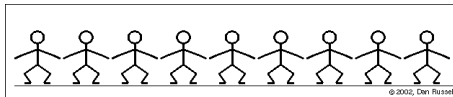


Scanning Electron Microscopy (SEM) & Electron Back Scattered Diffraction (EBSD)

David Mainprice

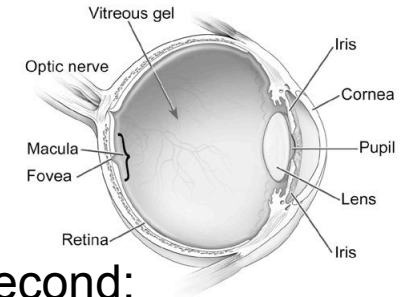


(Géosciences, Montpellier, France)



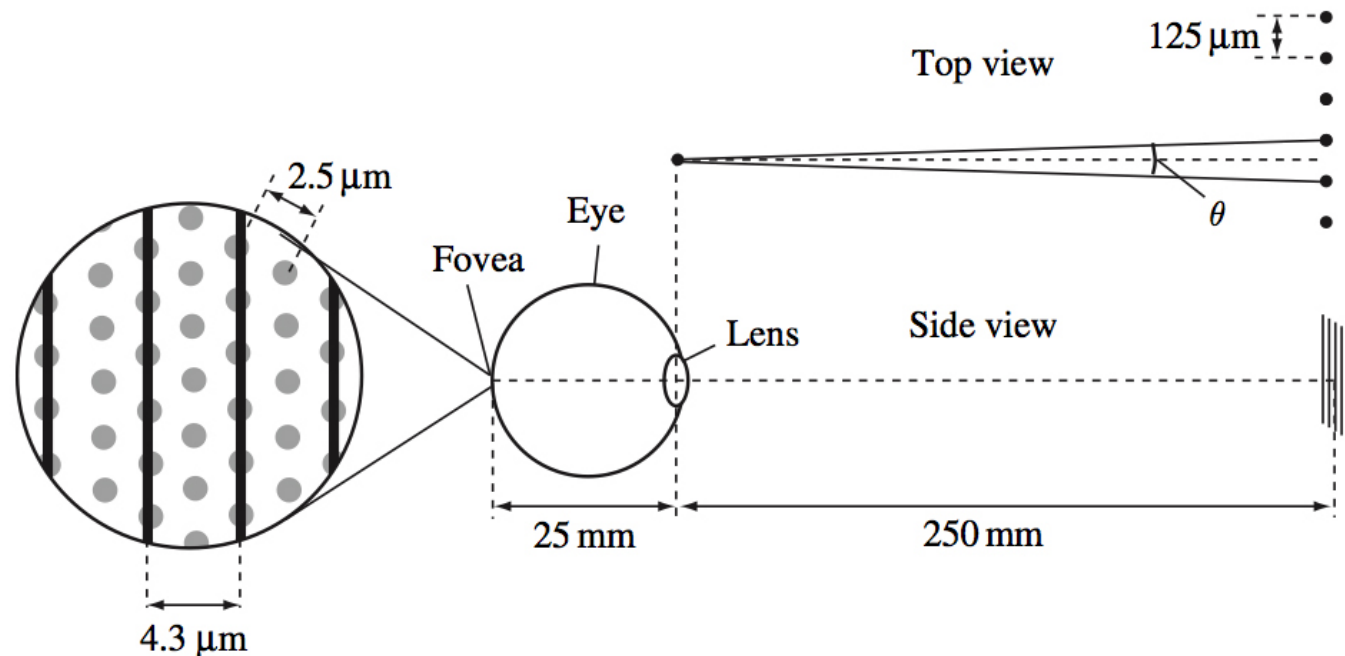
CNRS - Université Montpellier II, 34095 Montpellier, France

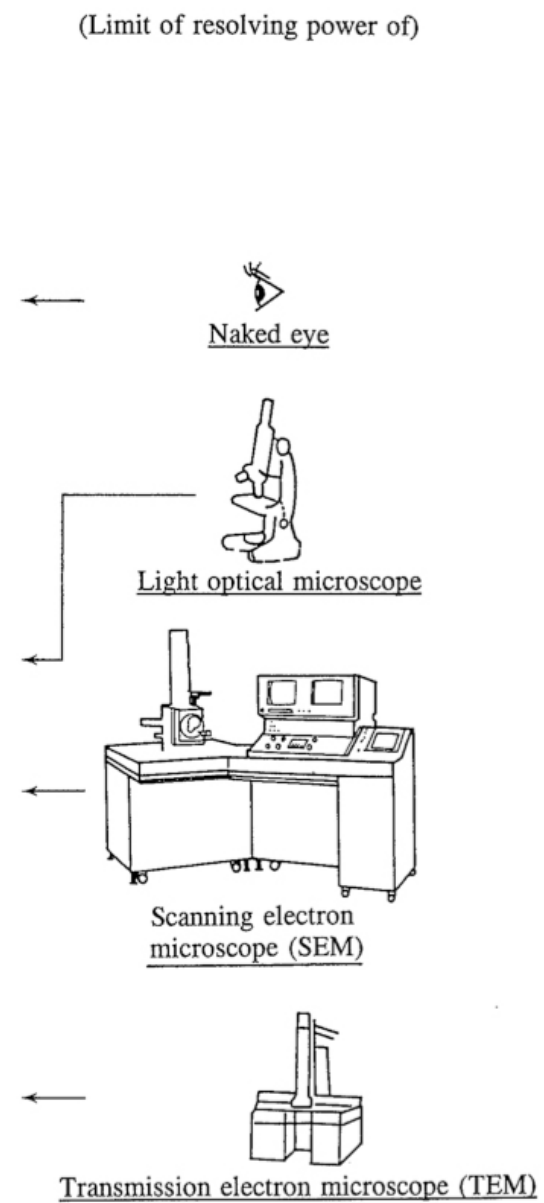
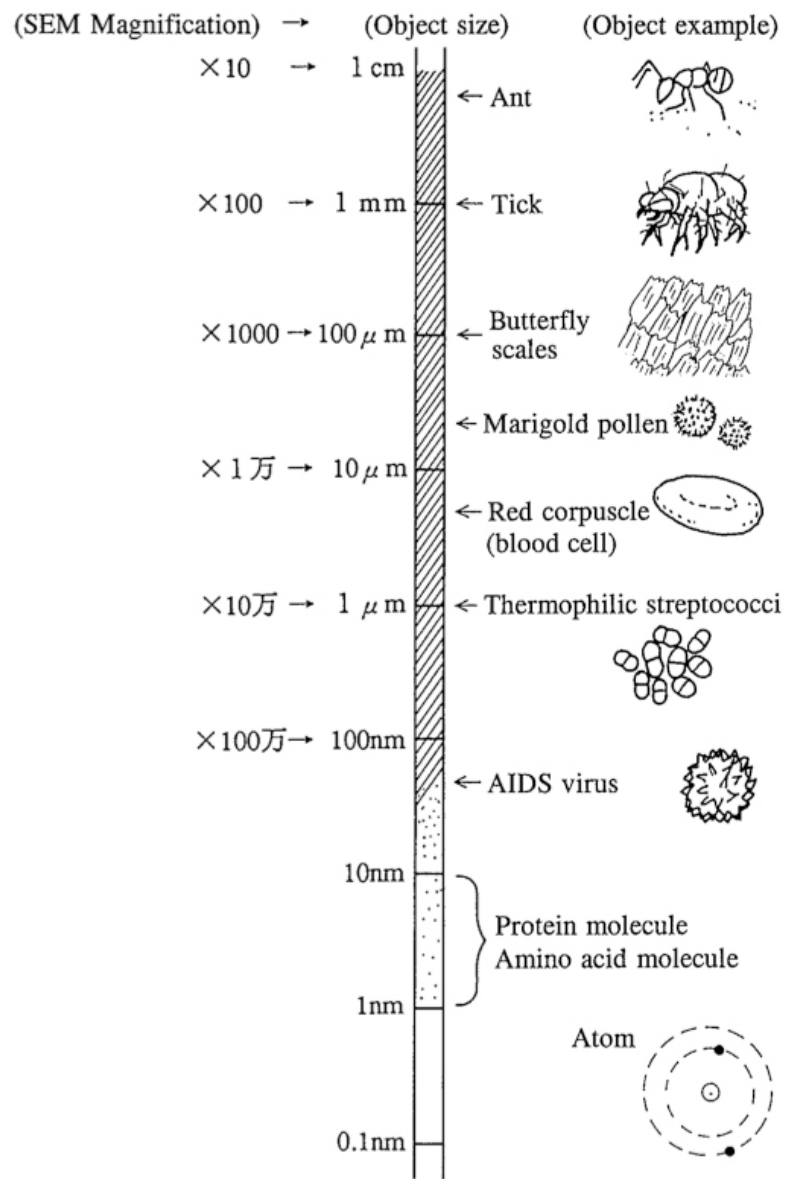
The human eye – your microscope



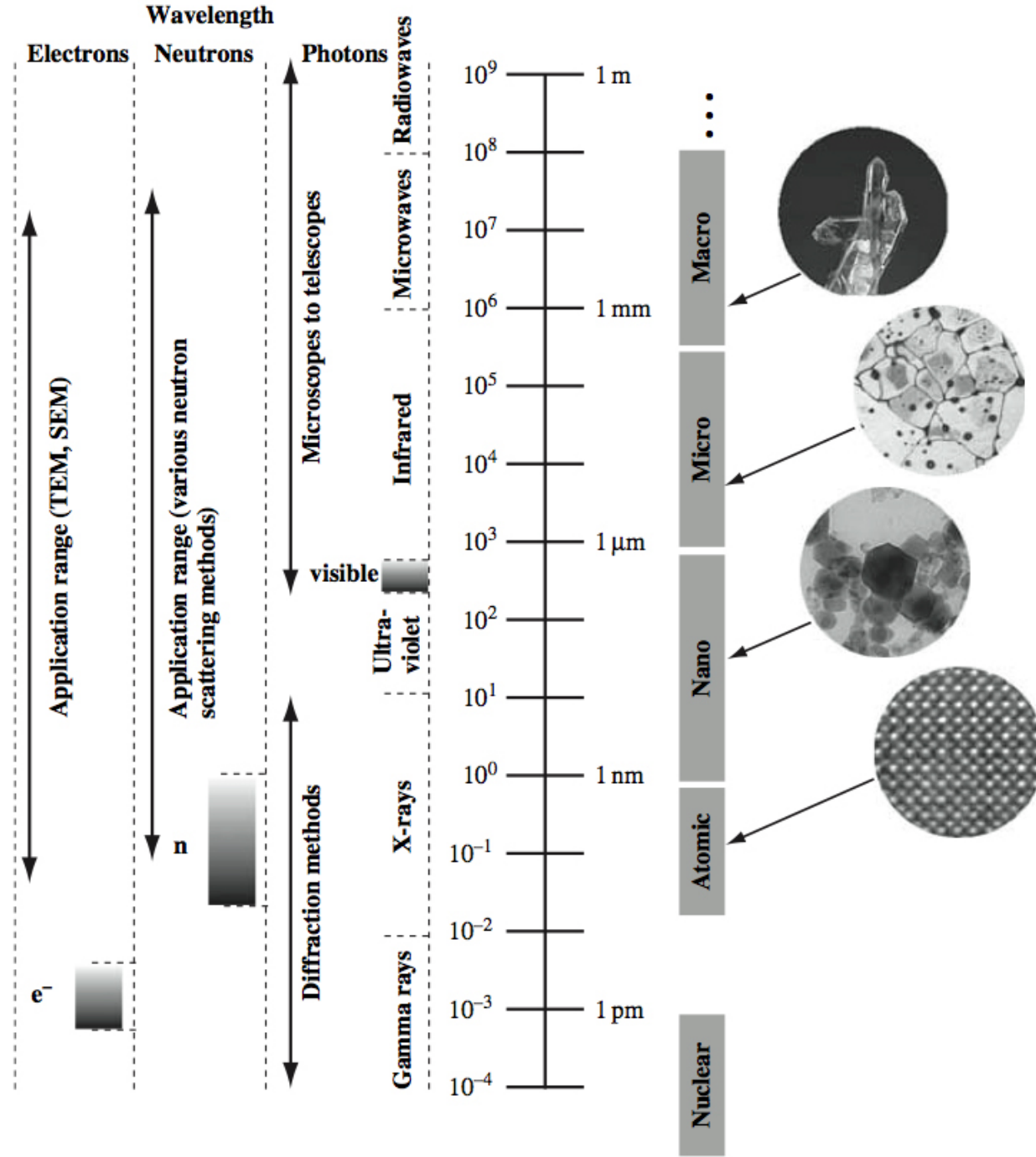
1. The remanence time of an image on the retina is about 1/24 of a second: this why television screens scanned 25 times per second and in the cinema the film advanced at 24 images per second.
2. The number of grey levels an eye can resolve is about 16 to 20. The human eye can discern 350 000 different shades of colour, but is bad observer of black and white images
3. The resolving power of the eye is about 0.125 mm at a distance of 250 mm

Schematic illustration of the resolution of the human eye. The lower portion shows the fovea as a hexagonal array of cones, the top view shows the angular resolution of the eye in terms of the eye-object distance, the angle θ , and the distance between individual object lines.

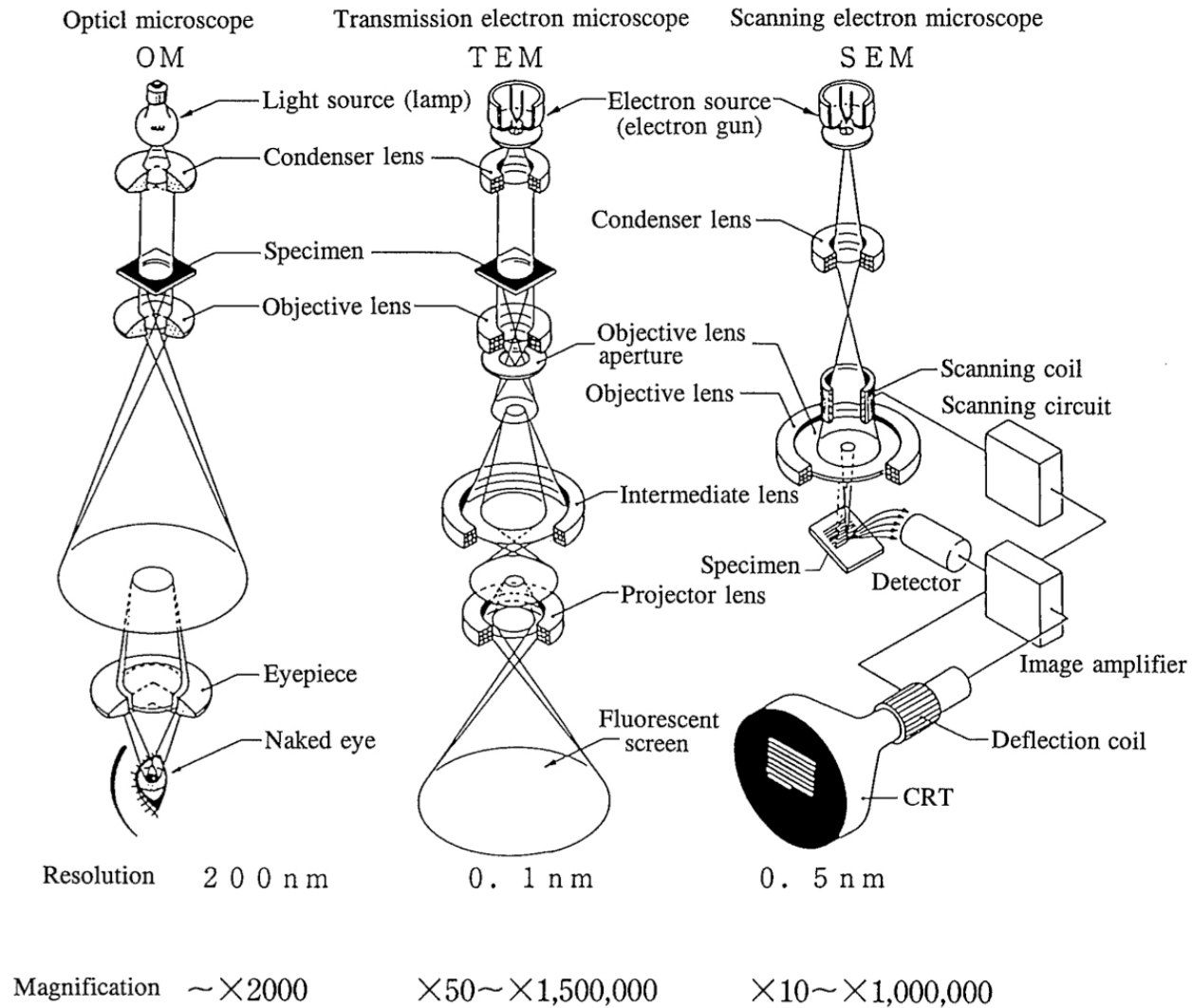




Schematic illustration of the various length scales, from macroscopic, to microscopic, to nanoscale, to the subatomic. The left hand side of the figure shows the experimental techniques that are used to cover the various length scales. The images in the circles on the right are (from the top down): a quartz crystal (courtesy of D. Wilson); grains in a SrTiO_3 ceramic (courtesy of G. Rohrer); nano-crystalline particles of $\text{Mn}_{0.5}\text{Zn}_{0.5}\text{Fe}_2\text{O}_4$ (courtesy of R. Swaminathan); atomic resolution image of BaTiO_3 .



Optical and Electronic Microscopes



Optical Microscope

Ernest Abbe 1874 ([University of Jena](#)) defined the resolution of an optical microscope to be the minimum distance of two structural elements to be imaged (d),

$$d = \lambda / \text{NA} = \lambda / n \sin \alpha$$

where λ is the wavelength and NA is the numerical aperture of the objective .
NA is defined as the sine of the half aperture angle α multiplied by the refractive index of the medium filling the space between the cover glass and the front lens

With $\alpha = 70^\circ$ $n = 1.5$ $\lambda = 0.5 \mu\text{m} = 500 \text{ nm}$

The resolution $d = 0.35 \mu\text{m} = 350 \text{ nm}$

N.B. The resolution is same order as wave length λ

Electron microscope

Louis de Broglie in 1924 in his PhD thesis associated the wave length of electrons with the accelerating voltage for which he was awarded the Nobel Prize for Physics in 1929 for this work, which made him the first person to receive a Nobel Prize for a PhD thesis. *Recherches sur la théorie des quanta*, Thesis (Paris).

$$\lambda = h / m v$$

with h = Planck's constant

m = electron's rest mass

v = velocity of the electron

The velocity is related to the kinetic energy of the particule (electron with charge e) accelerated by the voltage V given by :

$$\frac{1}{2} m v^2 = e V$$

where

$$\lambda = h / (2 m e V)^{1/2} = (1.5 / V)^{1/2} \text{ with } \lambda \text{ in nm and } V \text{ in volts}$$

$$\text{For exemple } V = 20 \text{ kV} \quad \lambda = 0.008 \text{ nm}$$

$$V = 100 \text{ kV} \quad \lambda = 0.004 \text{ nm}$$

Compared with optics with $\lambda = 500 \text{ nm}$ ($\times 125\,000 \lambda_{\text{optic}}$ à 100 kV)

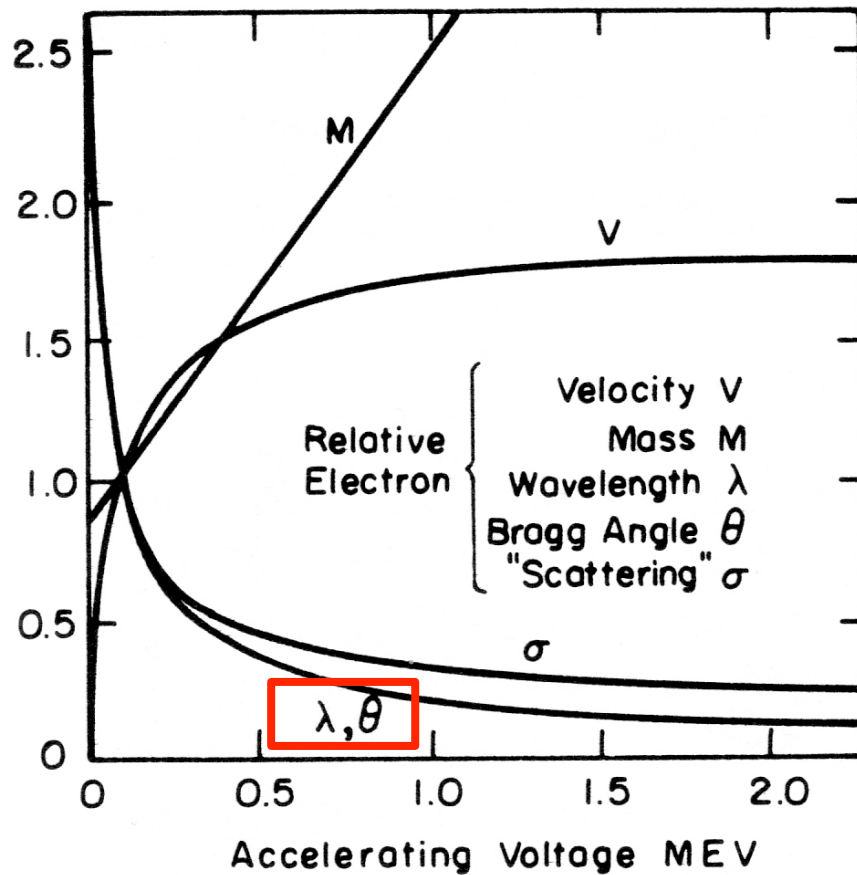
Today the best electron microscopes have a point to point resolution of about 0.1 nm.

N.B. a resolution of about 100λ ! For optical microscope resolution = λ !!

Average diffraction properties of radiation used for texture measurement by diffraction, with light also included for comparison

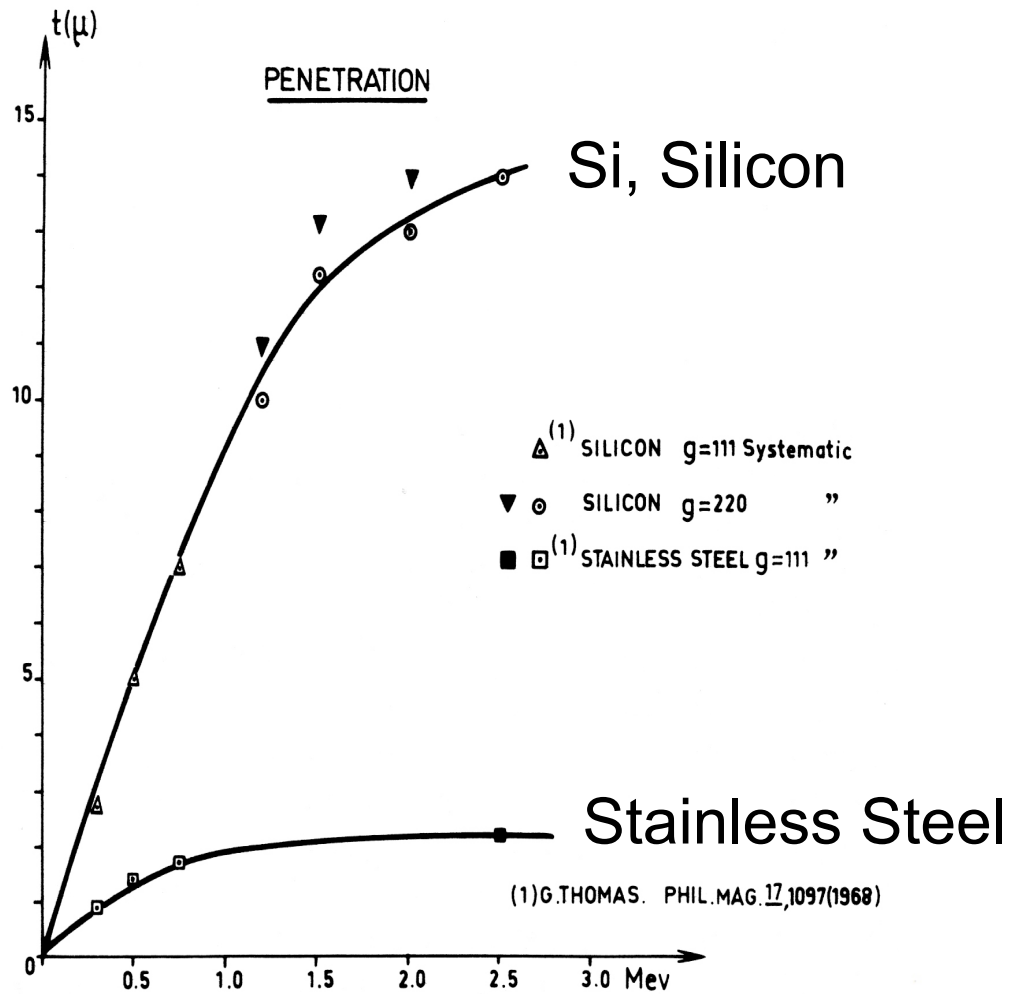
	Light	Neutrons	X-rays	Electrons
Wavelength [nm]	400–700	0.05–0.3	0.05–0.3	0.001–0.01
Energy [eV]	1	10^{-2}	10^4	10^5
Charge [C]	0	0	0	-1.602×10^{-19}
Rest mass [g]	0	1.67×10^{-24}	0	9.11×10^{-28}
Penetration depth, absorption length [mm]	–	10–100	0.01–0.1	10^{-3}

Wavelength – Voltage

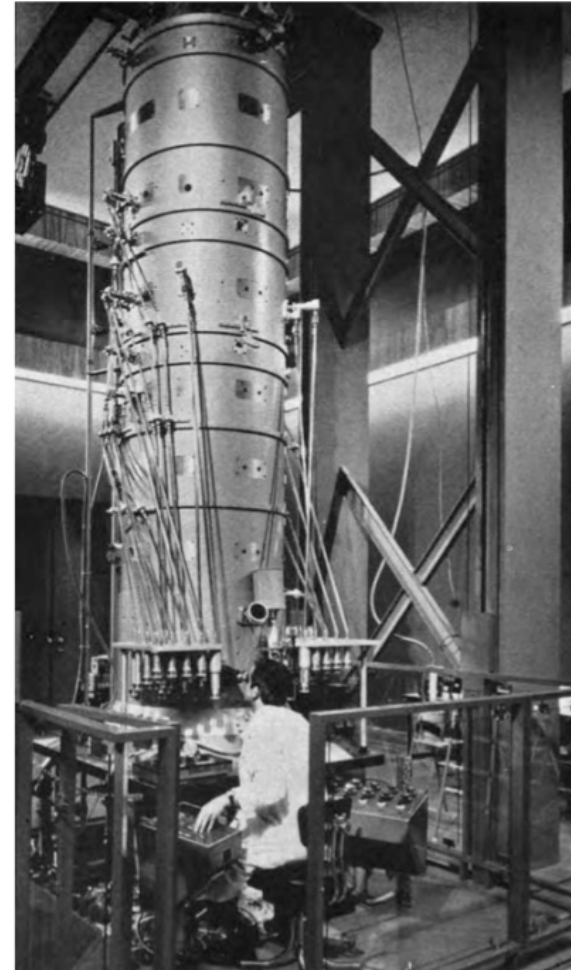


SEM – 10-30 kV

Properties of electrons as a function of voltage, relative to those at 100 kV. Courtesy R. M. Fisher.



Experimental data on penetration in silicon and stainless steel.

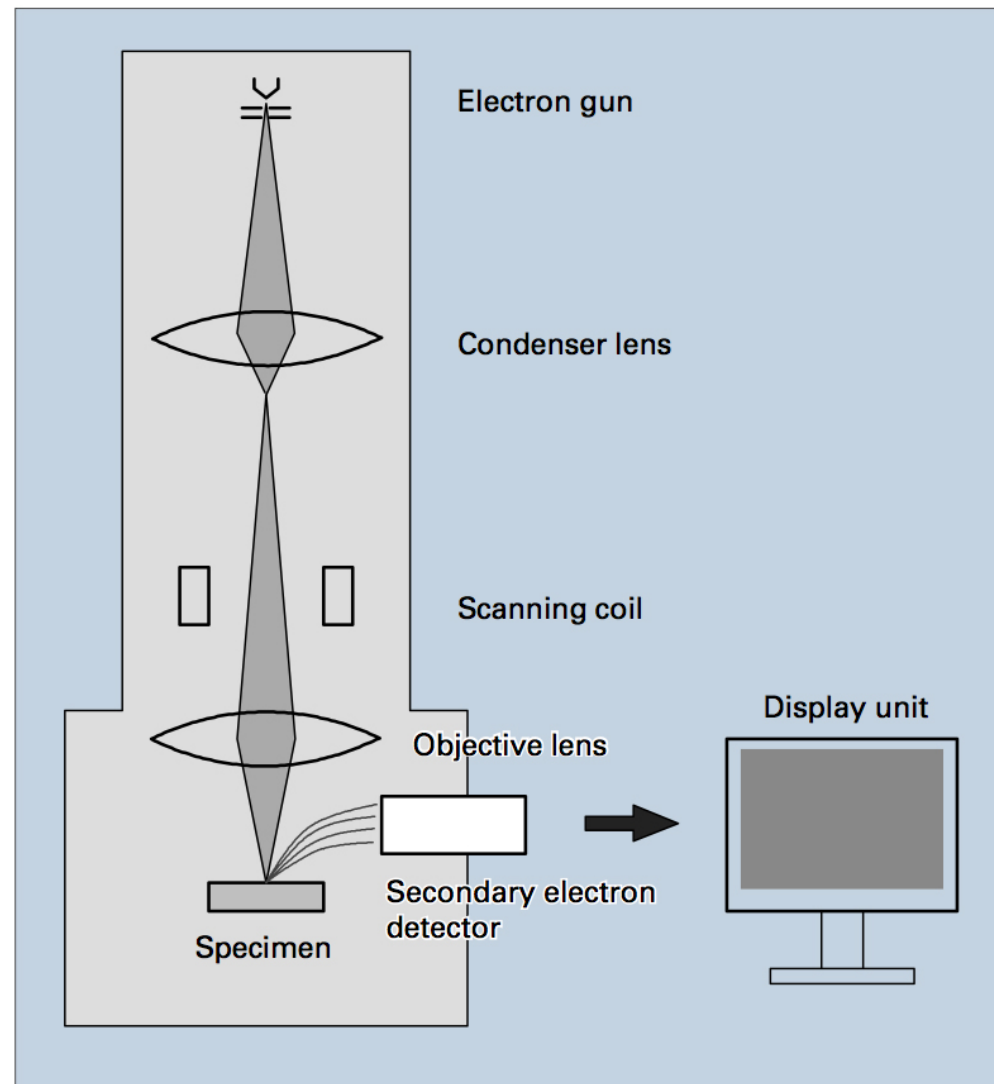


A 3 MV HVEM constructed at the C.N.R.S. Laboratories in Toulouse and in operation by 1970. To focus the high-energy electrons, large-diameter lenses were required, and the TEM column became so high that long control rods were needed between the operator and the moving parts (for example, to provide specimen motion). Courtesy of G. Dupouy, personal communication.

Some important dates

- 1924 De Broglie associated the notion of wave length to particles
- 1931 Ruska made first electron microscope
- 1939 Siemens delivered the first commercial transmission electron microscope (TEM)
- 1951 Castaing built the first micro-probe with an x-ray analyser
- 1965 Cambridge Instruments delivered the first commercial scanning electron microscope

Basic SEM column



Basic construction of a SEM.

Characteristic Information: SEM

Topography

The surface features of an object or "how it looks", its texture; direct relation between these features and materials properties

Morphology

The shape and size of the particles making up the object; direct relation between these structures and materials properties

Composition

The elements and compounds that the object is composed of and the relative amounts of them; direct relationship between composition and materials properties

Crystallographic Information

How the atoms are arranged in the object; direct relation between these arrangements and material properties

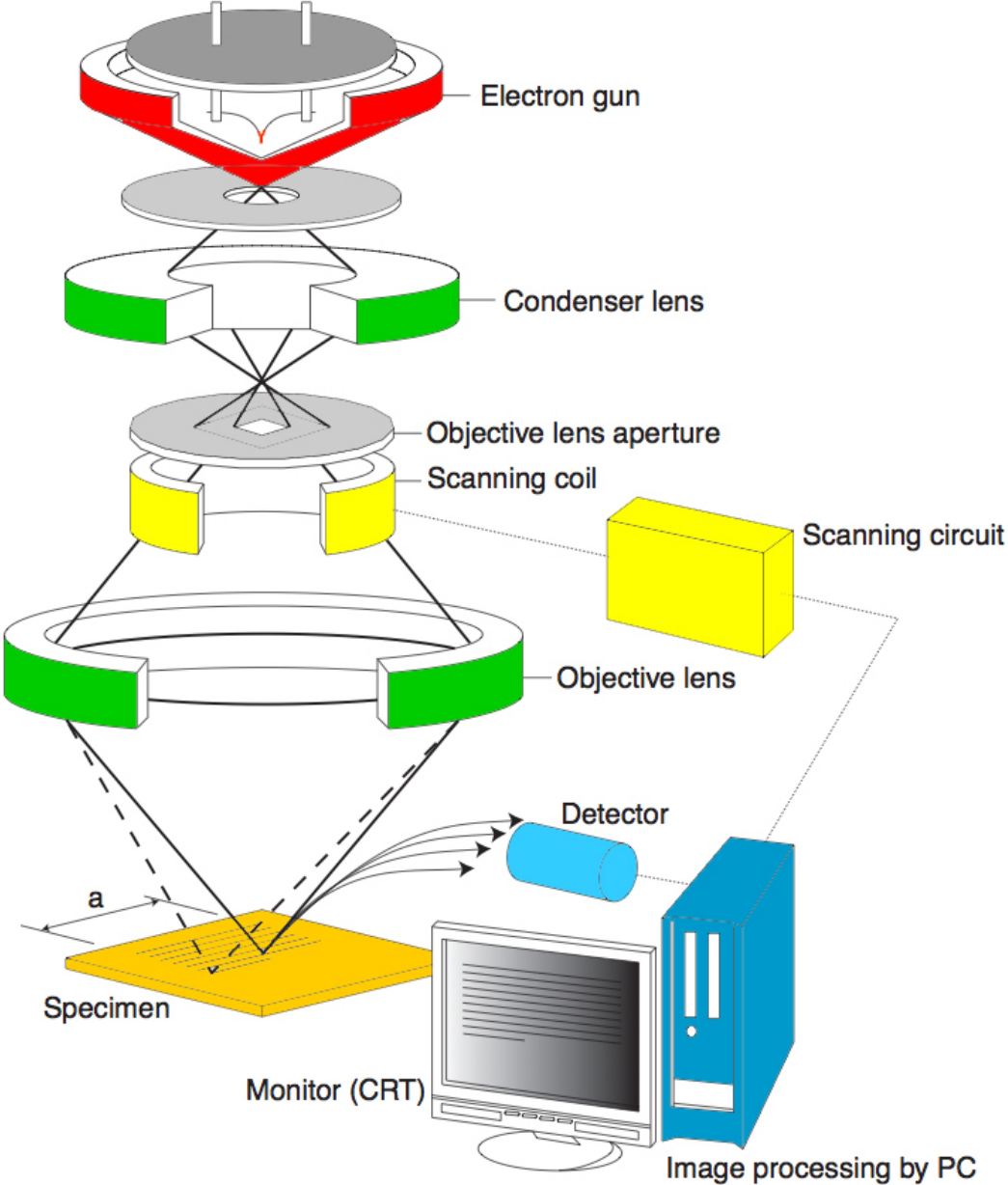
Advantages of Using SEM over OM

Mag	Depth of Field	Resolution
OM: 4x – 1400x	0.5mm	~ 0.2mm
SEM: 10x – 500Kx	30mm	1.5nm

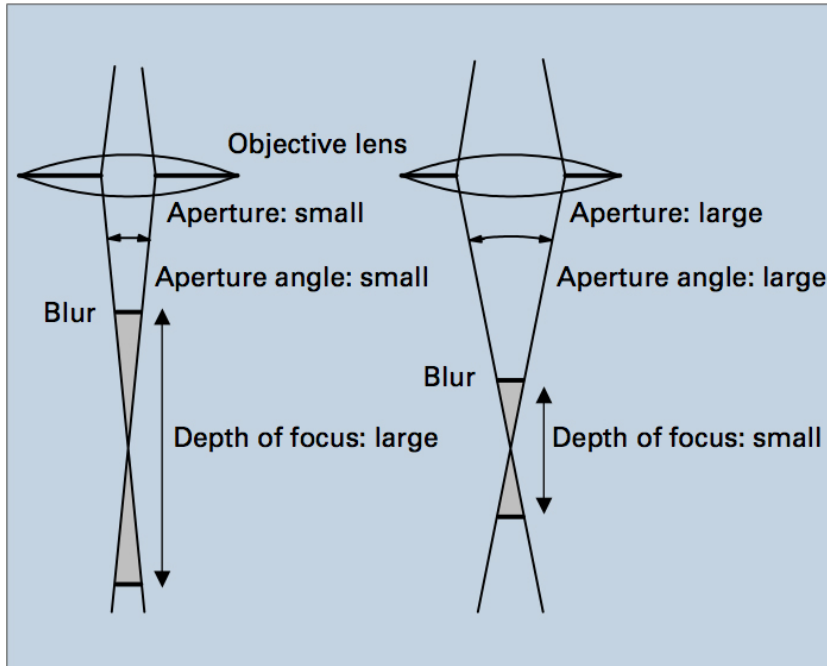
The SEM has a large depth of field, which allows a large amount of the sample to be in focus at one time and produces an image that is a good representation of the three-dimensional sample.

The combination of higher magnification, larger depth of field, greater resolution, compositional and crystallographic information makes the SEM one of the most heavily used instruments in academic/national lab research areas and industry.

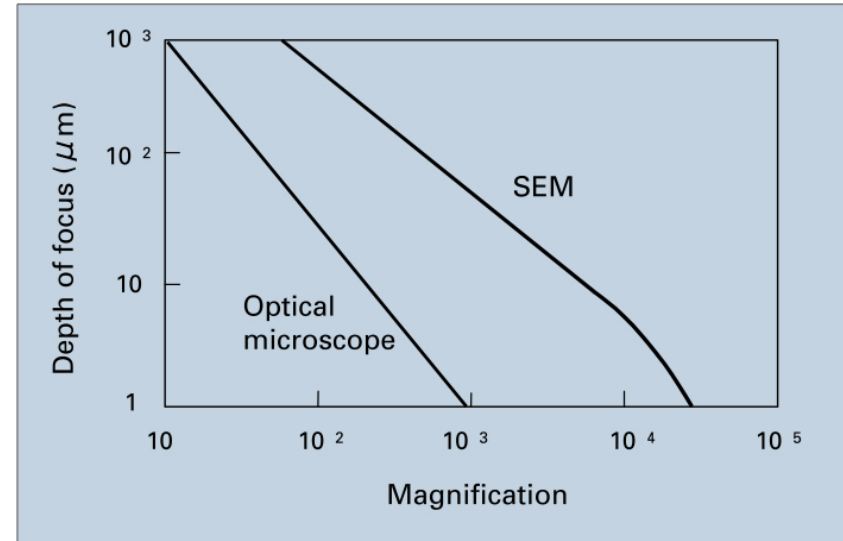
Elements of an SEM



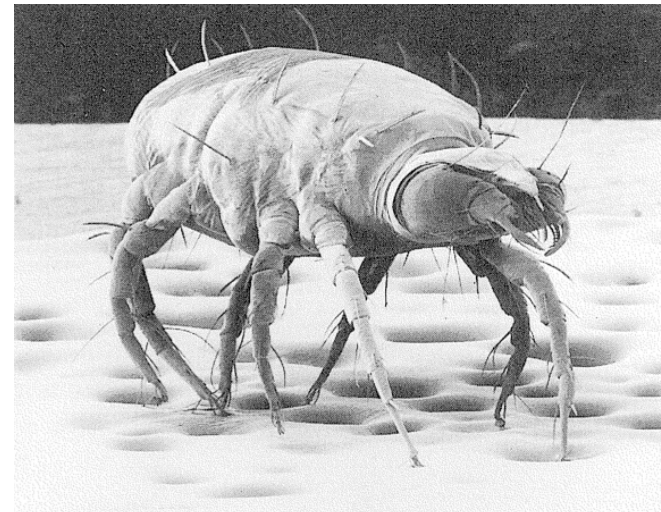
SEM : Depth of focus



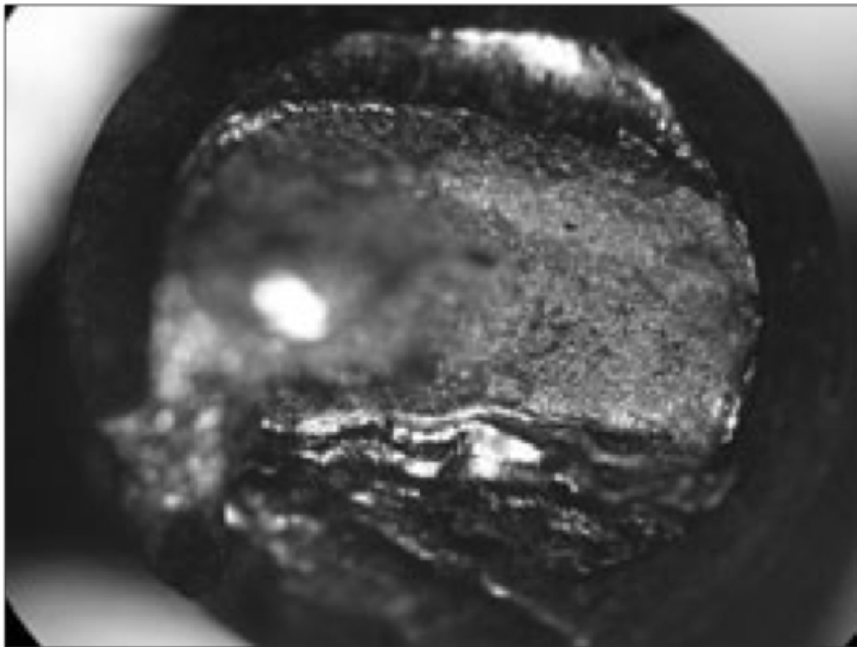
Relation between the aperture angle of the electron probe and the depth of focus.



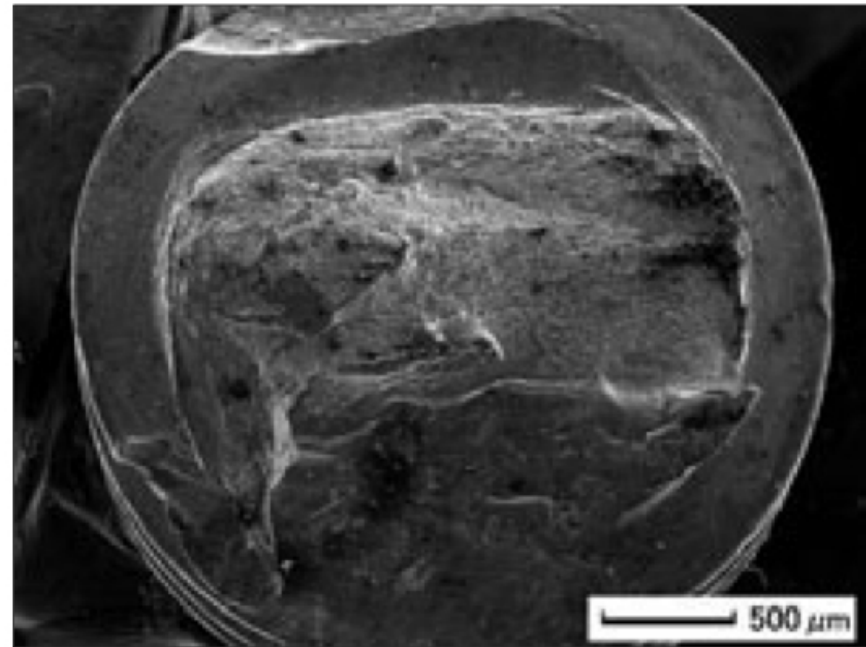
Difference of the depth of focus between SEM and optical microscope.



OM image



SEM image



OM image and SEM image of the same field of view.

Depth of Field

The height over which a sample can be clearly focused is called the Depth of Field. The SEM has a large depth of field which produces the images that appear 3-dimensional in nature.

Depth of field is improved by:

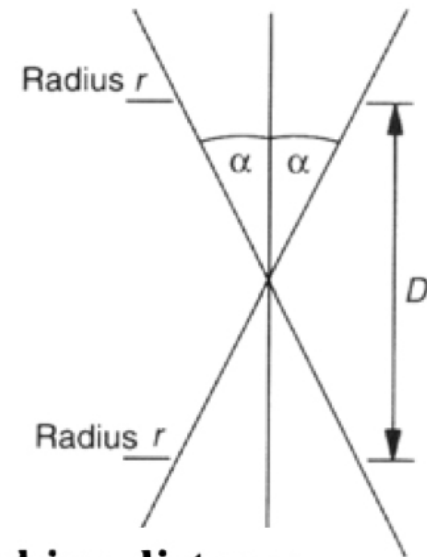
- Longer working distance**
- Smaller objective apertures**
- Lower magnifications**

Depth of Field

The angle α is determined by:

$$\alpha = r/WD$$

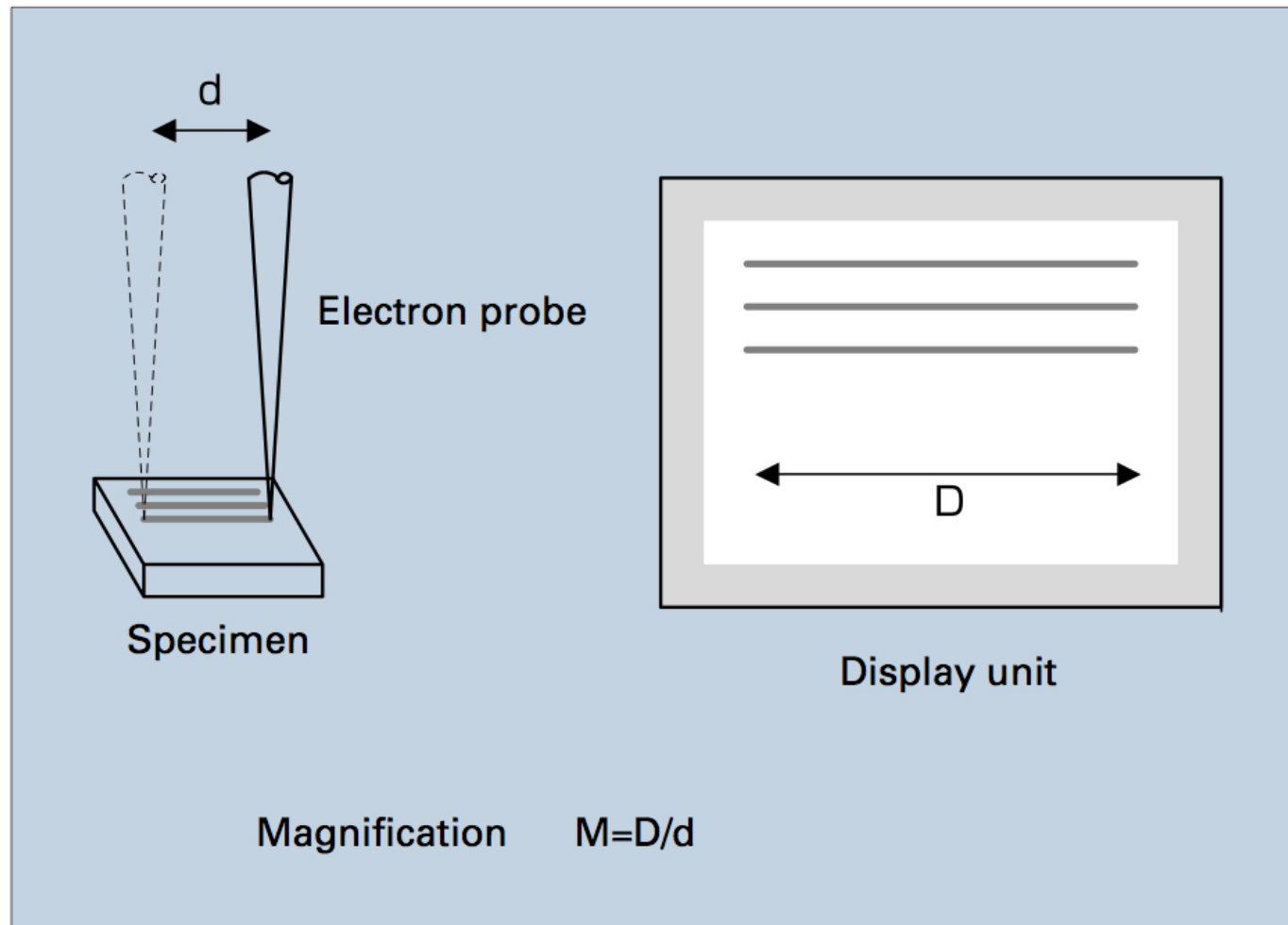
r = radius of the aperture used, and WD is the working distance of the aperture from the specimen.



Depth of field in μm with 10-mm working distance

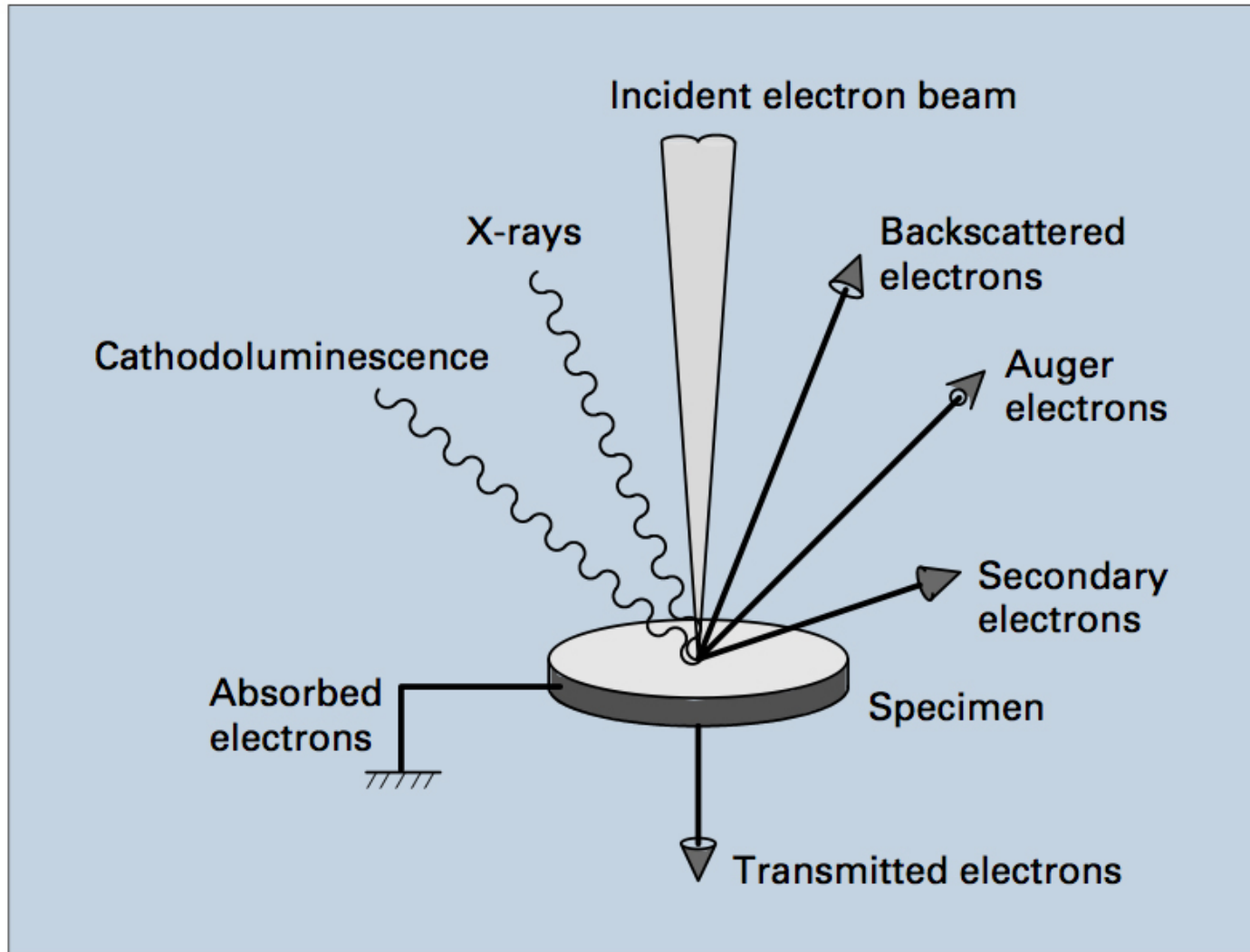
<i>Magnification</i>	<i>With 100-μm aperture</i>	<i>With 400-μm aperture</i>
100	400	100
1000	40	10
10000	4	1
100000	0.4	0.1

Concept of SEM magnification

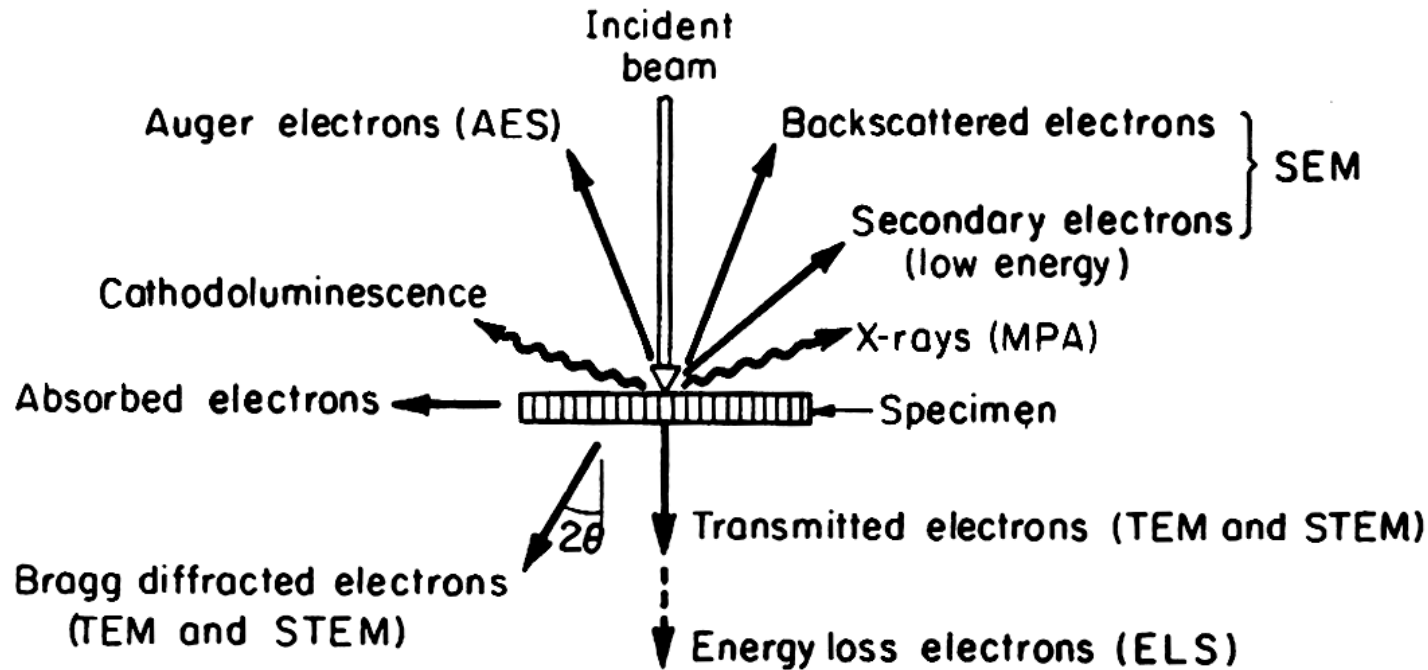


Concept of SEM magnification.

Electron beam – specimen interaction



Interaction - TEM



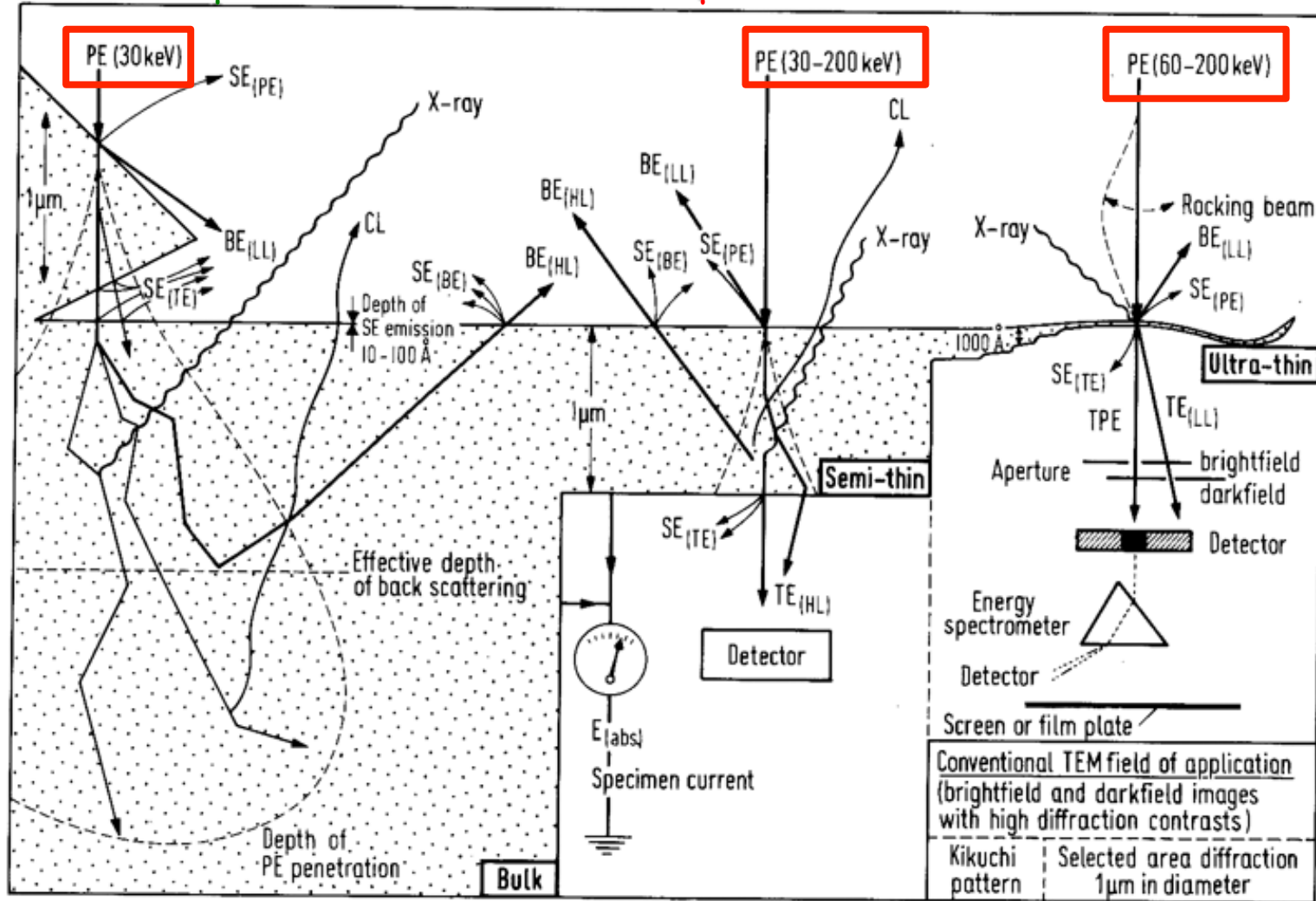
Schematic showing electrons and electromagnetic waves emitted from a specimen as a result of elastic and inelastic scattering of the incident electron waves

Interactions - TEM

3 μm

1 $\mu\text{m} = 1000 \text{ nm}$

100-10 nm



Signals excited by the scanning electron beam and their relation to specimen morphology

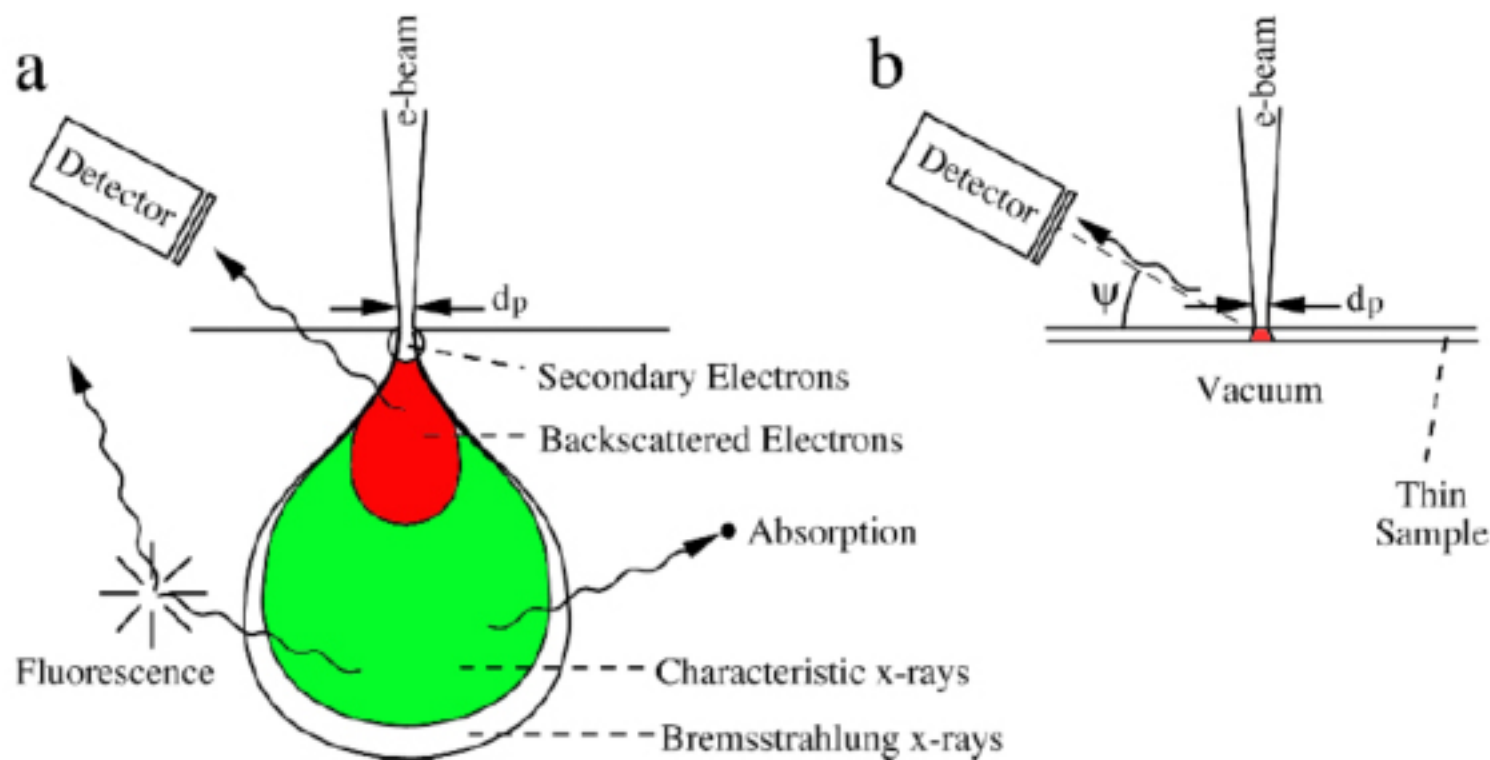
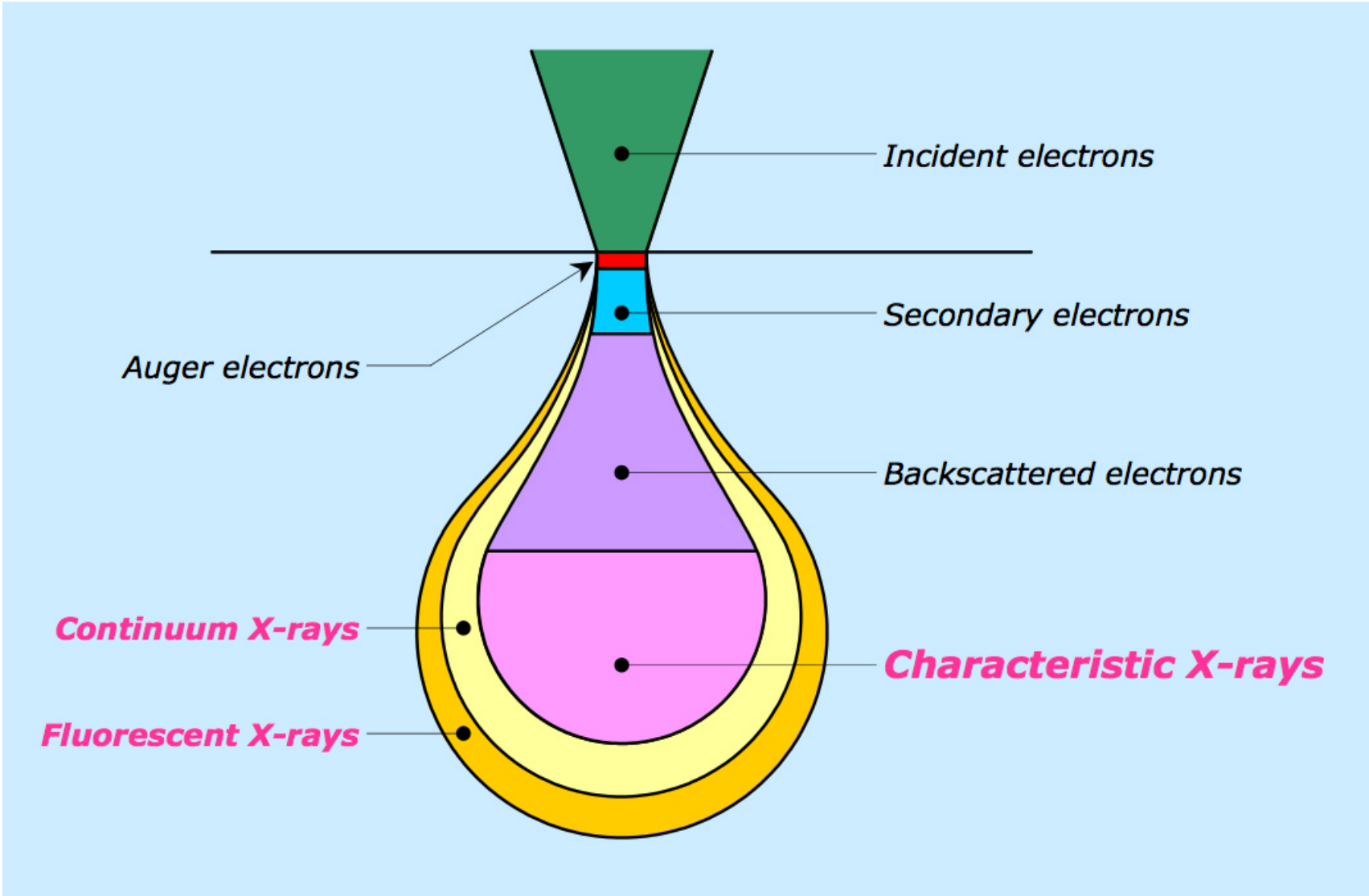


Fig. 4.20. Differences in beam broadening in a bulk specimen (a), and a thin film (b). Part a shows regions of electron penetration, electron escape, and x-ray emission. For high-energy electrons, dimensions of regions of x-ray emission are typically a few microns, microns for backscattered electrons, tens of Å for secondary electrons. The larger dimensions do not exist for the thin specimen in b.

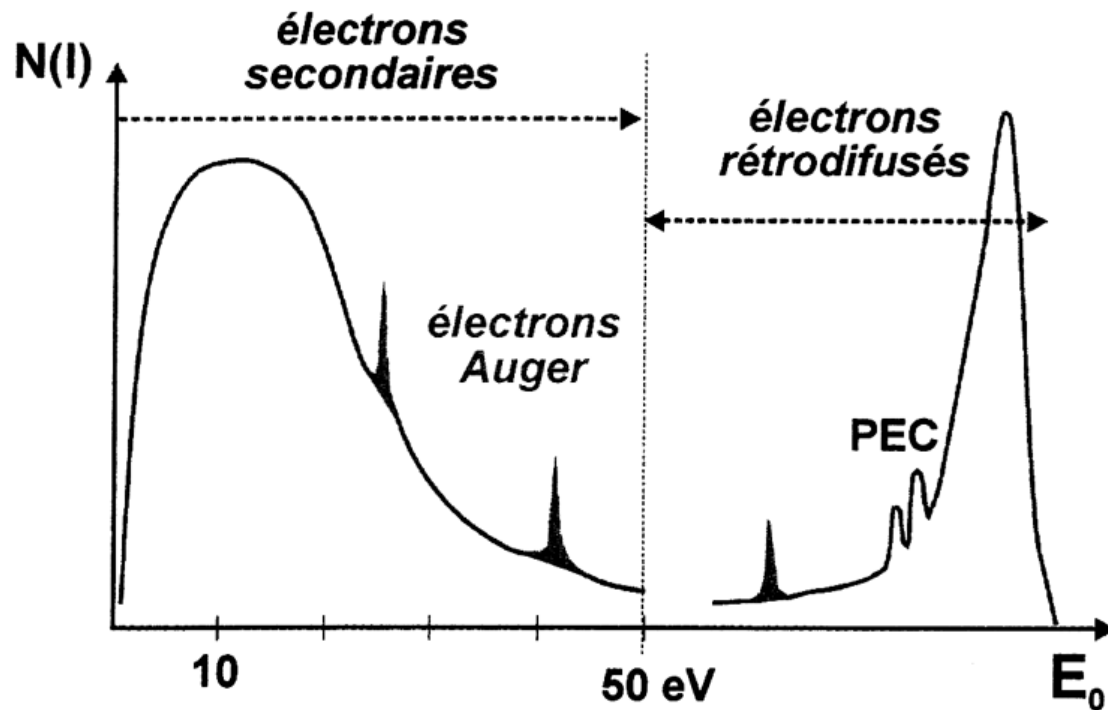


Specimen Interaction Volume

The volume inside the specimen in which interactions occur while interacting with an electron beam. This volume depends on the following factors:

- Atomic number of the material being examined; higher atomic number materials absorb or stop more electrons , smaller interaction volume.**
- Accelerating voltage: higher voltages penetrate farther into the sample and generate a larger interaction volume**
- Angle of incidence for the electron beam; the greater the angle (further from normal) the smaller the interaction volume.**

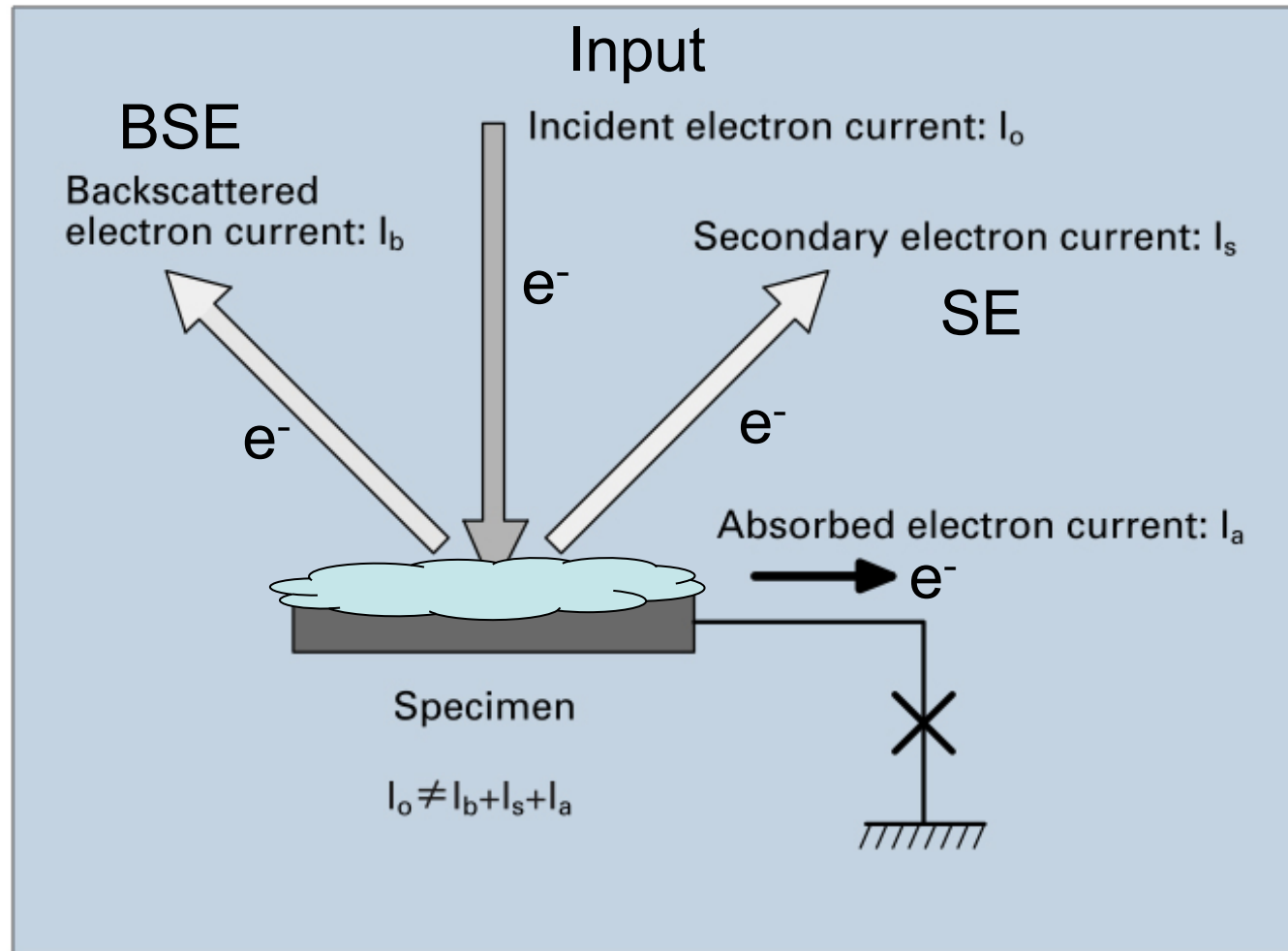
Secondary (SE) and back-scattered electrons (BSE)



Distribution énergétique de l'émission électronique d'une cible.

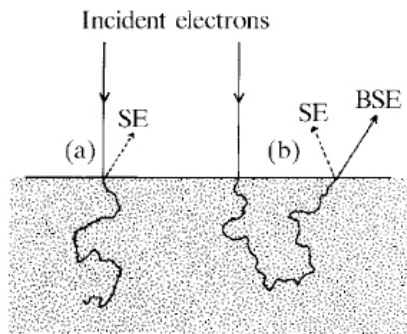
PEC : pic d'énergie caractéristique
(interactions avec les phonons)

Non-conductive specimen

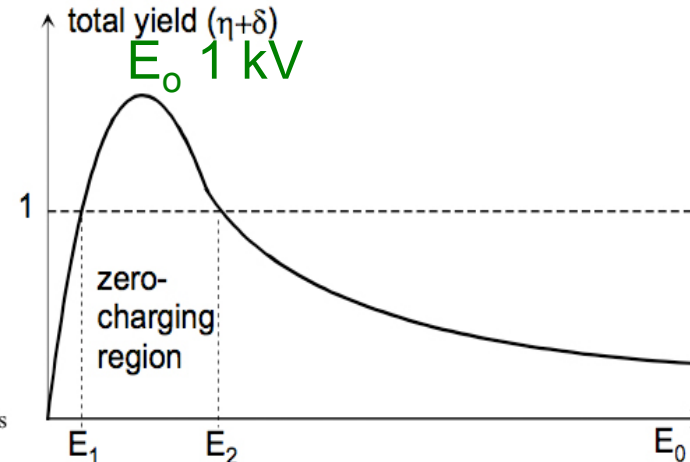


Electric flow in a nonconductive specimen.

Total electron yield – Back-scattered(η) + Secondary (δ) Low voltage microscopy



Production of secondary electrons (SE): (a) by incident electrons entering target; and (b) by backscattered electrons (BSE) as they leave.



$E_1 = 0.1 \text{ kV}$ $E_2 = 1.3 \text{ kV}$

Total electron yield ($\eta + \delta$) as a function of primary energy, showing the range (E_1 to E_2) over which electrostatic charging of an insulating specimen is not a problem.

$$I_{\text{specimen}} = I_{\text{primary}} - I_{\text{BSE}} - I_{\text{SE}} = I_{\text{primary}} - (I_{\text{BSE}} + I_{\text{SE}}) = I_p - (\eta + \delta)$$

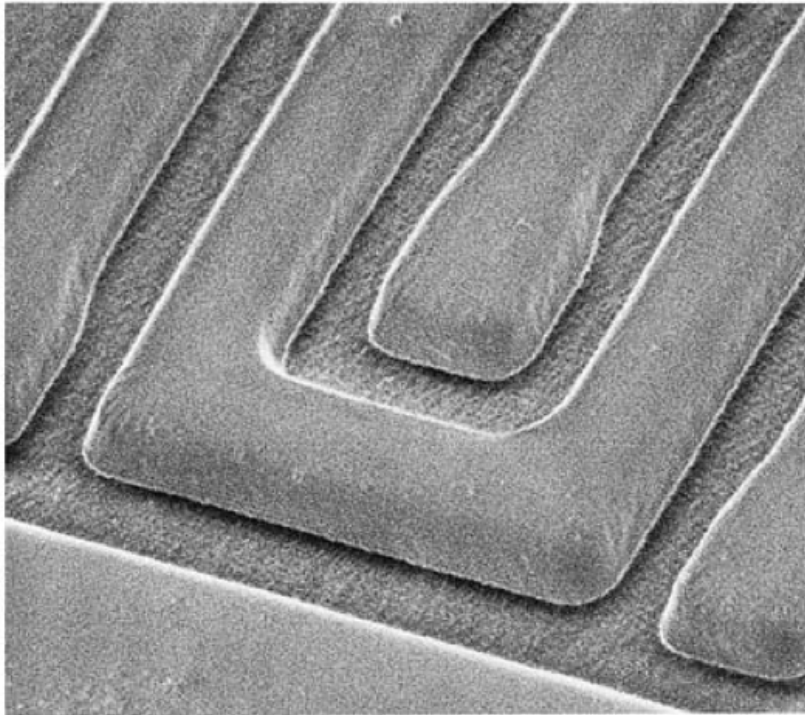
$E_1 = \eta + \delta = 1$ (specimen +ve charged to neutral) $\approx 100\text{-}500\text{V}$

$E_1 < E_0 < E_2$ no charge $I_p \approx (\eta + \delta)$ Input Beam $E_0 \approx$ Output SE+BSE

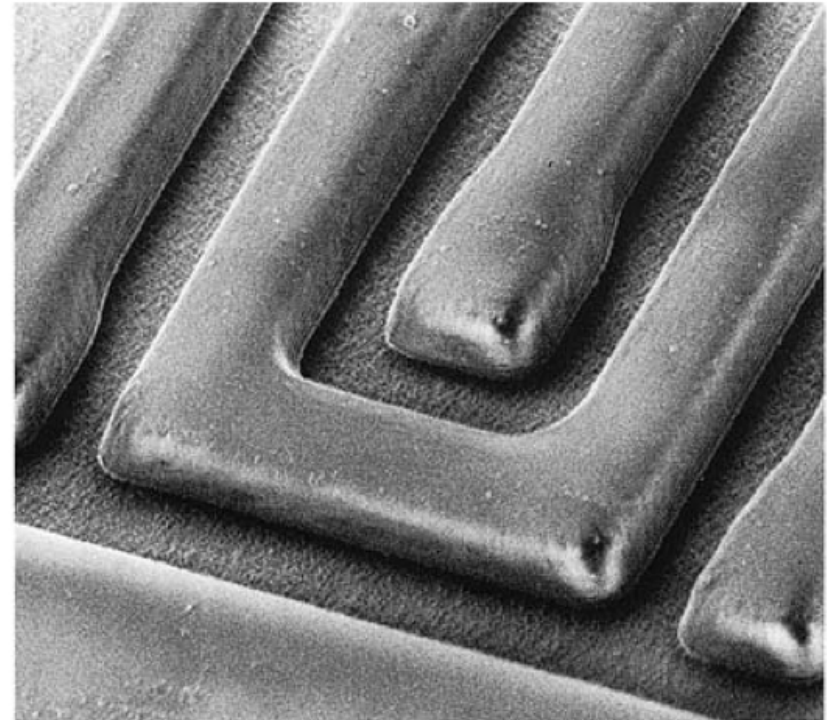
e.g. $E_1 = 0.1 \text{ kV}$ $E_0 = 1 \text{ kV}$ $E_2 = 1.3 \text{ kV}$

$E_2 = \eta + \delta = 1$ (specimen -ve charged to neutral) $\approx 1\text{-}10 \text{ kV}$

No charging at 1.0 kV



(a) 1.0kV Image without charging because the charge equilibrium is obtained. $\times 3,200$



(b) 1.3kV Image with charging $\times 3,200$

Coating

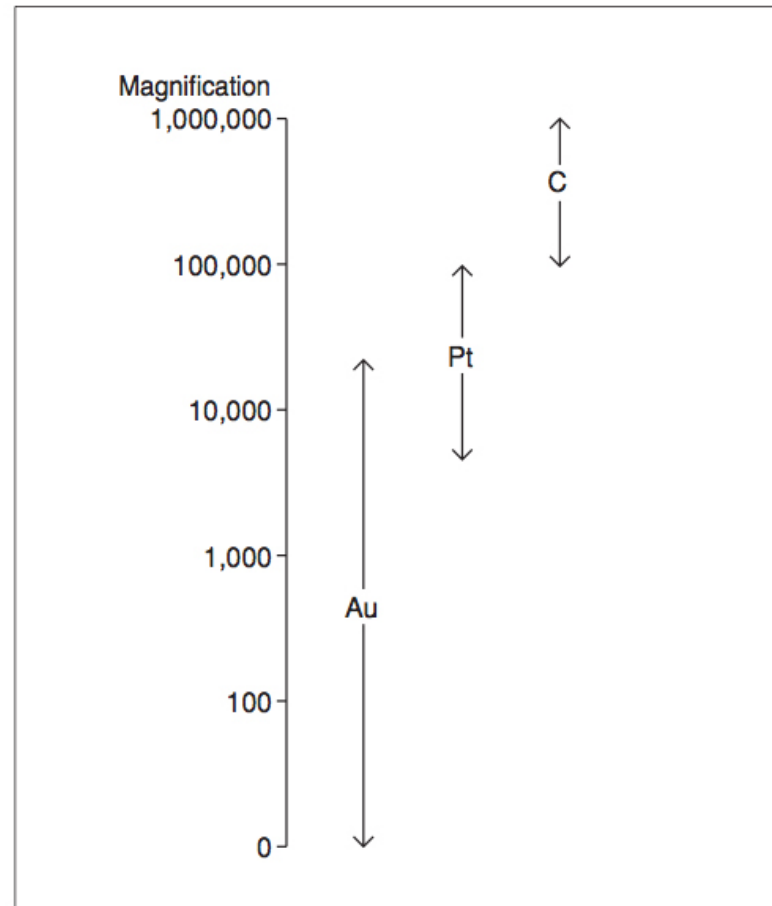
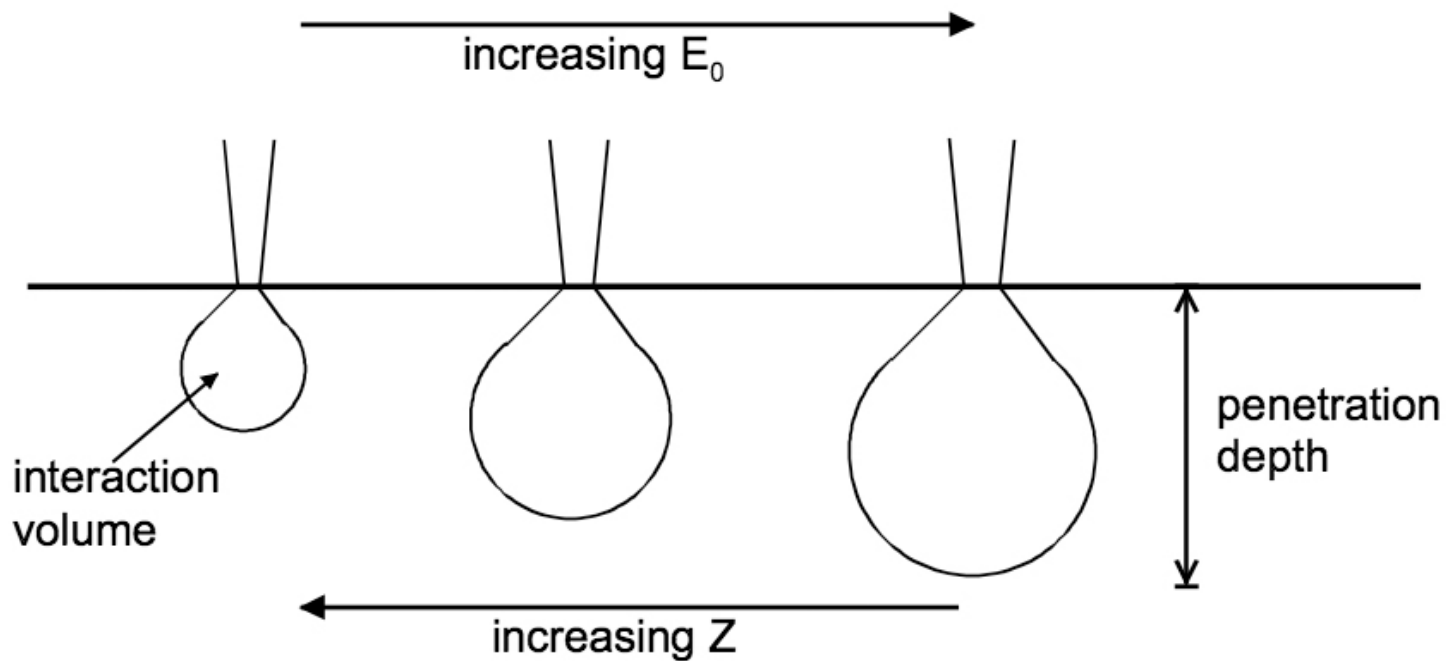


Fig.1 Usage of the coating material according to the granularity (for the SEM observation).

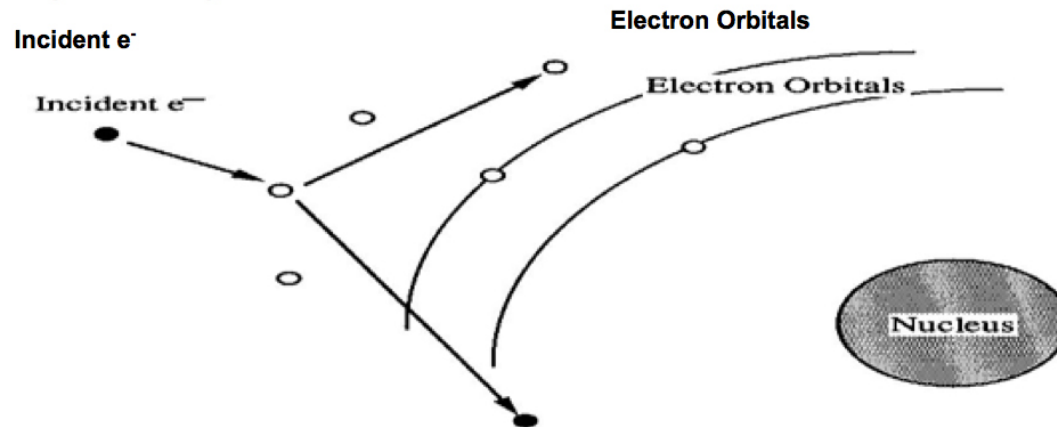
Purpose	Major coating material
SEM observation (secondary electron image)	Au, Pt, Au-Pd
Observation of backscattered electron image	C
Elemental analysis	C, Al, Au
Magnetic domain or channeling pattern of nonconductive specimens	C



Schematic dependence of the interaction volume and penetration depth as a function of incident energy E_0 and atomic number Z of the incident (primary) electrons.

Secondary Electrons

These electrons arise due to inelastic collisions between primary electrons (the beam) and loosely bound electrons of the conduction band (more probable) or tightly bound valence electrons. The energy transferred is sufficient to overcome the work function which binds them to the solid and they are ejected.

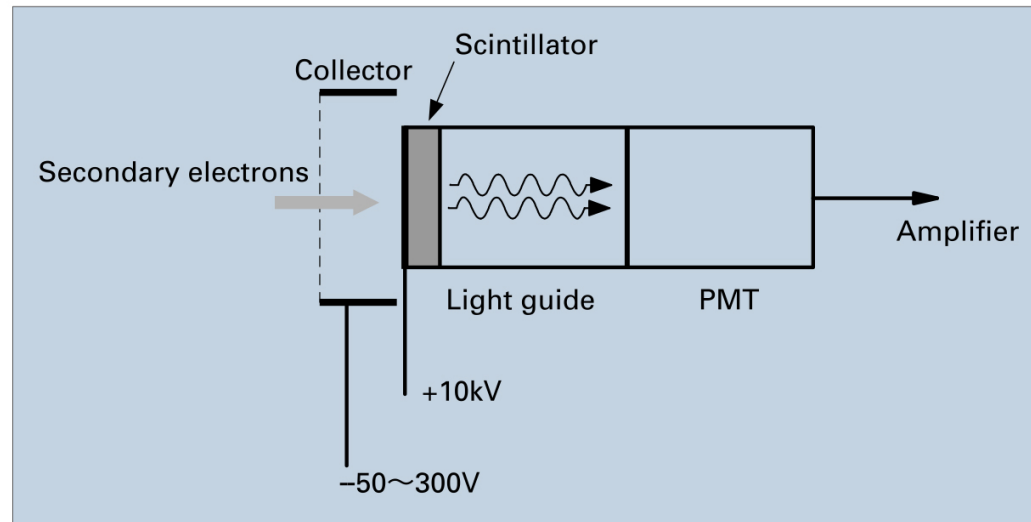


The interaction is Coulombic in nature and the ejected electrons typically have $\approx 5 - 10$ eV. 50 eV is an arbitrary cut-off below which they are said to be secondary electrons.

Detection

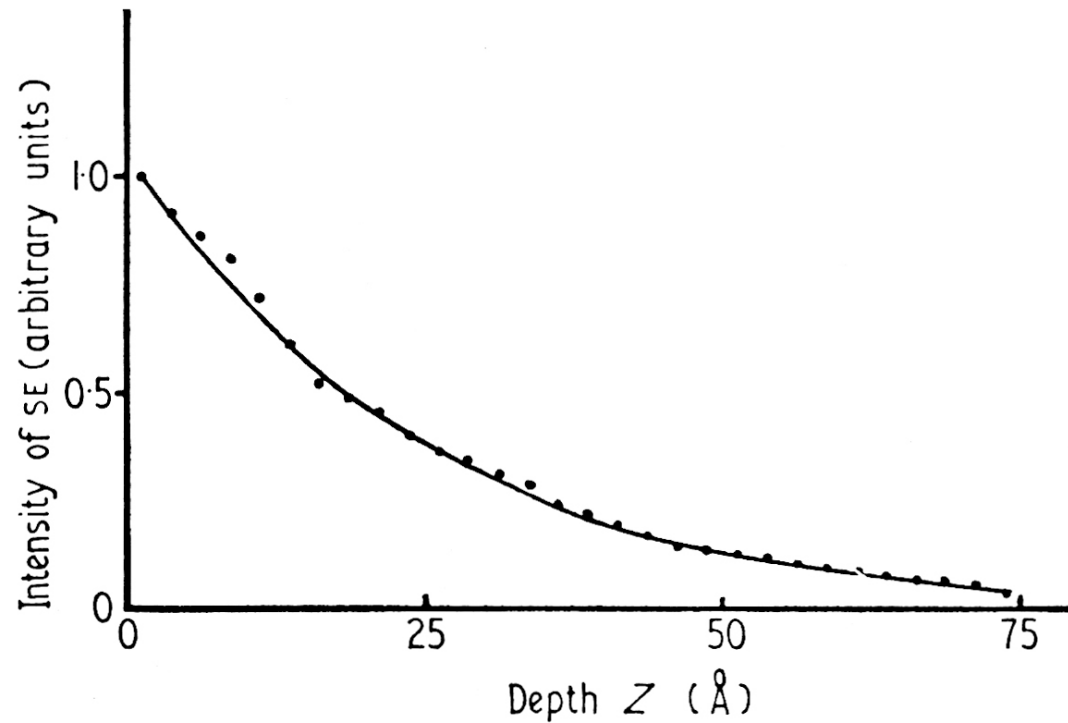
Remember, secondary electrons are low energy electrons. We can easily collect them by placing a positive voltage (100 - 300V) on the front of our detector. Since this lets us collect a large number of the secondaries (50 - 100%), we produce a “3D” type of image of the sample with a large depth of field.

The type of detector used is called a scintillator / photo-multiplier tube.



Construction of the secondary electron detector.

SE : Secondary Electrons



Probability of escape of secondary electrons generated at a depth Z below the sample surface (Koshikawa and Shimizu 1974).

Secondary Electrons : SE Topography

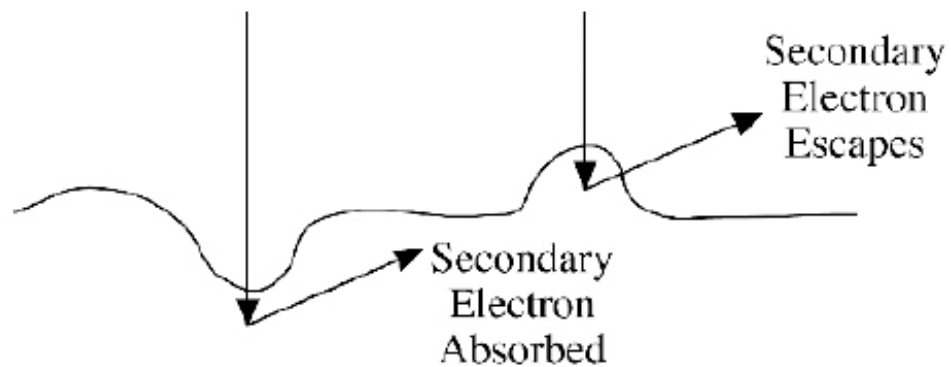
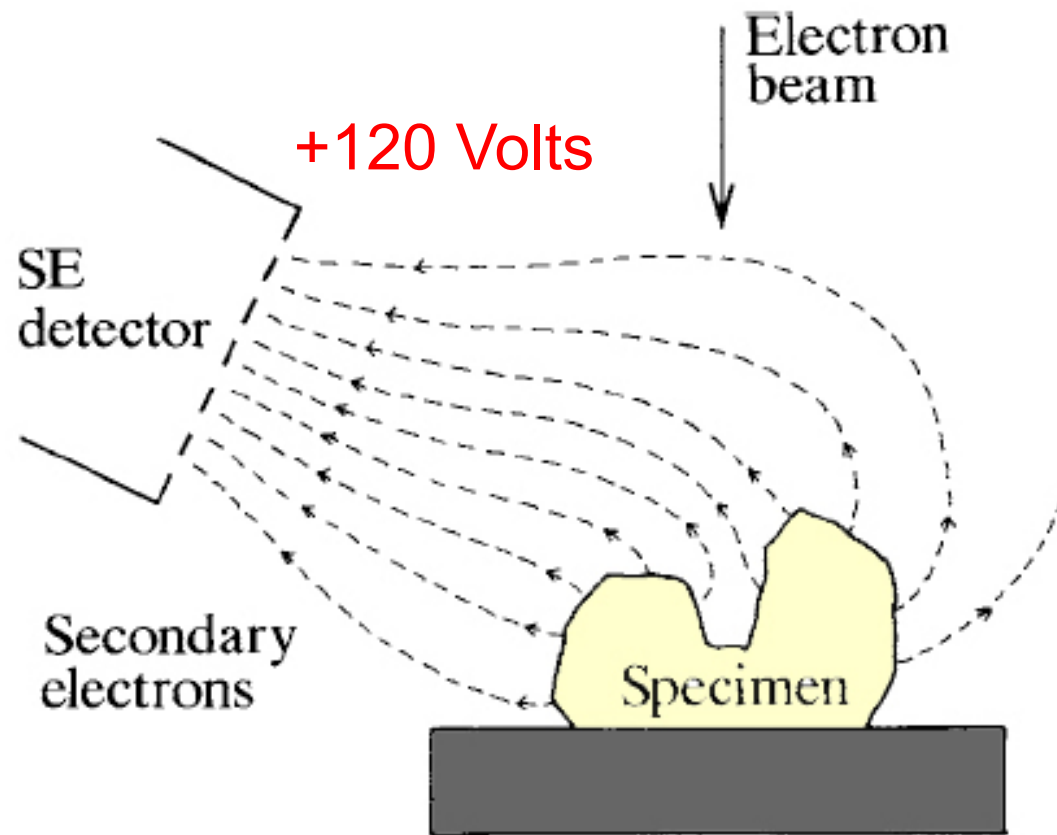
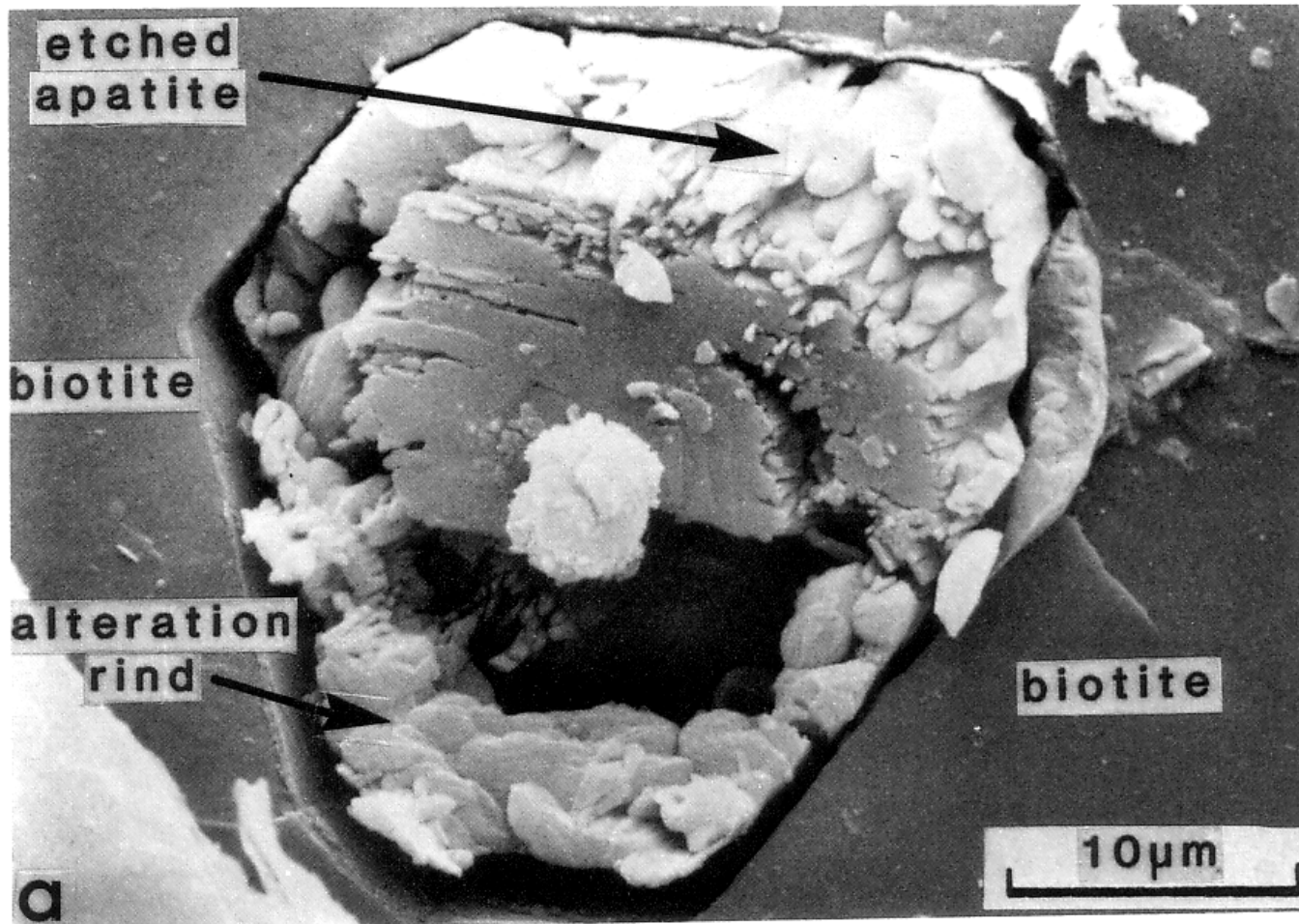


Fig. 4.21. The escape probability of a secondary electron depends on the surface topography.



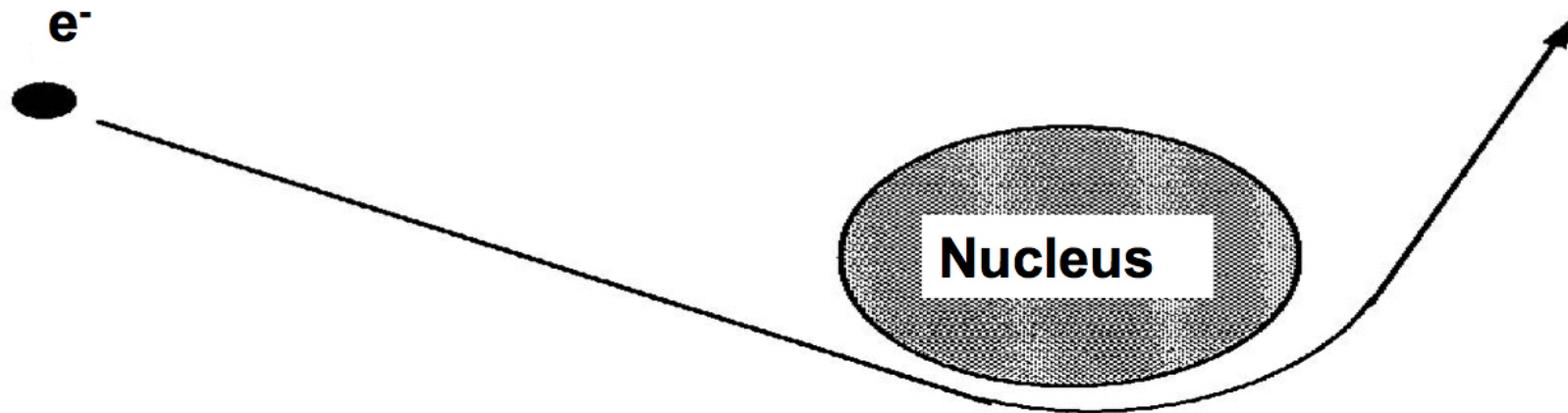
Collection of secondary electrons from a three-dimensional specimen by a detector with a positively biased grid.

SE – strong topographic contrast



Backscattered Electrons

Backscattered electrons (BSE) arise due to elastic collisions between the incoming electron and the nucleus of the target atom (i.e. Rutherford scattering). Higher Z, more BSE emitted.



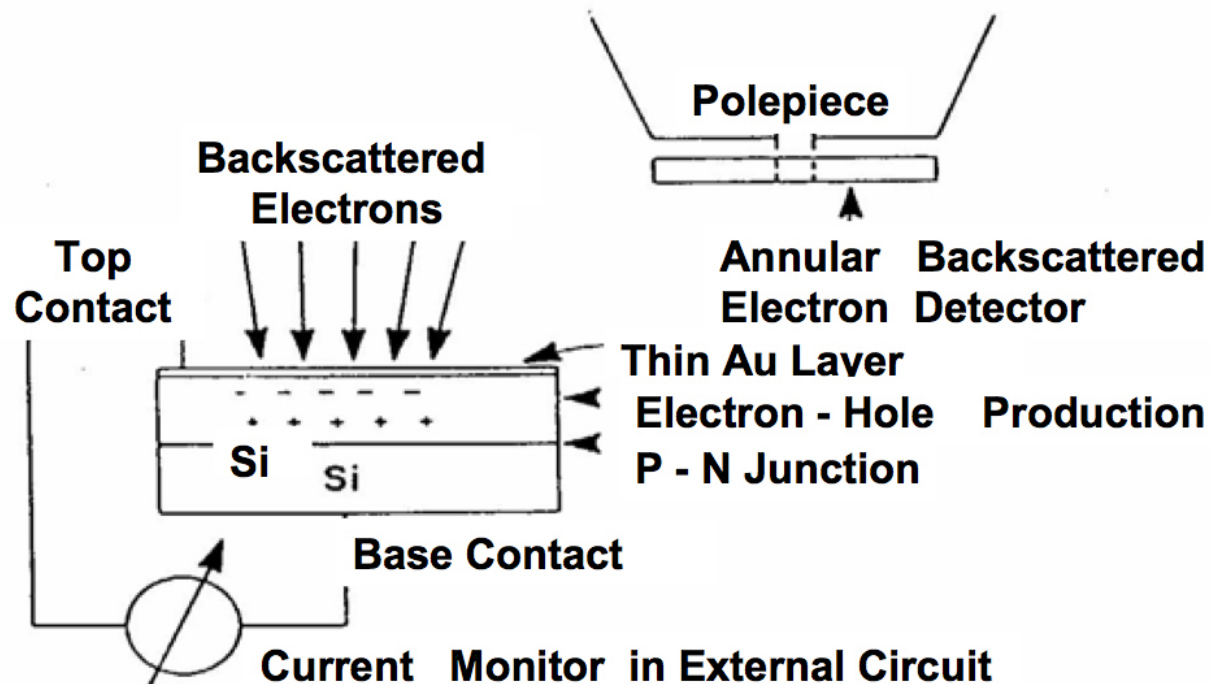
As the name implies, elastic scattering results in little (< 1 eV) or no change in energy of the scattered electrons, although there is a change in momentum (p). Since $p = mv$ and the mass of the electron doesn't change, the direction of the velocity vector must change. The angle of scattering can range from 0 to 180° .

BSE

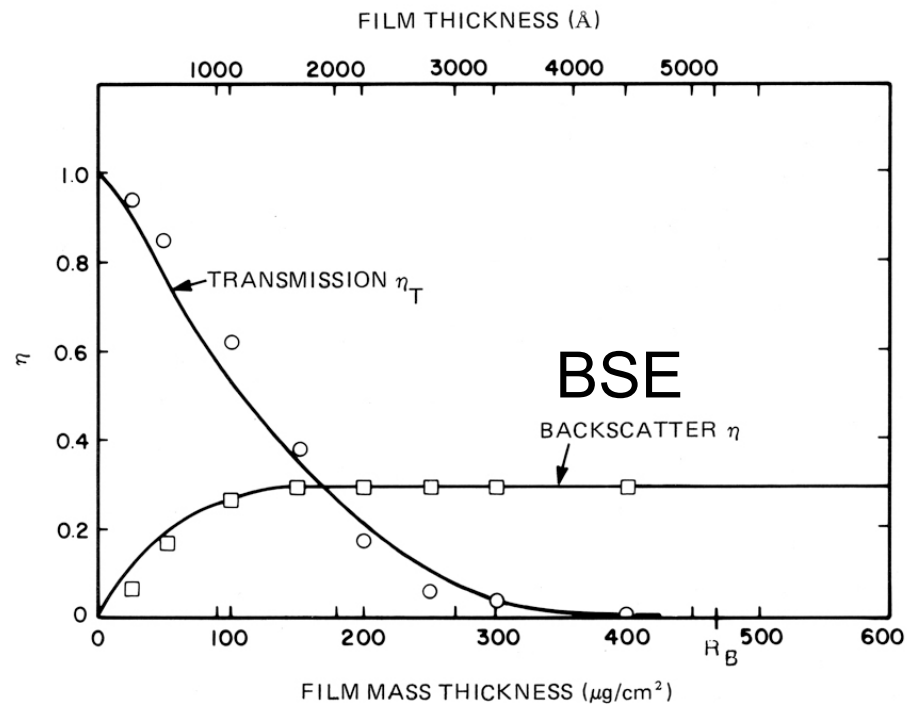
Detection

Since BSE have high energies, they can't be pulled in like secondaries. If you placed a potential on a grid to attract them, you would also attract the incident beam!!

The most common detector used is called a surface barrier detector. It sits above the sample, below the objective lens. BSE which strike it are detected.

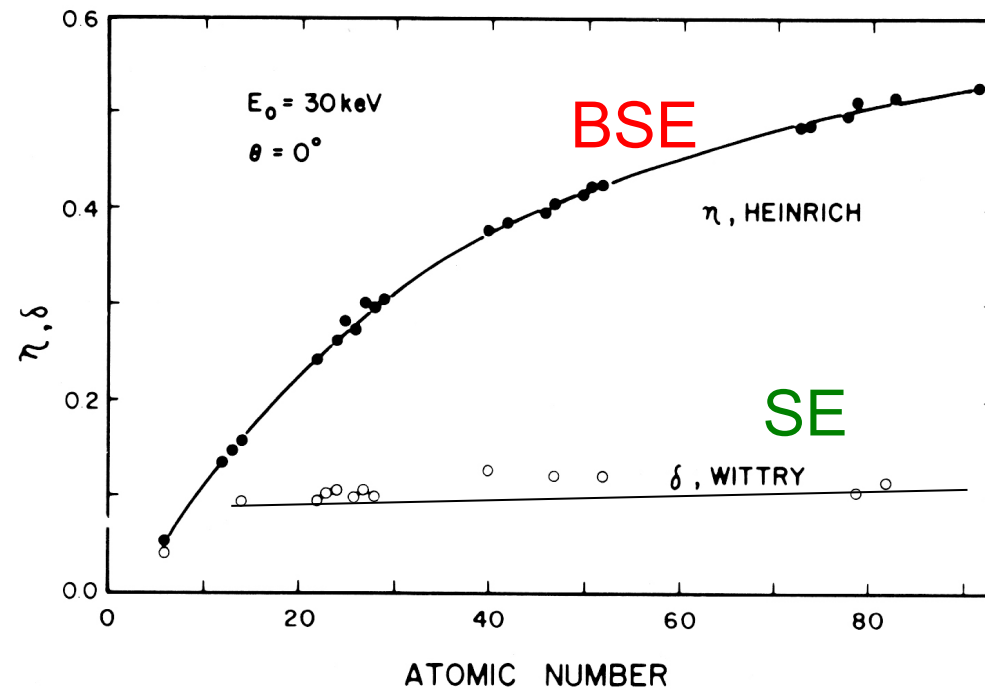


Back-scattered Electrons : BSE 1000 Å (1 μm) depth



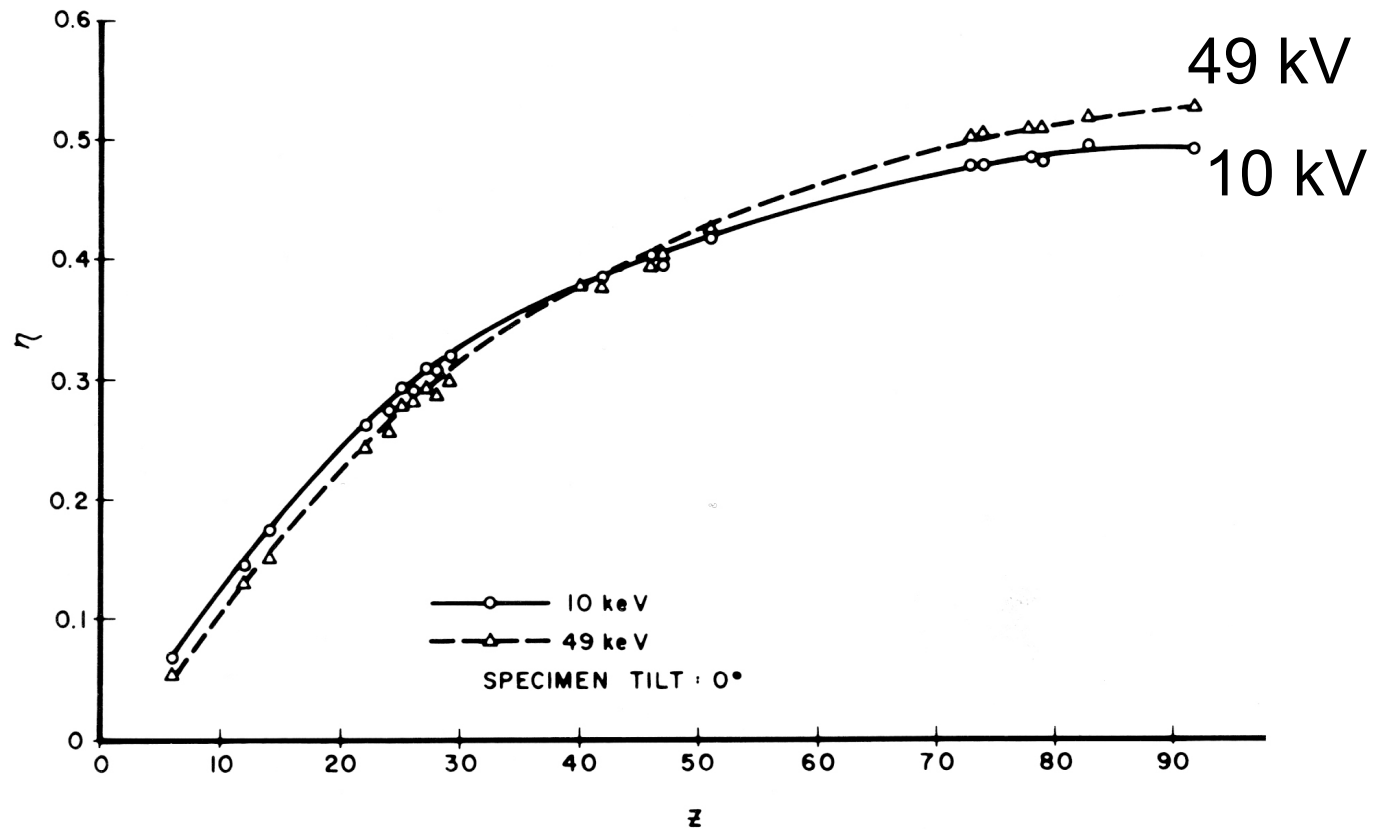
Transmission coefficient η_T and backscatter coefficient η as a function of film thickness for a copper target, $E_0 = 10$ keV. Solid lines represent experimental results (Cosslett, 1966); points represent individual Monte Carlo calculations (Newbury and Yakowitz, 1976).

BSE versus SE: Z atomic number



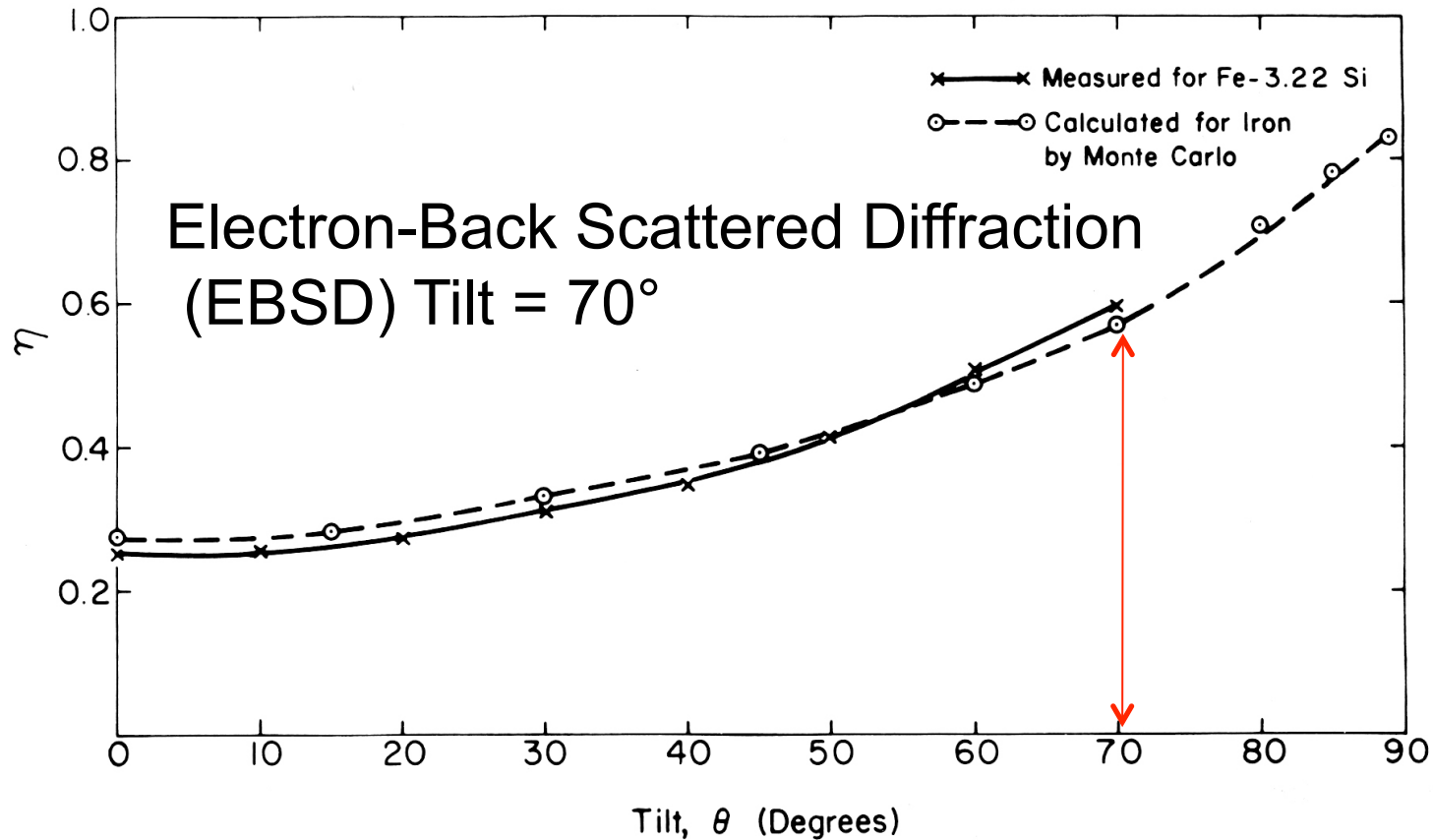
Comparison of backscattered electron coefficients and secondary-electron coefficients as a function of atomic number (Wittry, 1966; Heinrich, 1966).

BSE – effect of kV



Variation of the backscatter coefficient as a function of atomic number at $E_0 = 10$ keV and $E_0 = 49$ keV. Data of Heinrich (1966a).

BSE – effect of Tilt



Backscatter coefficient of iron as a function of tilt. Beam energy 30 keV. Monte Carlo calculations and experimental measurements. Newbury *et al.* (1973).

Mean Z for Minerals

Table 4.2. *Minerals in order of mean atomic number*

Mean Z	Mineral	Mean Z	Mineral
6.0	Graphite	16.4	Brookite
7.7	Borax	16.4	Rutile
9.4	Magnesite	16.5	Perovskite
10.0	Zoisite	16.5	Siderite
10.0	Spodumene	16.9	Ferrosilite
10.2	Clinochlore	17.2	Tephroite
10.3	Serpentine	18.6	Malachite
10.4	Humite	18.7	Fayalite
10.4	Kaolinite	19.0	Ilmenite
10.4	Periclase	19.9	Chromite
10.5	Analcite	20.0	Ulvospinel
10.6	Forsterite	20.6	Haematite
10.6	Glaucophanes	20.7	Pyrite
10.6	Spinel	21.0	Magnetite
10.6	Topaz	22.2	Pyrrhotite
10.7	Albite	22.9	Pentlandite
10.7	Andalusite	23.5	Chalcopyrite
10.7	Corundum	23.7	Celestine
10.7	Enstatite	24.2	Apophyllite
10.7	Jadeite	24.2	Xenotime
10.7	Kyanite	24.6	Columbite
10.7	Pyrope	24.6	Willemite
10.7	Sillimanite	24.8	Zircon
10.8	Quartz	25.3	Bornite
11.1	Lepidolite	25.4	Sphalerite
11.1	Mullite	25.6	Strontianite
11.1	Muscovite	26.4	Chalcocite
11.1	Sodalite	26.7	Cuprite
11.9	Anorthite	26.8	Benitoite
11.9	Orthoclase	27.2	Celsian
12.1	Leucite	27.3	Arsenopyrite
12.4	Aragonite	27.6	Cobaltite
12.4	Calcite	29.0	Copper
12.4	Gypsum	31.7	Baddeleyite
12.9	Grossular	32.5	Tetrahedrite
13.4	Anhydrite	37.3	Barite
		13.6	Wollastonite
		13.8	Montecellite
		14.1	Apatite
		14.2	Arfvedsonite
		14.7	Fluorite
		14.7	Titanite
		15.0	Riebeckite
		15.2	Spessartine
		15.3	Hercynite
		15.3	Uvarovite
		15.6	Almandine
		15.8	Andradite
		15.9	Rhodochrosite
		38.7	Monazite
		41.1	Cassiterite
		41.1	Stibnite
		41.3	Witherite
		43.0	Argentite
		59.4	Anglesite
		65.3	Cerussite
		65.4	Tantalite
		70.5	Bismuthinite
		73.2	Galena
		78.0	Platinum
		79.0	Gold
		82.0	Uraninite

Argile - électrons rétrodiffusés - contraste Z

(3)
Brightest
is Pyrite,
 FeS_2

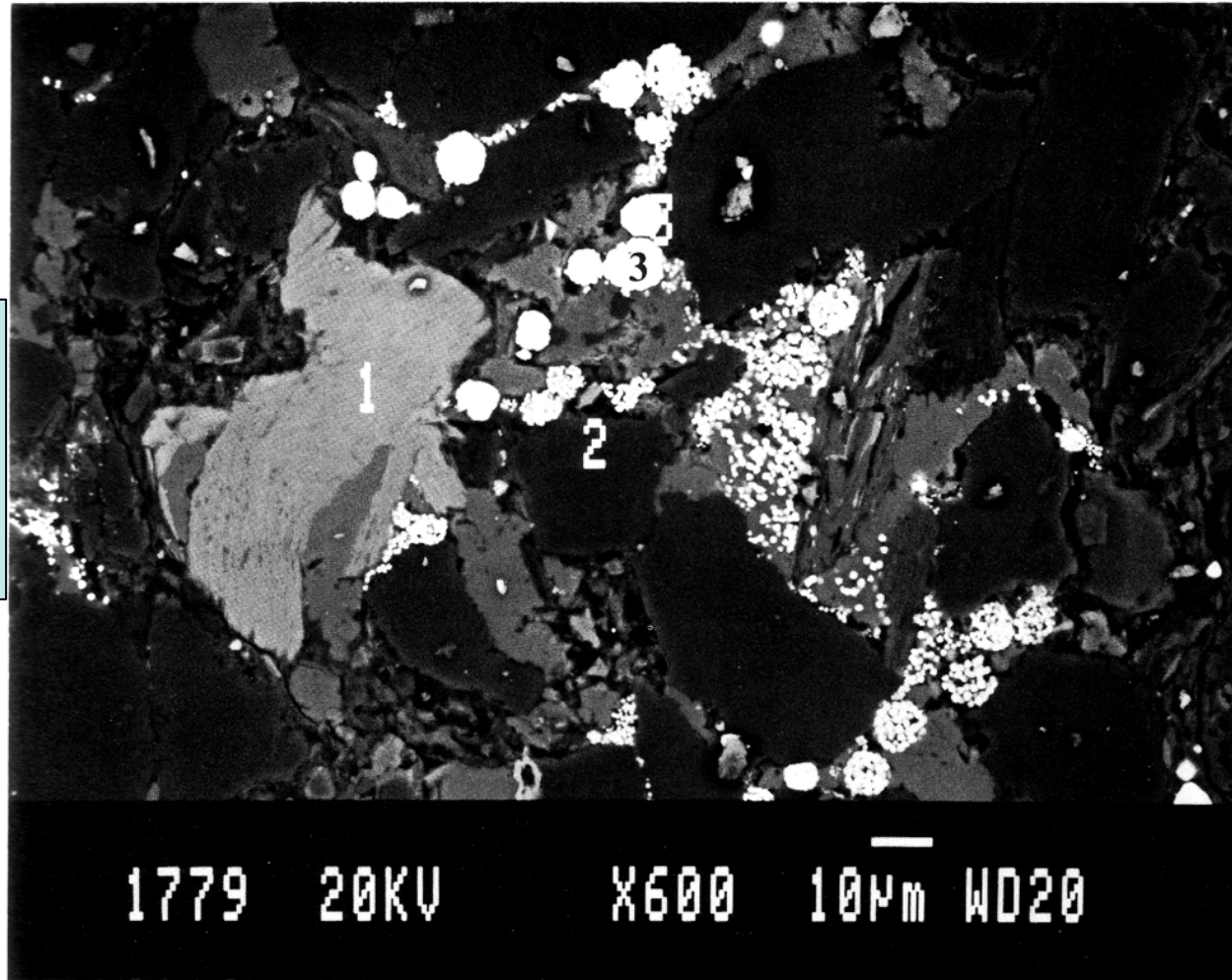
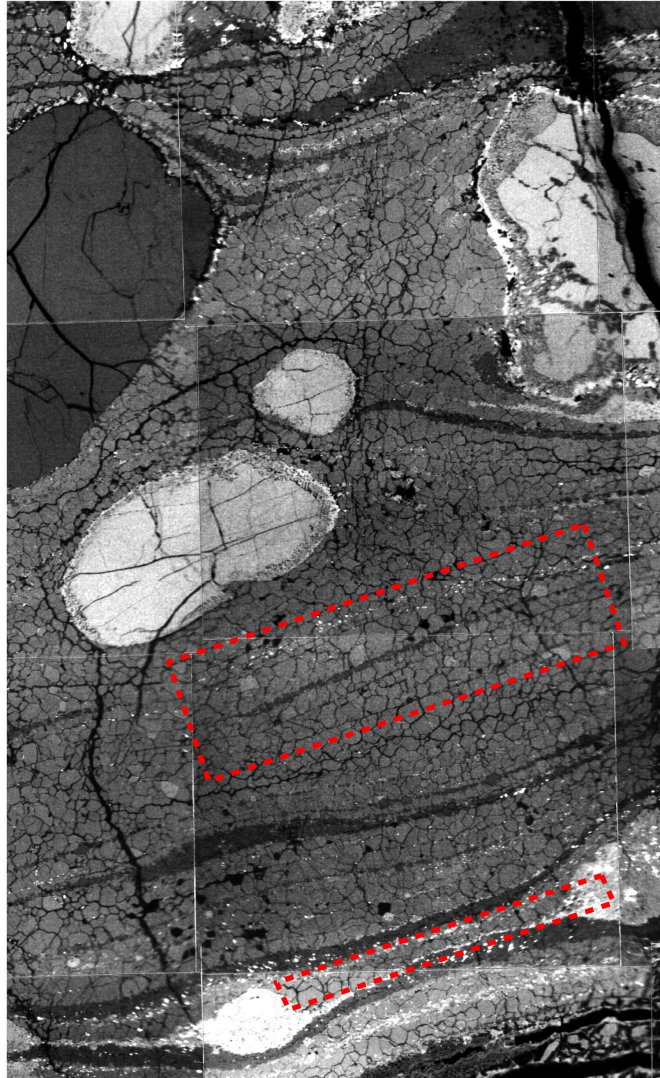


Figure 3.49. An SEM image formed from the backscattered electrons whose intensity depends on the average atomic number of the specimen being bombarded. The specimen shown here is a polished rock slice of shale. The brightest grains are pyrite, FeS_2 , the grey grains are ferromagnesian silicates such as mica and pyroxene, and the darkest contrast grains are quartz SiO_2 . The numbered labels refer to crystals whose X-ray spectra are shown in Figure 3.50.

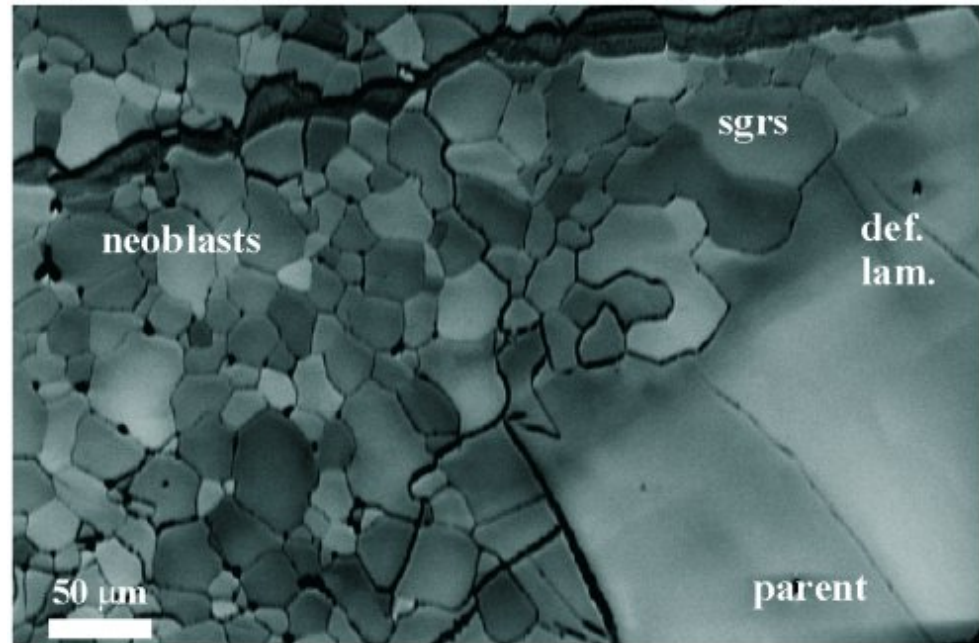
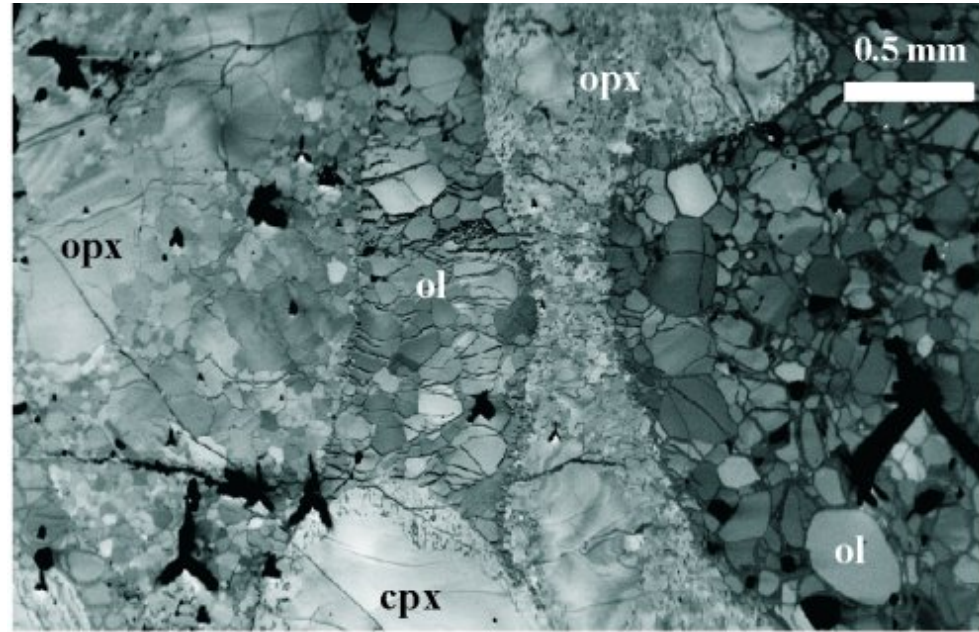
PHN 1611 - 220 km 1600°C



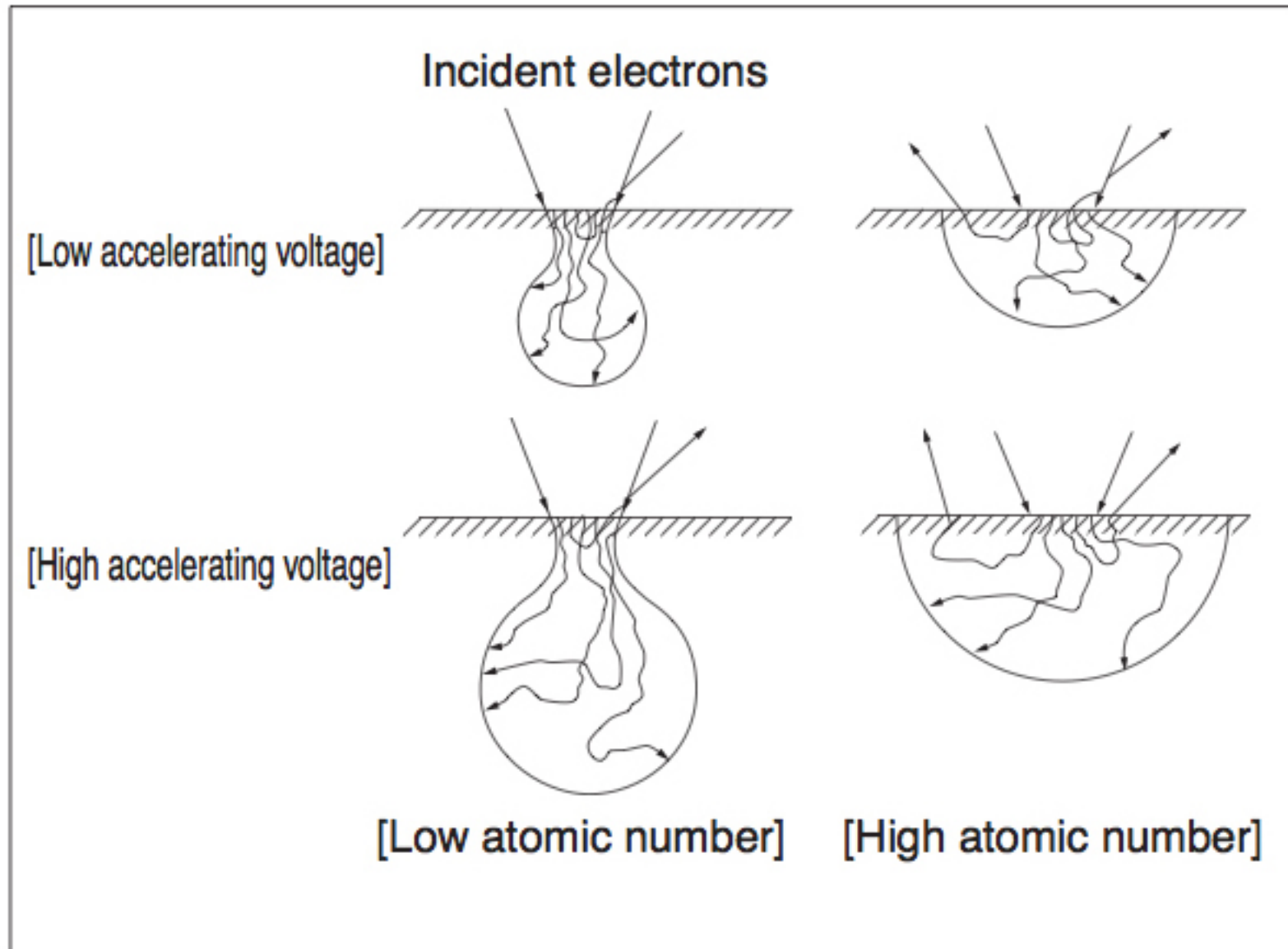
100 μm

Kimberlite nodules
From South Africa

Geoff Lloyd (Leeds,UK)

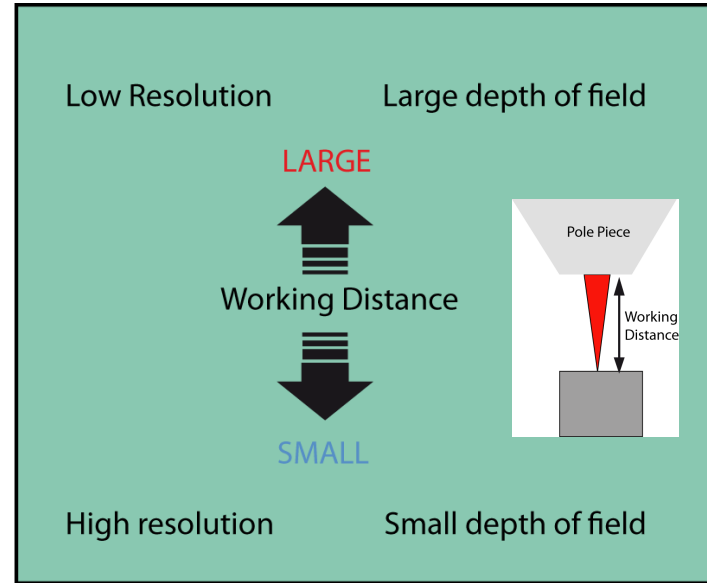
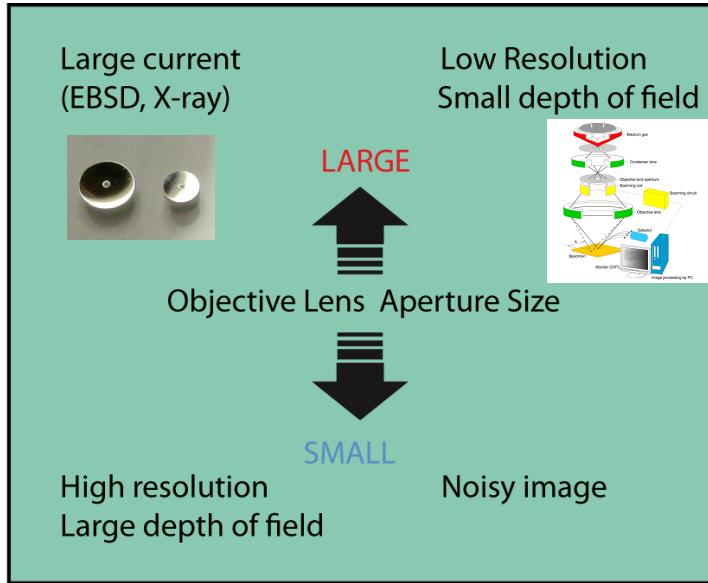


Accelerating Voltage (kV) : depth

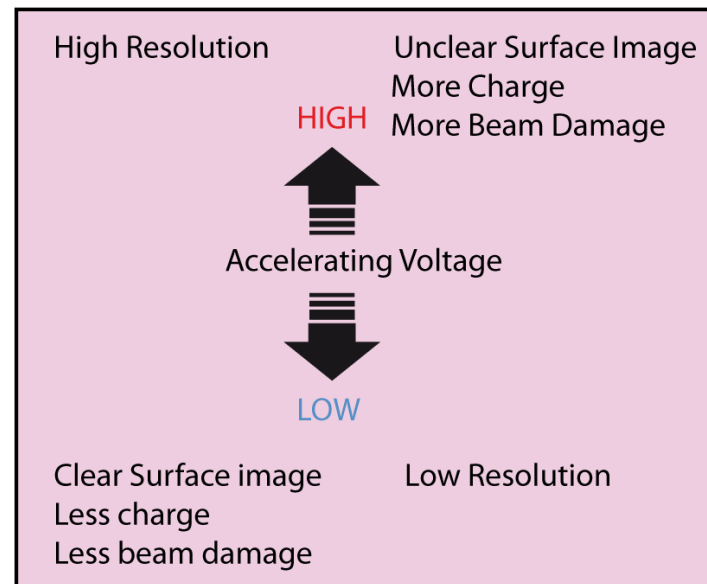
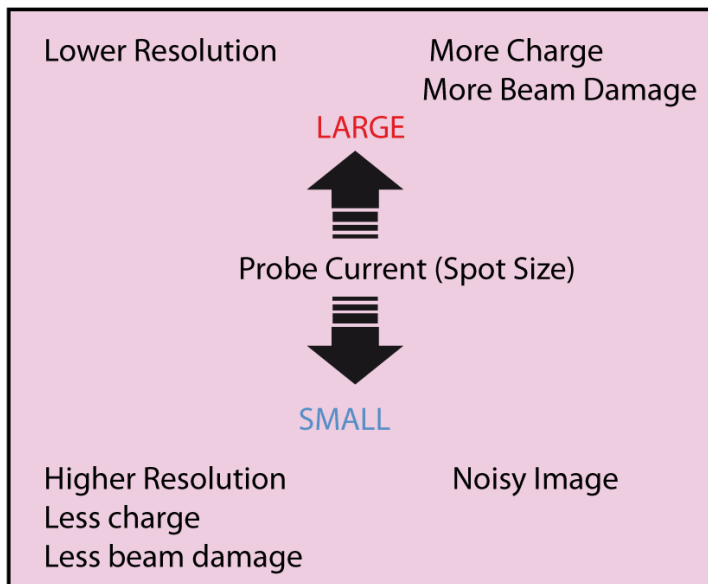


Four Key Parameters for SEM

Mechanical



Electronic



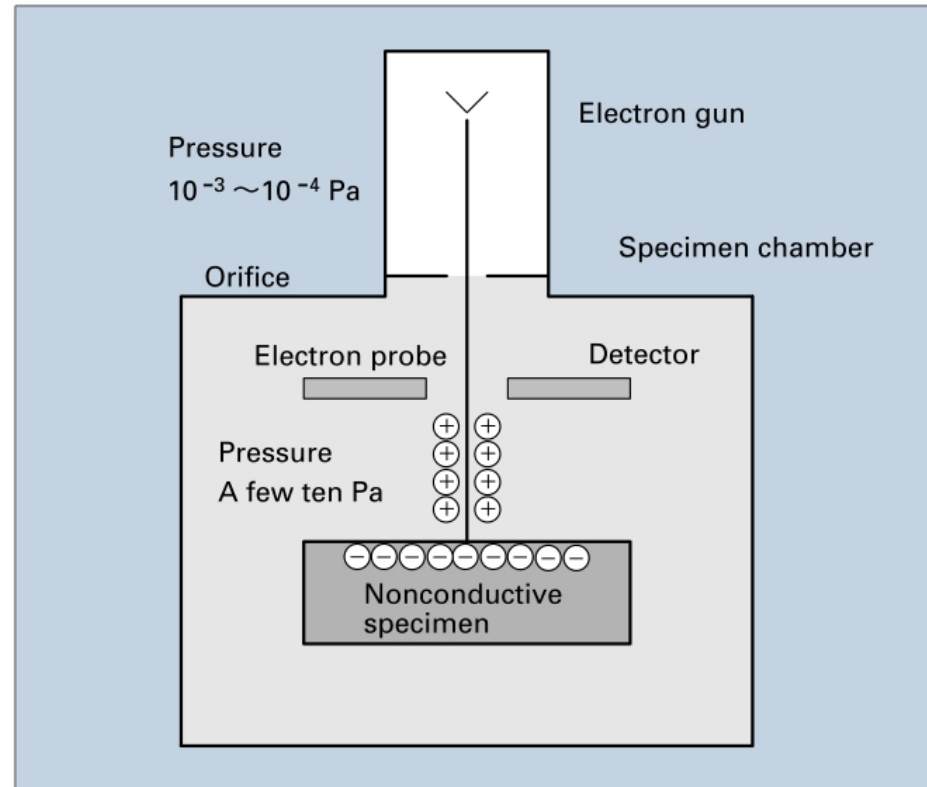
Unités de pression

Conversions entre les principales unités de pression

	Pa	bar	mbar	torr	mmHg	atm
Pa	1	10^{-5}	10^{-2}	$7,5 \cdot 10^{-3}$	$7,5 \cdot 10^{-3}$	$9,869 \cdot 10^{-6}$
bar	10^5	1	10^3	750	750	0,9869
mbar	10^2	10^{-3}	1	0,75	0,75	$9,869 \cdot 10^{-4}$
torr	133,3224	$1,333 \cdot 10^{-3}$	1,33322	1	1	$1,3158 \cdot 10^{-3}$
mmHg	133,3	$1,333 \cdot 10^{-3}$	1,33322	1	1	$1,3158 \cdot 10^{-3}$
atm	$1,013 \cdot 10^5$	1,013	1013	760	760	1

Pour résumer, rappelons-nous que le millibar vaut un hectoPa, qu'une atmosphère correspond à 1013 millibars ou à 760 mmHg, et qu'un torr est équivalent à un mmHg.

Pressure variable (PV), low vacuum (LV) or Environmental SEM



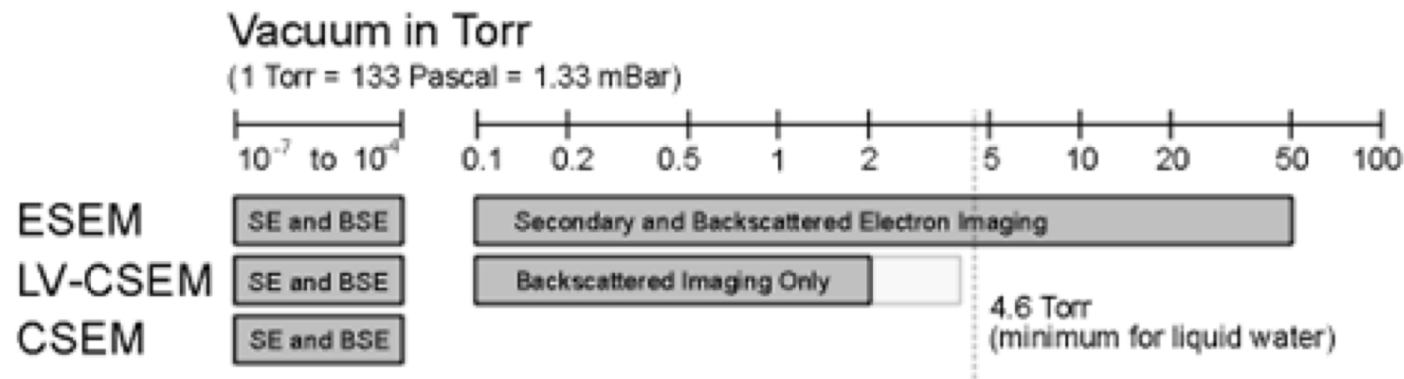
Schematic diagram illustrating the principle of the LVSEM for observation of nonconductive specimens.

- Decreasing the vacuum to from 10^{-4} to 15 Pa increases the number of residual gas molecules in the chamber.
- The electron beam ionizes residual gas molecules in vacuum to create a number of positive (+ve) ions.
- The positive ions neutralizes the excess electron negative (-ve) charge on the specimen surface.

Environmental Scanning Electron Microscope

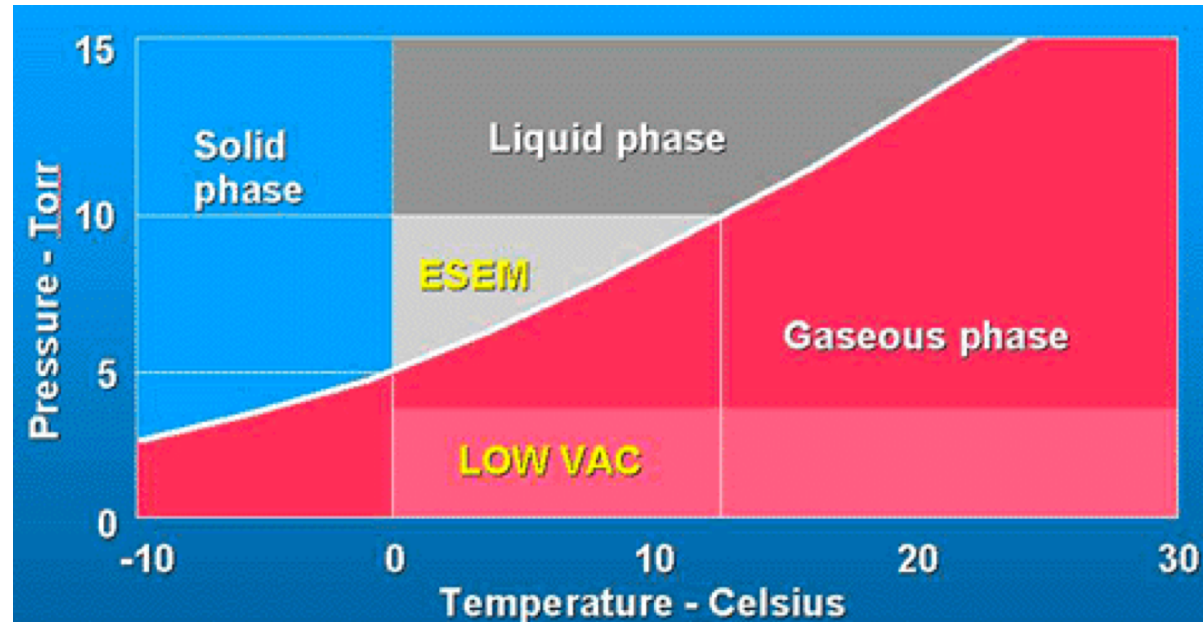
Le microscope environnement est un microscope présentant l'avantage de pouvoir travailler en trois modes qui sont :

- Le mode balayage classique (CSEM) sous vide secondaire (10^{-7} à 10^{-4} Torr) pour des échantillons conducteurs et non déshydratés.
- Le mode Low Vacuum (LV-CMEM), la chambre est en vide partiel de 0.1 à 2 Torr pour des échantillons non métallisés.
- Le mode environnemental (E-SEM), sous vide partiel de 0.1 à 50 Torr en présence d'un gaz tel que la vapeur d'eau, qui permet d'étudier des échantillons fragiles, hydratés et non métallisés.



CrystalProbe = LV-CSEM <http://www.gm.univ-montp2.fr/PERSO/mainprice/CrystalProbe.html>

Phase Diagram for water at SEM pressures and temperatures

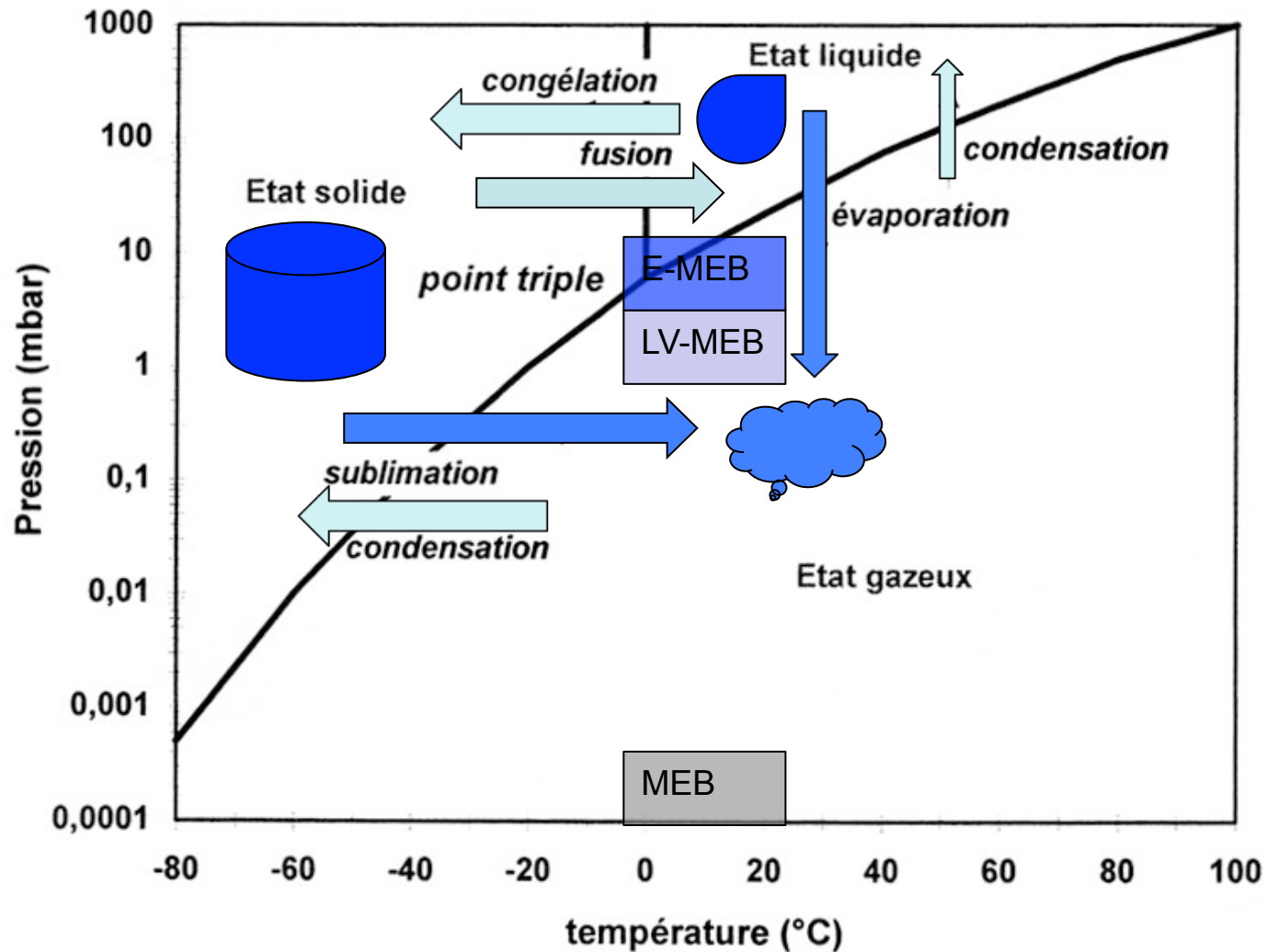


Hydrocarbon
particule in diesel

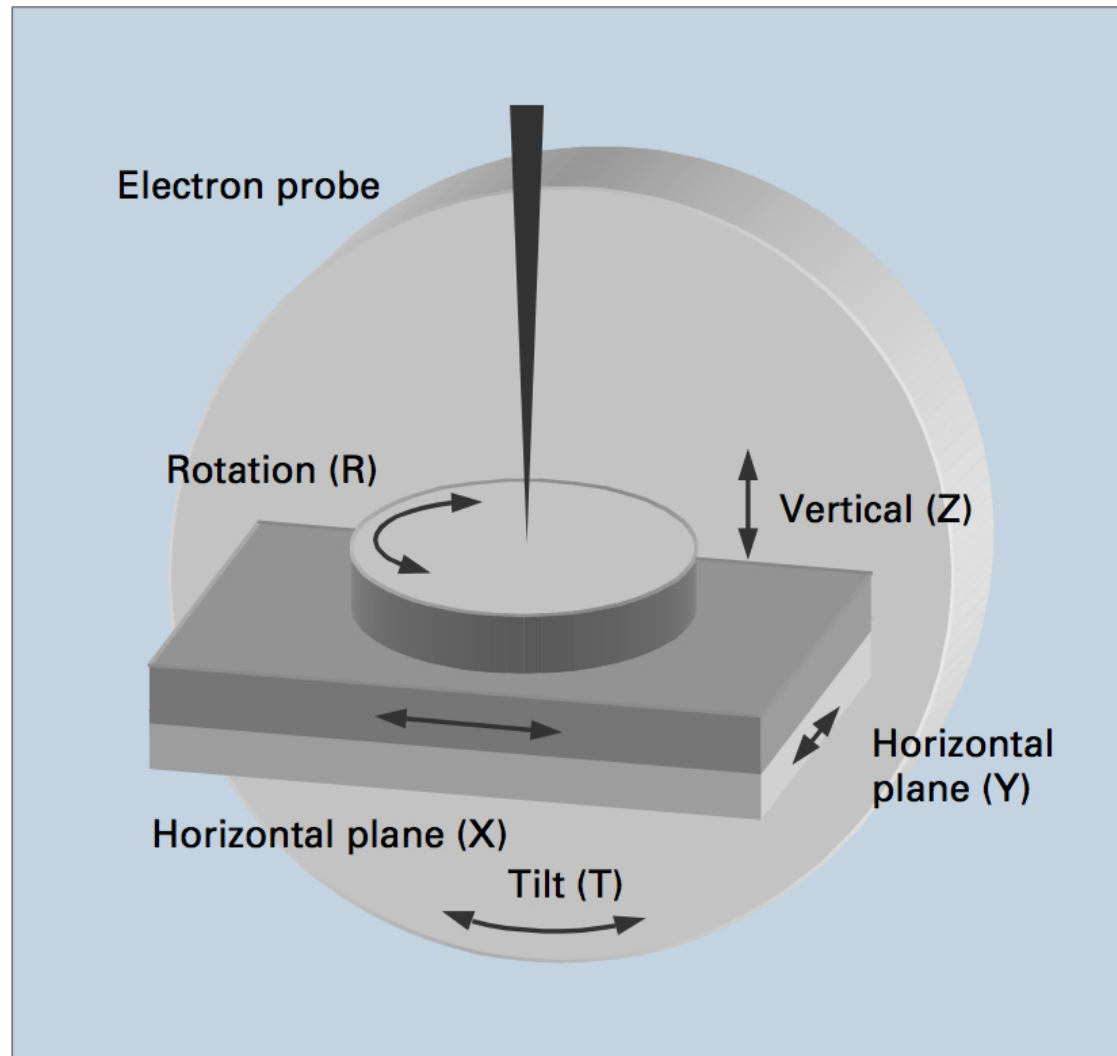


Diagramme d'équilibre Pression Température de l'eau

Courbe de tension de vapeur de l'eau

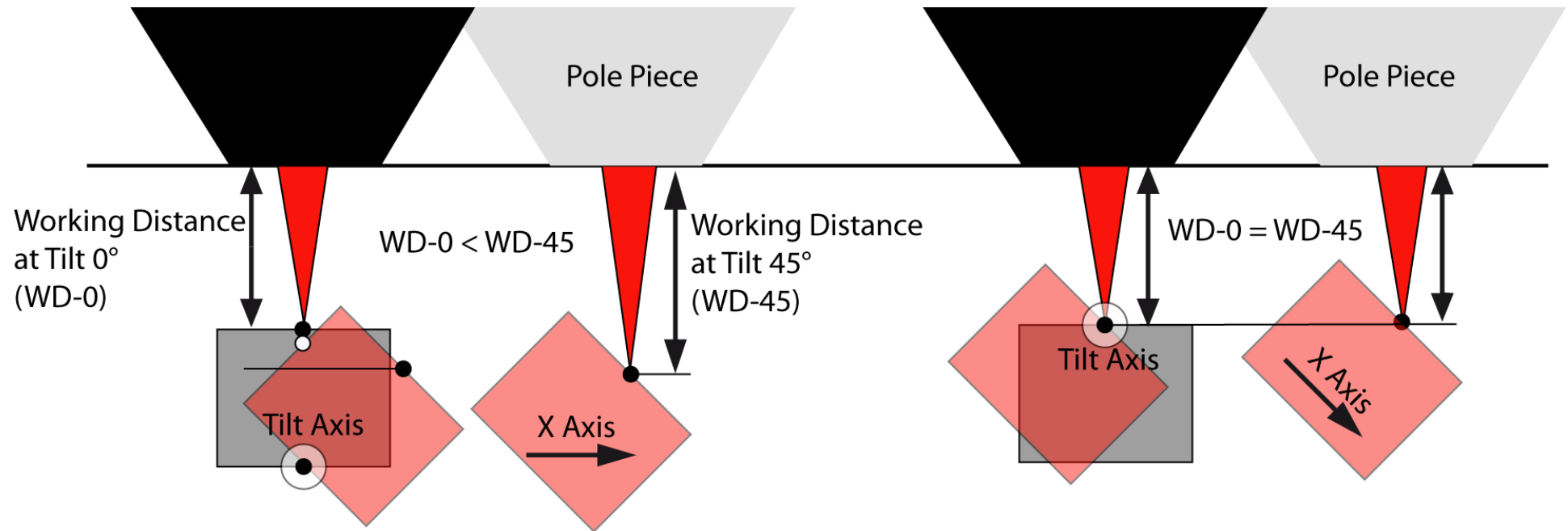


Elements of SEM : specimen stage



Construction of the specimen stage.

Tilting Stage



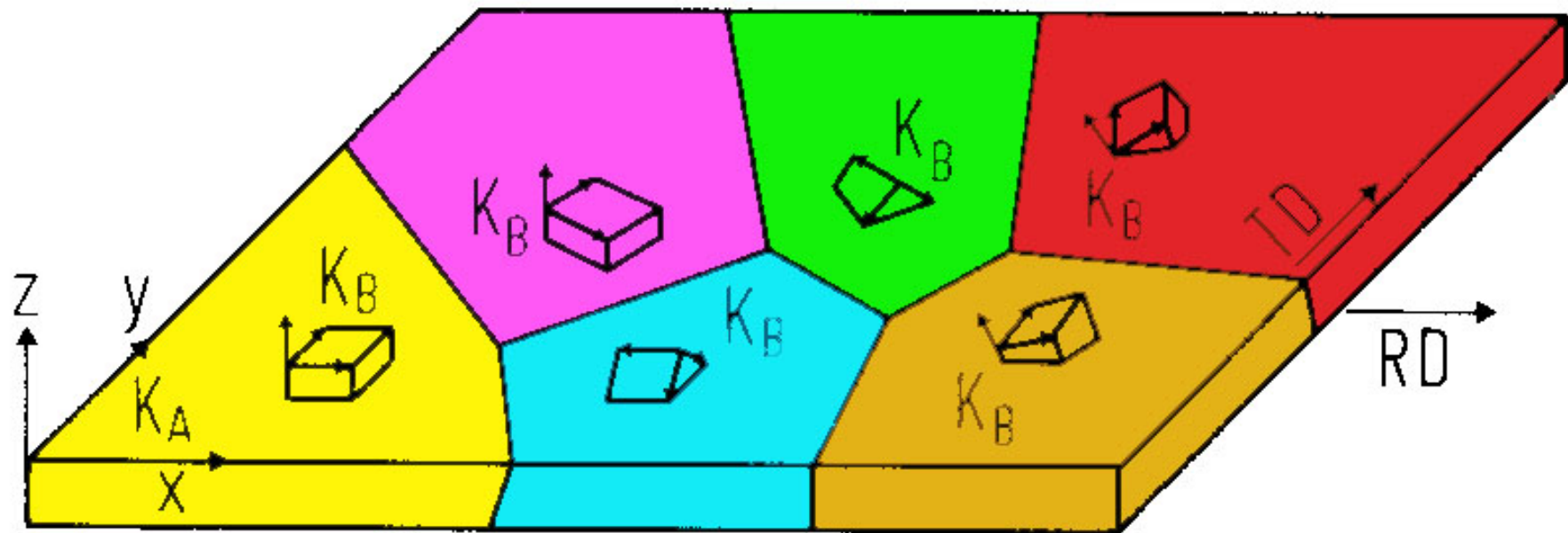
Non-Eucentric Stage

- Beam position on specimen is changed when stage is tilted (black to white dot)
- The focus position (WD) is changed for a for tilted specimen when moved in the X-direction

Eucentric Stage

- Beam position on specimen is NOT changed when stage is tilted
- The focus position (WD) is NOT changed for a for tilted specimen when moved in the X-direction

EBSD = Electron Back Scattered Diffraction

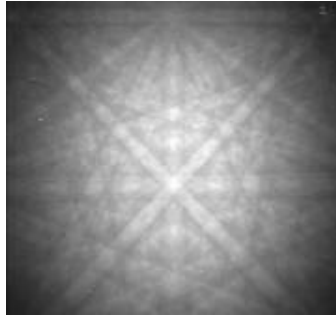


Why should we be interested in EBSD ?

- Can work with tradition petrographic thin sections (combine with studies using probes...)
- Measure the orientation of transparent and opaque minerals of any symmetry
- Measure orientations of rocks with complex mineralogies (real rocks !)
- Measure orientations and misorientation of crystals (e.g.twins, subgrains..) in the microstructure at submicron to cm scale

Table: Spatial and angular resolution of orientation measurements

Diffraction Pattern	Microscope	Spatial	Angular	Specimens
Spot	TEM	0.5 μm	1°	thin films
Kikuchi	TEM	0.5 μm	0.1°	thick films
Kikuchi	STEM	10 nm	0.2°	thick films
ECP	SEM	1-10 μm	0.1°	bulk samples
EBSD	SEM	1-2 μm	1°	bulk samples
EBSD	FEG-SEM	100 nm	1°	bulk samples

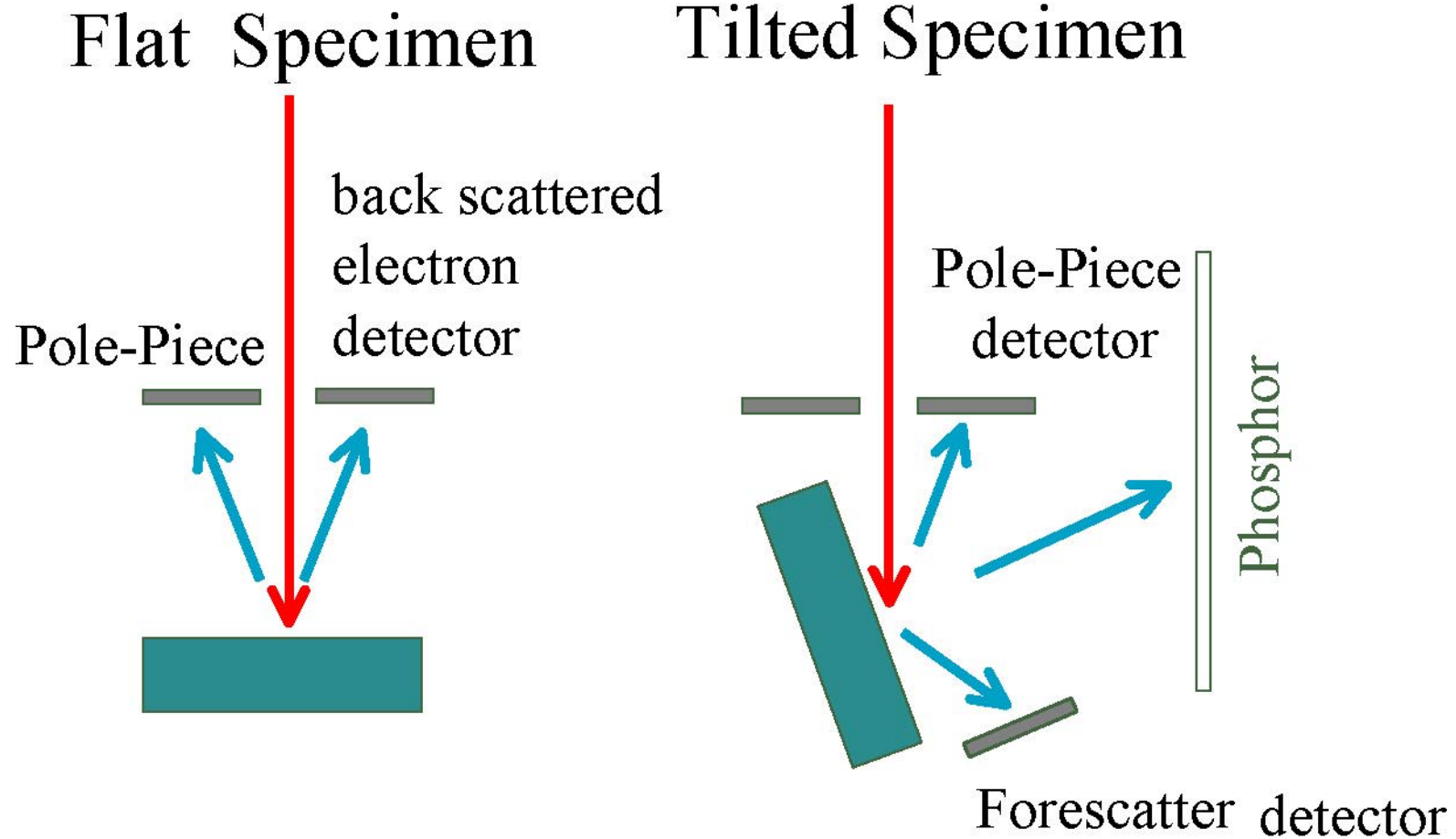


A little history

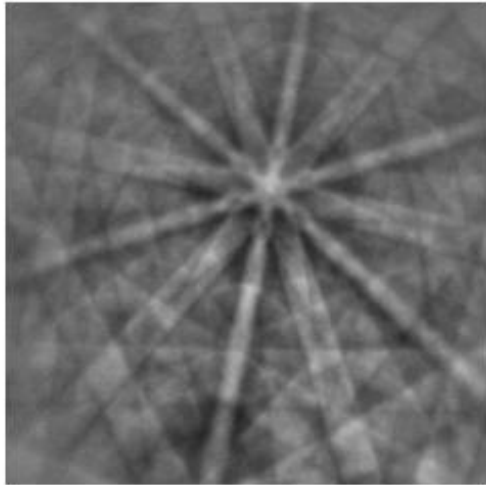


- First electron backscattered diffraction by Kikuchi in 1928 on a thin mica crystal.
- Later in 1954 Alum et al. published patterns of lead sulfide.
- First SEM based work by Coates in 1967.
- First SEM/EBSD by Venables in 1972.
- First EBSD on polycrystalline materials by Dingley in 1981.
- 1985 first computer controlled system... 21 years ago

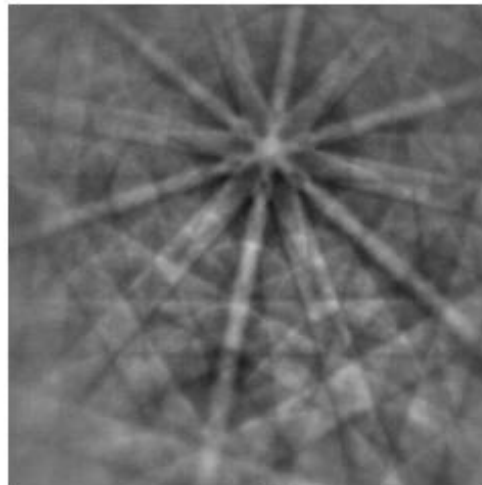
Flat & Tilted Specimens



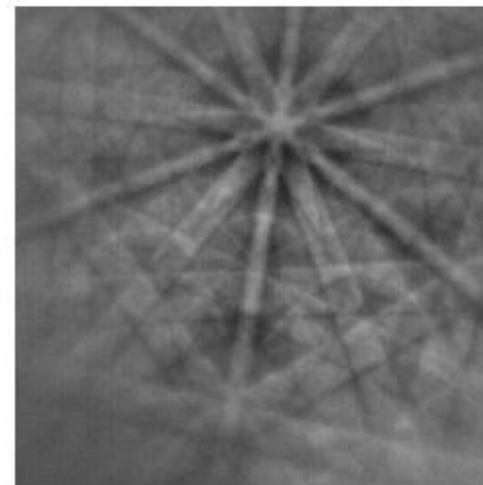
Effect of tilt angle on EBSD patterns



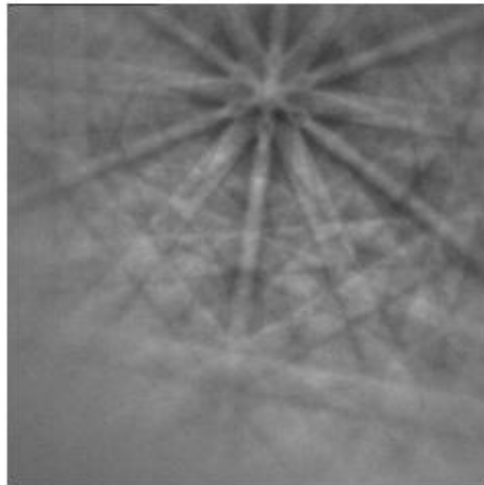
75°



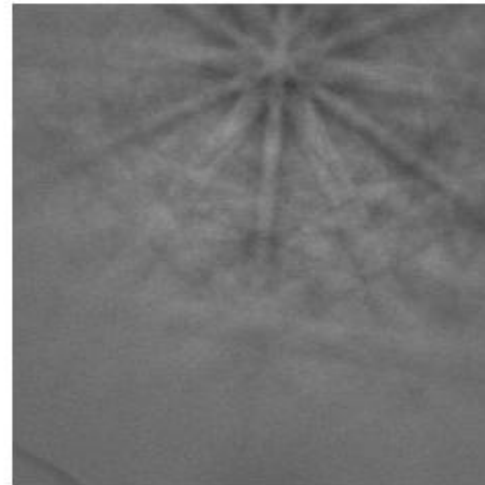
70°



65°

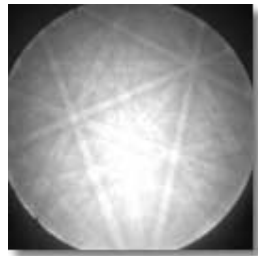
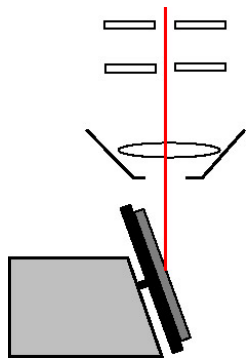


60°

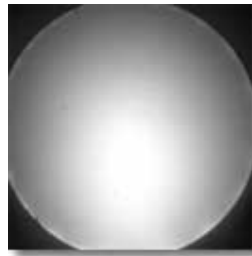
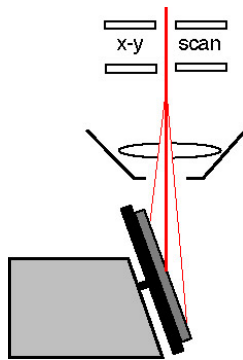


55°

Background correction



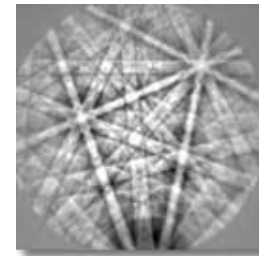
Raw pattern
recorded
in spot mode



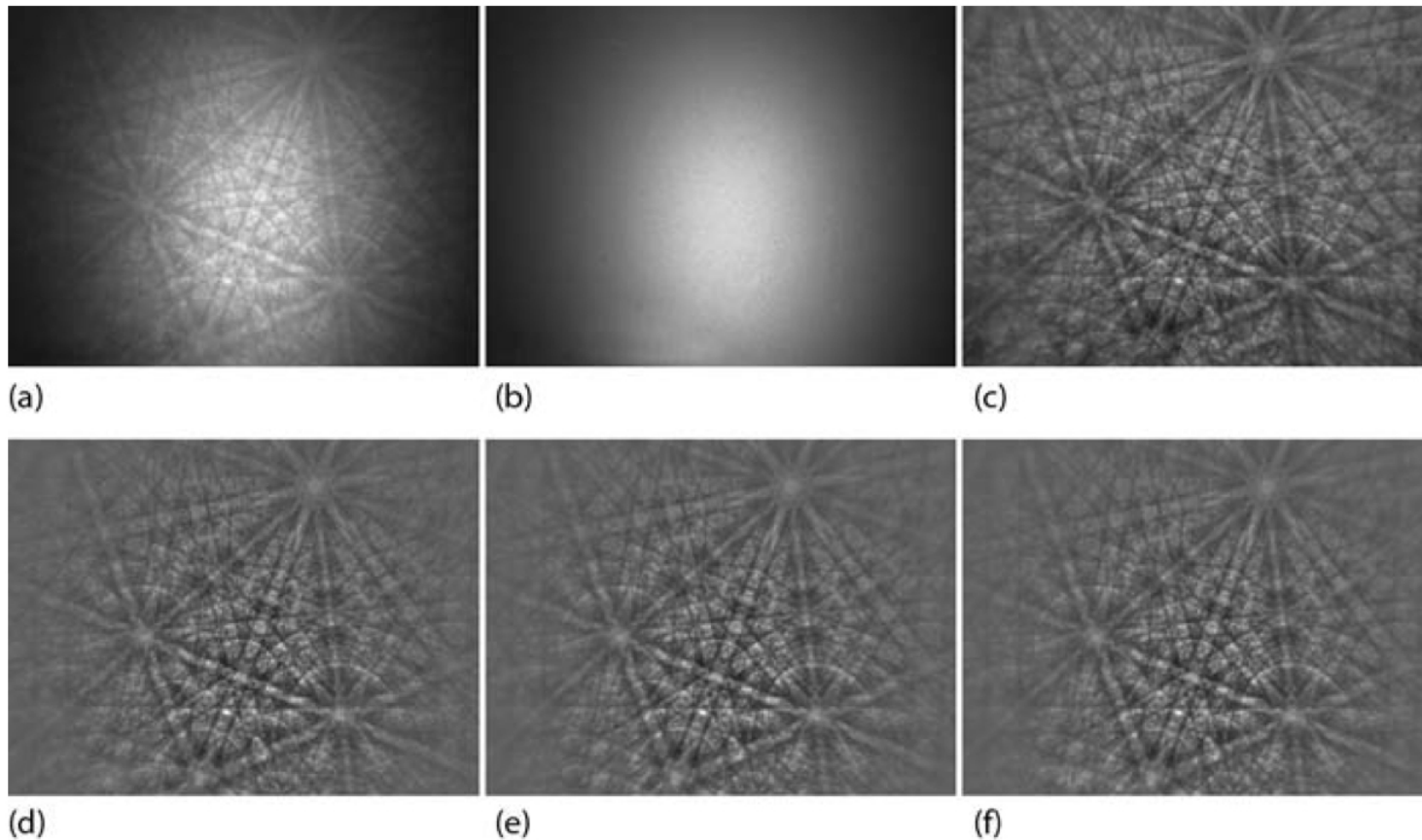
Background pattern
recorded
in scanning mode

-

=

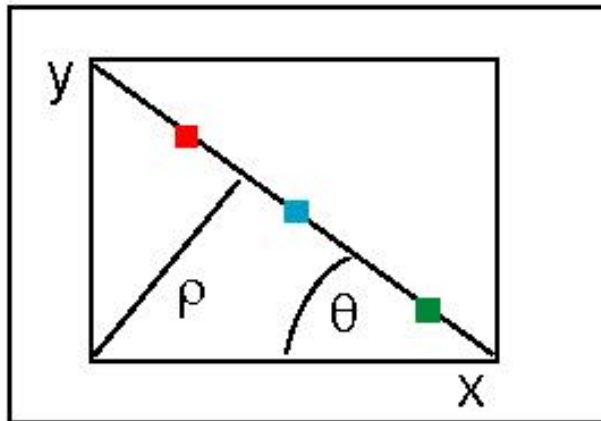


Background corrected
pattern



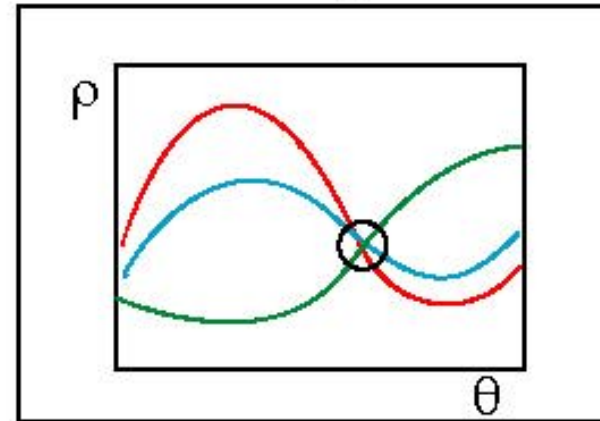
Example of EBSD image processing. (a) A raw EBSD pattern from tungsten carbide. (b) The EBSD pattern background signal. (c) The corrected EBSD pattern produced by dividing the raw pattern by the background and then adjusting the brightness and contrast of the resulting image to fit the available gray-level range. (d) Pattern after single frame averaging. (e) Pattern after frame averaging over three frames. (f) Pattern after frame averaging over 20 frames. (Courtesy of K. Mingard and A. Day.)

Image



A straight line is defined by the ρ and θ

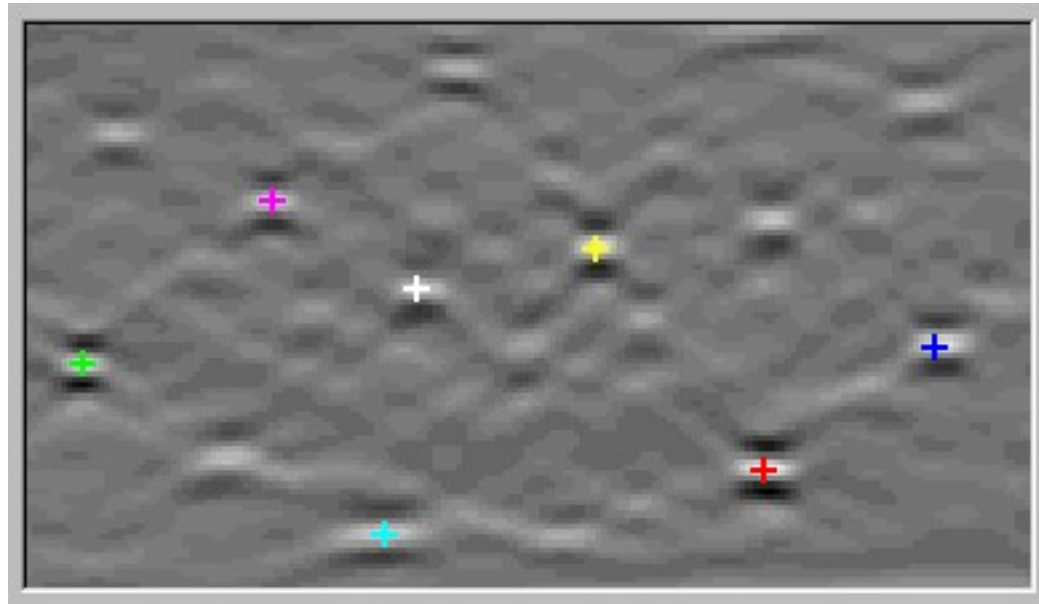
Hough

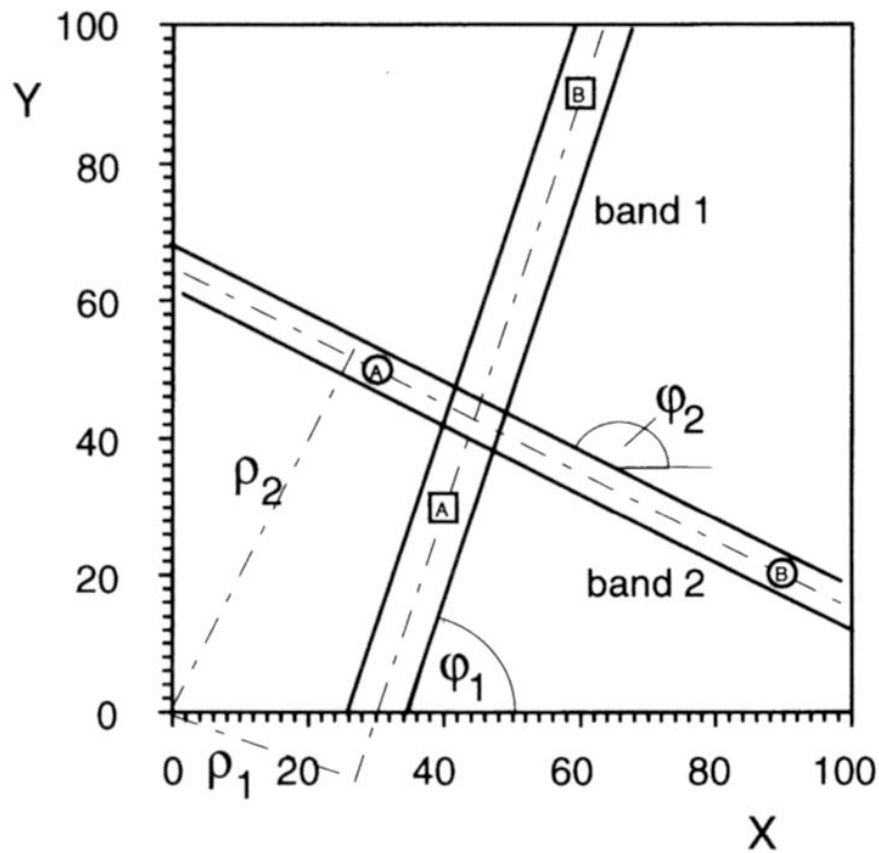


In Hough space a straight line corresponds to a point

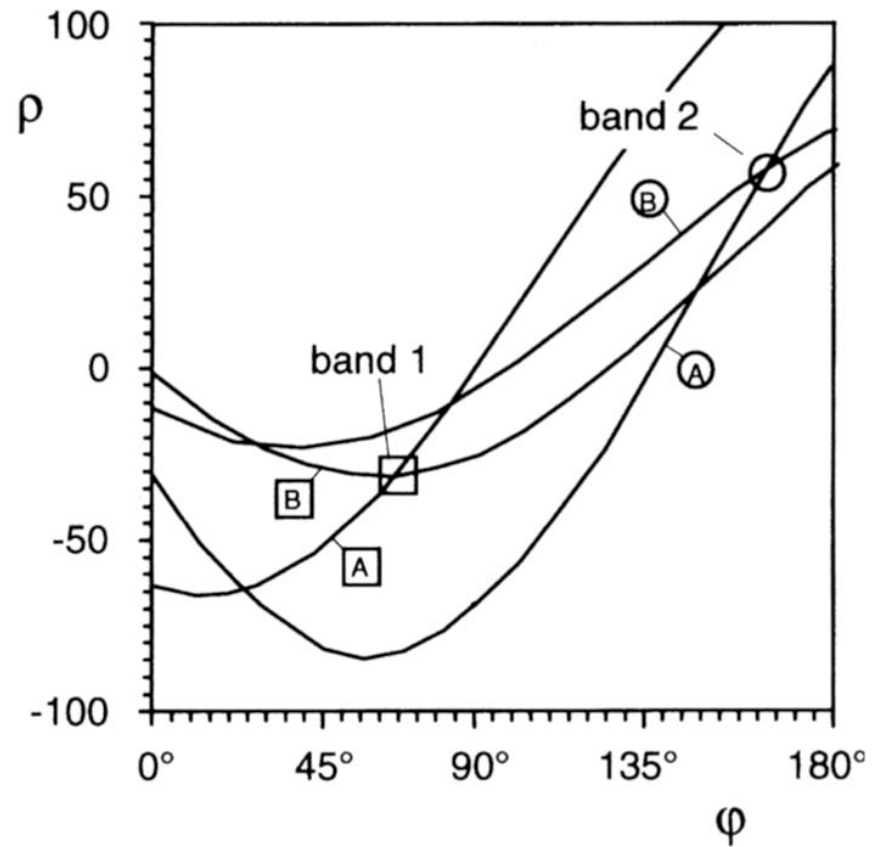
$$x \cos \theta + y \sin \theta = \rho$$

Hough Space





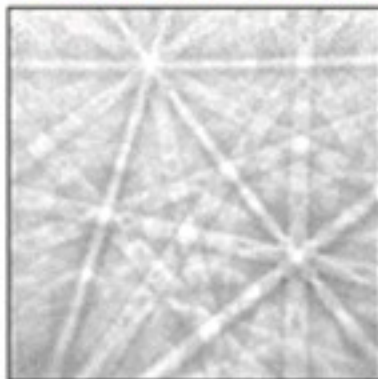
(a) original image



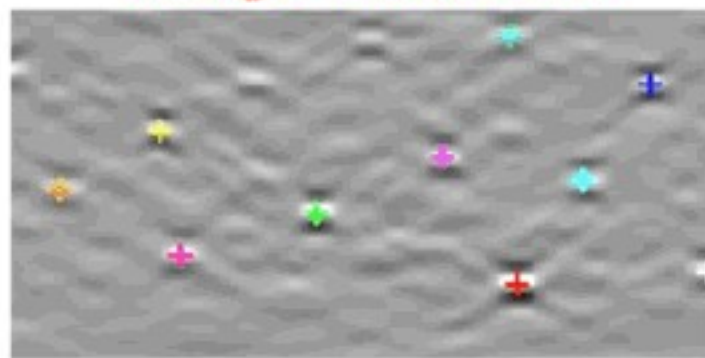
(b) Hough-space

Figure 6.8 Schematic representation of the Hough transform. (a) Two bands in the original image; (b) bands-from (a) in the Hough space.

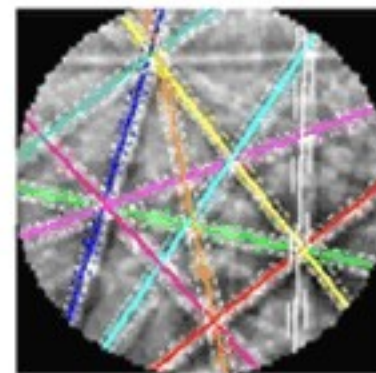
Diffraction Pattern



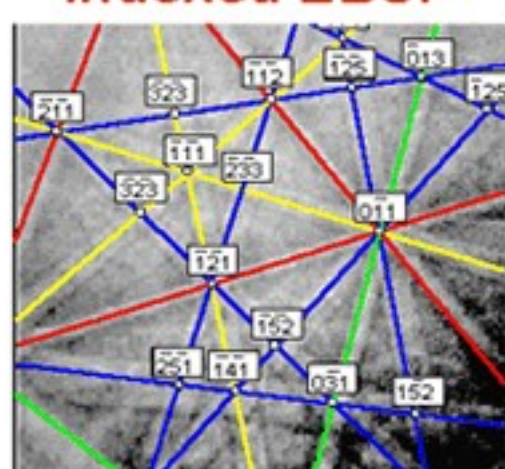
Hough Transform



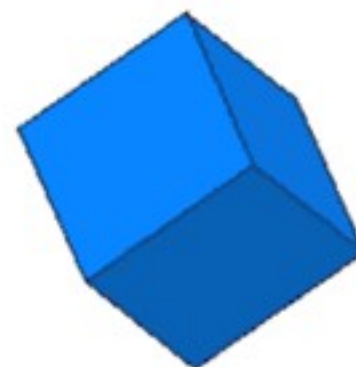
Detected Bands

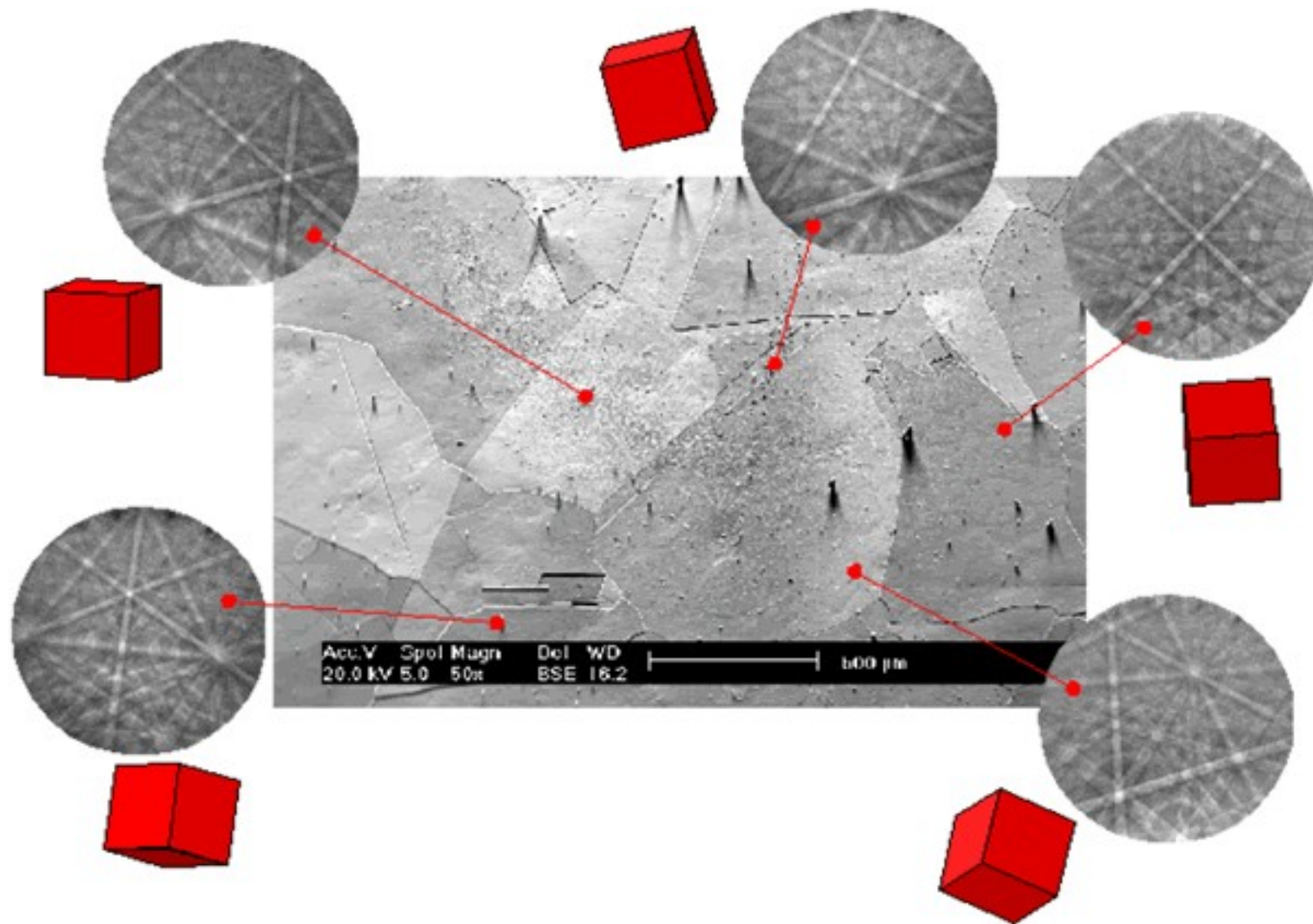


Indexed EBSP

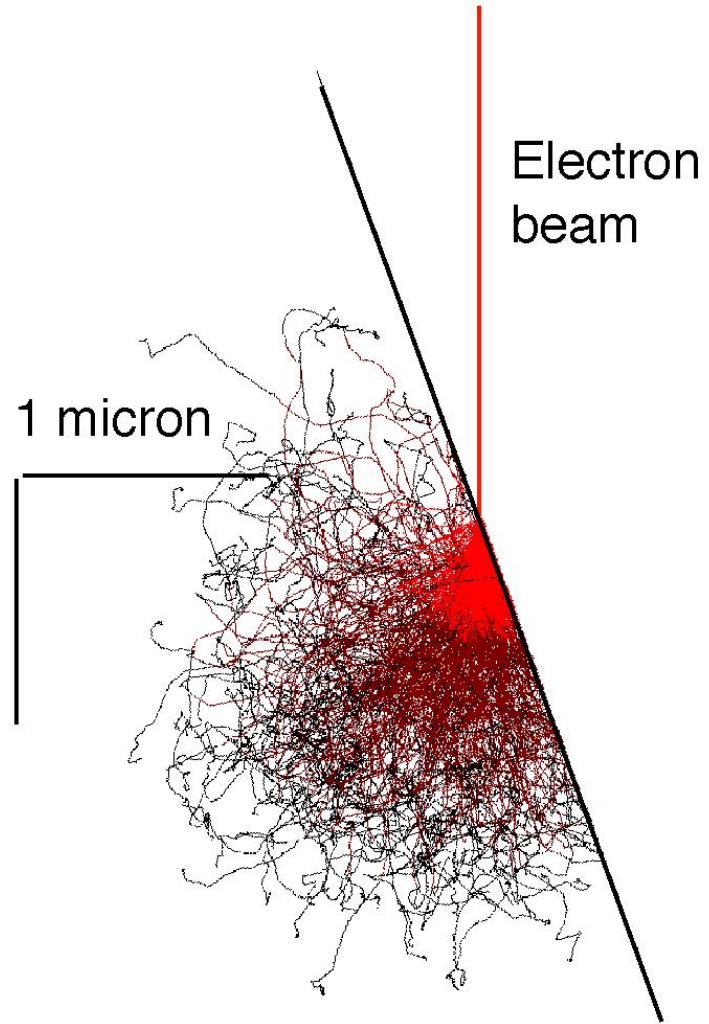


Crystallographic Orientation



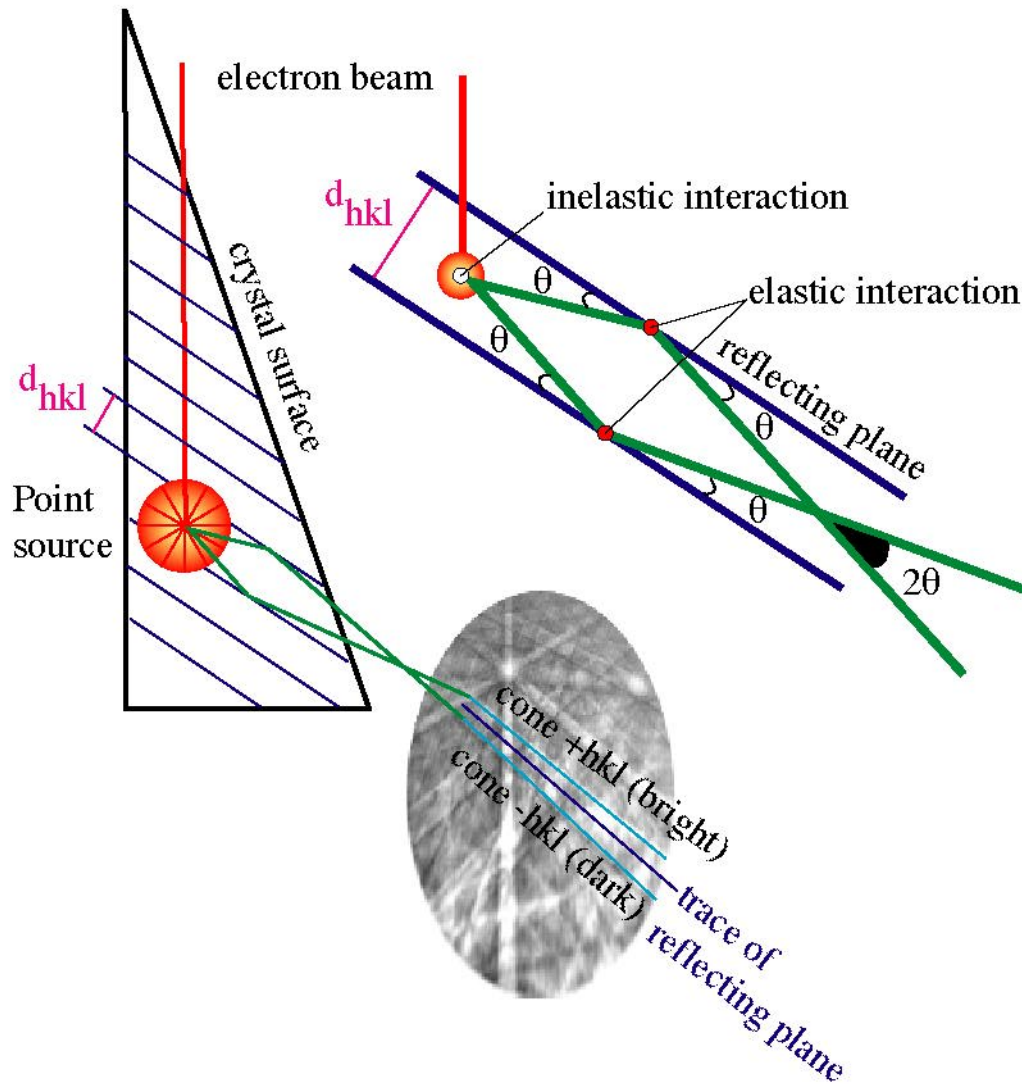


Beam-Specimen Interaction

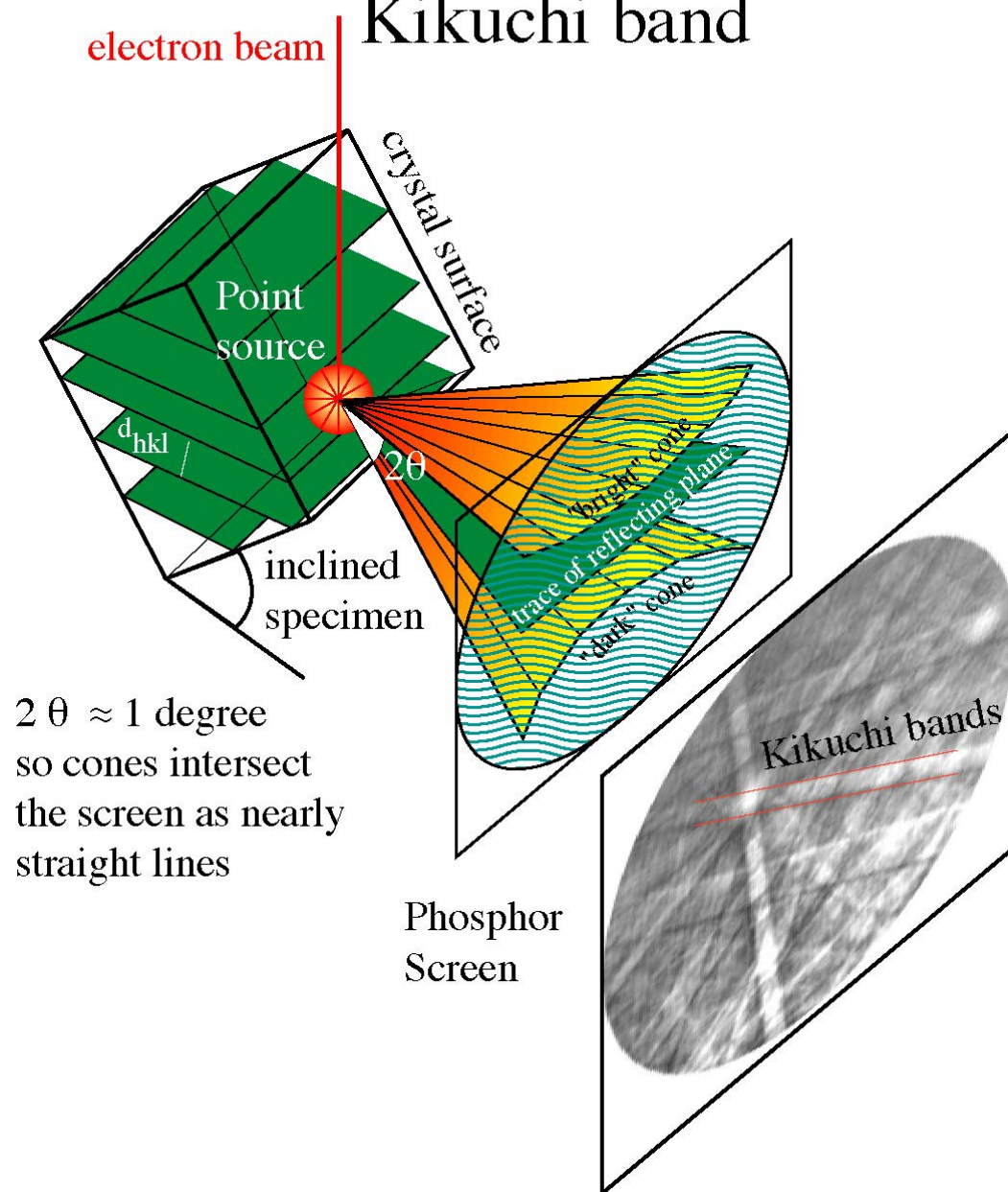


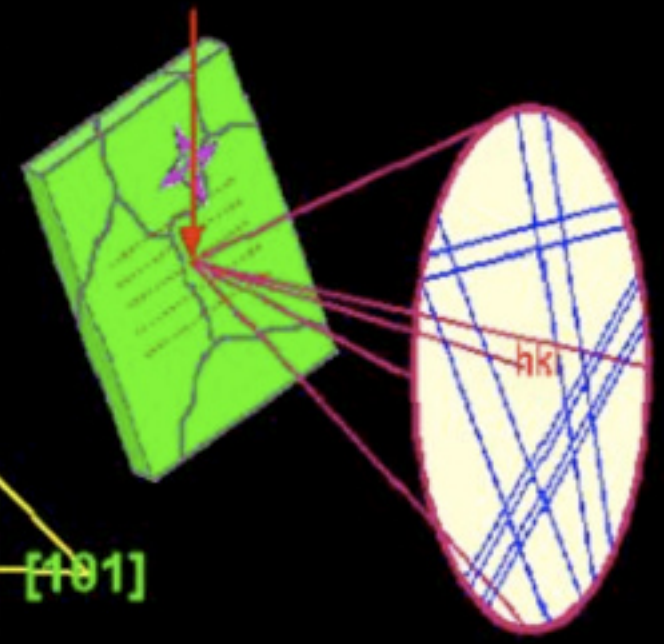
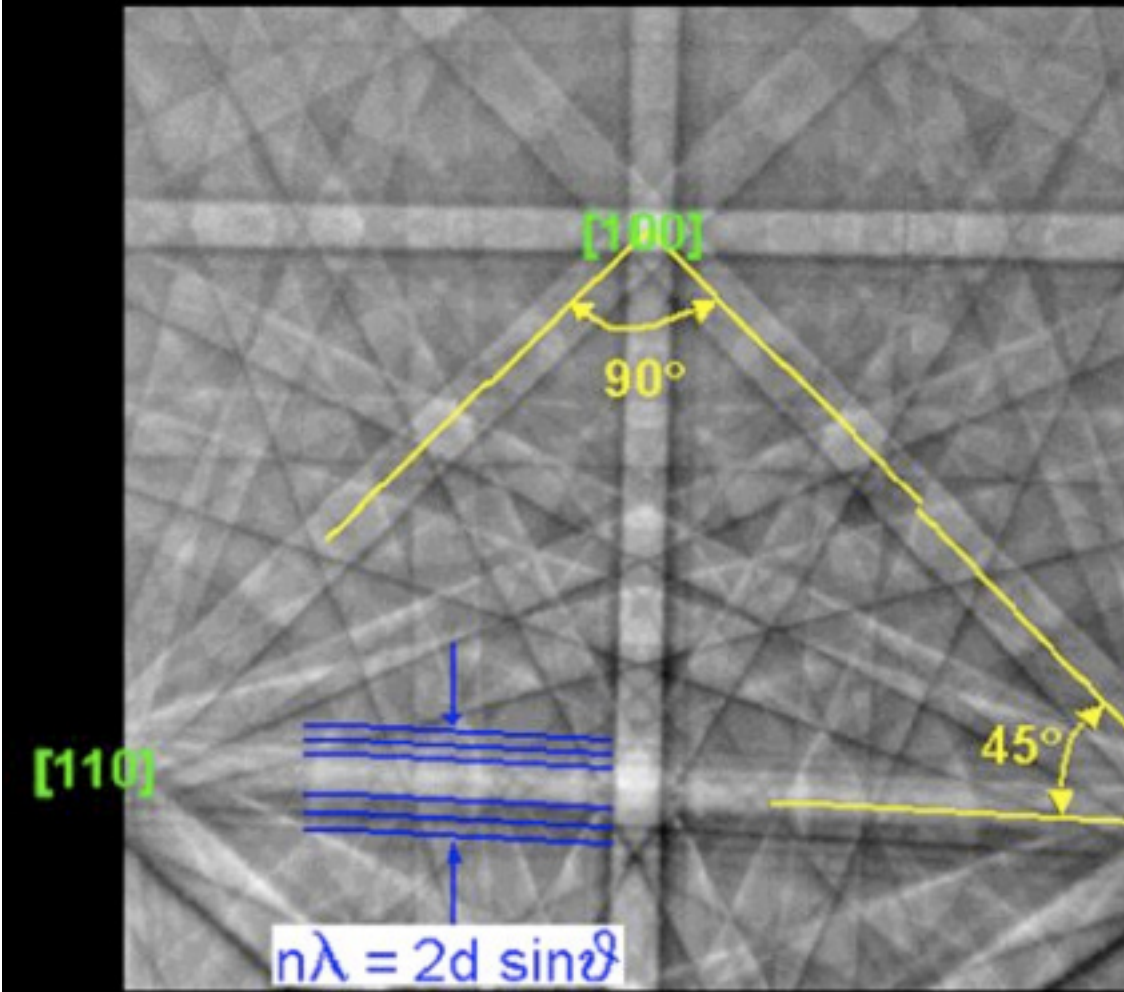
Tilt 70° 15 kV

Geometry of a backscattered Kikuchi bands

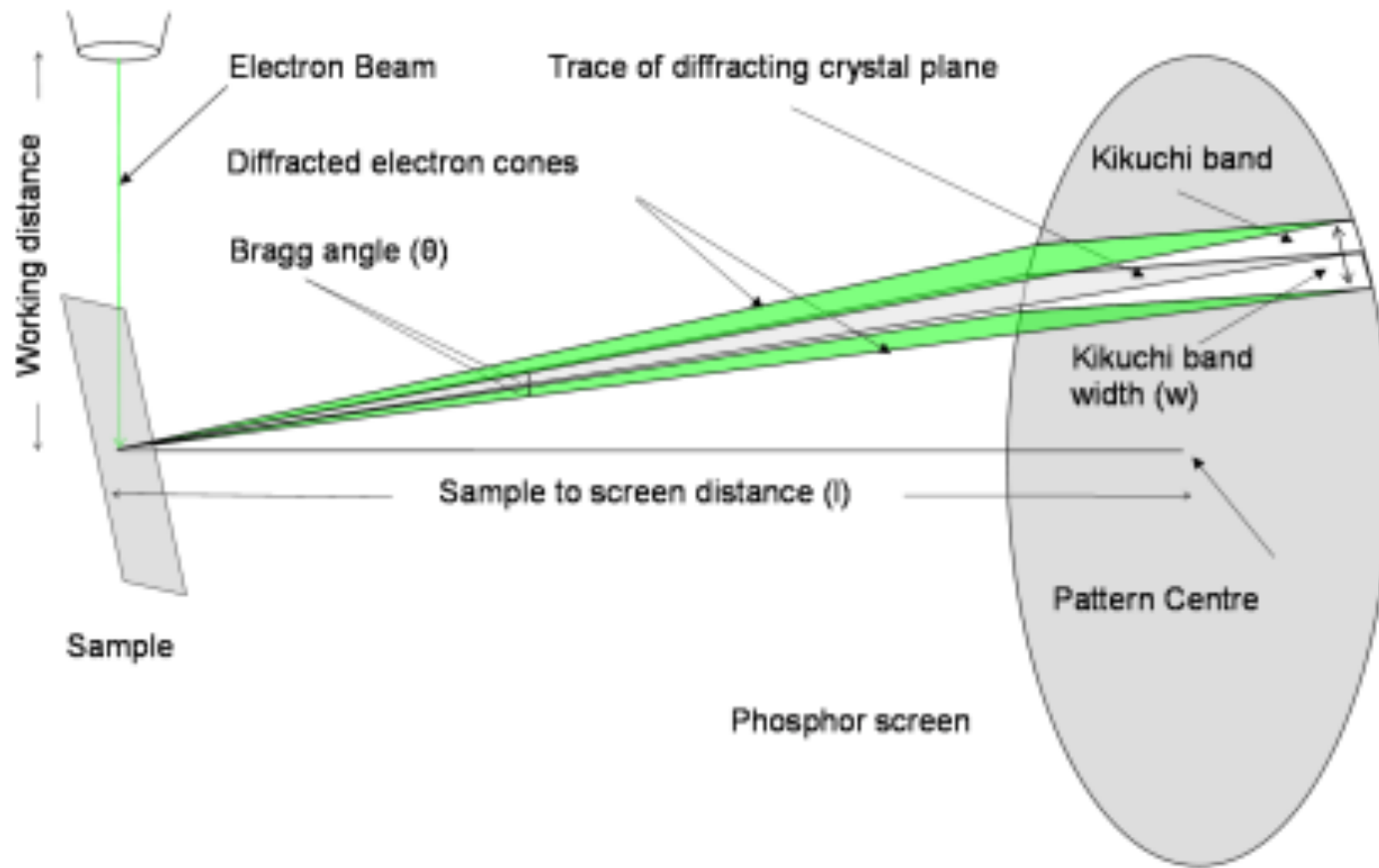


Formation of a backscattered Kikuchi band





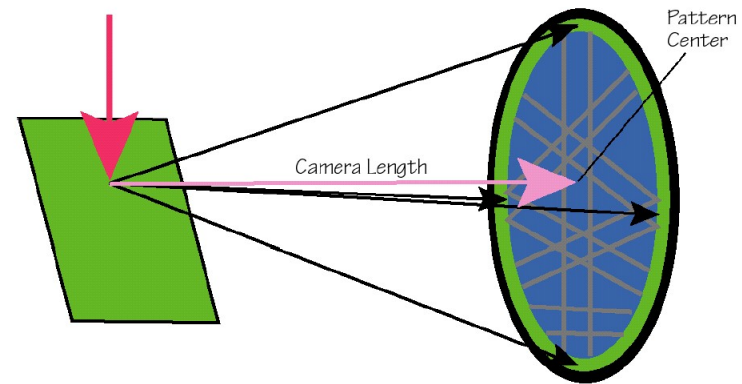
Working Distance & Pattern Centre



Si [100] wafer calibration of camera length and PC

Calibrating the Phase ID Geometry

In order to accurately analyze the Kikuchi pattern, the identification geometry is first calibrated. Using a pattern from a standard Si [100] wafer specimen, the software automatically performs the calibration. It finds the exact location of the pattern center on the Kikuchi pattern and the diffraction camera length. The pattern center is the (x, y) location on the pattern that traces back to the impact position on the specimen of the electron beam. The camera length is the distance from the impact position on the specimen to the pattern center. This image *must* be used to accurately index all patterns acquired using this analysis geometry.



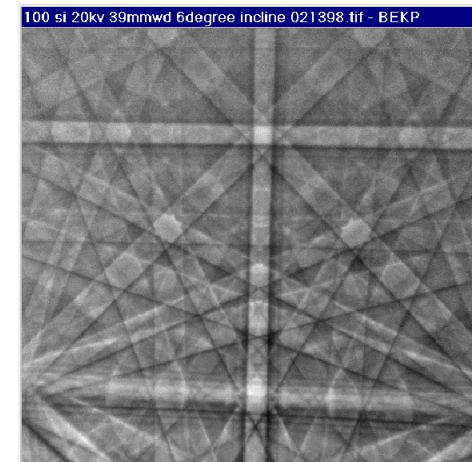
Pattern Loaded

A flat field corrected pattern is loaded for phase analysis.

Analyzing the Pattern

Once the software is calibrated for the analysis geometry, a Kikuchi pattern is analyzed. The extracted parameters are used in a search of the ICDD phase database. Most of the tedious work and all of the mathematics have been automated so that the optimum phase selection is done in a timely manner.

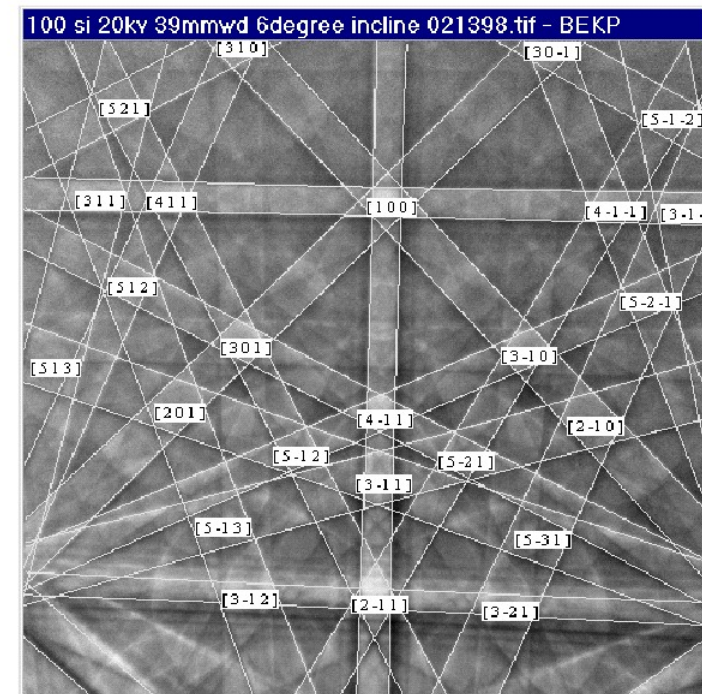
The software performs a Hough transform, which extracts the dominant Kikuchi bands from image. The widths of the bands and their relative angles are calculated.



Si [100] wafer calibration

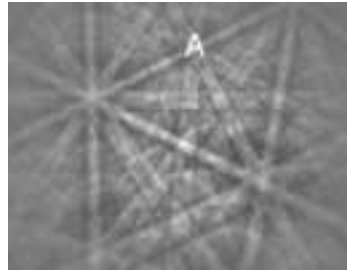
Pattern Simulation

If requested, a simulation of the Kikuchi pattern for the selected crystal can be overlaid on the pattern. The complete line pattern and zone index markers are overlaid on the Kikuchi pattern. Zone text markers are automatically provided and planar text markers can be shown, if desired.

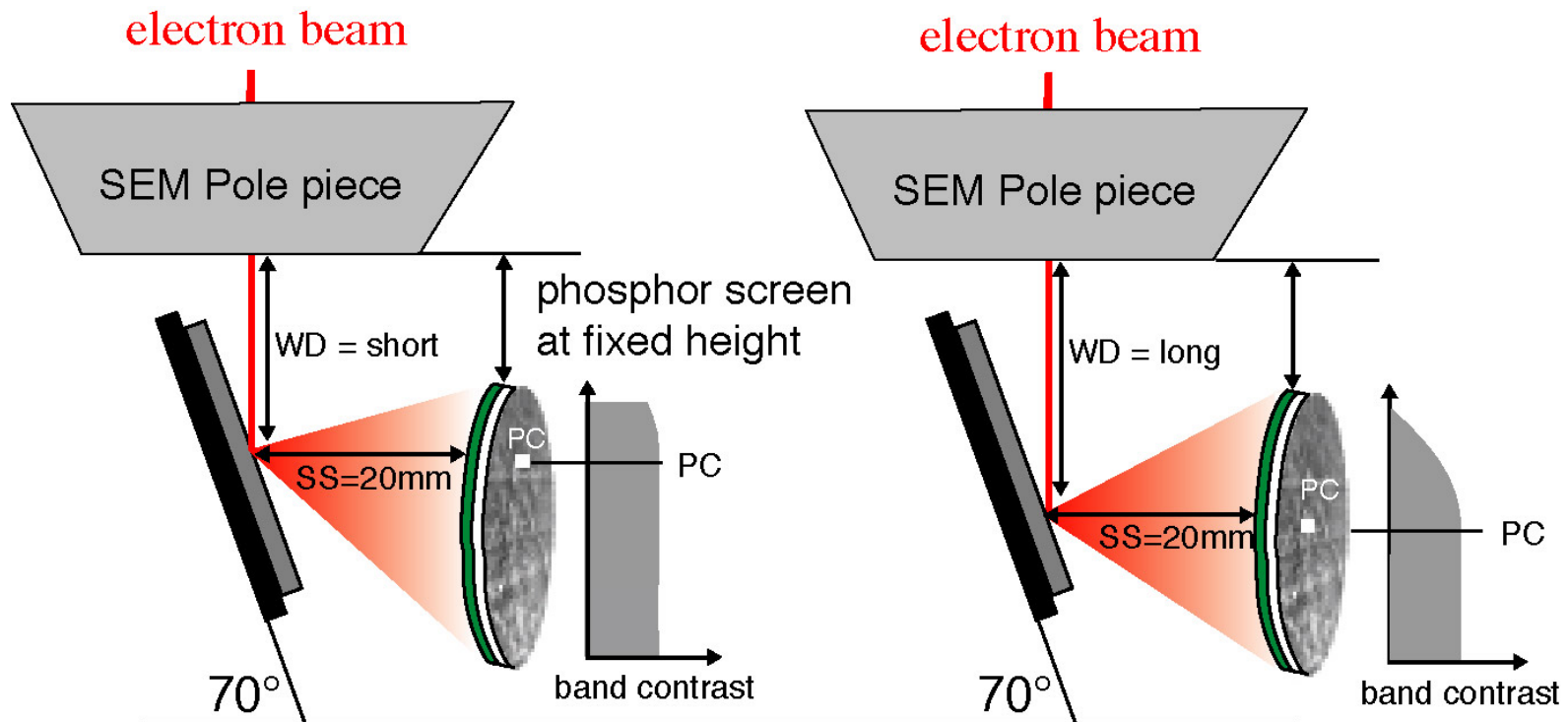
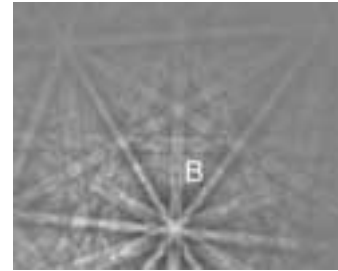


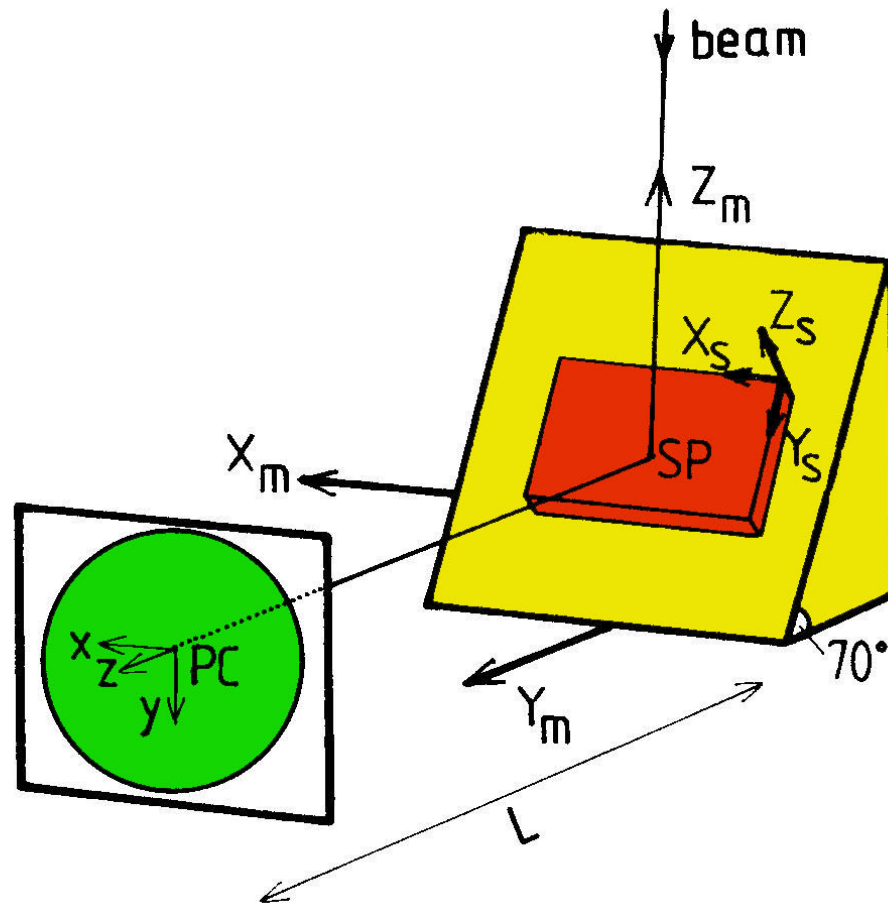
Pattern Center (PC) and Working Distance (WD)

A) Near top of screen

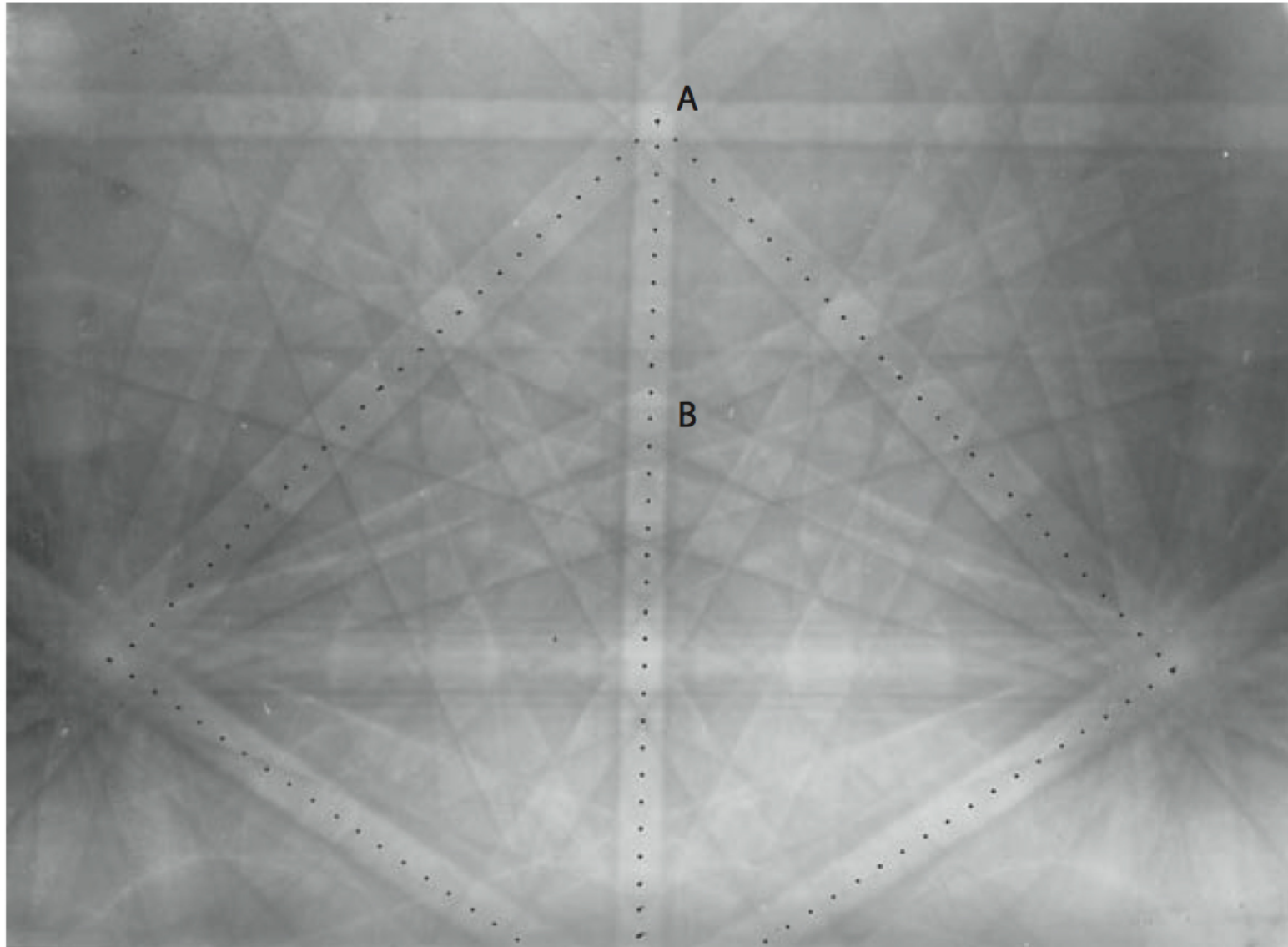


B) Middle of screen



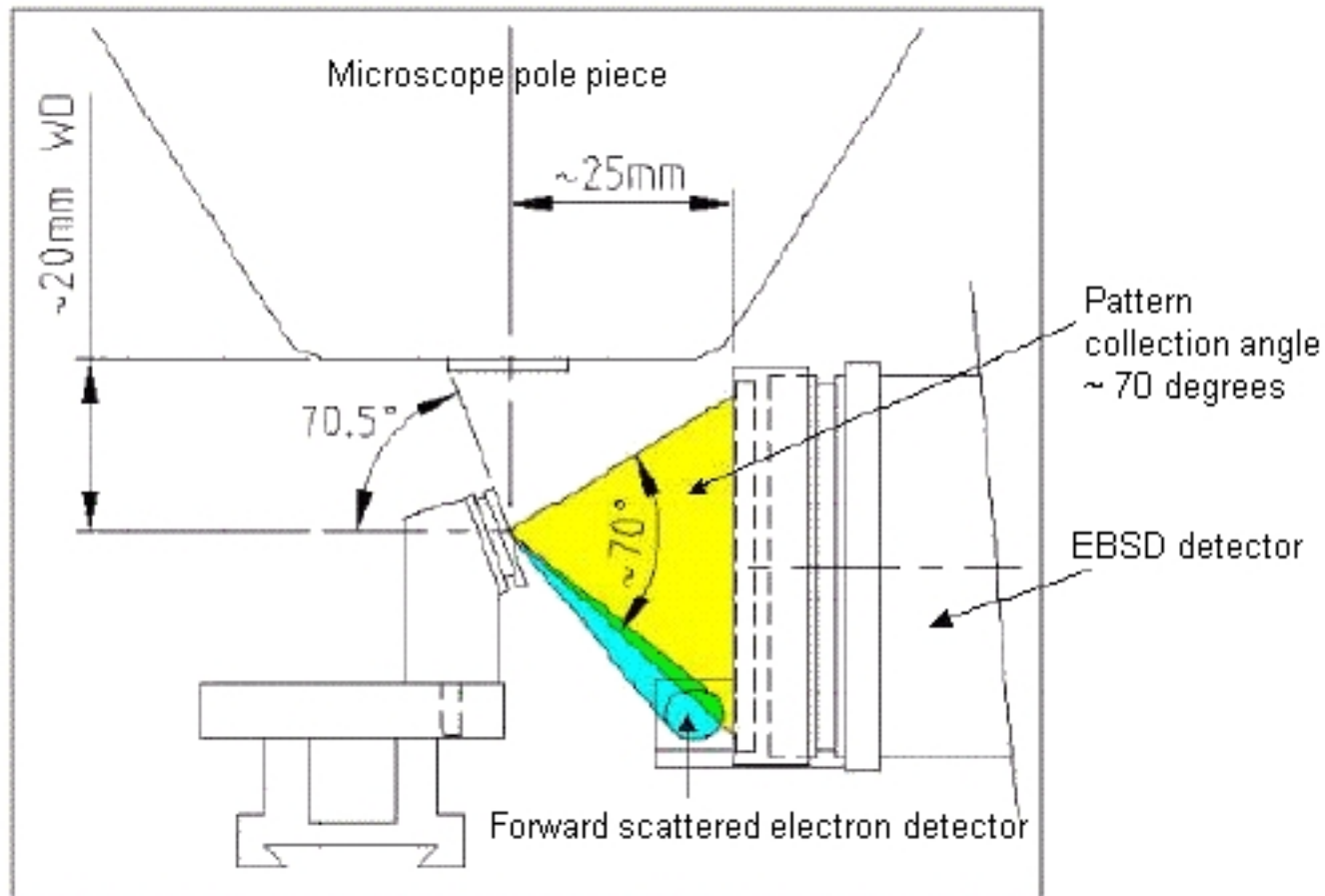


Parameters required for EBSD orientations measurements: pattern source point on the specimen, SP , pattern centre on the recording screen, PC , specimen-to-screen distance L (or Z_{SSD}), and three sets of orthogonal axes, xyz (screen/pattern axes), $X_s Y_s Z_s$ (specimen axes) and $X_m Y_m Z_m$ (microscope axes).



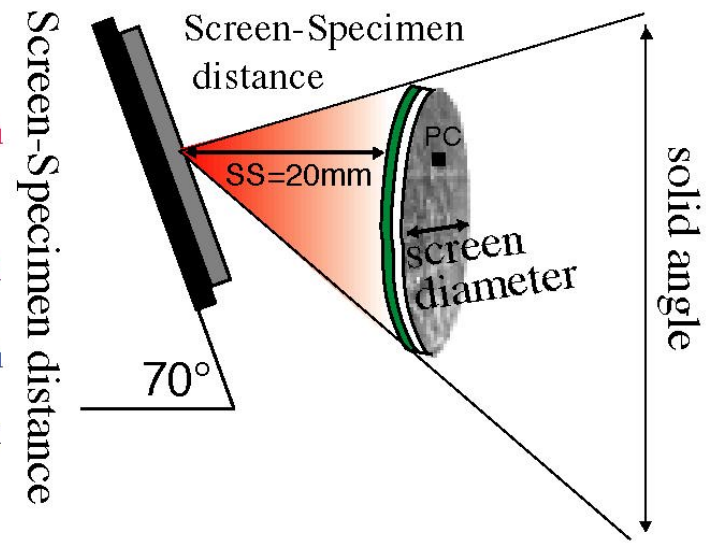
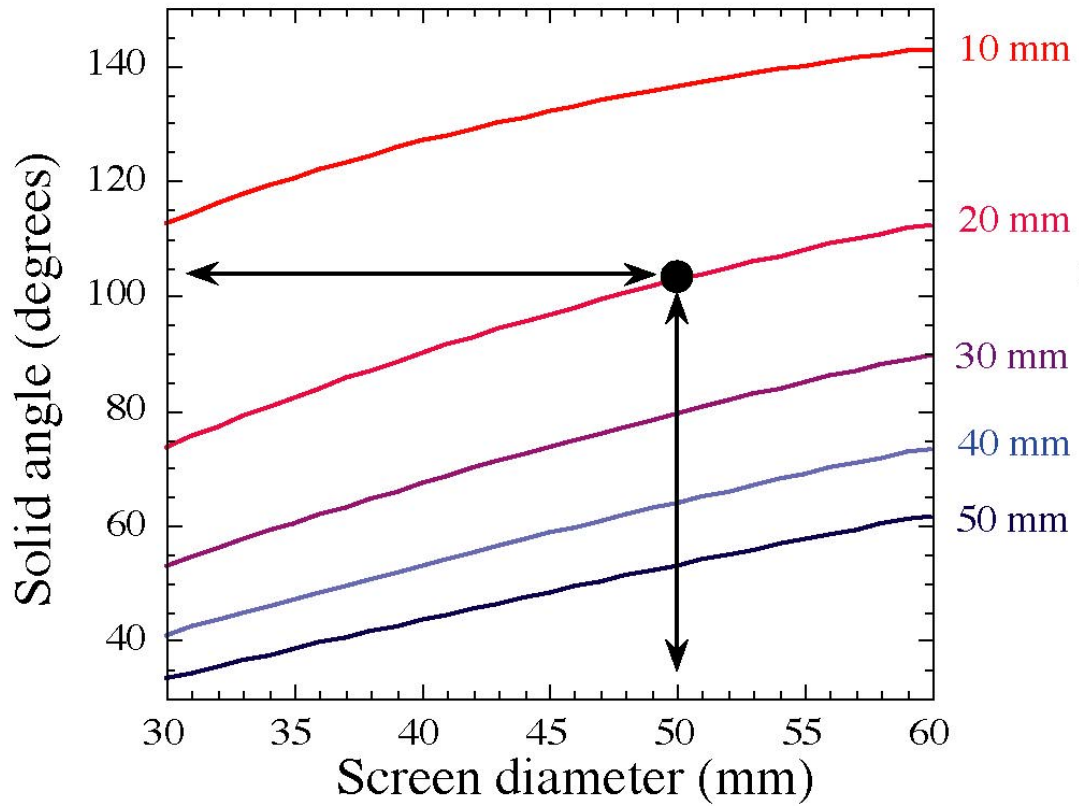
An EBSD pattern of (001) silicon with the specimen normal direction labeled A and the pattern center labeled B.

Typical commercial geometry



Oxford Instruments (UK)

Screen geometrical parameters for EBSD



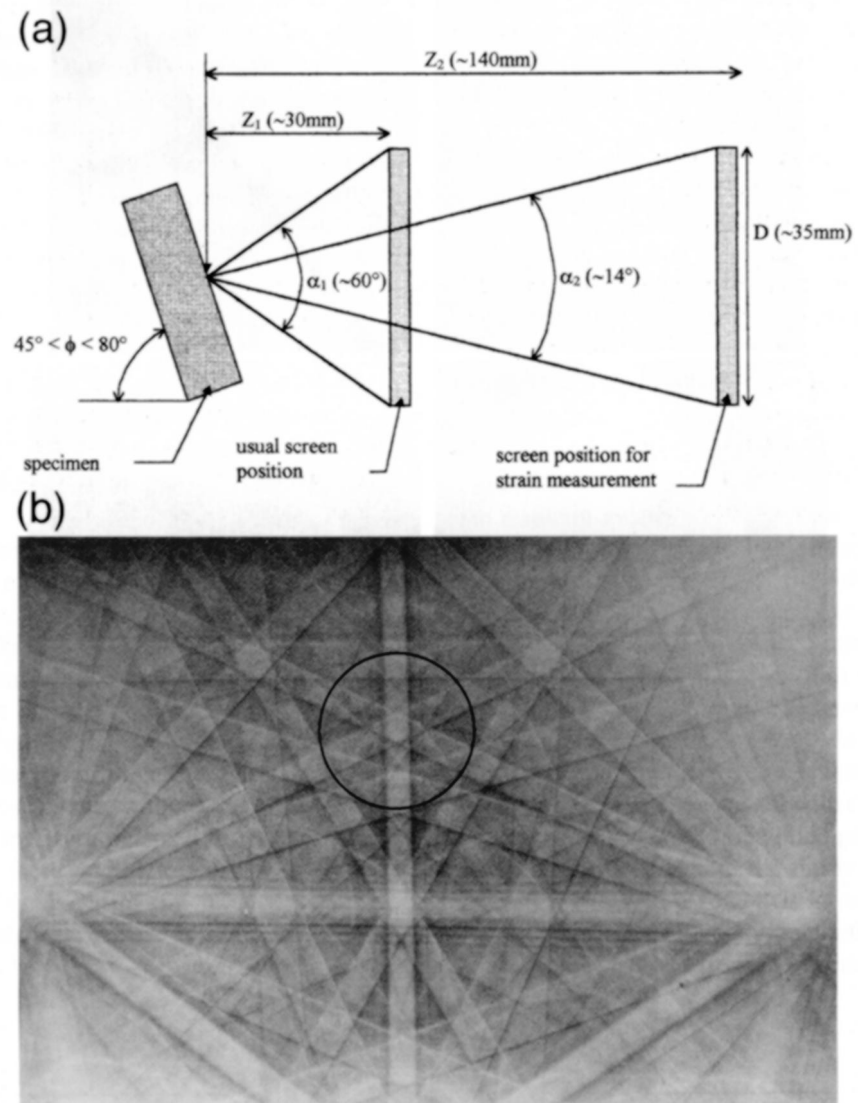
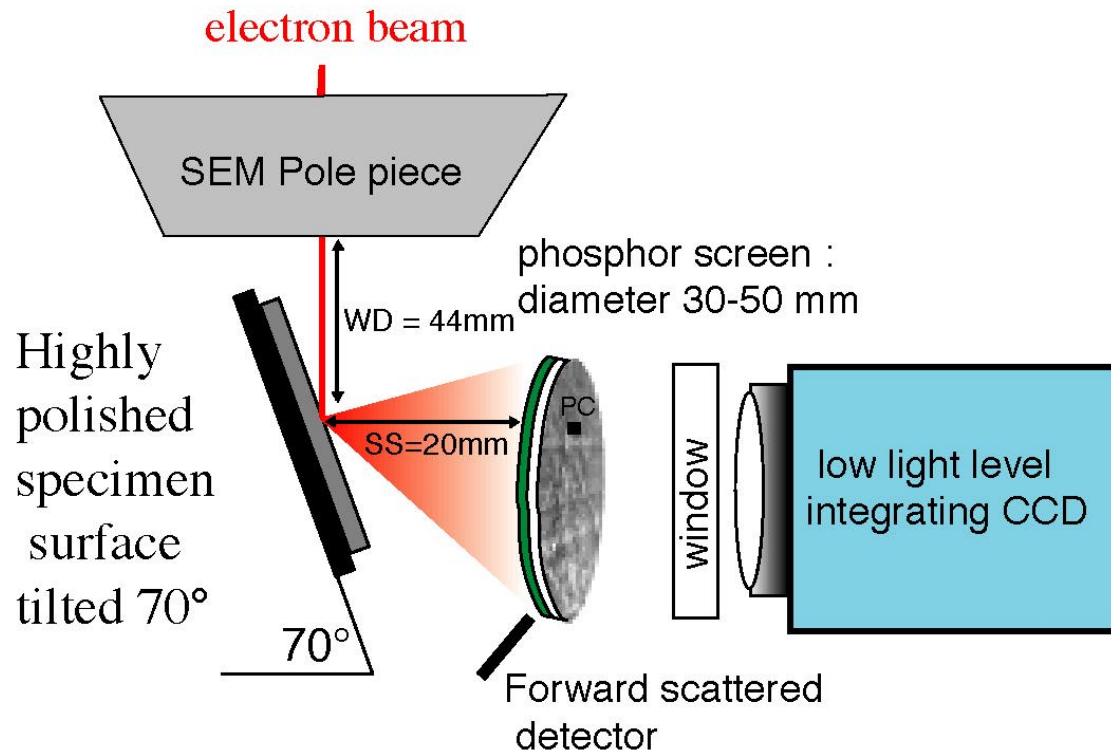


Fig. 1. (a) schematic diagram showing the geometry of the specimen and scintillator configuration used for EBSD. (b) an EBSD pattern from Si obtained by exposing an em film plate in the SEM specimen chamber. The circle marked on this pattern indicates the reduced capture angle ($\sim 14^\circ$) used in this work.

The geometry of an EBSD system

electron beam : 15-25 kV, 0.01-50 nA **working distance (WD)** : 8 - 45 mm
determines spatial resolution
and max. specimen area

specimen to screen distance (SS): 10-40 mm
determines solid angle (60 - 90°)
large angles->short SS



Kinematic intensities - good approximation for EBSD ?

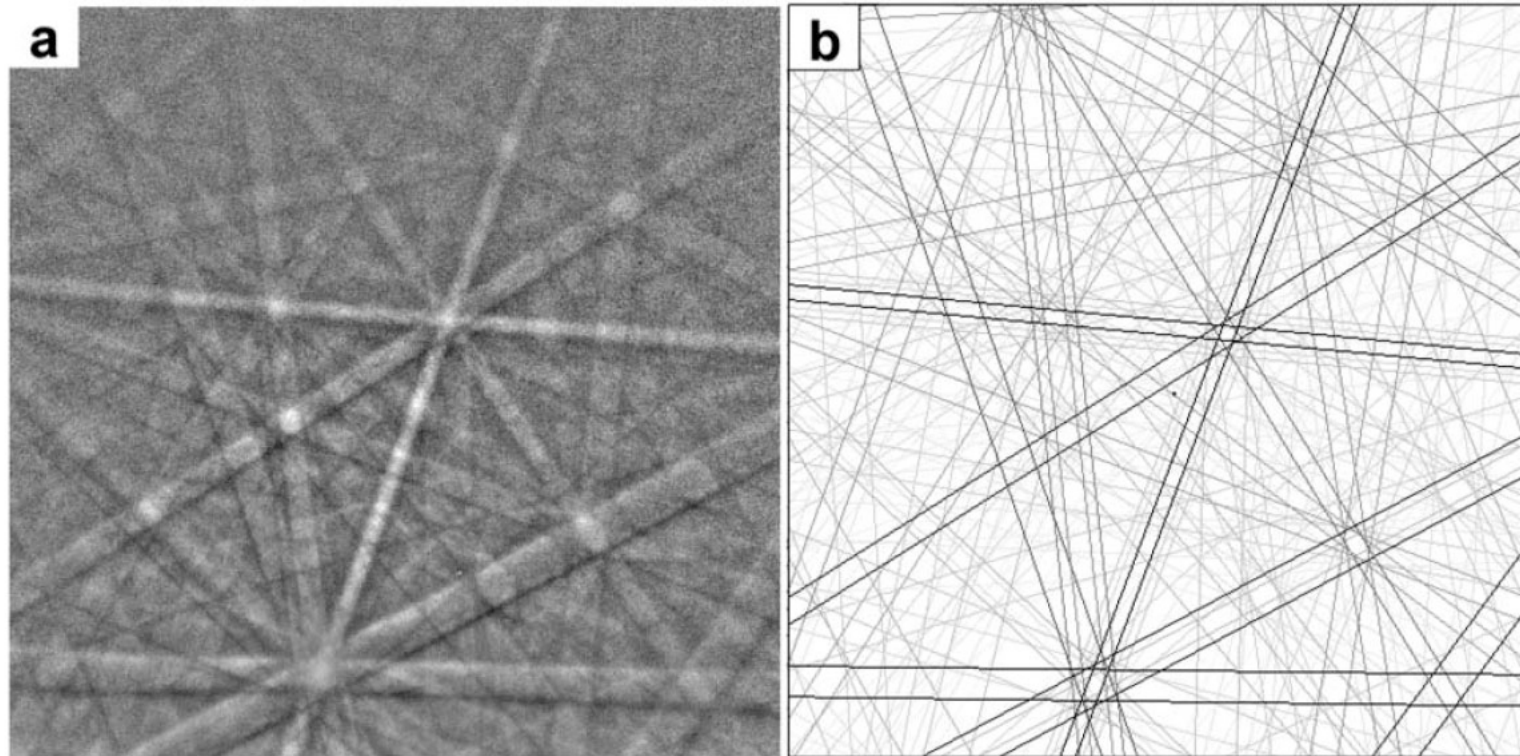
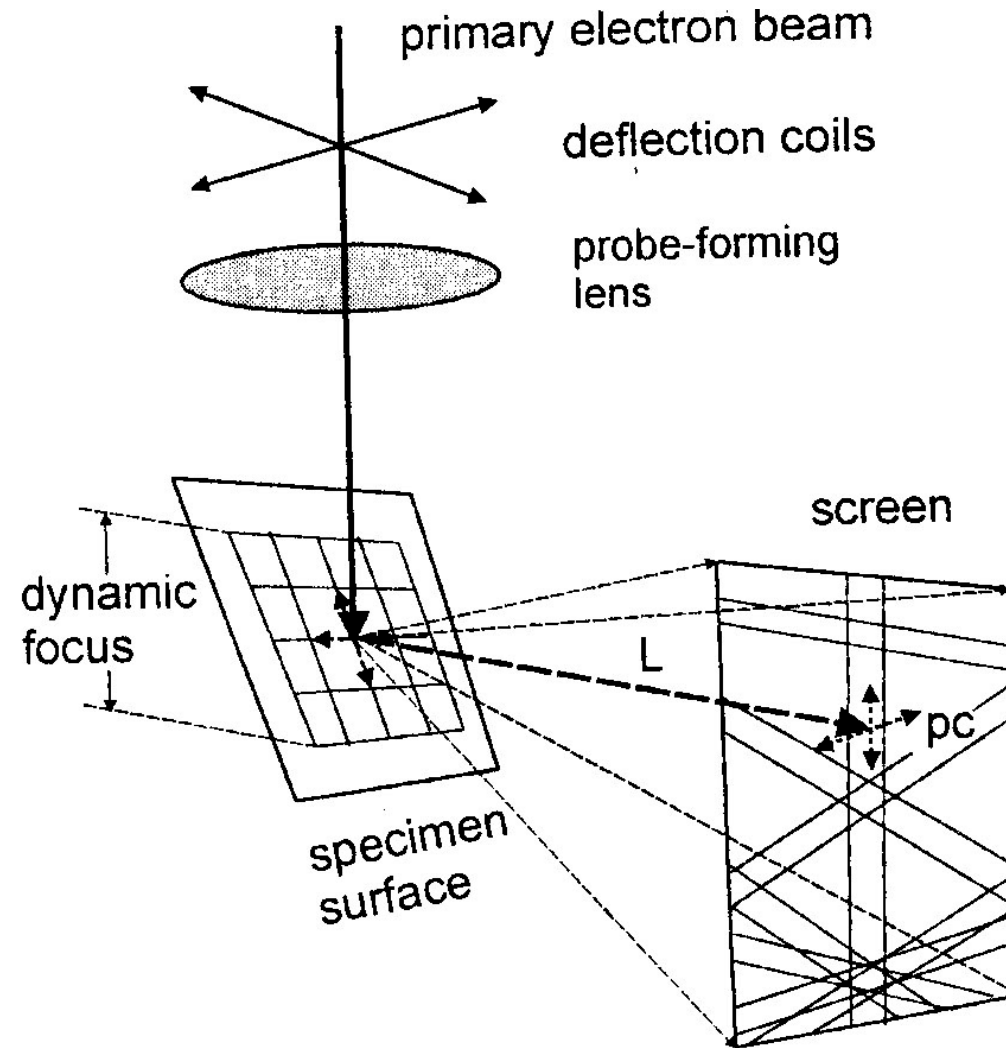


FIGURE 2. (a) EBSD patterns from calcite (CaCO_3), with a $\{10\bar{1}4\}$ cleavage surface inclined by 70° toward the phosphor screen. (b) Calculated pattern for calcite in the same orientation. In (b), Kikuchi bands are shown as a pair of straight lines whose color (depth) is proportional to the kinematic-diffraction amplitude of the corresponding reflections.

Calcite $\{1\ 0\ -1\ 4\}$ cleavage

Kogure 2002 AM

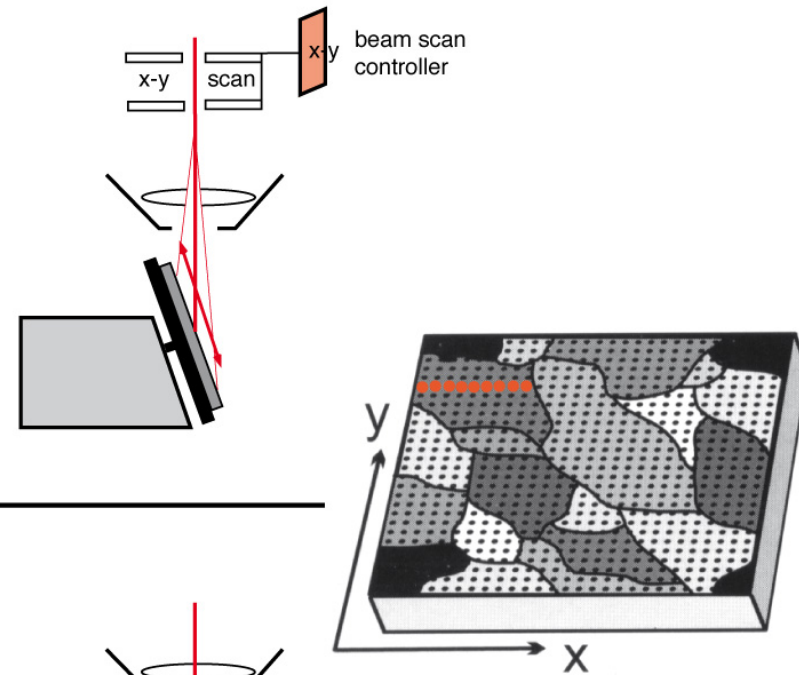
Beam Scanning



EBSD Maps - Beam or Stage scanning

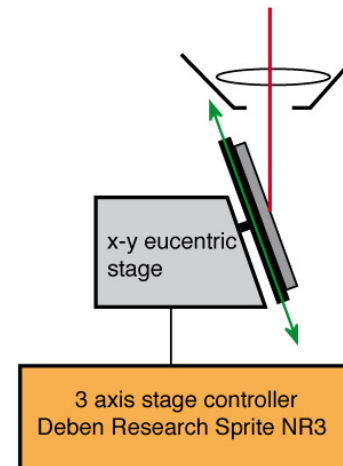
Beam scanning

- + fast (no moving parts)
- small steps & areas (1x1 mm)
- changing beam geometry



Stage scanning

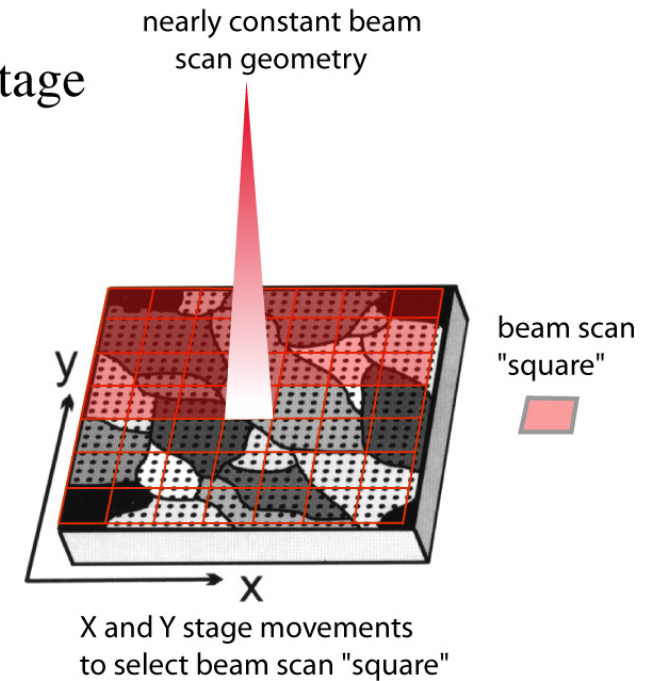
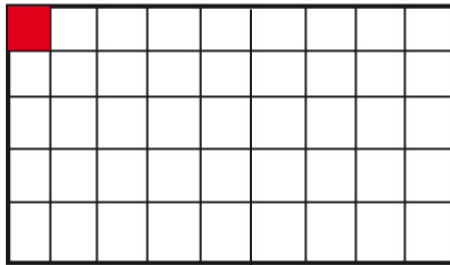
- + constant beam geometry (eucentric stage)
- + large steps & areas (20 x 30 mm)
- slow (but still over 1000 points per hour !)



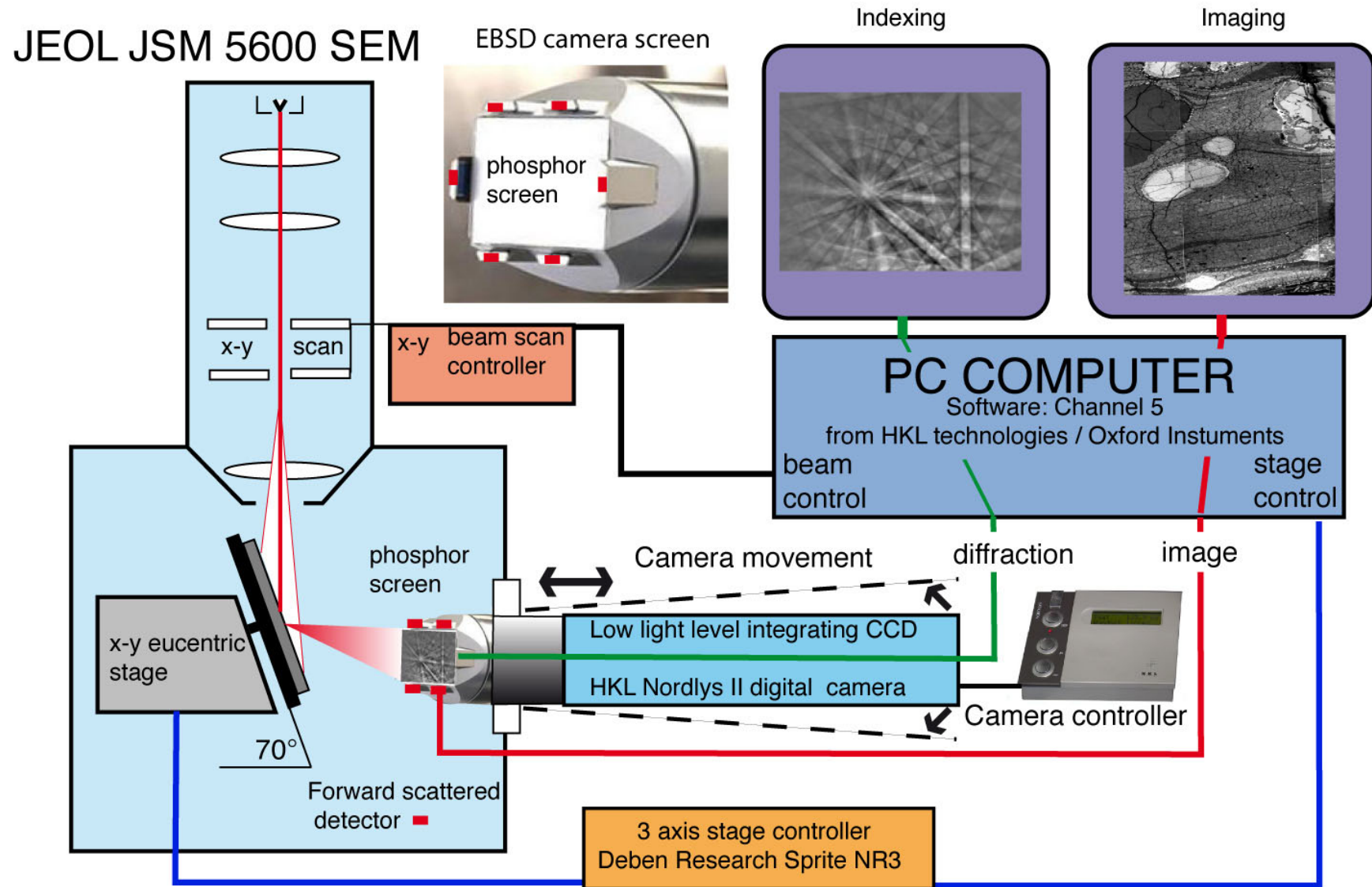
EBSD Maps - Combined Beam and Stage scanning

- + nearly constant beam geometry
(eucentric stage) - stage
- + large steps & areas (20 x 30 mm) using X and Y stage
- + fast over small area - beam

Beam scan mosaic, origin displaced
by stage movement



EBSD System : UMR Tectonophysique - Université Montpellier 2



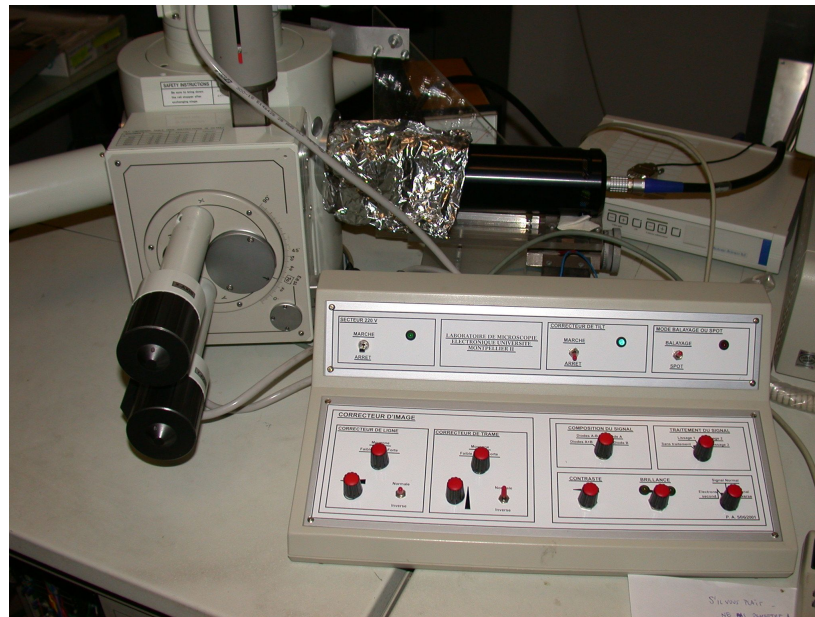
Tilt (70°) corrected images



No correction

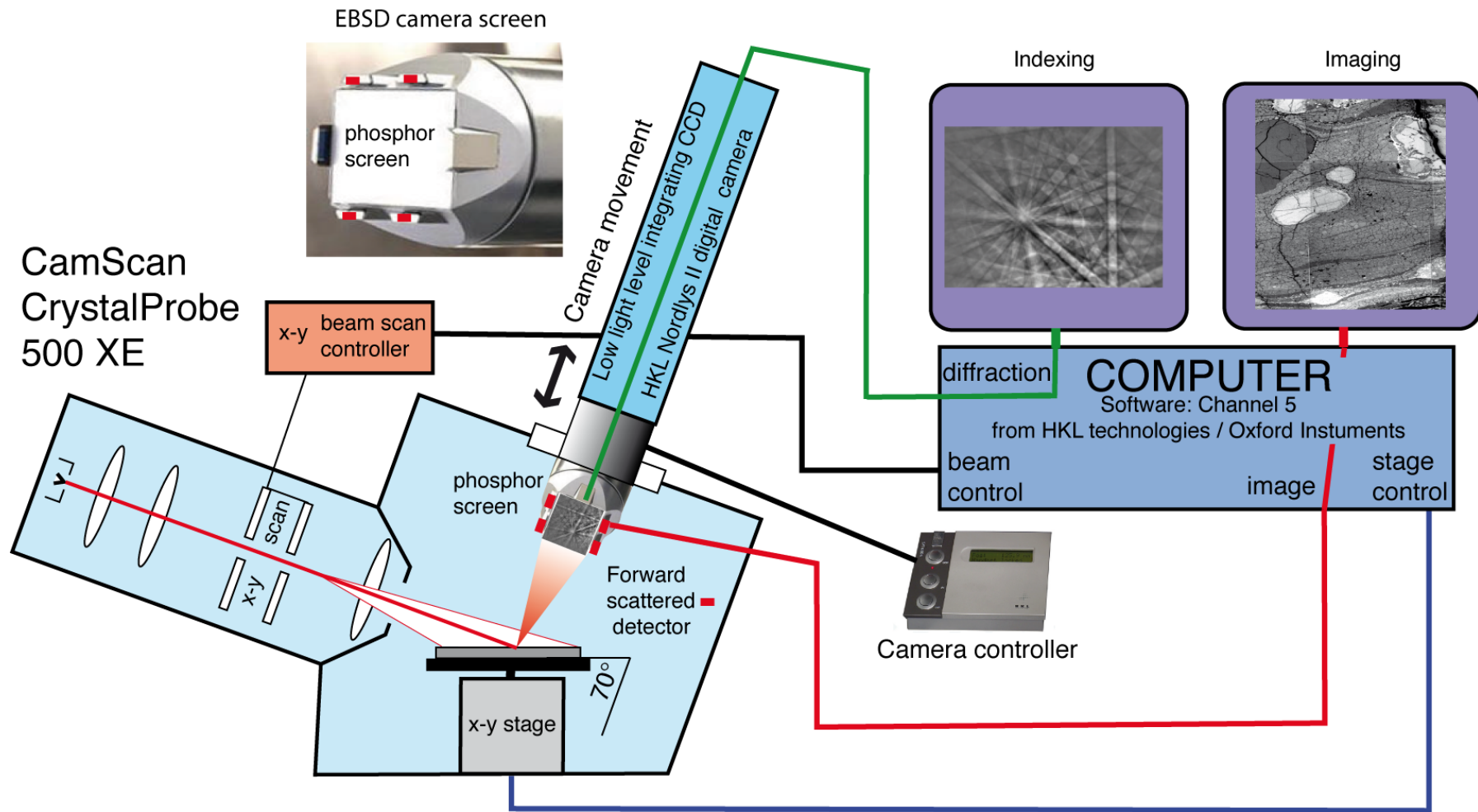


Corrected



Home-made
Tilt correction
electronics

Géosciences - Université Montpellier II EBSD system



Specimen Preparation

- 1) Polished thin sections or blocks.
- 2) The mechanical surface damage can be removed by:
 - a) Chemical-mechanical (SYTON) polish.
 - b) Etching.
 - c) Electro-polishing.
 - d) Ion beam milling.
- 3) Natural fracture or growth surfaces.
- 4) Uncoated or very thin carbon or Pt coat.

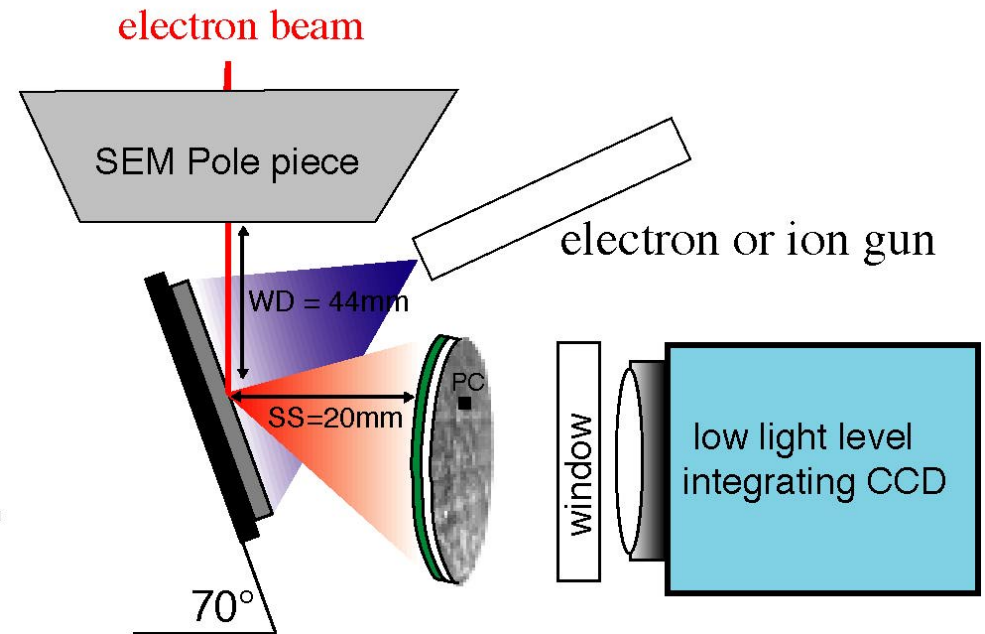
Typical sample preparation for EBSD

Impregnate sample with resin to avoid holes & surface topography

- A) Lap with 220 grit silicon carbide until flat.
- B) Lap with 500 grit silicon carbide for 5 mins.
- C) Polish with 9 micron diamond for 15 mins.
- D) Polish with 3 micron diamond for 15 mins.
- E) Polish with 1 micron diamond for 15 mins.
- F) Syton polish for 1 - 20 hours.

The charging problem....

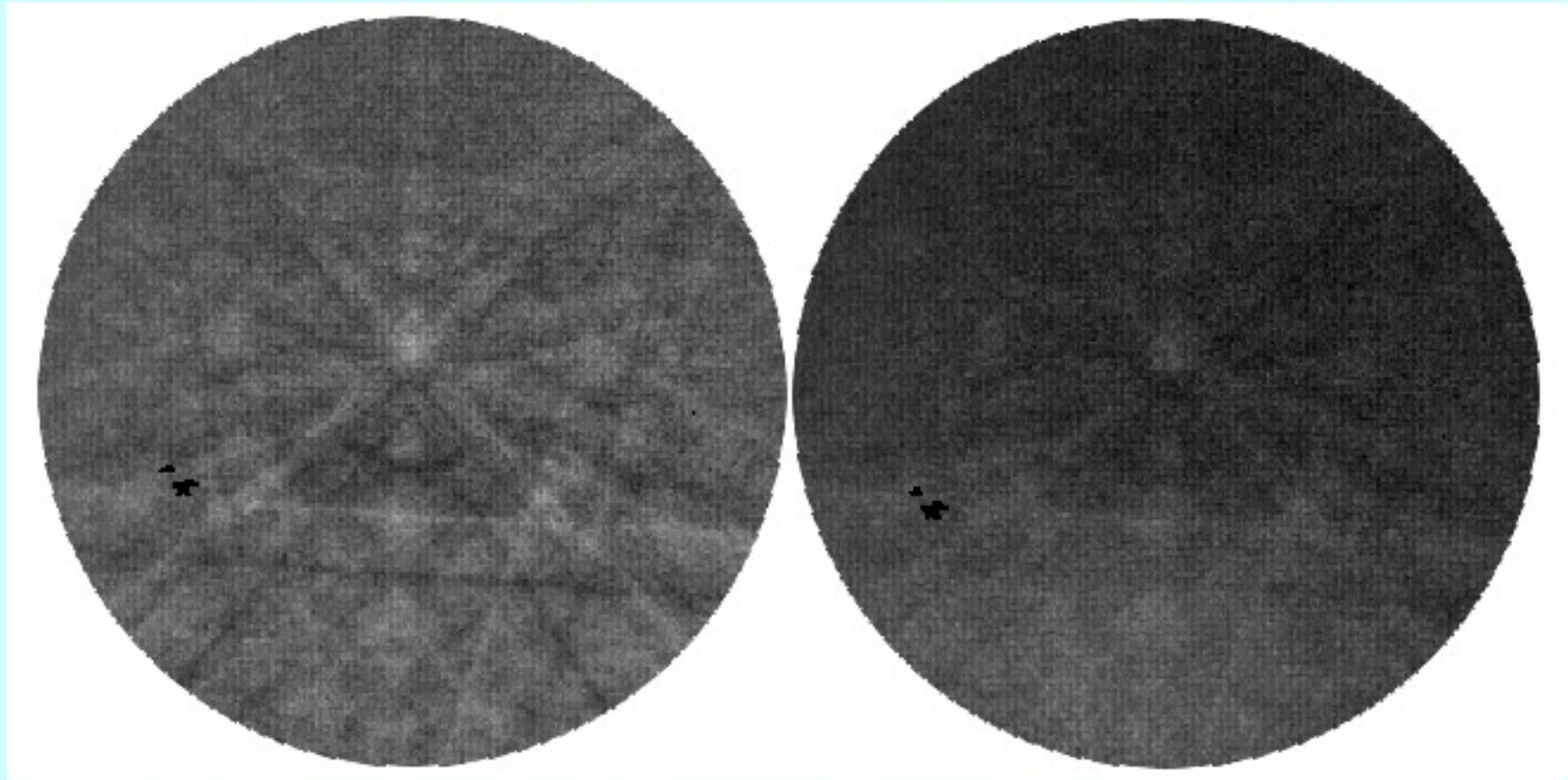
- A) Low energy (0.1-3 kV) electron beam (only negative charge)
- B) Ion beam (positive or negative charges)
- C) Ultraviolet light
- D) Low vacuum SEM (need NEW SEM !)



Coat dependence

Uncoated

3-5nm C coat



K-feldspar. 20keV ~15nA

Image from David Prior, University of Liverpool, UK

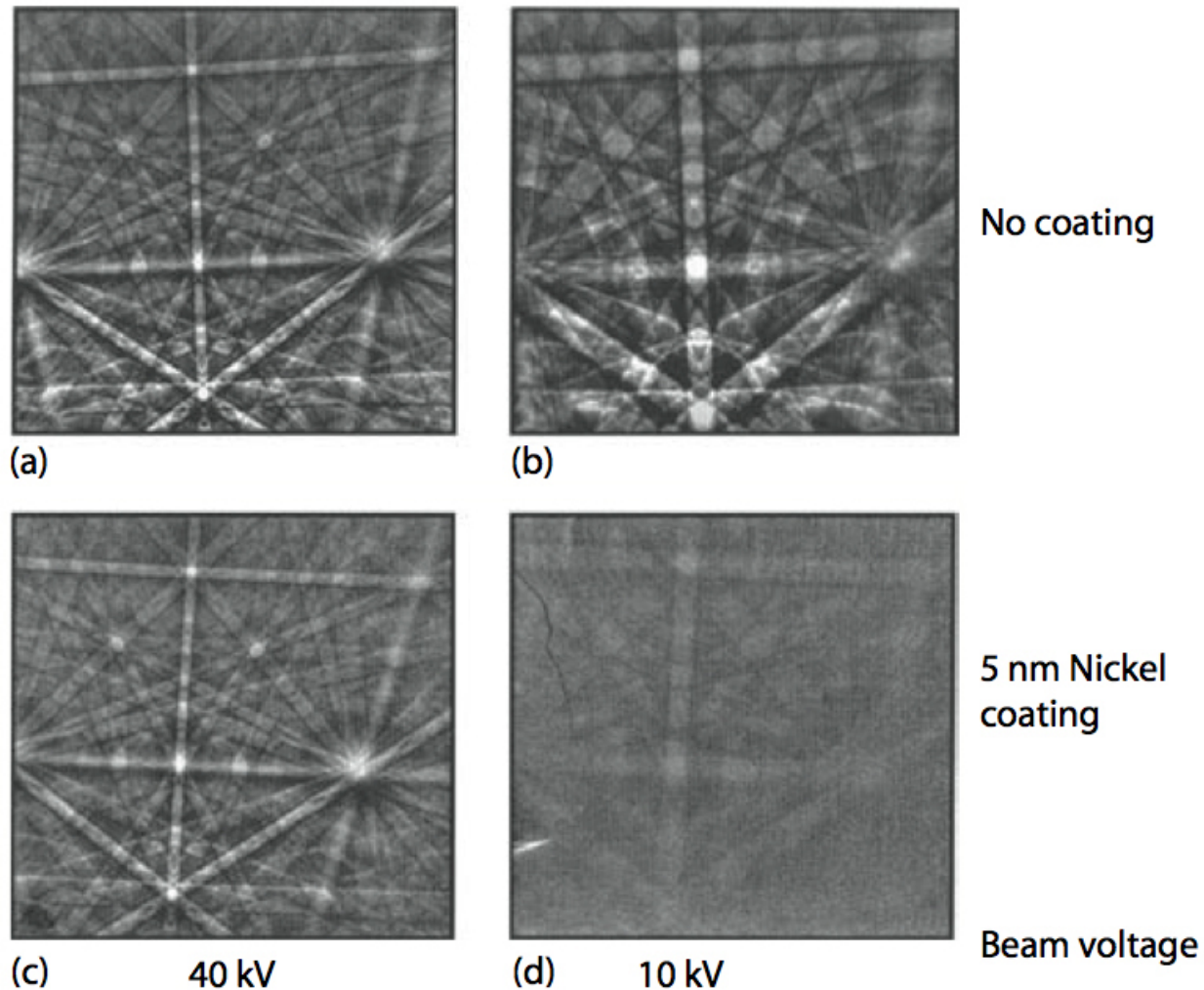
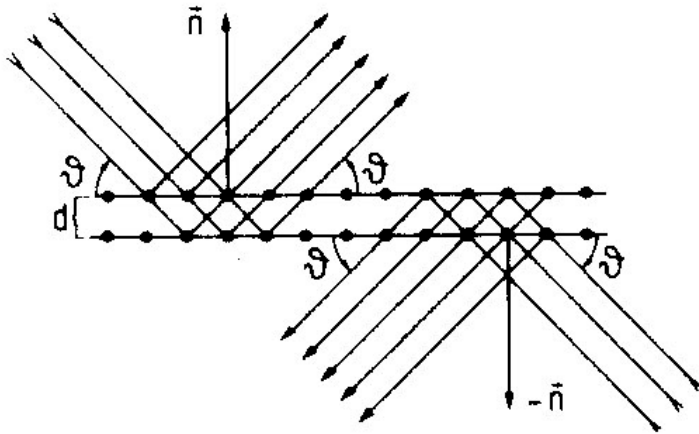


Illustration of the penetration depth of the electron beam in a silicon EBSD specimen. (a) No coating, 40 kV accelerating voltage; (b) no coating, 10 kV accelerating voltage; (c) coating with 5 nm of nickel, 40 kV accelerating voltage; (d) coating with 5 nm nickel, 10 kV accelerating voltage. There is less beam penetration at 10 kV since the underlying silicon pattern is indistinct. (Courtesy of J.R. Michael.)

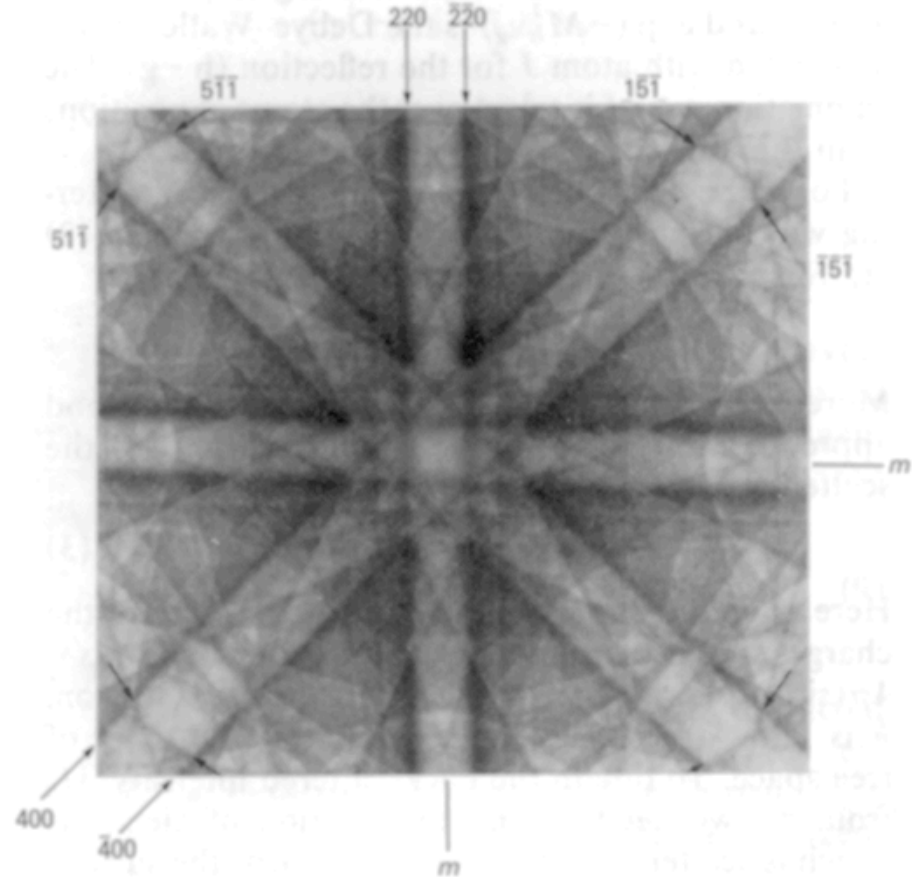
1. What is EBSD ?
- 2. Symmetry and EBSD**
3. Applications
4. Future developments

Symmetry
for routine indexing of known
phases

Diffraction symmetry – Friedel's law



X-ray reflection at both sides
of a set of lattice planes
(Friedel's law)



Friedel's Law: The intensities of reflections
(structure factors) hkl et $-h-k-l$ are equal:
 $|F(hkl)|^2 = |F(-h-k-l)|^2$

11 Laue Classes or Groups

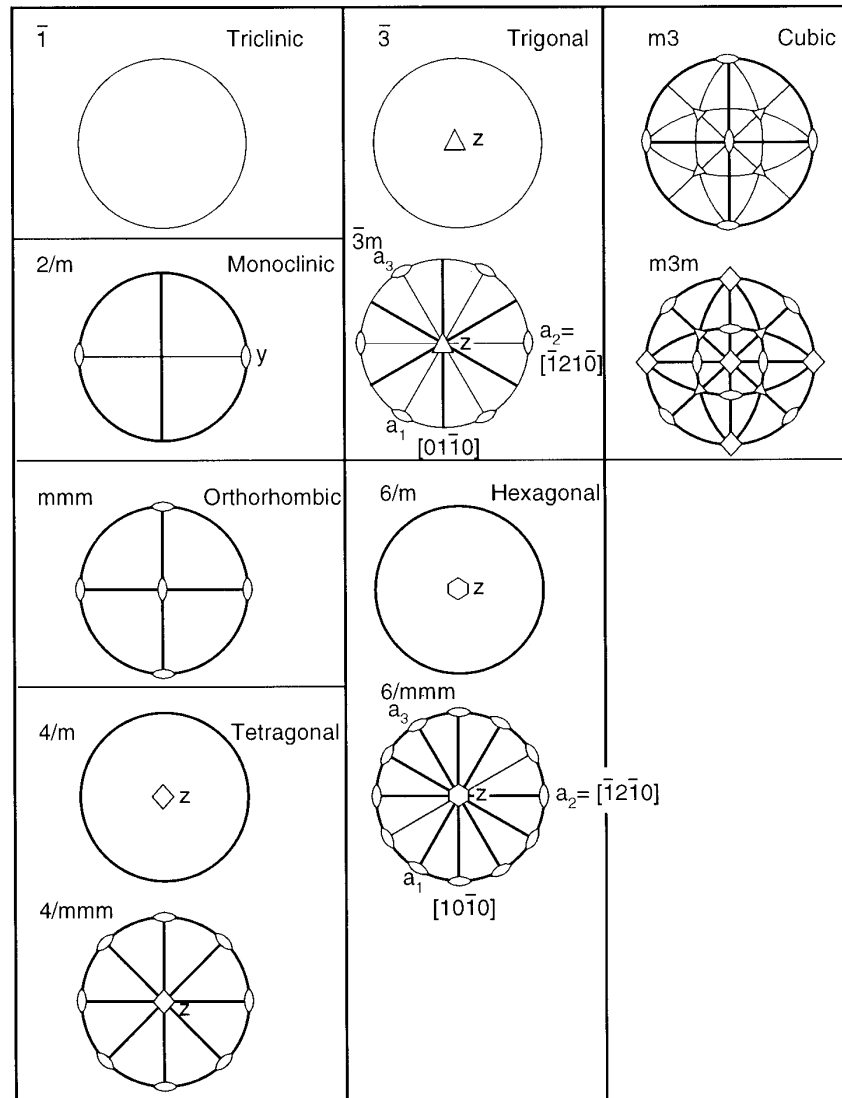


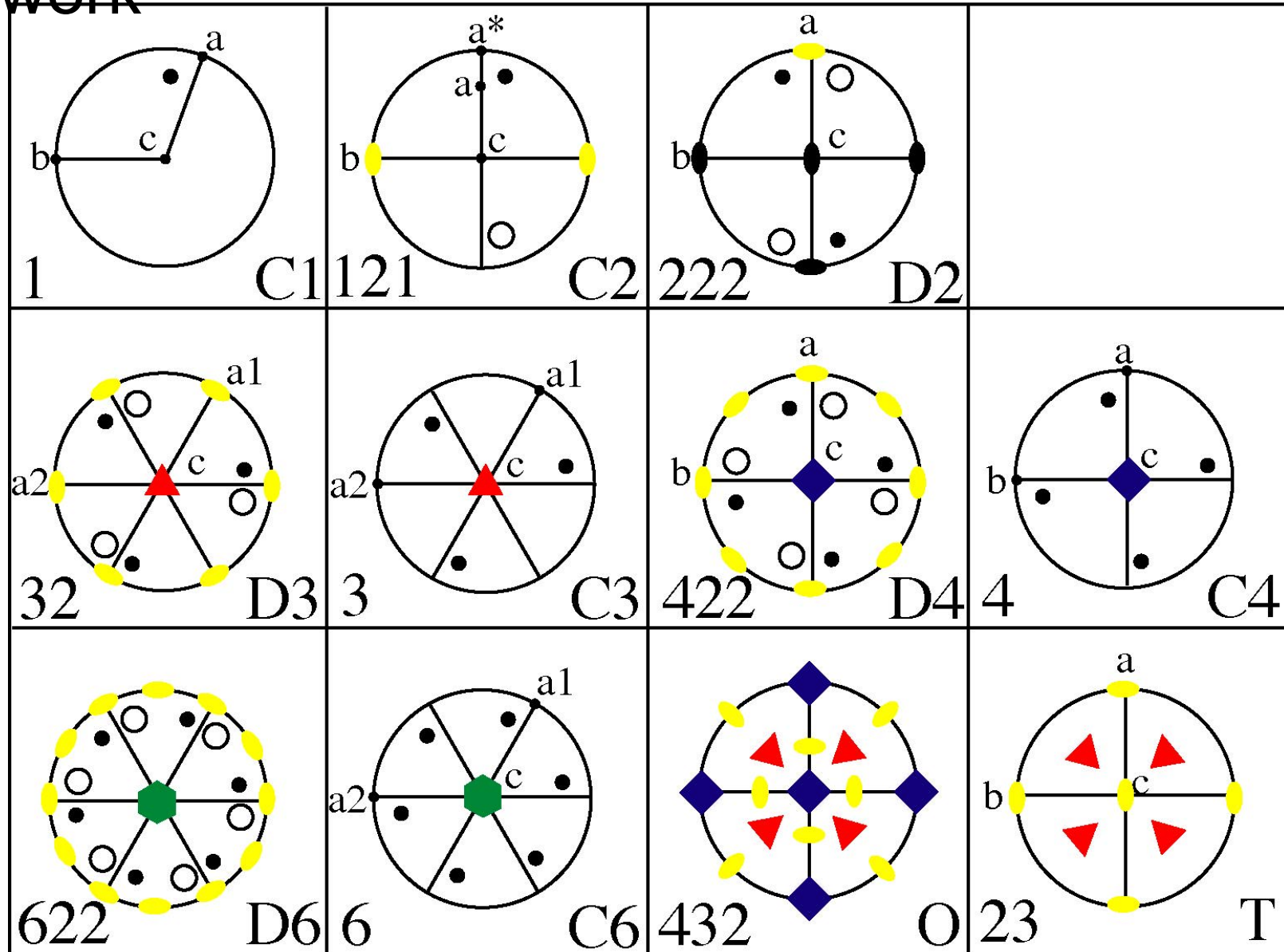
Fig. 5. Symmetry elements and crystallographers' conventions for the choice of axes in the 11 Laue groups (which are all centrosymmetric). (Note that, elsewhere in this book, x and y are usually used such that the quadrant with positive x and positive y is the upper right one.)

Table I. Crystal symmetries relevant for orientations

CRYSTAL SYSTEM	crystal class		no. of sym. el.	no. of centro-sym. tensor prop's.	
	Laue	rot.		sym. 2 nd -rank	sym. 4 th -rank
triclinic	$\bar{1}$	1	1	6	21
monoclinic	2/m	2	2	4	13
orthorhombic	mmm	222	4	3	9
tetragonal	† 4/m	4	4	2	7
	4/mmm	422	8	2	6
trigonal	† $\bar{3}$	3	3	2	7
	† $\bar{3}m$	3	6	2	6
	† 6/m	6	6	2	5
hexagonal	6/mmm	622	12	2	5
cubic	† m3	23	12	1	3
	m3m	432	24	1	3

† These groups have lattice planes which have the same spacing but are not symmetrically equivalent; thus they exhibit overlapping peaks in diffraction patterns; an example is (121) and (211) in crystal class 4/m.

11 Rotational classes used in orientation work



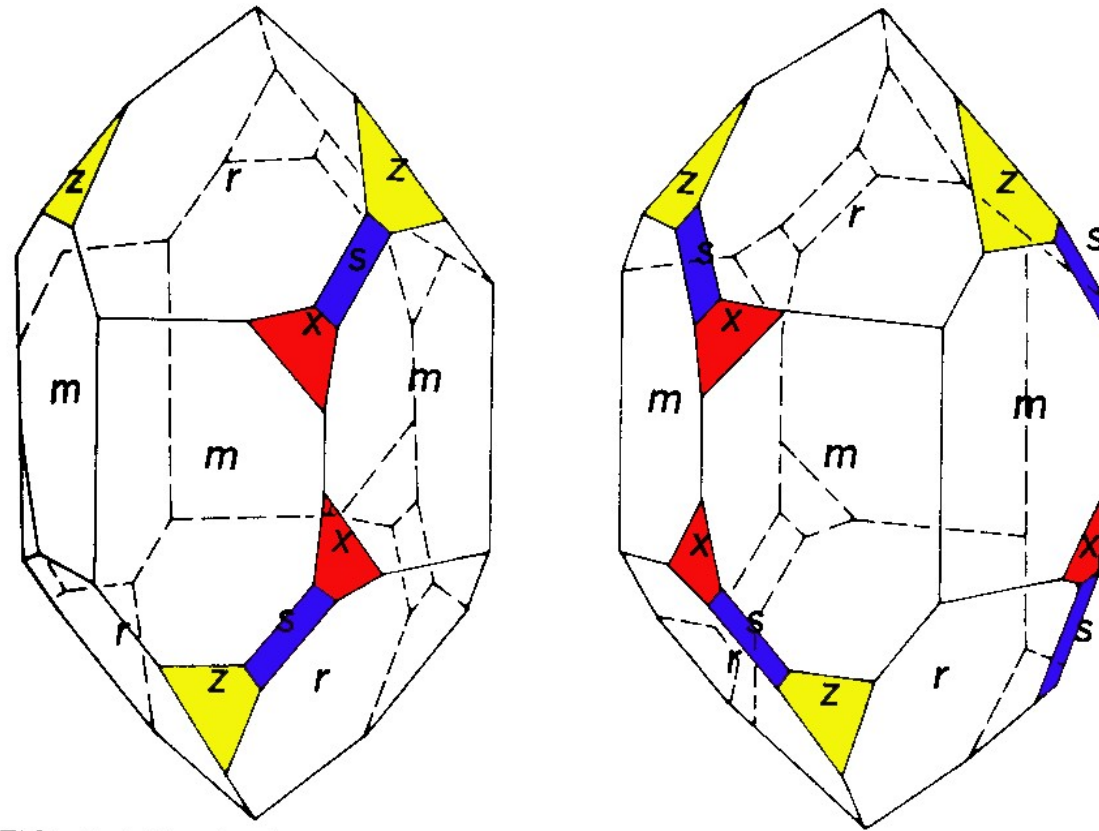
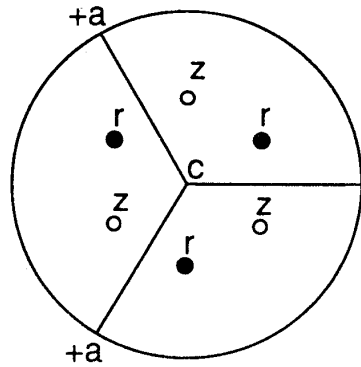


FIG. 2-51 Left-handed and right-handed quartz crystals.
(After E. S. Dana, *A Textbook of Mineralogy*, revised by
W. E. Ford, 4th ed., Wiley, 1955.)

QUARTZ TWIN LAWS

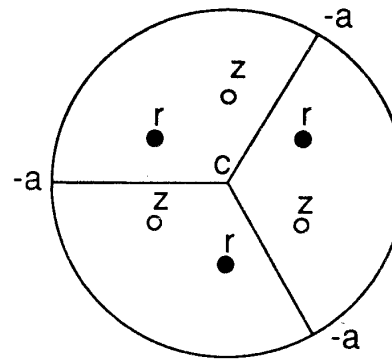
RIGHT-HANDED HELIX



a)



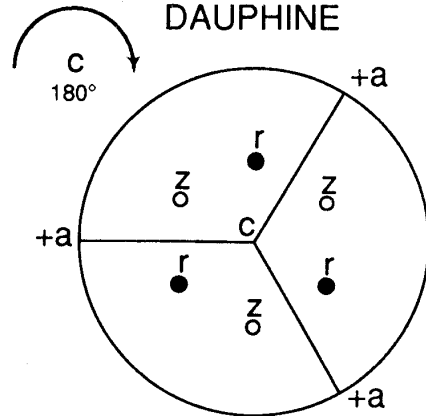
BRAZIL



b)

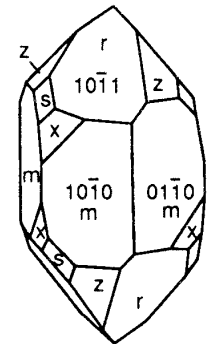
reflection on (a)

DAUPHINE



c)

RIGHT-HANDED HELIX



d)

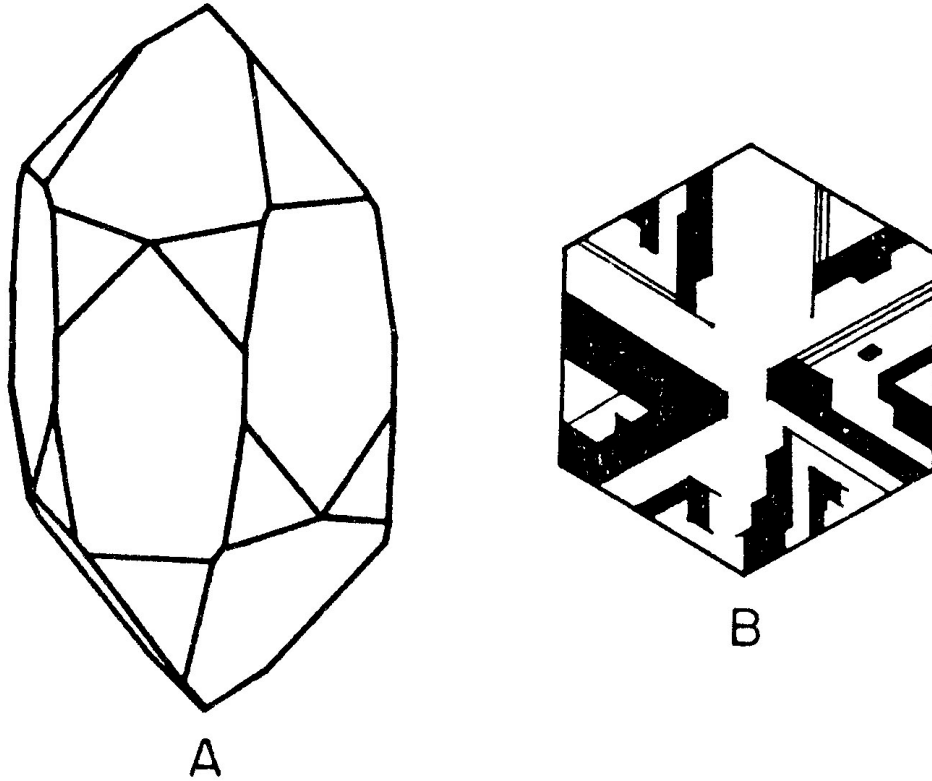
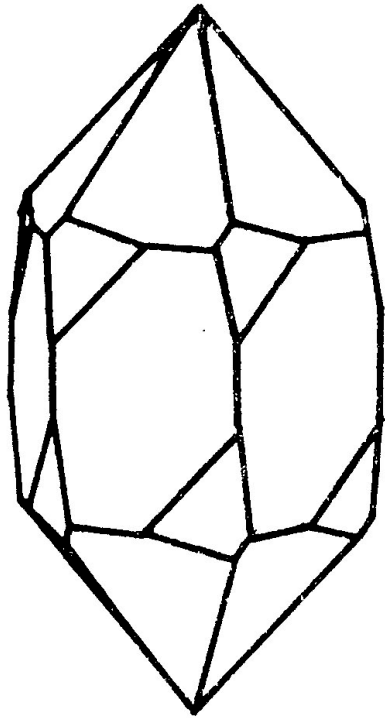


Fig. 200 Growth twinning (Brazil twinning) of quartz.
 A. The morphology of a Brazil twin: forms present; prism $\{10\bar{1}0\}$; rhombohedra $\{10\bar{1}1\}$ and $\{01\bar{1}1\}$ and trigonal trapezohedra $\{51\bar{6}1\}$.
 B. An etched basal section showing plane composition surfaces.



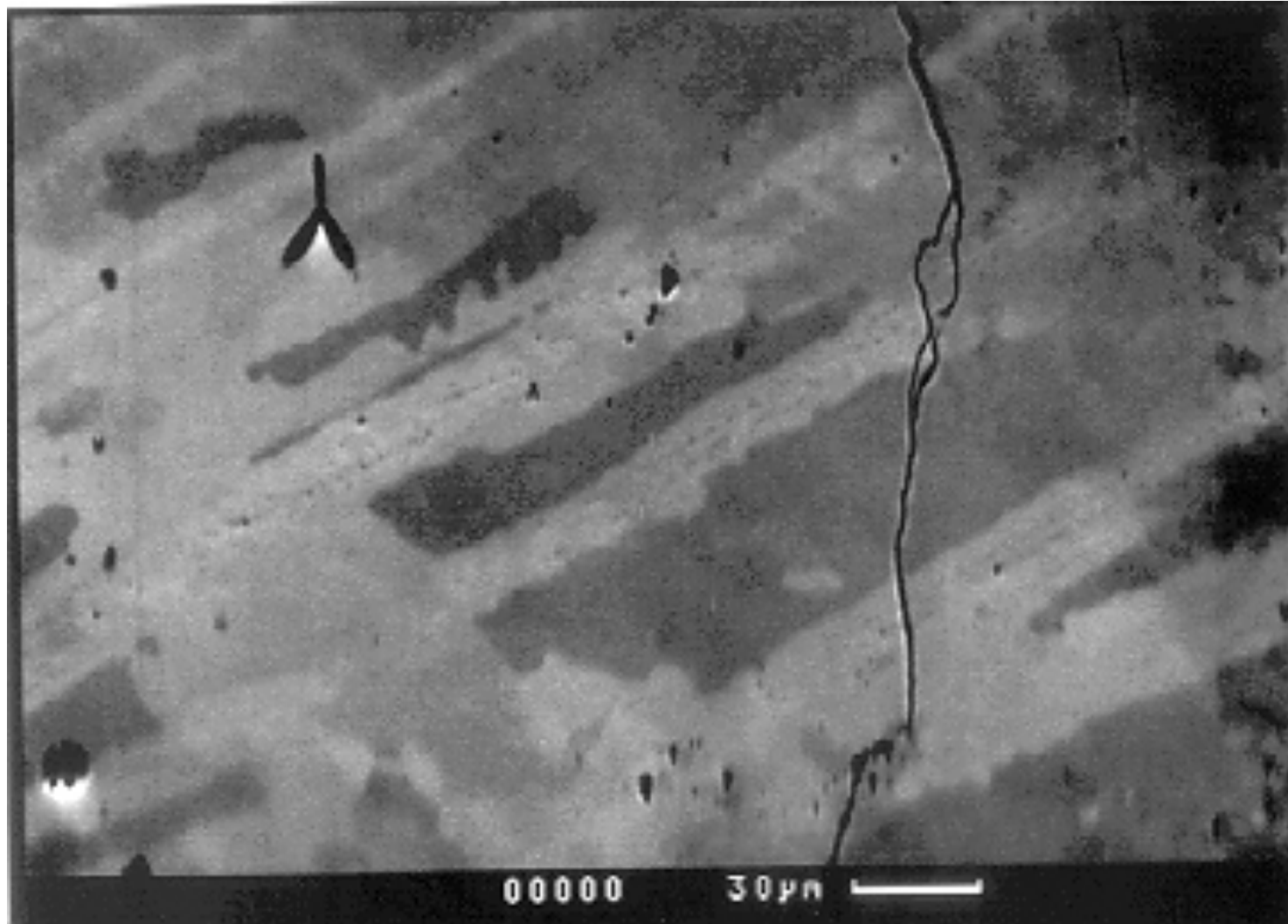
A



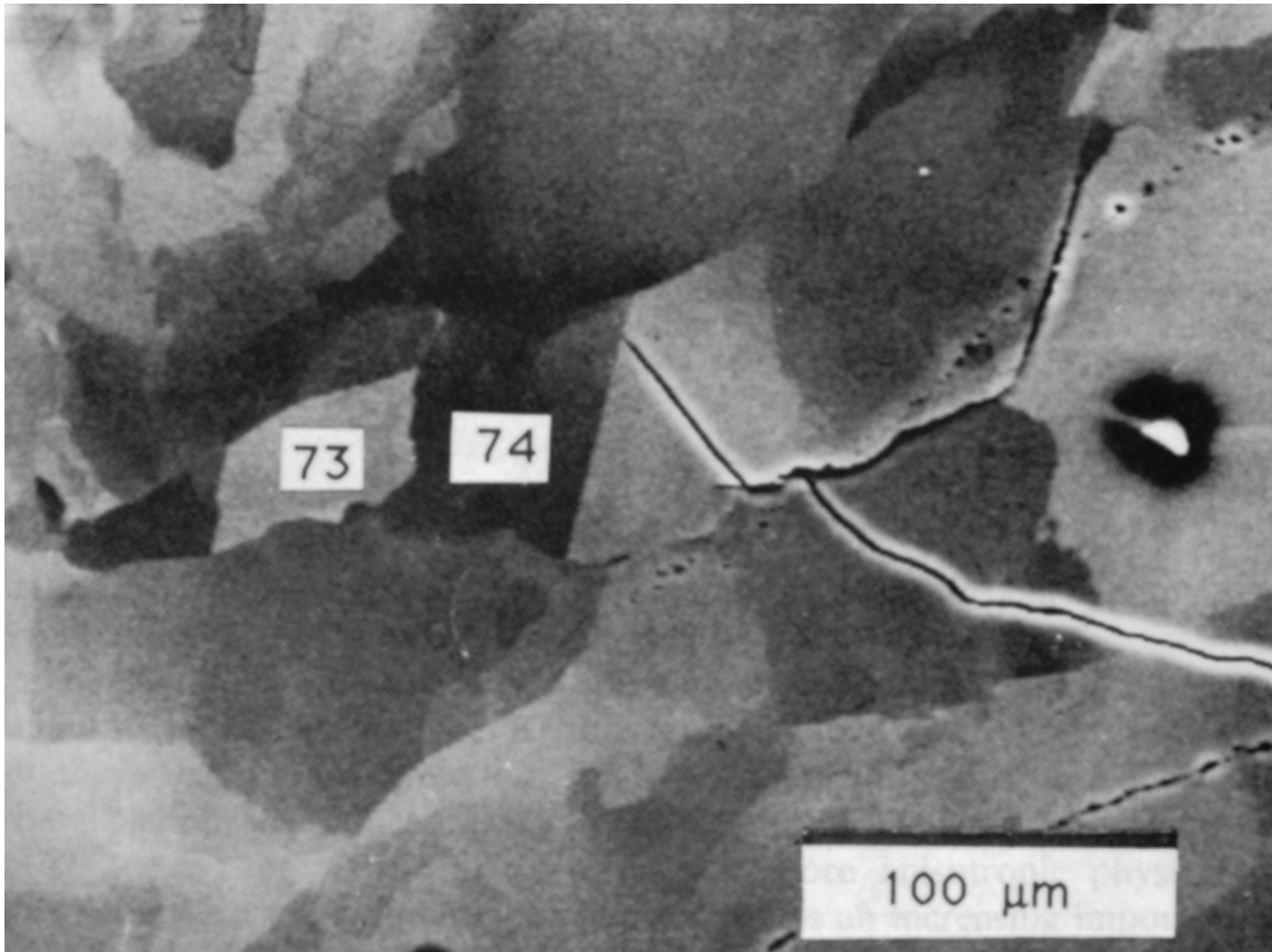
B

Fig. 202 Dauphiné twinning of quartz.
A. The morphology of a Dauphiné twin.
B. An etched basal section showing irregular composition surfaces.
Brazil twinning shown to right.

EBSD - forward scattering image : Dauphiné Twins



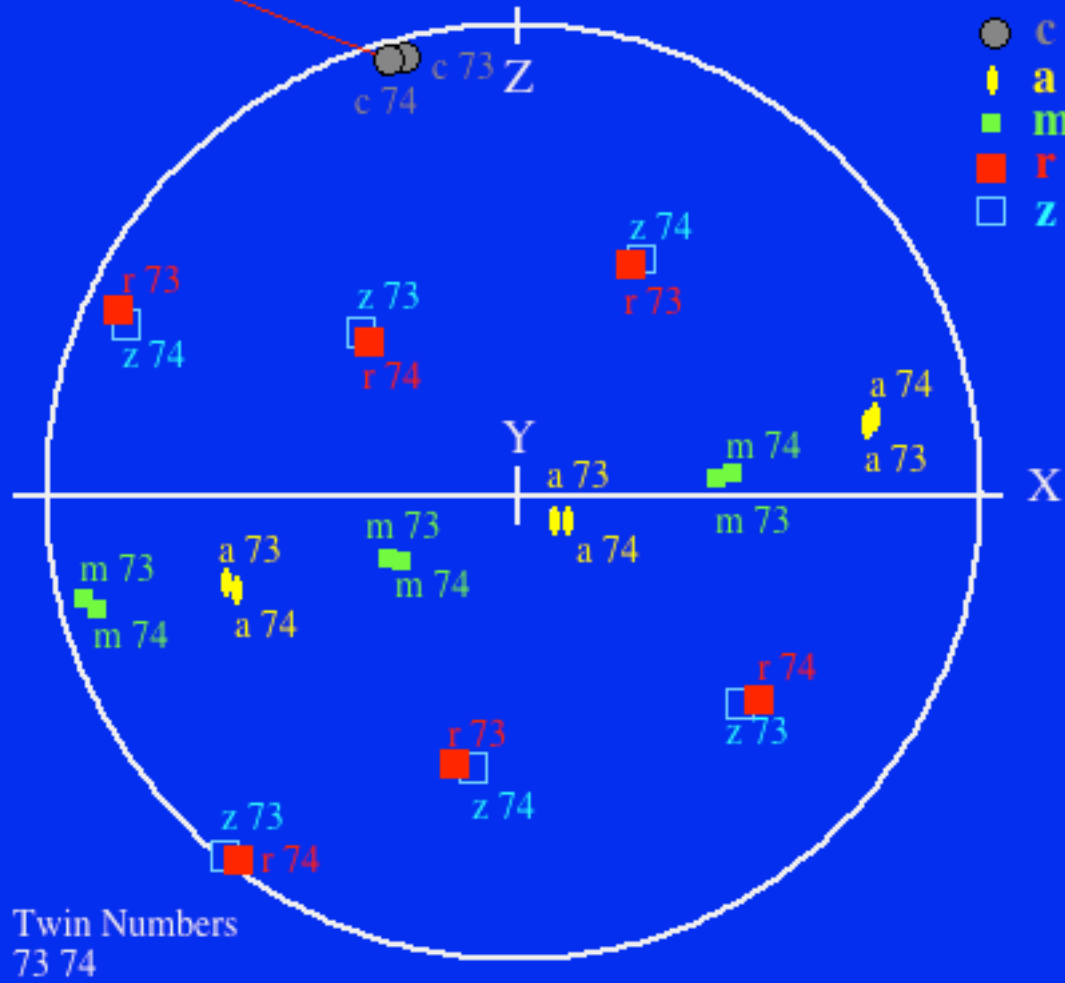
ECP orientation contrast of Dauphiné twins



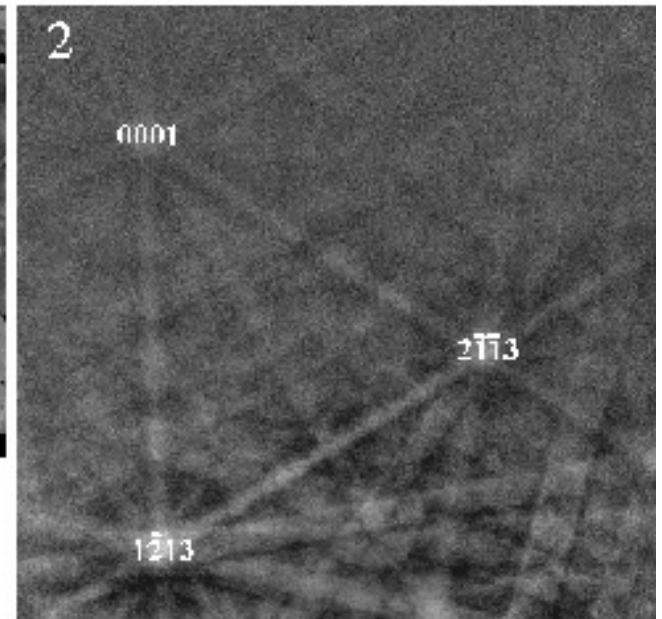
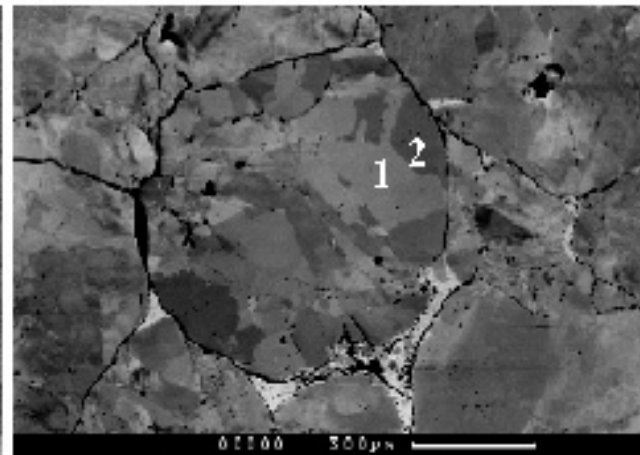
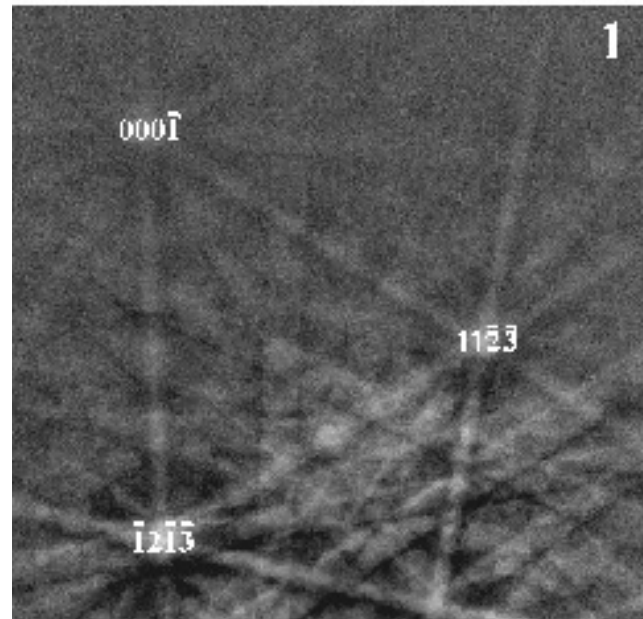
Mainprice, Lloyd and Casey 1993

Dauphiné Twin related orientations

rotation axis [-0.00 0.03 -0.03 1.85] / 61.99 °

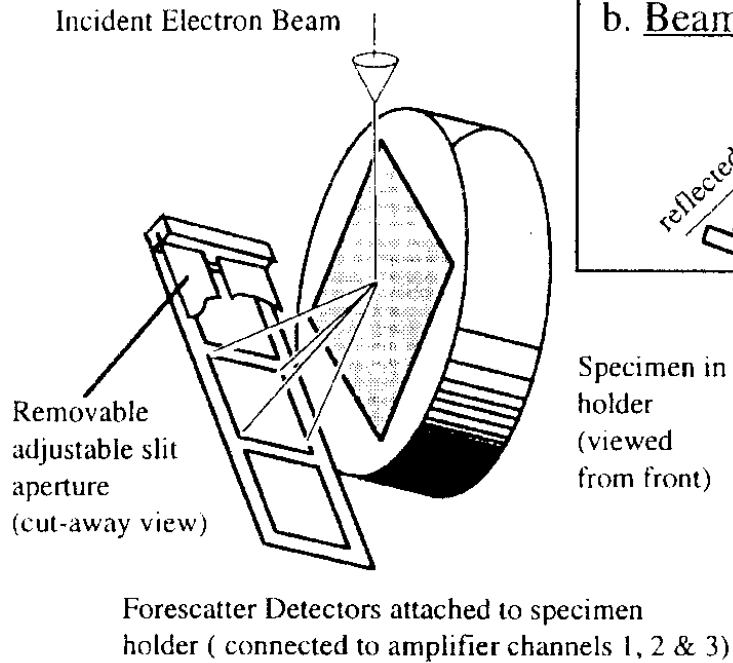


Quartz : - Indexing Dauphiné Twins

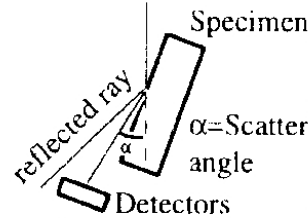


EBSP EULER ANGLES			
	Psi1	Phi	Psi2
Grain 1	68	165	77
Grain 2	68	165	18

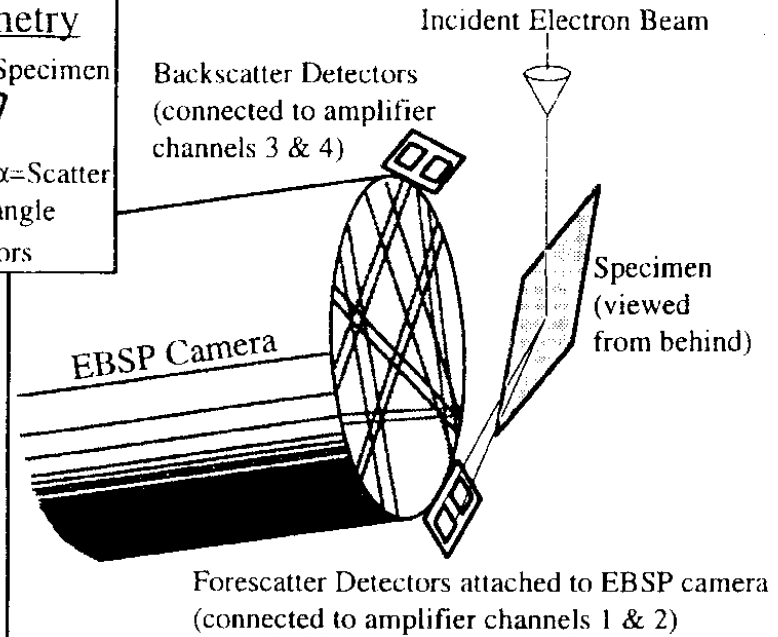
a. Forescatter Detector Geometry 1

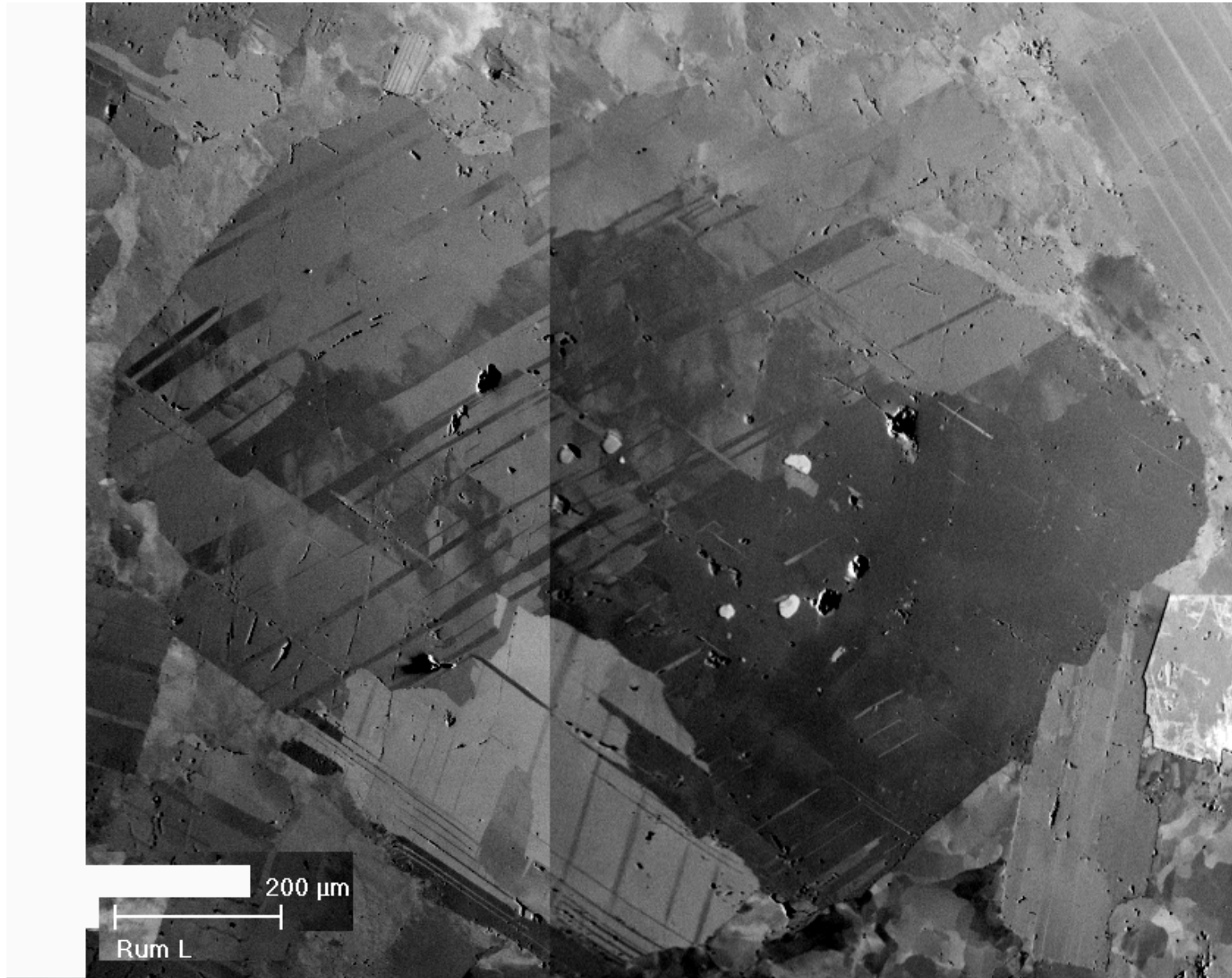


b. Beam Geometry



c. Forescatter Detector Geometry 2

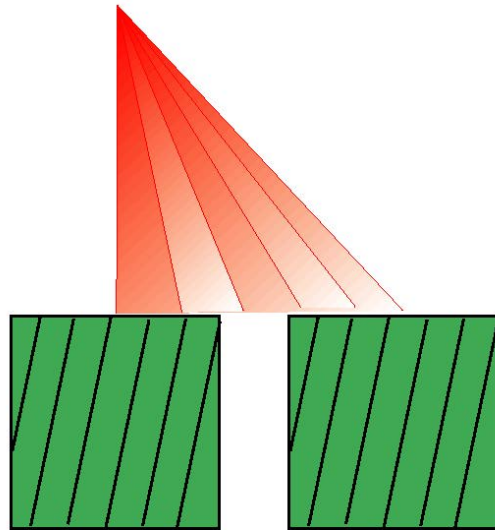




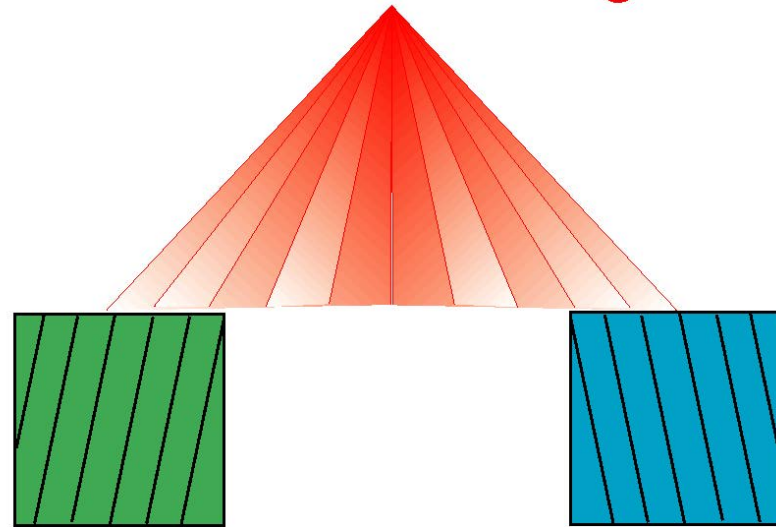
Feldspar forward scattered image Dr. David Prior (Liverpool,UK)

Orientation contrast images are not quantitative

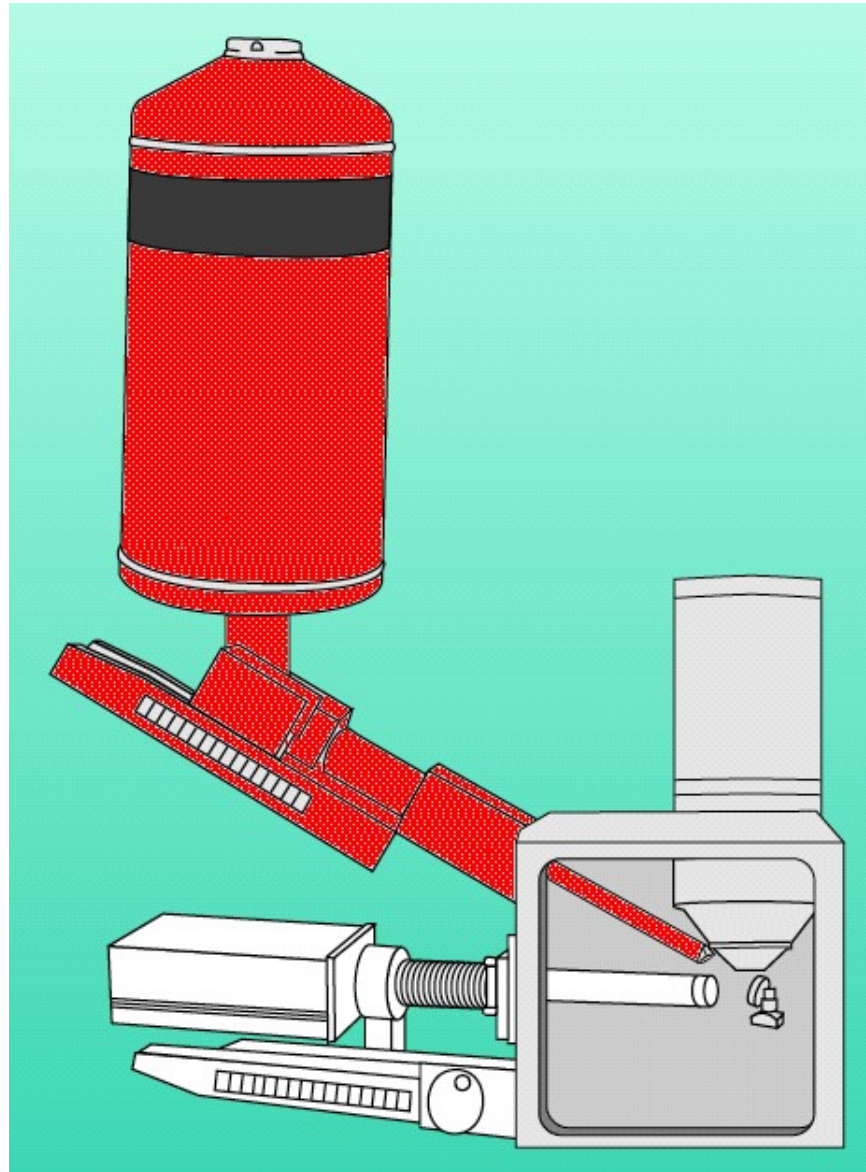
Two grains of the **same orientation**
can have **different signals**



Two grains of **different orientation**
can have the **same signal**

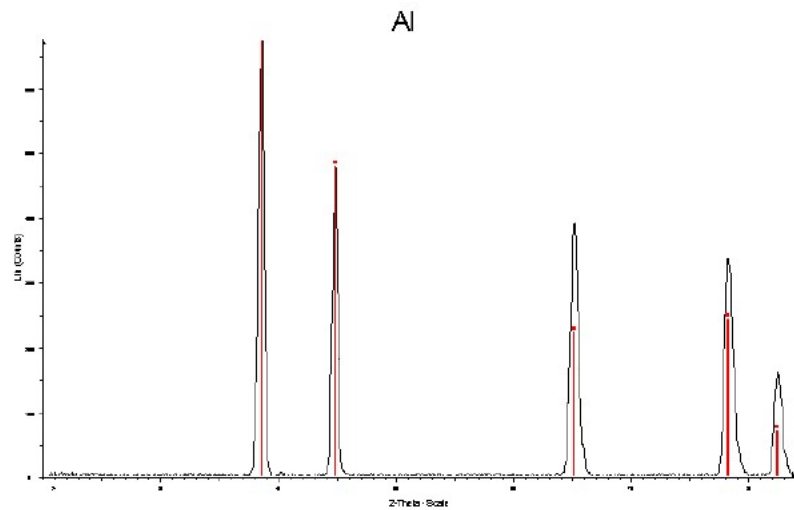


EDS X-ray detector and EBSD



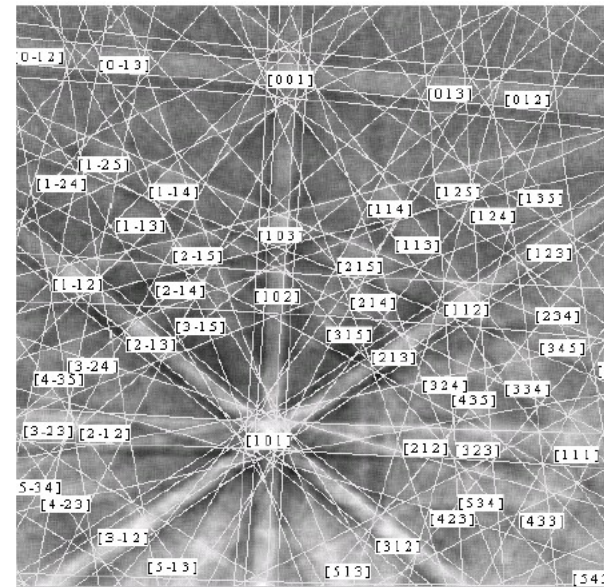
Phase ID : EDS + EBSD

EDS data

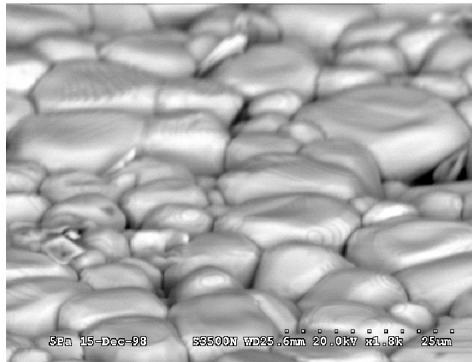


XRD also identifies the same ICDD Card #4-787 for Aluminum.

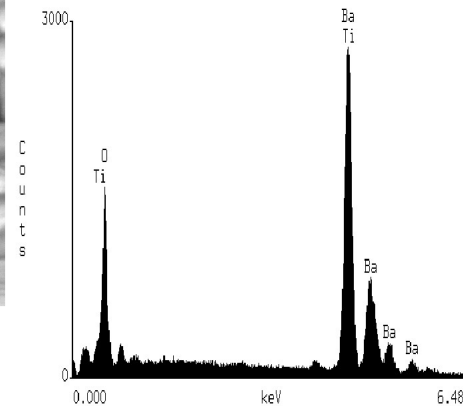
EBSD data



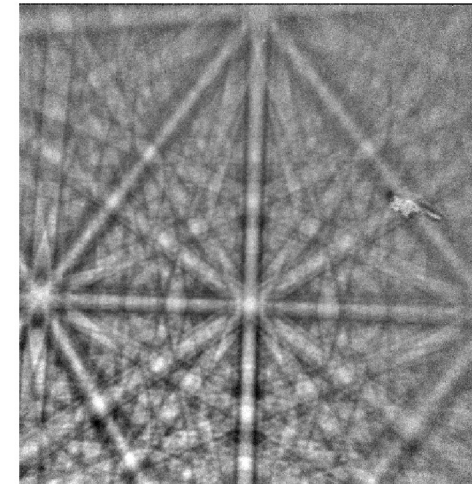
Example - BaTiO₃ powder



SEM image of compressed powder sample (70 degree tilt).



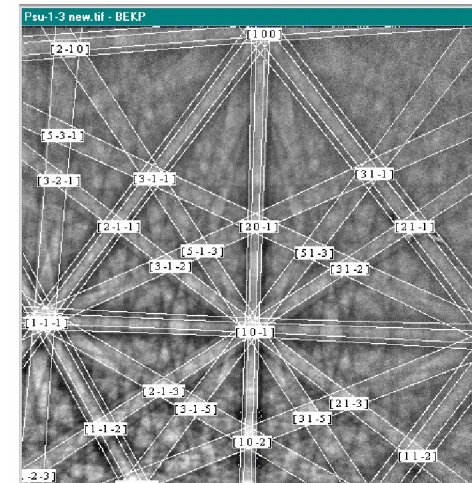
EDS spectrum of compressed powder sample.



Pattern of compressed powder sample.

Data for card #05-0626			
Crystal Identification			
Card #:	05-0626	Entry #:	2 of 101 found.
Name:	Barium Titanium Oxide		
Mineral:			
Formula:	Ba Ti O3		

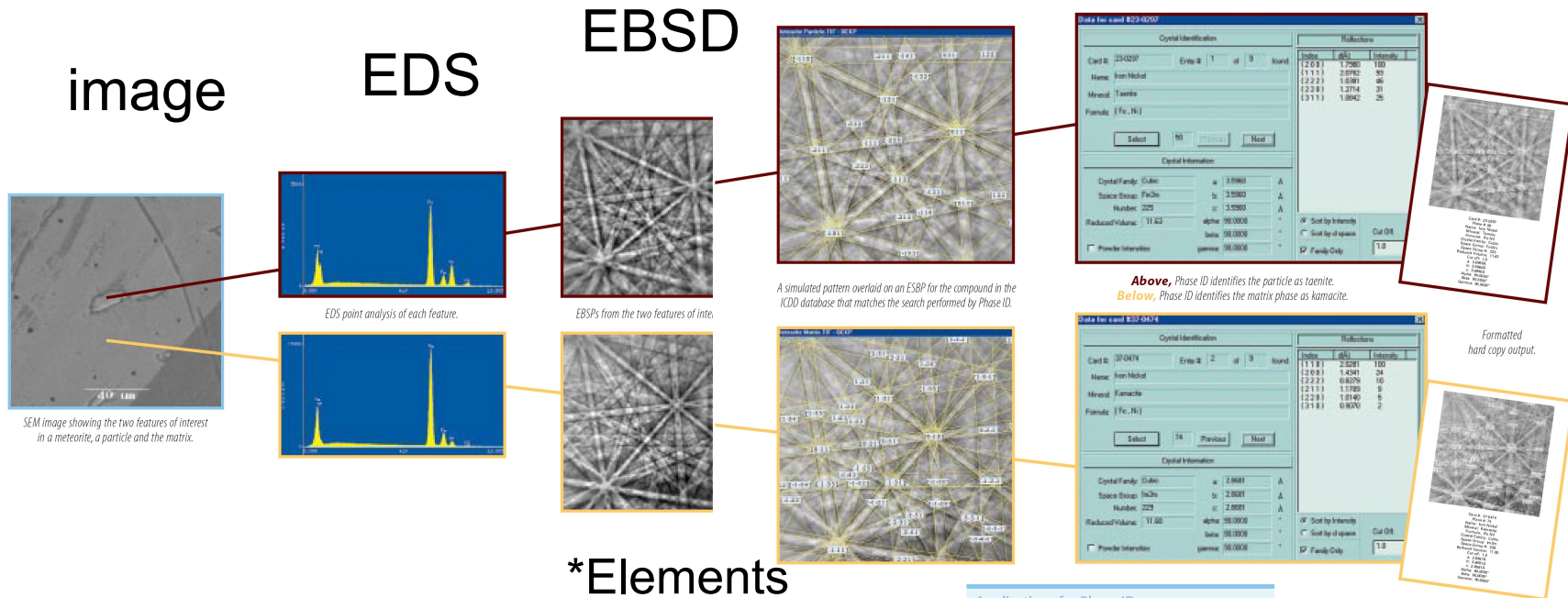
Summary of selected crystal: tetragonal Barium Titanium Oxide (BaTiO₃).



Simulation of BaTiO₃ overlaid on pattern.

'Real' Phase ID

INDEXING REPORT



- *Elements
- *D-space & angles
- HOLZ
- Pattern Symmetry
- Cell determination

Applications for Phase ID
The phase ID solution can be applied to many areas in materials analysis, including:

- Semiconductors
- Superconductors
- Ceramics
- Metals
- Minerals
- Composites
- Steels
- Super Alloys
- Films

* 'Classical' Phase ID
Compared with list of possible phases

1. What is EBSD ?
2. Symmetry and EBSD
- 3. Applications**
4. Future developments

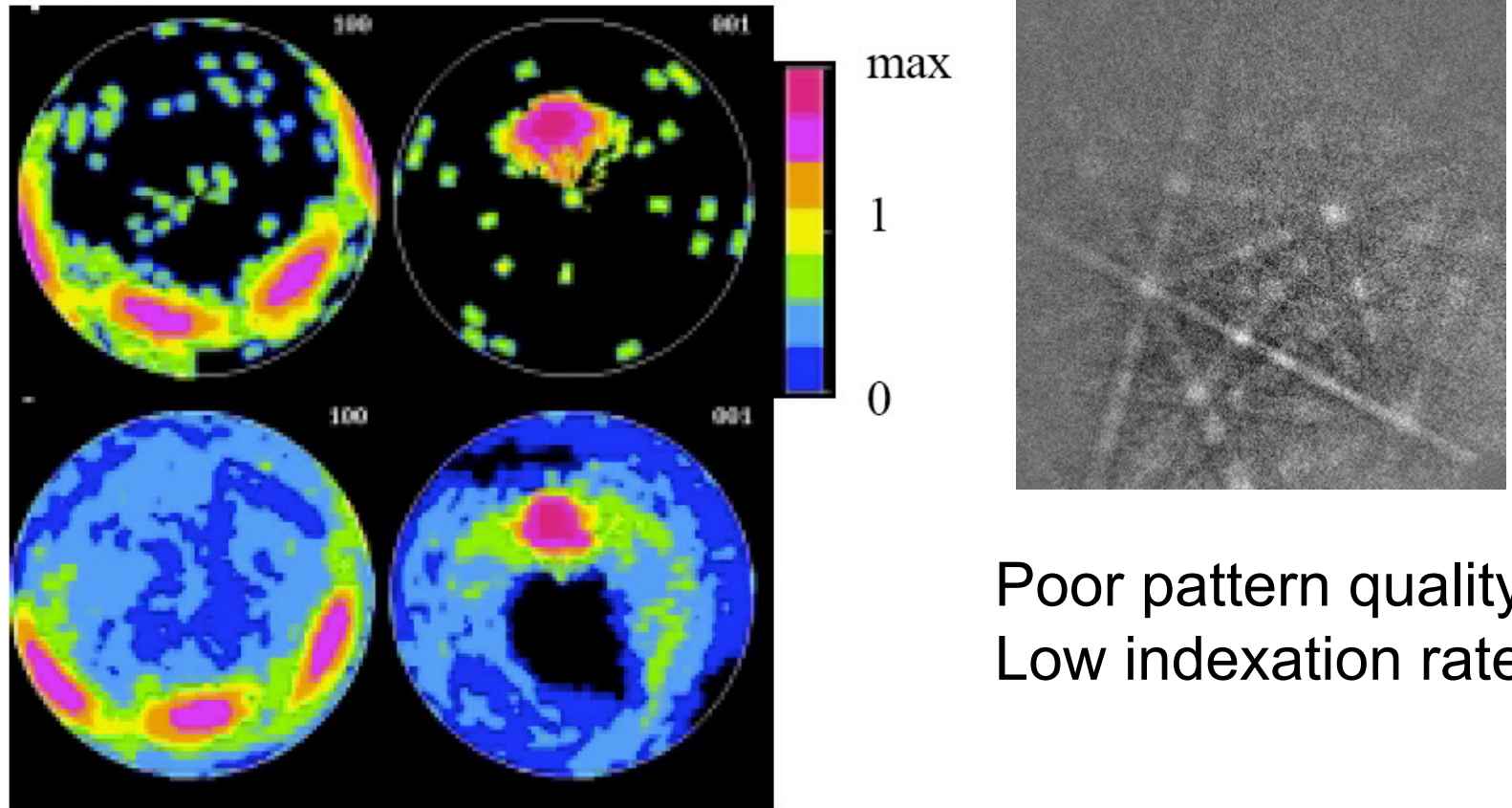
Applications of EBSD

1. Orientation of crystals (most common use).
2. Measuring elastic strain from diffraction pattern distortion -> elastic stress
3. Estimating plastic strain from quality of diffraction pattern.
4. Aiding phase identification (e.g. coupled with EDS X-rays).
5. Determination of lattice constants.

Table 2. Comparison of EBSD with conventional methods of quantitative metallography for a typical sample.

Application	Conventional technique(s)	Approximate EBSD data acquisition time (min)	Advantages of EBSD	Limitations of EBSD
Phase fractions (point count)	Optical SEM	20	Speed, Accuracy, Automation	Phases must diffract
Grain size (linear intercept)	Optical SEM	20	Speed, Accuracy, Automation, Boundary information	Requires undeformed or coarse subgrain structure
Grain size (image reconstruction)	Optical SEM + image analysis	120	Boundary characterization	Speed Requires undeformed or coarse subgrain structure
Boundary misorientation distributions (linear intercept)	TEM	20	Speed, Automation	Requires undeformed or coarse subgrain structure
Subgrain size (linear intercept)	TEM SEM	20	Speed Automation	Minimum size $\sim 2 \mu\text{m}$
Subgrain size (image reconstruction)	TEM SEM	120	Full characterization	Minimum size $\sim 2 \mu\text{m}$
Subgrain misorientation (linear intercept)	TEM	20	Speed Automation	Minimum size $\sim 2 \mu\text{m}$ Minimum misorientation $\sim 1^\circ$
Fraction recrystallized (point count)	Optical SEM	20		Requires careful calibration Unsuitable for many samples
Fraction recrystallized (linear intercept)	Optical SEM	20	Early stages of recrystallization	Requires coarse subgrain structure
Bulk texture (point count)	X-ray	20	Speed Through thickness measurements possible	Small samples Requires undeformed or coarse subgrain structure

Bio-materials - Mollusc shell



Poor pattern quality
Low indexation rate

{100} and {001} pole figures of *Crassostrea gigas*, obtained from EBSD (top row) and x-ray (bottom) analyses. Max = 100 m.r.d. Logarithmic density scale, equal area projections.

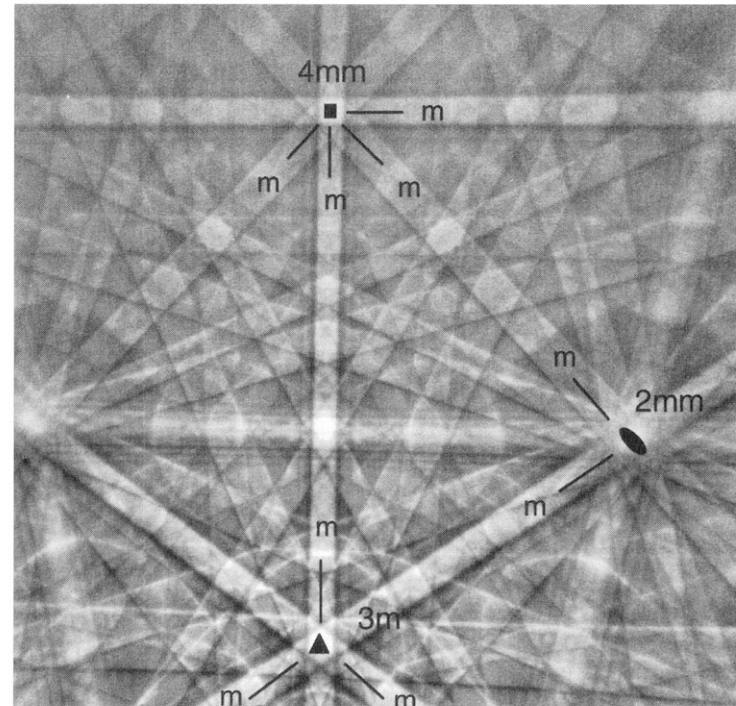
Aragonite

Daniel Chateigner HDR
2000

Pattern symmetry analysis : Silicon

Zone axes with 4mm, 3m and 2mm point group symmetries

Identification as m3m

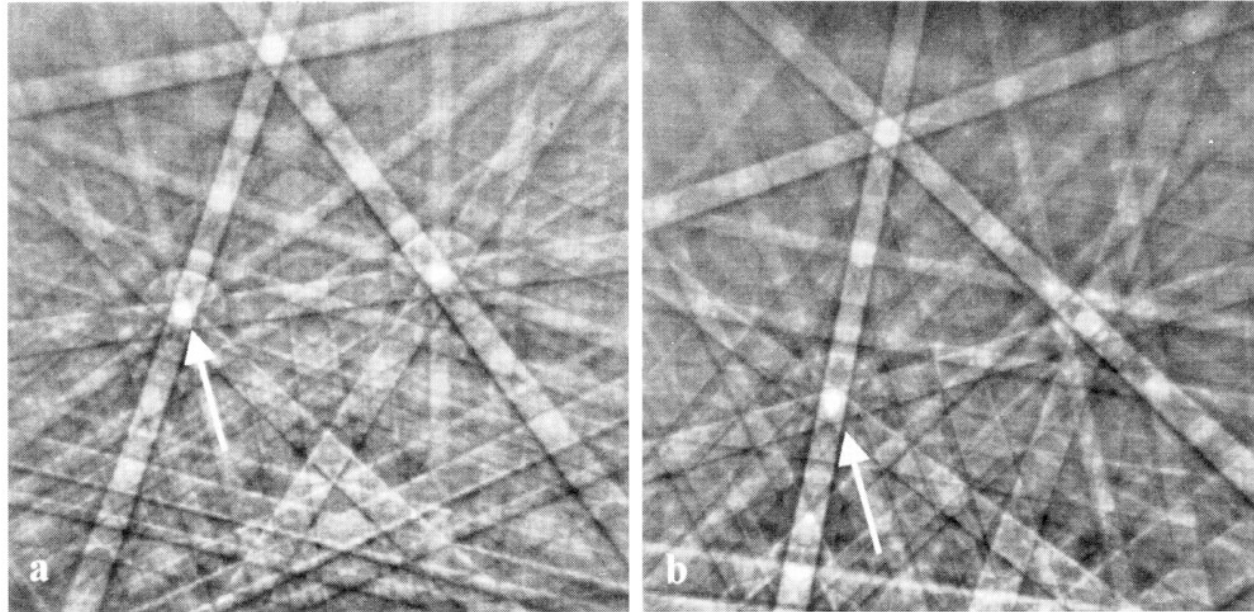


EBSD pattern of Si with symmetry axes indicated.

Some cubic whole pattern symmetries for EBSD point group determination.

Point Group	$\langle 111 \rangle$	$\langle 100 \rangle$	$\langle 110 \rangle$	$\langle uu0 \rangle$	$\langle uuw \rangle$	$\langle uvw \rangle$
m3m	3m	4mm	2mm	m	m	1
43m	3m	2mm	m	1	m	1
432	3	4	2	1	1	1

Polymorphs - SiC using HOLZ rings



EBSD patterns obtained from two polytypes of SiC. The HOLZ rings analyzed are indicated by arrows. (a) EBSD pattern from 6H polytype, and (b) EBSD pattern from 15R polytype.

6H polymorph (1.858nm) 15R polymorph (1.545nm)

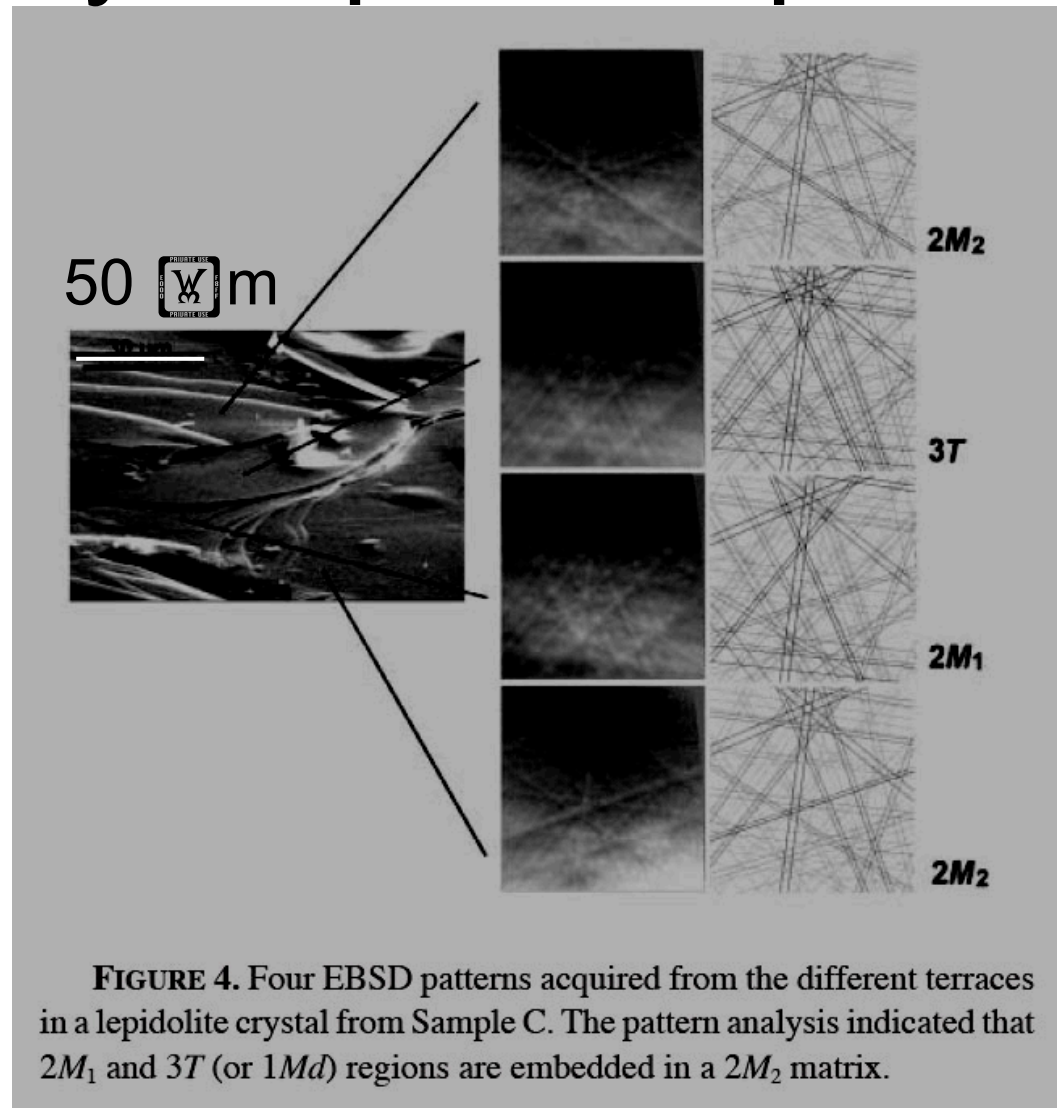
UVW = 2 4 1

UVW = 10 5 1

J.R. Michael & J.A. Eades (2000) Ultramicroscopy

Polymorphs - Lepidolite

Lithium
rich
mica



AFC Toulouse 2006

Kogure & Bunno 2004 AM

Exsolution : Diopside in Wollastonite

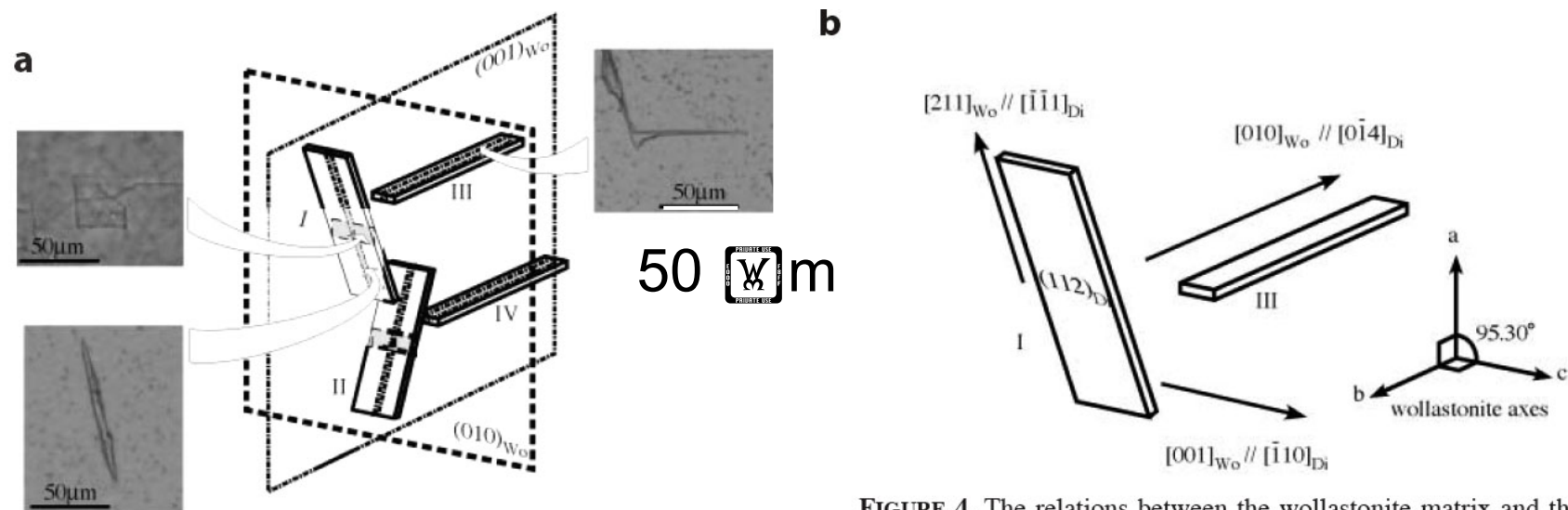


FIGURE 4. The relations between the wollastonite matrix and the diopside lamellae. (a) Shapes of the lamellae and the cross section (optical microscopy) and (b) the detailed crystallographic relation (see context).

Wollastonite - CaSiO_3 pyroxenoid

Diopside - $\text{CaMgSi}_2\text{O}_6$ pyroxene

Seto et al 2006 AM

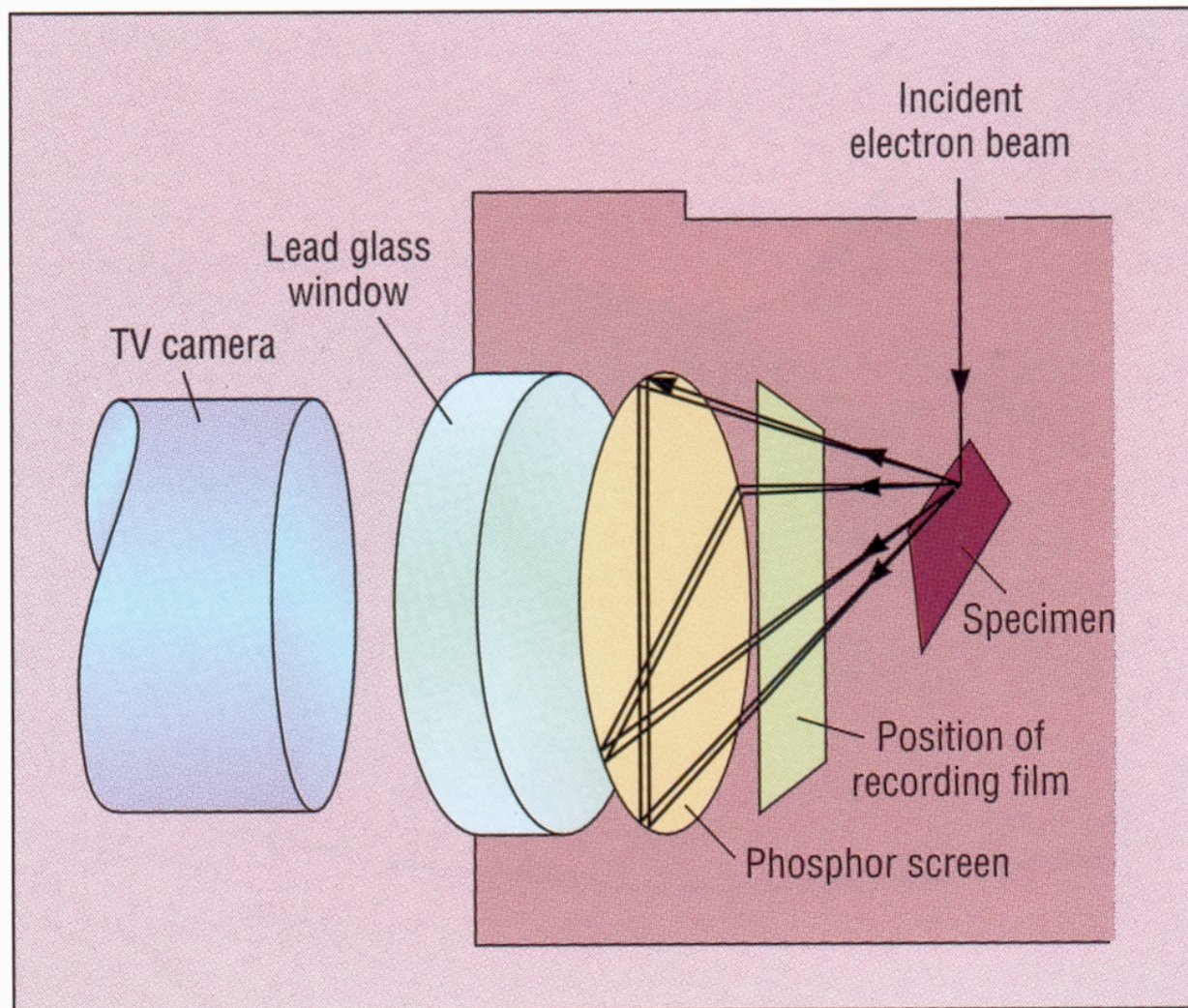
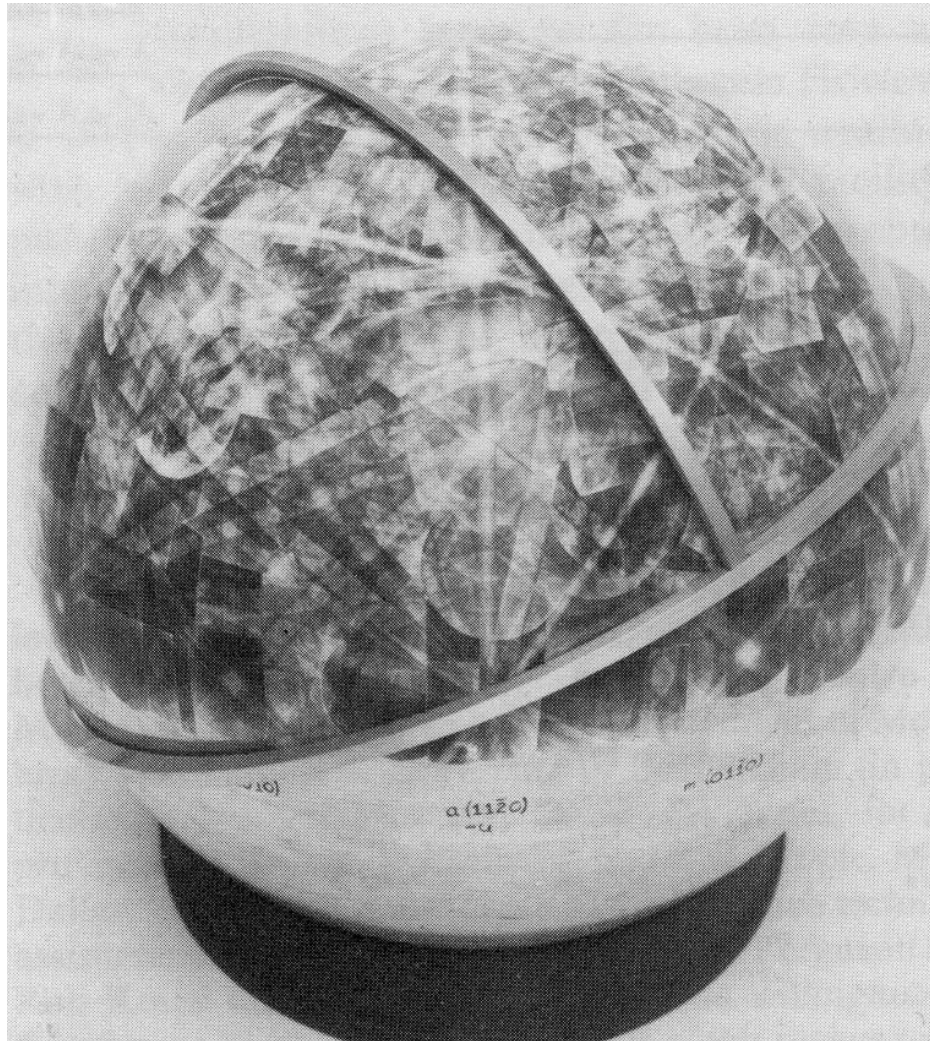


Figure 1. Schematic diagram for detection of EBSD patterns.

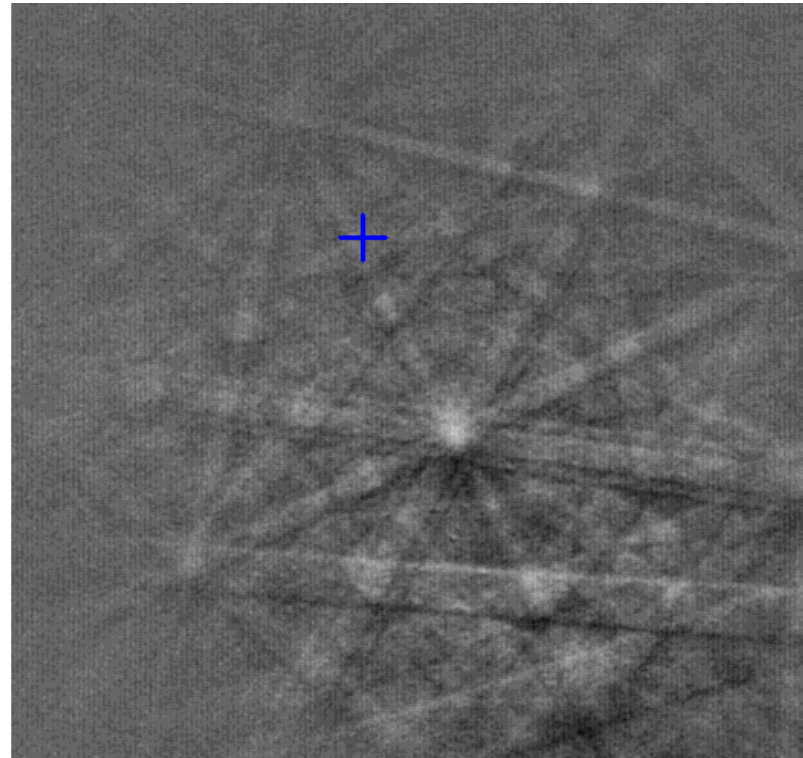
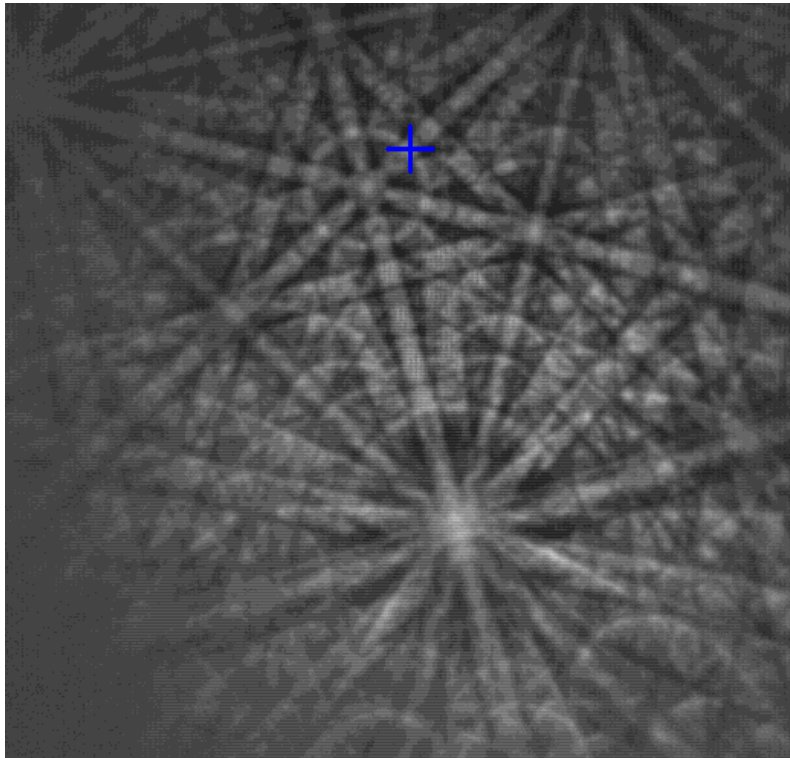
Quartz Sphere

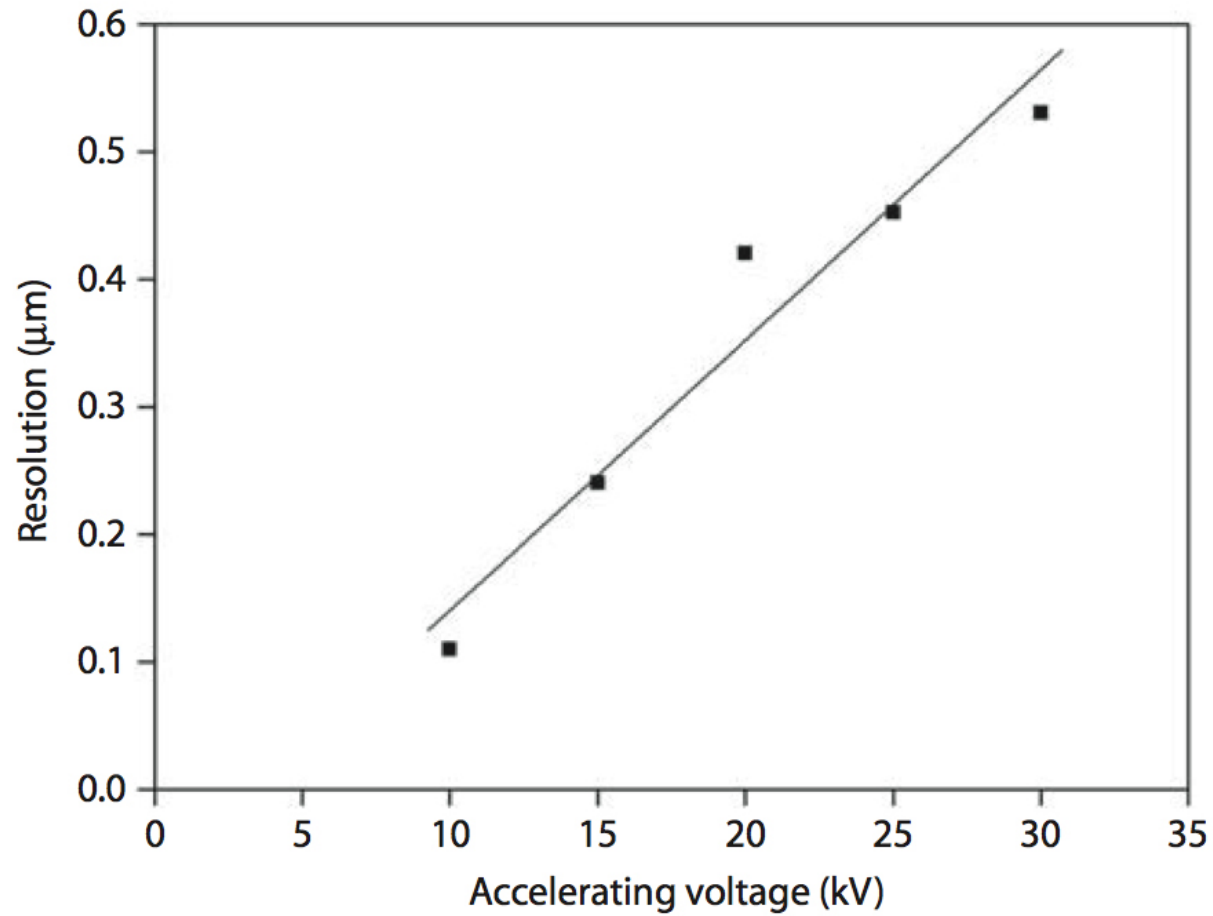


Indexing: The basis of this is to match a sample EBSP to some knowledge of all possible EBSPs for the crystal structure of interest

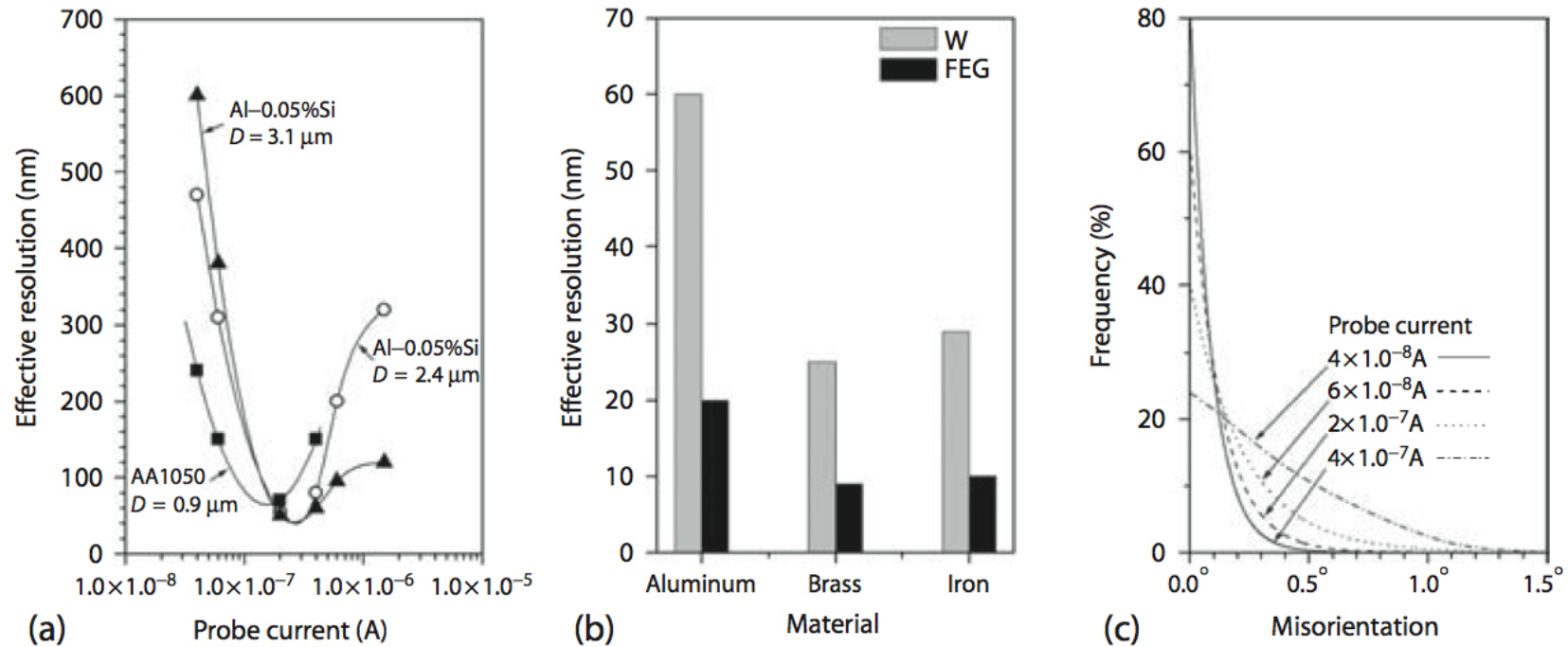
ECP « globe » for quartz
by
Geoff Lloyd (Leeds, UK)

Automatic indexing is now possible





Spatial resolution of EBSD in nickel as a function of accelerating voltage. (Adapted from Drake, A. and Vale, S.H., *Inst. Phys. Conf. Ser. 147*, 137, Inst. Phys. Pub. Inc., Bristol, 1995.)



(a) The effect of probe current on effective resolution for several aluminum specimens. The minima in the plots are caused by the reduced pattern-solving accuracy at low probe currents. (From Humphreys, F. J. et al., *J. Microsc.*, 195, 212, 1999.) (b) Effective EBSD spatial resolution for various metals in tungsten filament and FEG SEMs. (From Humphreys, F.J., *Scripta Mater.*, 51, 771, 2004.) (c) Misorientation measurements between adjacent points on a single-crystal silicon specimen for four different probe currents (in amperes). The highest-probe current provides the most accurate result. (Courtesy of F. J. Humphreys.)

EBSD Mapping

Crystallographic Mapping of Kimberlite xenolith : beam scanning

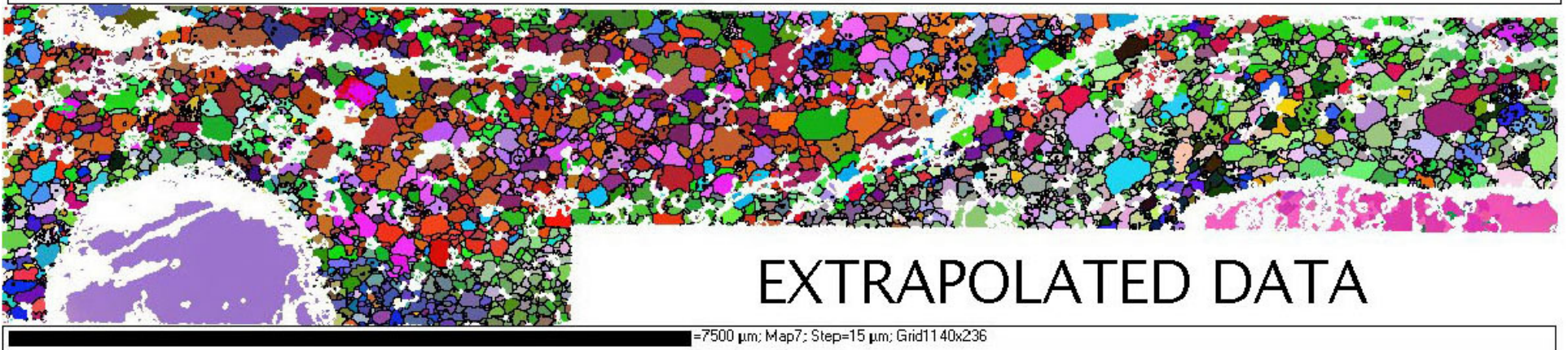
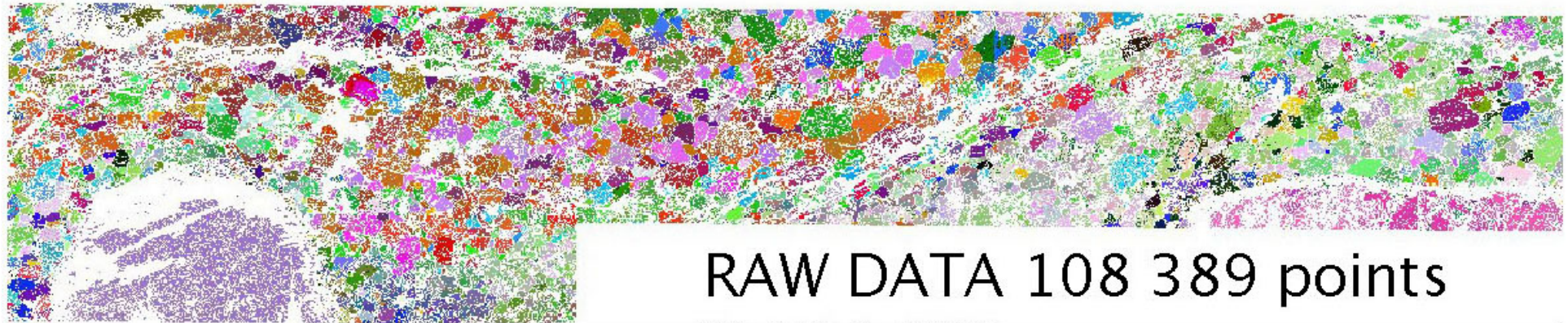


Raw data on SEM image

Raw Orientation Map

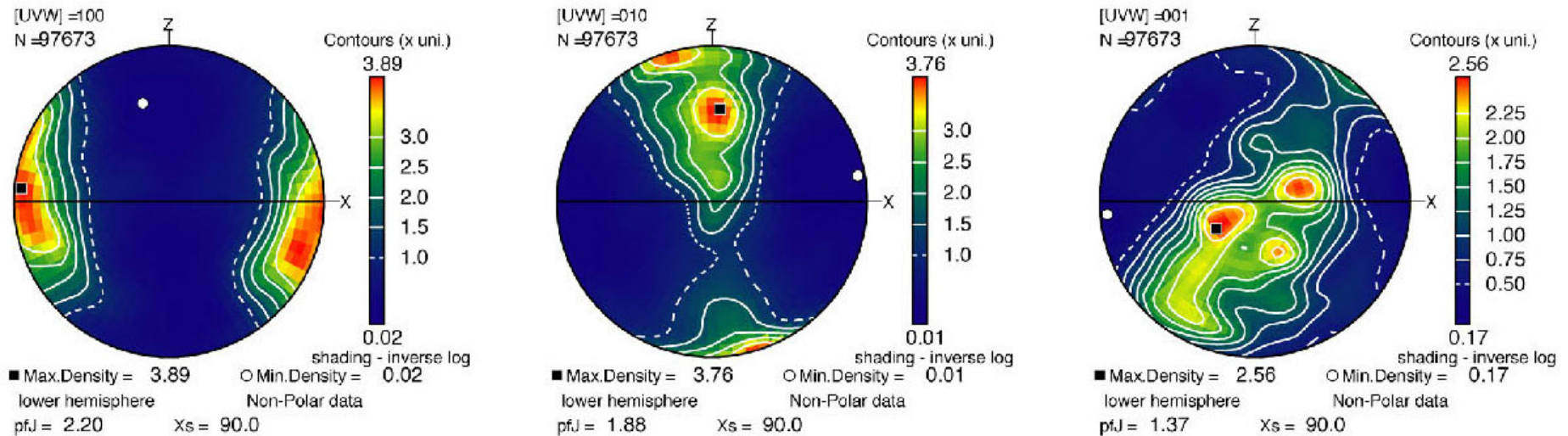
Extrapolated Map

Crystallographic Mapping of Kimberlite xenolith

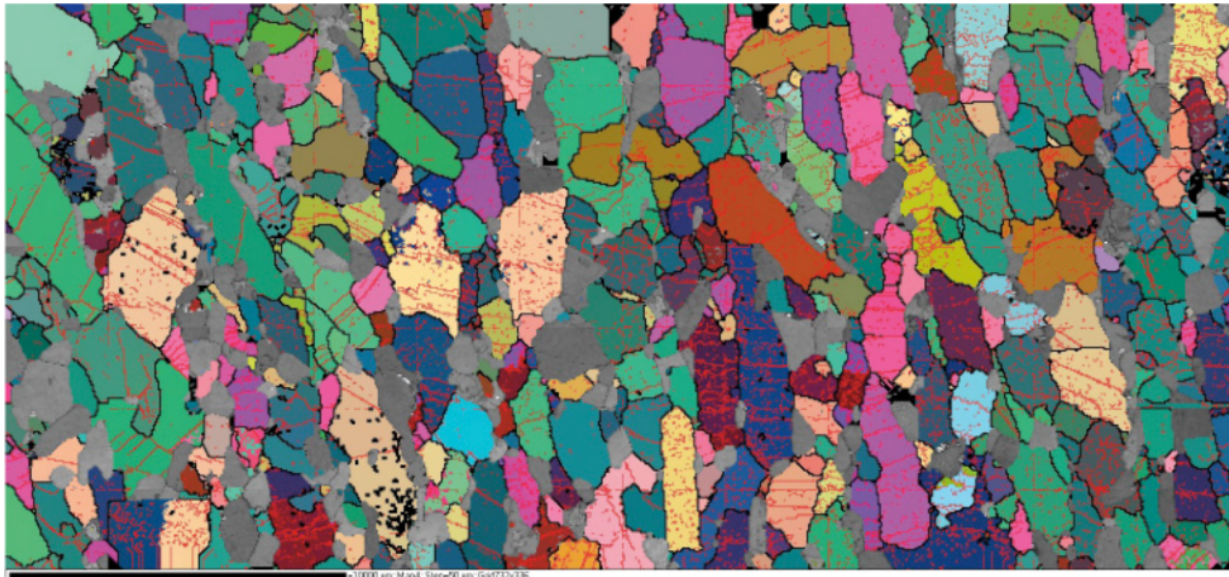


Kimberlite Xenolith

[100],[010] & [001] Olivine pole figures

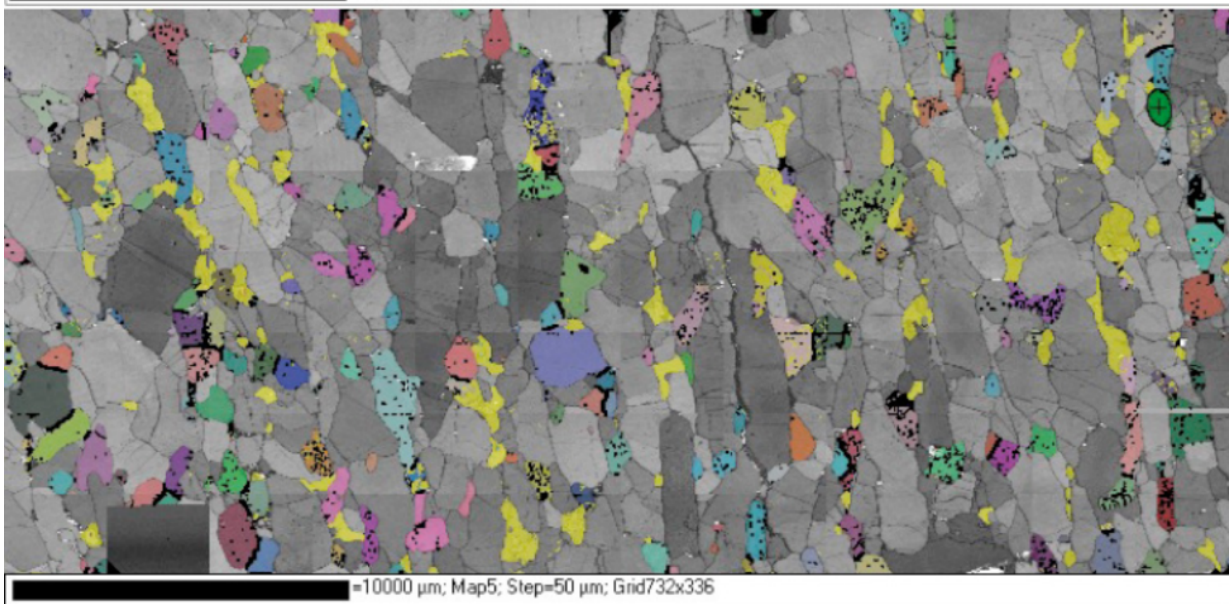


Current level of EBSD mapping



Olivine -
coloured by
orientation

Cpx – grey level
by band contrast



Cpx – coloured
by orientation

Olivine – grey
level by band
contrast

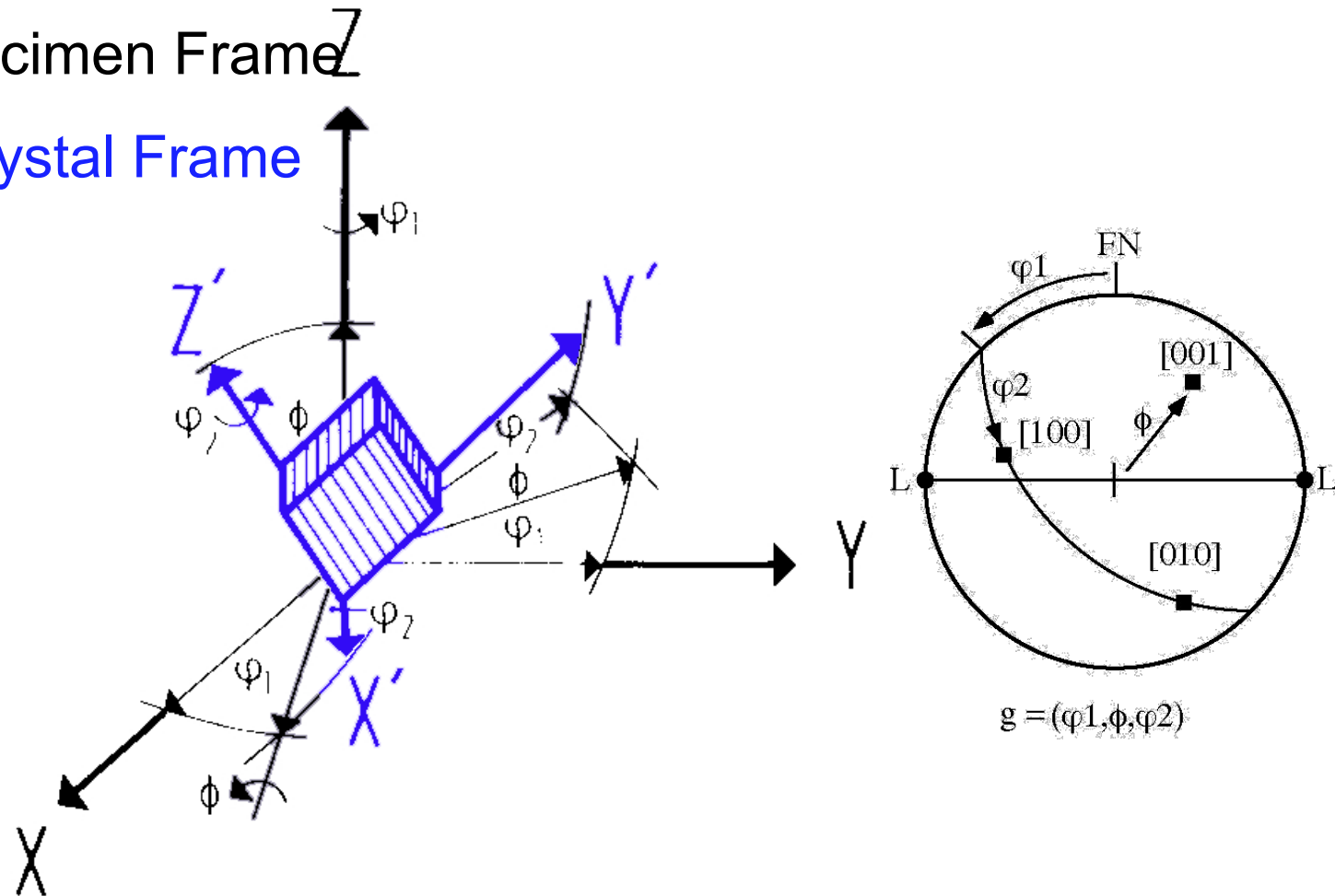
9510-16 Low cpx lherzolite

1cm scale bar 50 micron steps

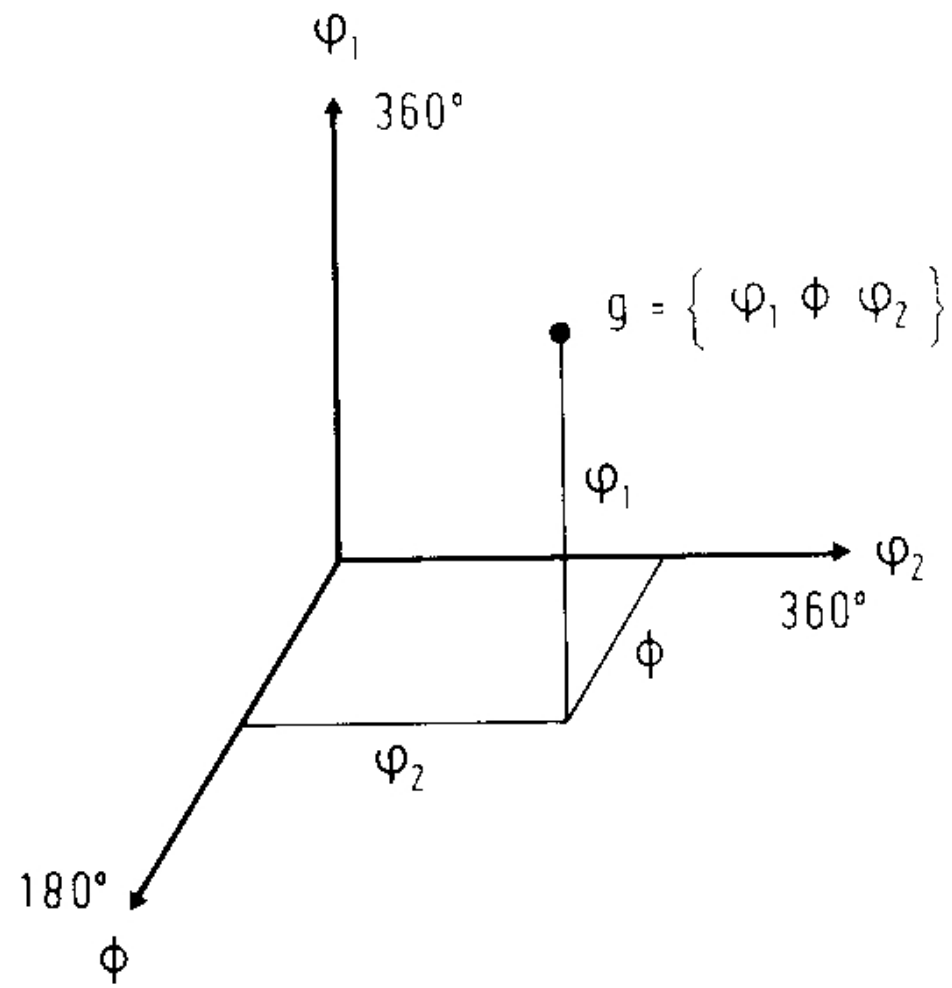
Orientation of a crystal defined by 3 Euler angles

XYZ - Specimen Frame

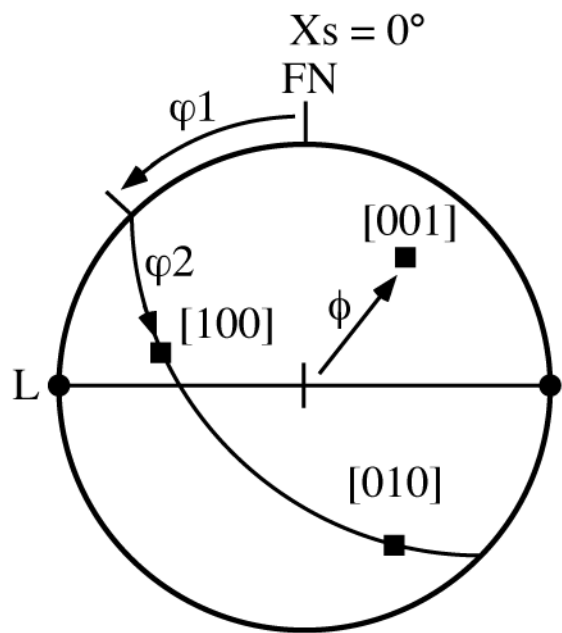
X'Y'Z' - Crystal Frame



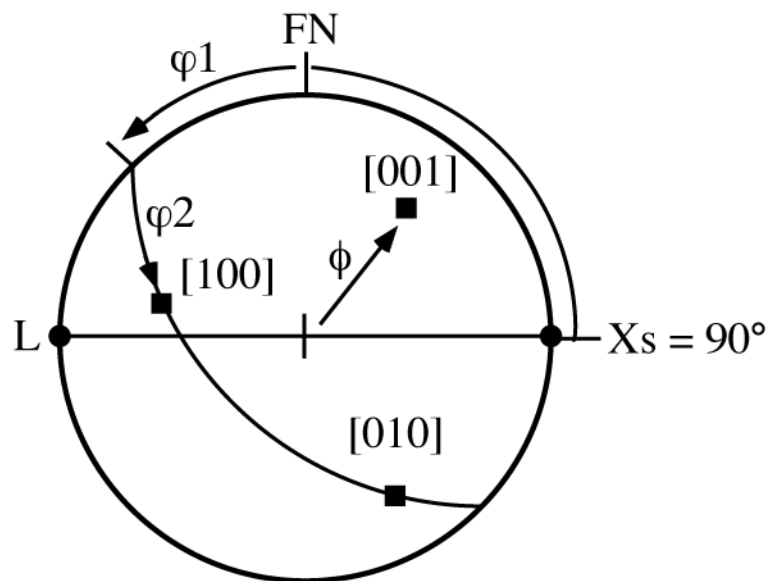
Beware there many different conventions - here the convention of Bunge (1982)



Euler Angles



$X_s = 0^\circ$ azimuth



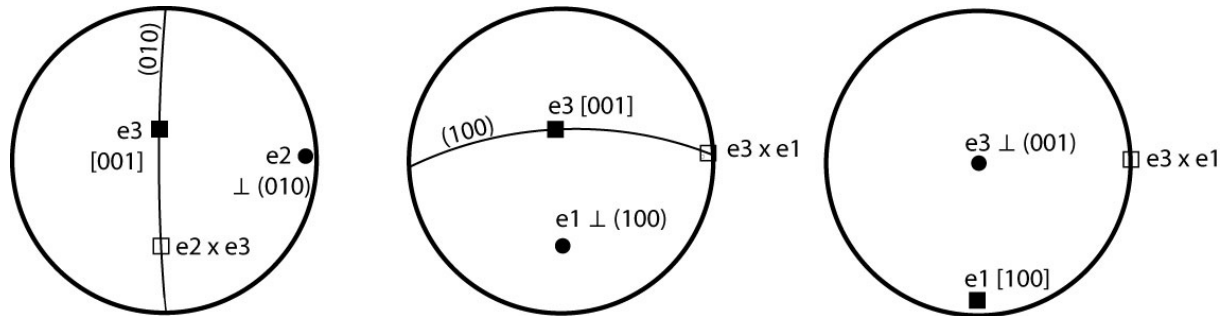
$X_s = 90^\circ$ azimuth

Cartesian Reference Frame I

- Measurement of orientation using Euler angles requires the definition of a right-handed Cartesian (also called orthonormal) system in crystal co-ordinates.
- For cubic, tetragonal and orthorhombic the obvious choice is to use the orthogonal lattice basis vectors **a**[100], **b**[010] and **c**[001] of the crystal axes. However, for most general case of triclinic crystal symmetry where **a**, **b**, and **c** are not orthogonal, there are many possible choices and no general convention.
- The choice of a specific reference frame is often imposed by the EBSD software, but users are often not aware what choice has been made.

Cartesian Reference Frame II

- Here are 3 possible choices, for the tensor Cartesian reference frame for Euler angles $(\mathbf{e}_1, \mathbf{e}_2, \mathbf{e}_3)$;
- a) $\mathbf{e}_3 = \mathbf{c}[001]$, $\mathbf{e}_2 = \mathbf{b}^* \perp (010)$ and hence for a right-handed system $\mathbf{e}_1 = \mathbf{e}_2 \times \mathbf{e}_3$ (e.g. BearTex software)
- b) $\mathbf{e}_3 = \mathbf{c}[001]$, $\mathbf{e}_1 = \mathbf{a}^* \perp (100)$ and $\mathbf{e}_2 = \mathbf{e}_3 \times \mathbf{e}_1$ (e.g. HKL Channel software)
- c) $\mathbf{e}_3 = \mathbf{c}^* \perp (001)$, $\mathbf{e}_1 = \mathbf{a}[100]$ and $\mathbf{e}_2 = \mathbf{e}_3 \times \mathbf{e}_1$



Reference Frames a), b) and c) for triclinic plagioclase Labradorite An66
 ($\mathbf{a}=0.817$ nm $\mathbf{b}=1.287$ nm $\mathbf{c}=1.420$ nm $\alpha=93.46^\circ$ $\beta=116.09^\circ$ $\gamma=90.51^\circ$)

Orientation Distribution Function & J index

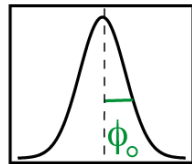
Measured ODF : $f(g)$ - series of individual orientations $g_1, g_2, g_3 \dots g_n$

$$g = \{\varphi_1 \ \phi \ \varphi_2\} \quad dV/V = f(g) dg \quad \int f(g) dg = 1 \quad dg = d\varphi_1 d\phi d\varphi_2 \sin \phi / 8\pi^2$$

$$J = \int f(g)^2 dg$$

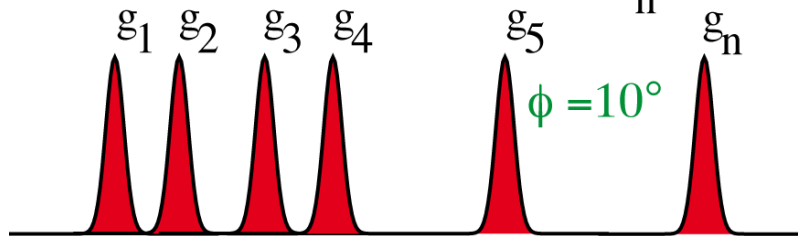
1-D Representation

Gaussian angle ϕ_0

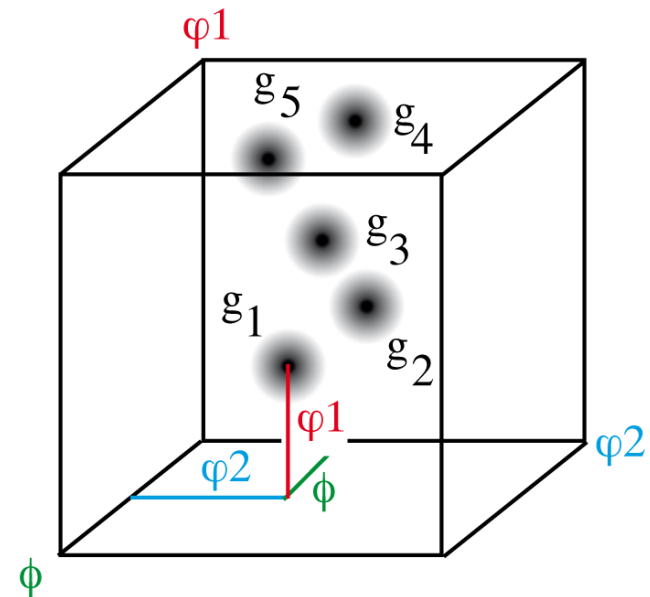


g_n

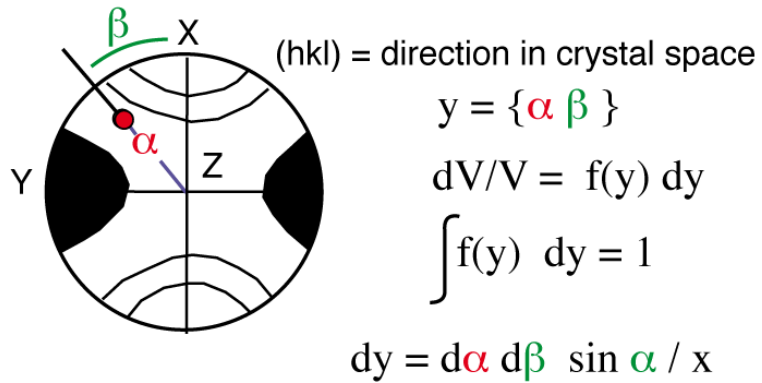
Individual orientations (g_n)



3-D Representation



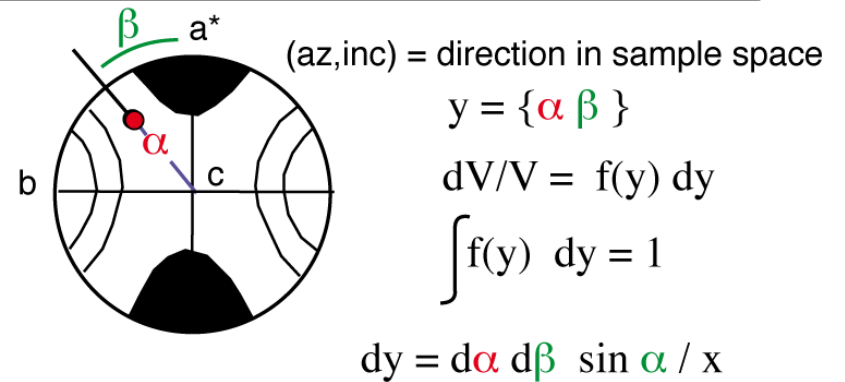
Definition of pole figure & Jpf index



for a hemisphere $x = 2 \pi$
 and a sphere $x = 4 \pi$

$$J_{pf} = \int f(y)^2 dy$$

Definition of inverse pole figure & Jipf index

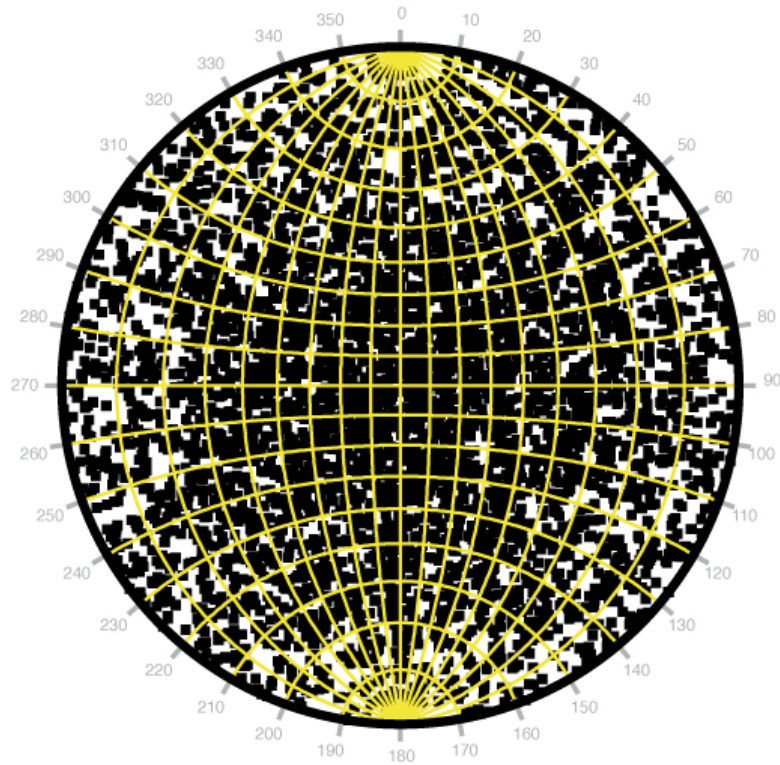


for a hemisphere $x = 2 \pi$
 and a sphere $x = 4 \pi$

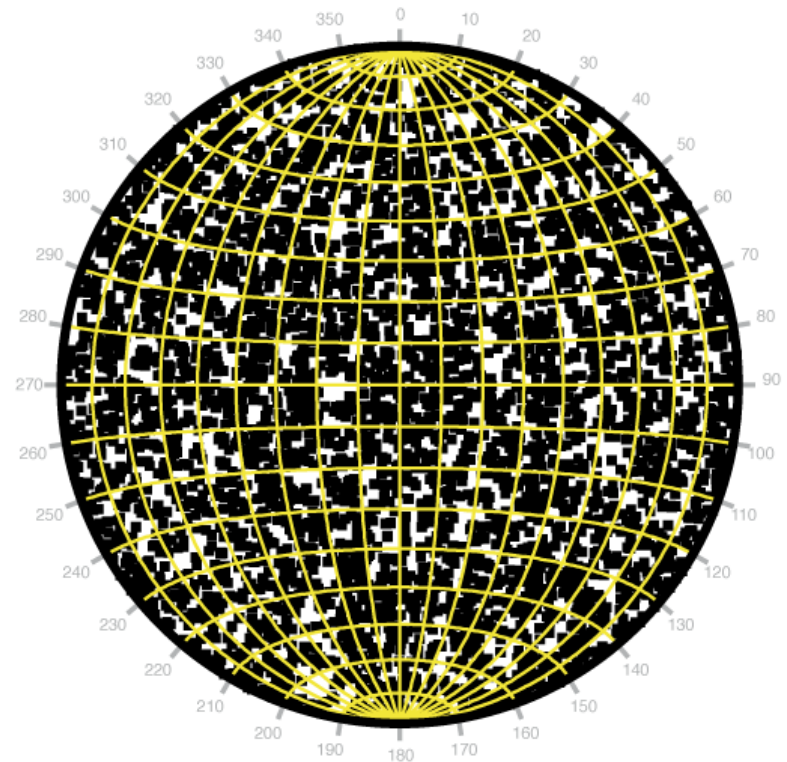
$$J_{ipf} = \int f(y)^2 dy$$

5000 Random orientations

Equal angle pole figure



Equal area pole figure



Rotation axis/angle; $[uvw]/\theta$

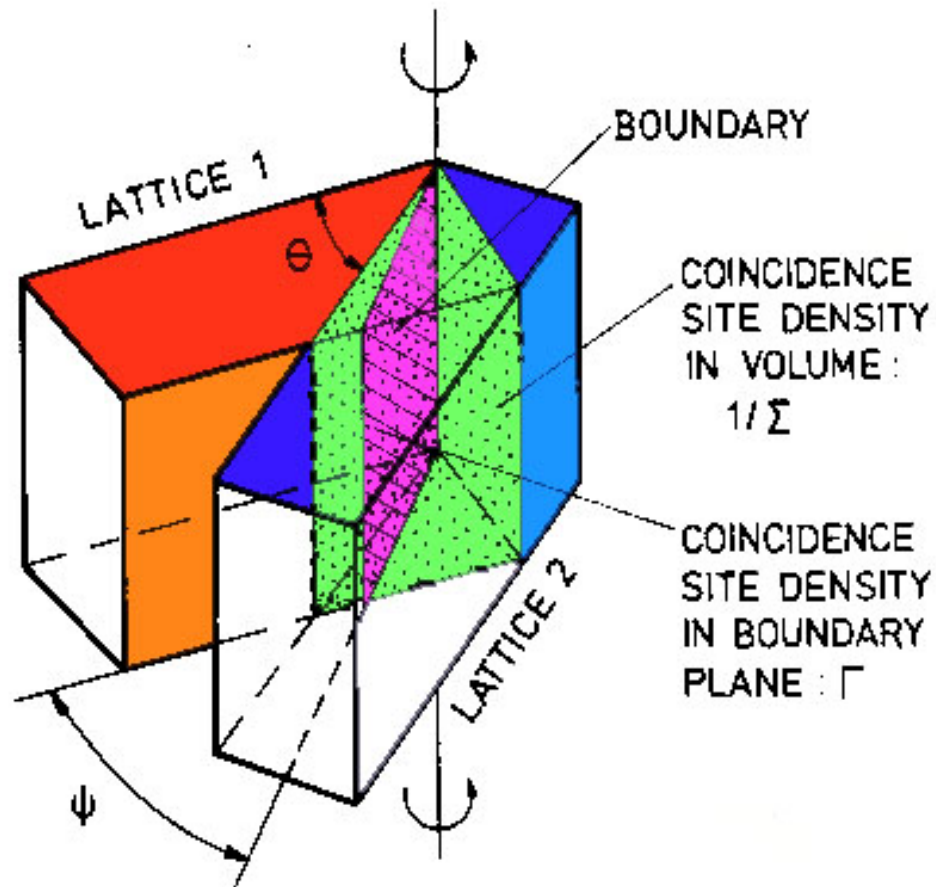
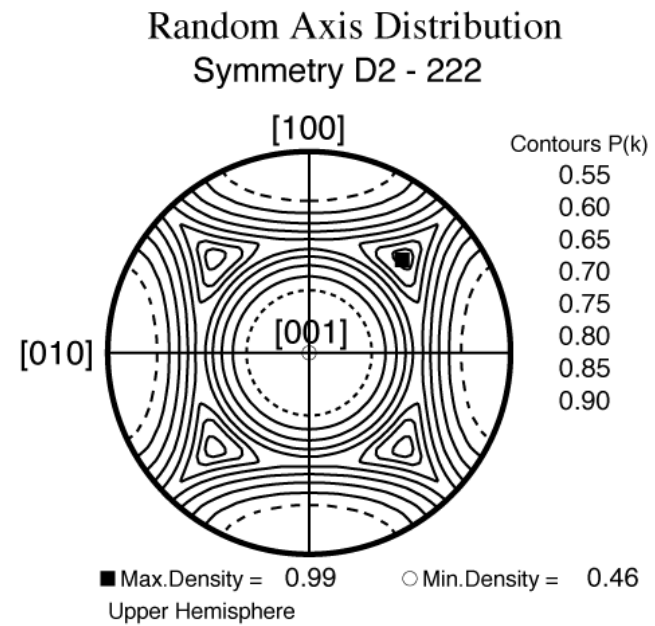
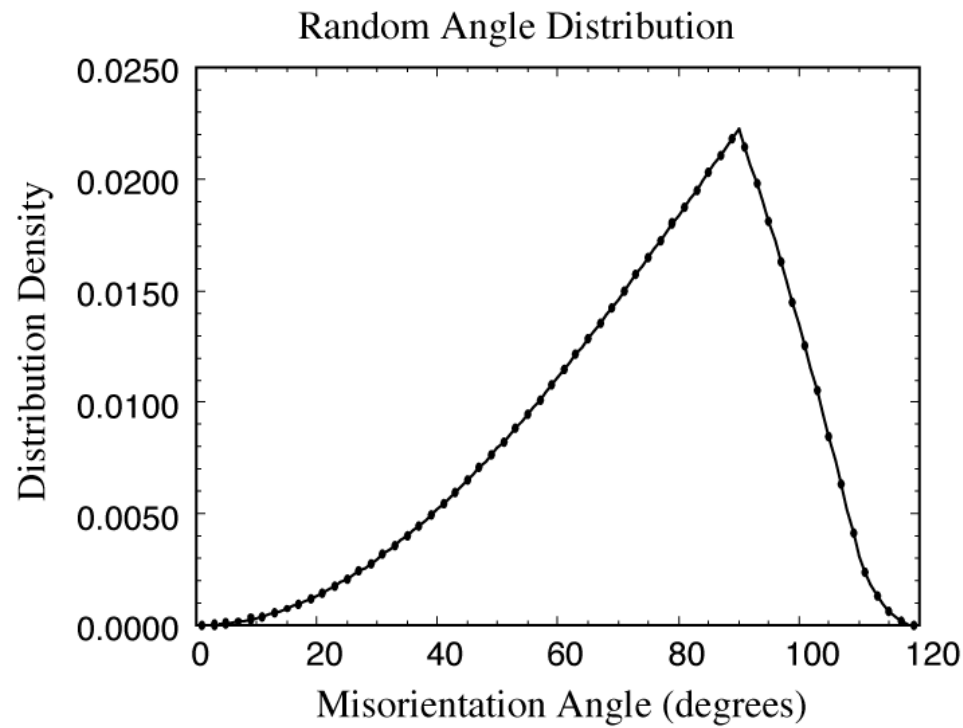


Fig. 1 - Two interpenetrating lattices with misorientation θ and boundary inclination ψ . Shown here is the special case of a tilt boundary (asymmetric); in the general case, the axes of θ and ψ would not be coincident.

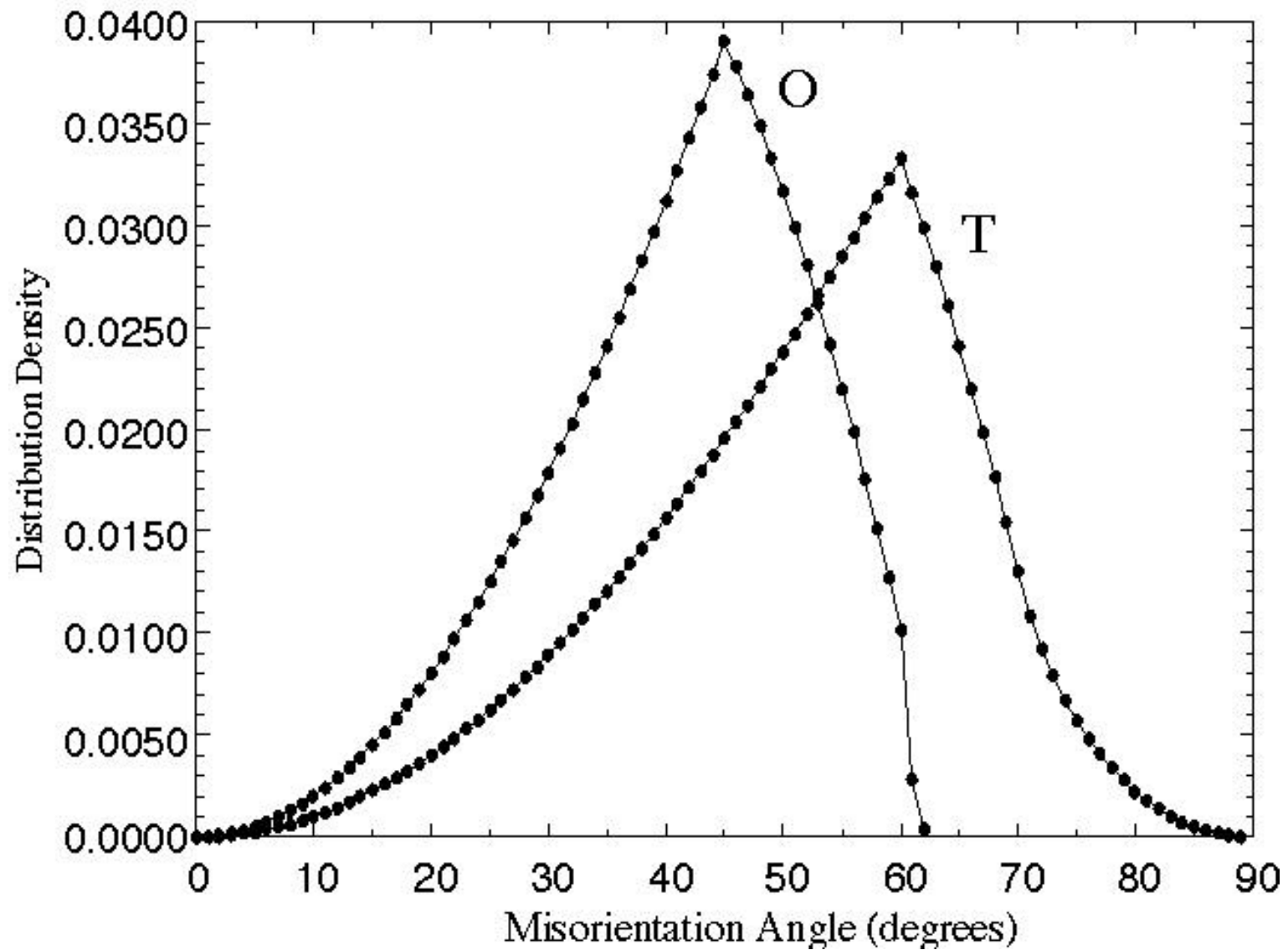
Misorientation

- Relative misorientation between crystal A and crystal B in crystal co-ordinates
- Rotation matrix; $\Delta g_{ij} = g^A_{ik} \cdot g^B_{jk} = g^A \cdot (g^B)^t$
- Rotation axis/angle; $[uvw]/\theta$
- Euler angles; $\varphi_1 \Phi \varphi_2$

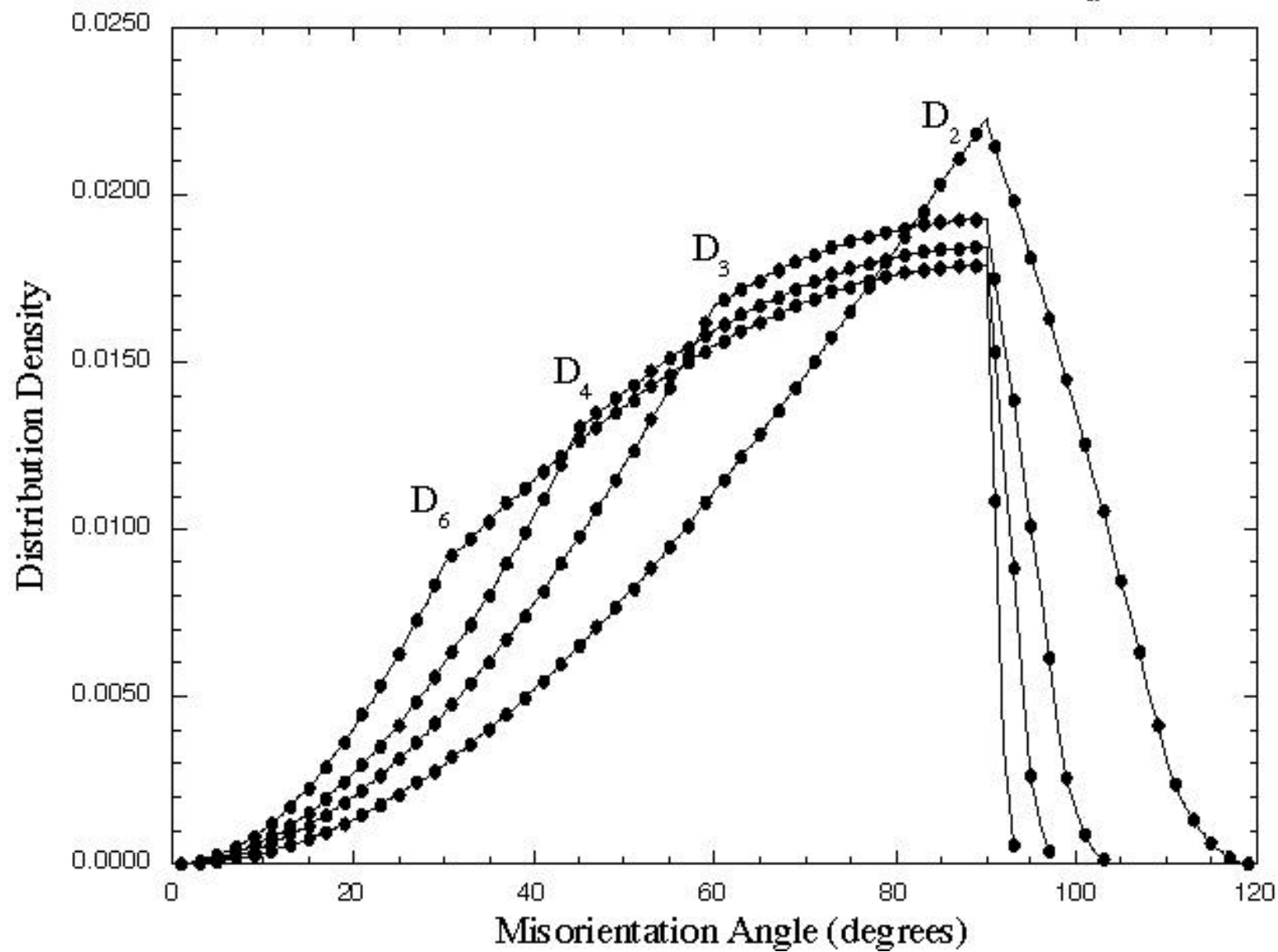
Rotation axis and angle distributions for random case - Orthorhombic crystal symmetry



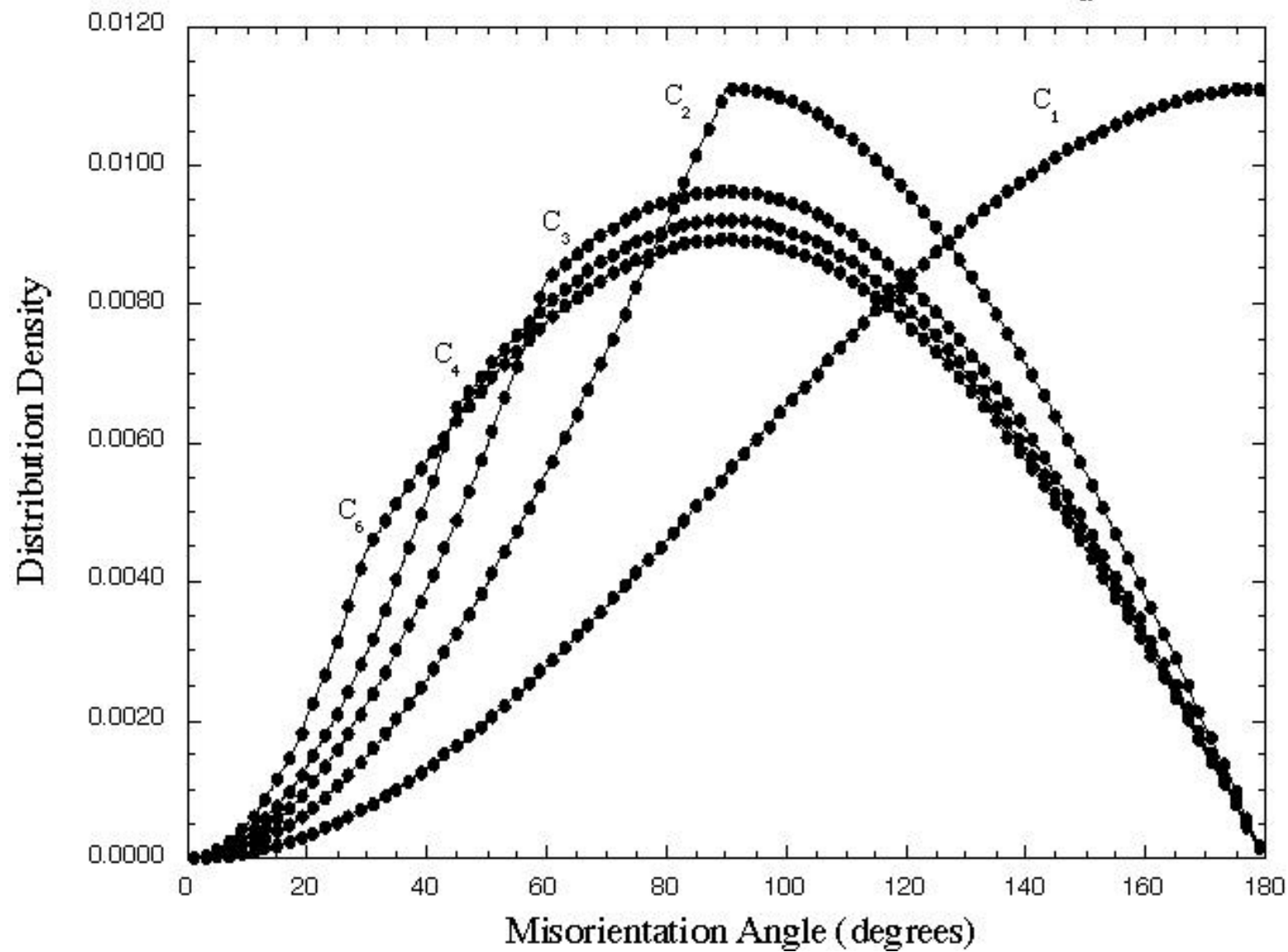
Random Angle Distributions - Cubic groups



Random Angle Distributions - Dihedral Groups D_n



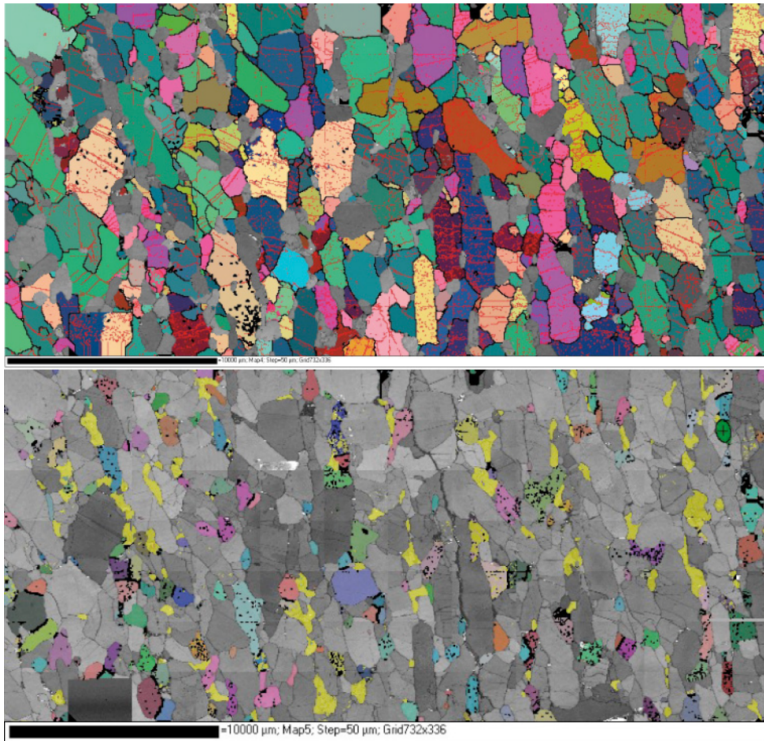
Random Angle Distributions - Cyclic Groups C_n



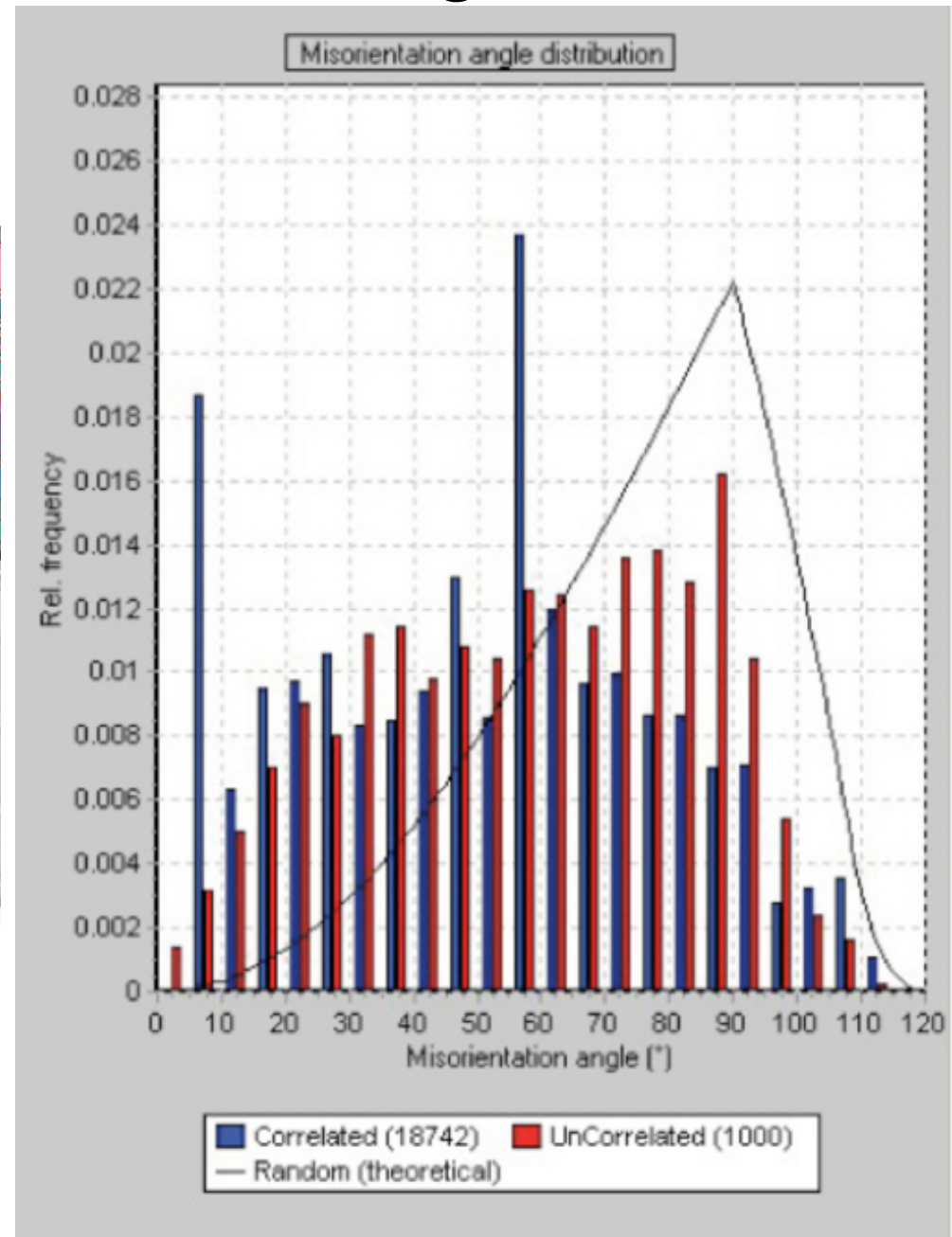
Misorientation

- Uncorrelated misorientation between random pairs A and B in the microstructure
- Correlated (physical) misorientation between neighbouring crystals A and B
- Autocorrelated misorientation between crystal A and every other pair B in the microstructure, similar to uncorrelated

Misorientation Histogram



9510-16 Low cpx lherzolite



Noise at low misorientation

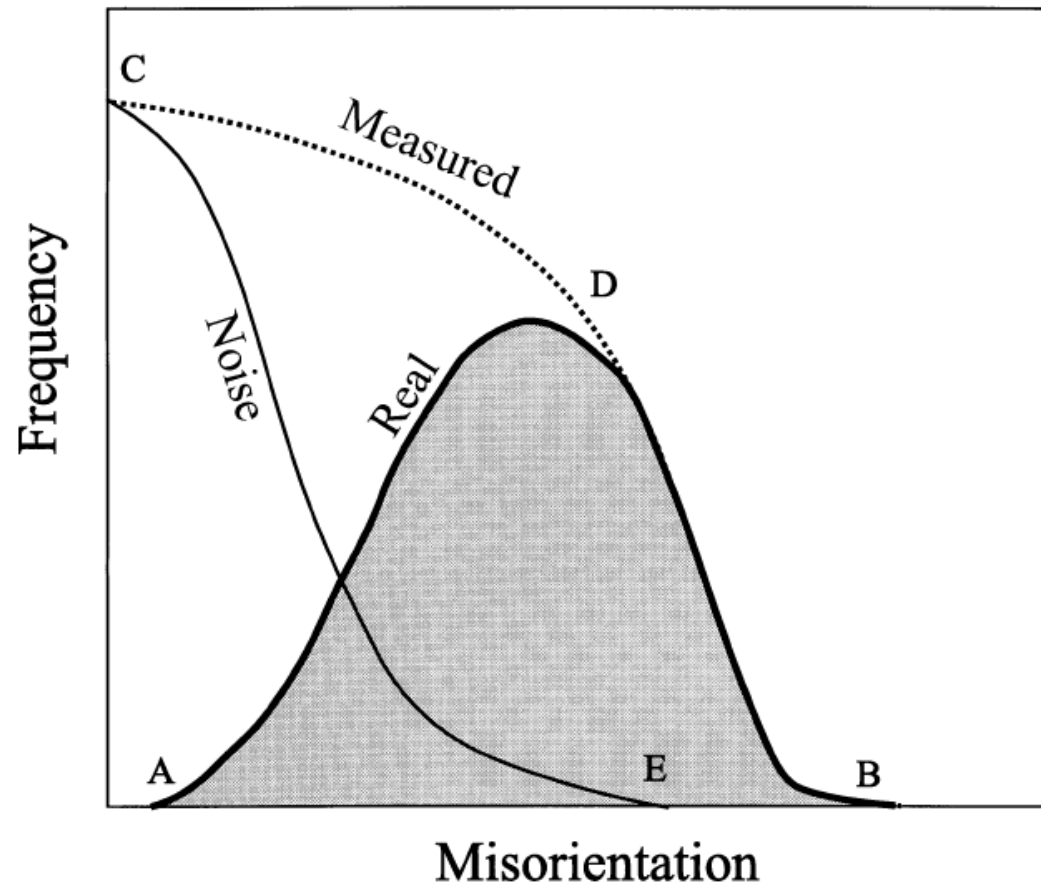
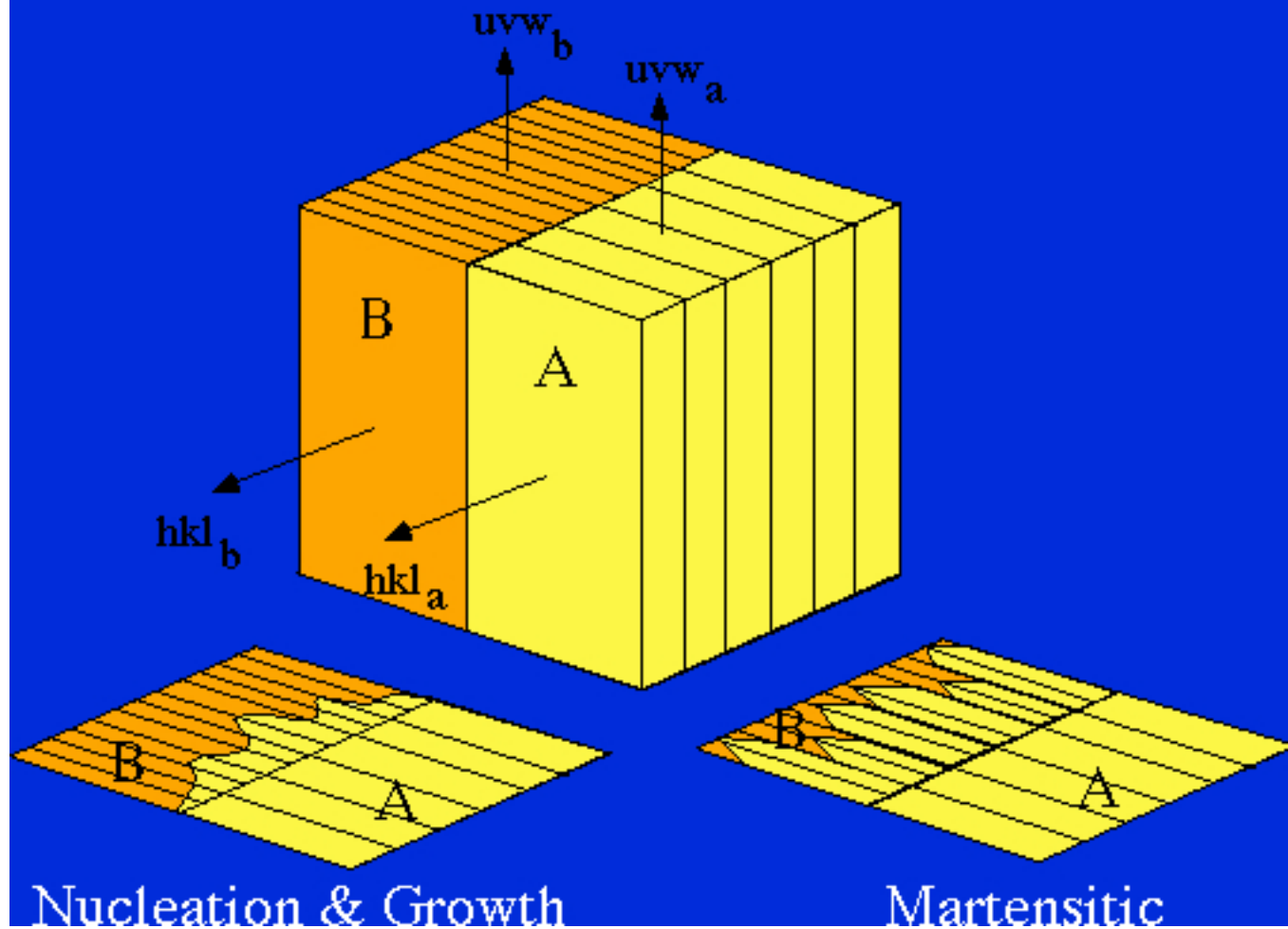


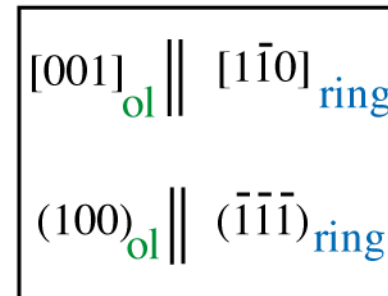
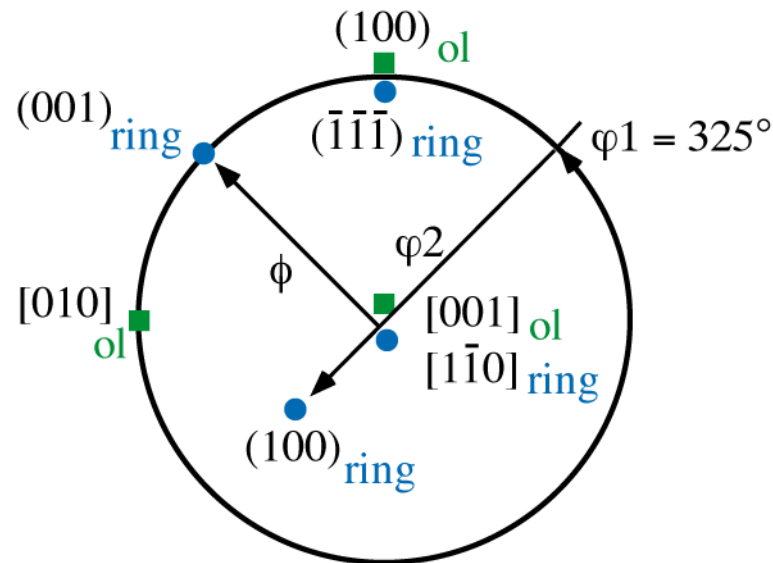
Fig. 8. Schematic diagram showing the relationship between the real and measured misorientation distributions and the orientation noise.

Phase Transition Orientation Relationships



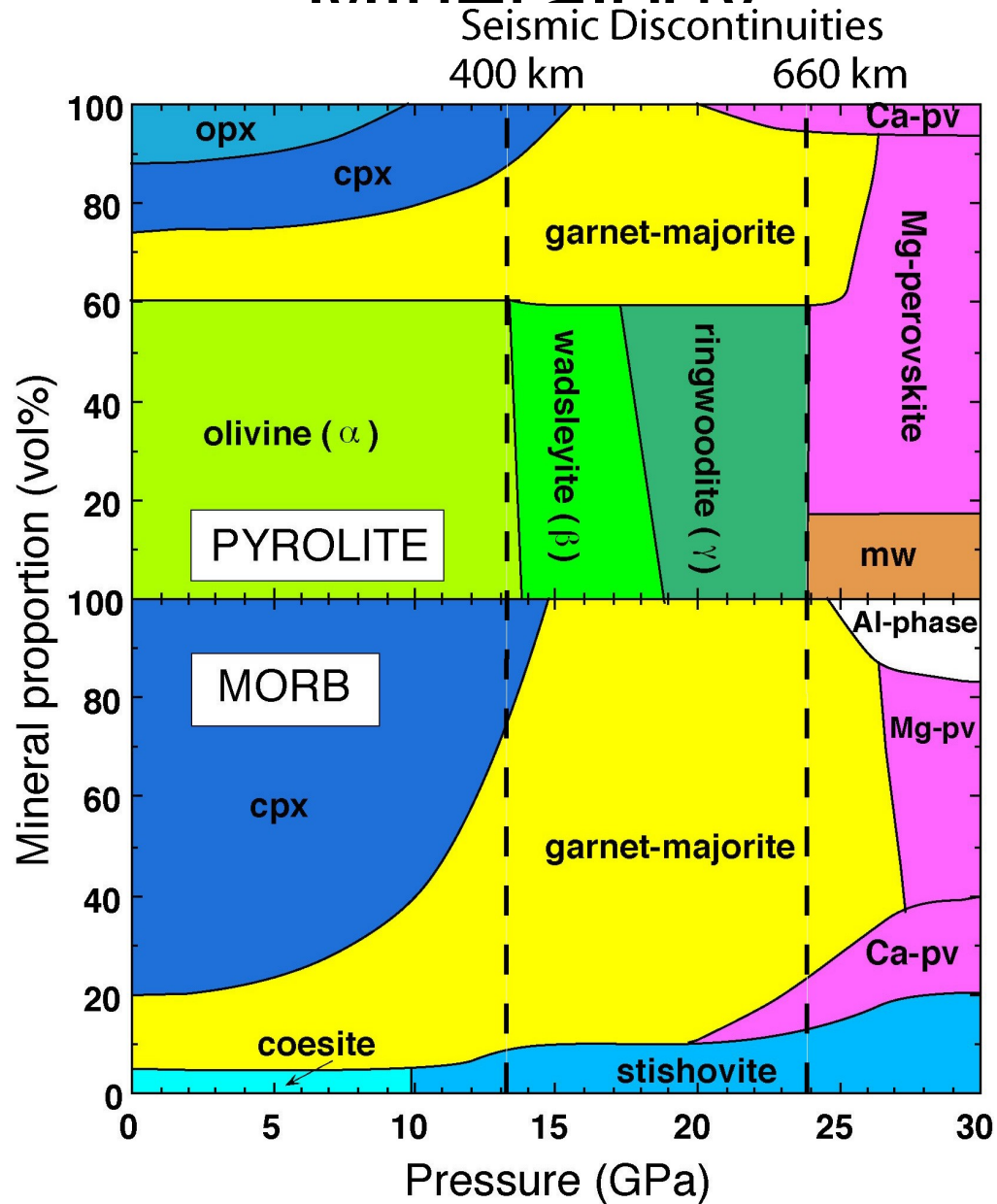
Crystallographic relationships

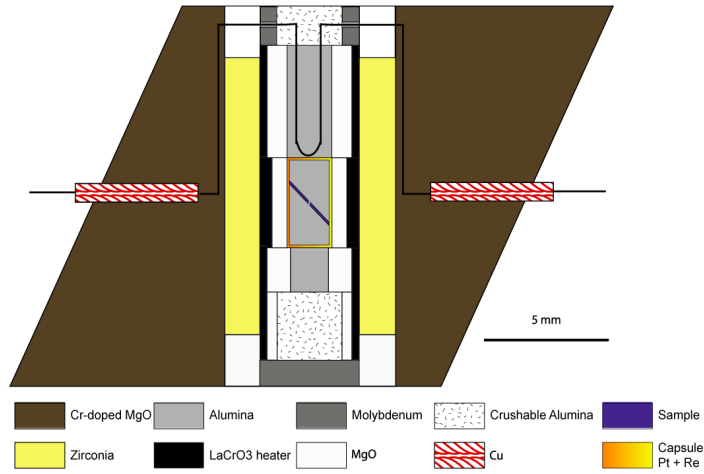
Misorientation Δg between lattices : **olivine** - **ringwoodite**



$$\Delta g = (\varphi_1, \phi, \varphi_2)$$

Mantle Phase Transitions and Mineralogy

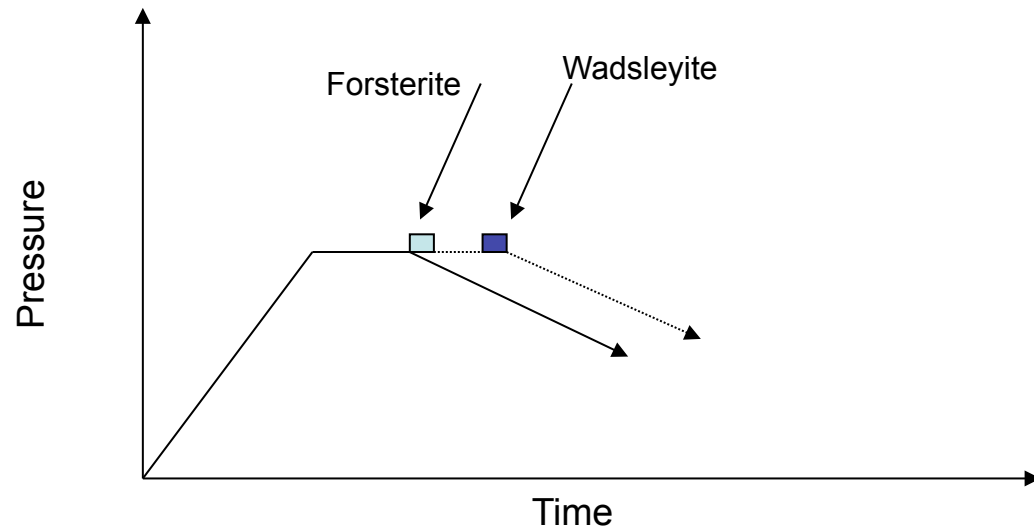
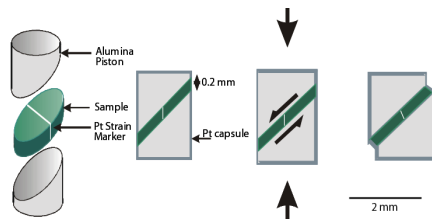
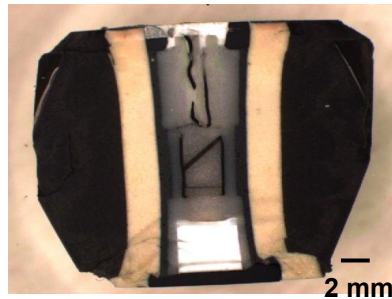




Starting material:
 Mg_2SiO_4 (sintered powder) at 11 GPa 1400°C

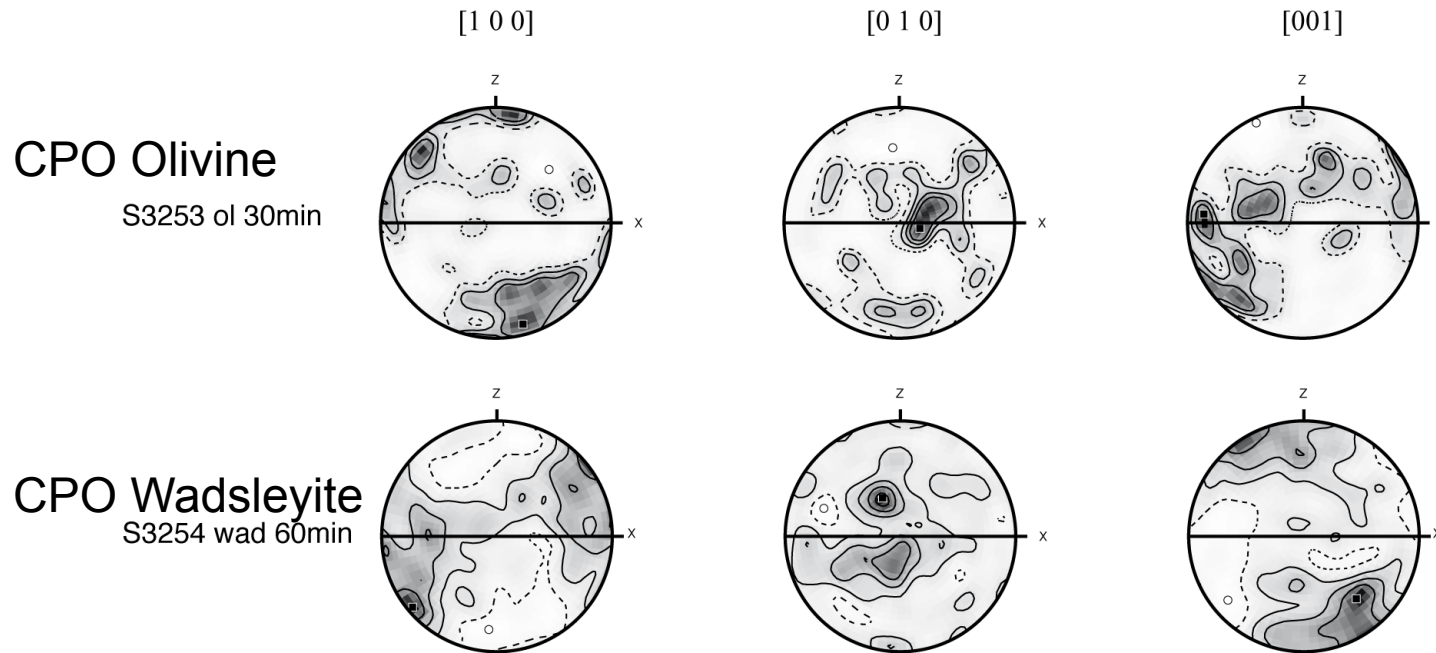
Conditions Pressure-Temperature :
 ~16 GPa – 1400°C

Deformation time:
 30 minutes
 1 hour

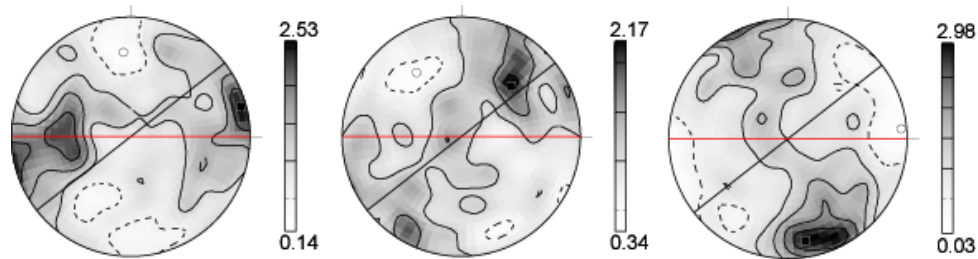


Hélène Couvy & Patrick Cordier
 Bayerisches Geoinstitut, Universitaet Bayreuth, Bayreuth, Allemagne
 LSPES, Université des sciences et technologies de Lille, Lille, France

CPO of Olivine and Wadsleyite in simple shear

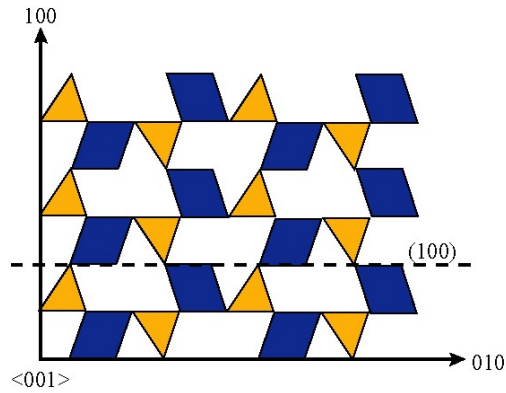


CPO Simulation for Wadsleyite



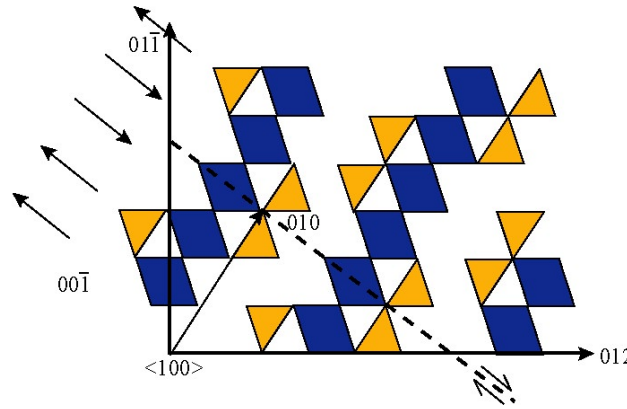
Oxygen Sublattices of Olivine polymorphs

Olivine
Pbnm
O-lattice h.c.p.
in $\langle 100 \rangle$ direction



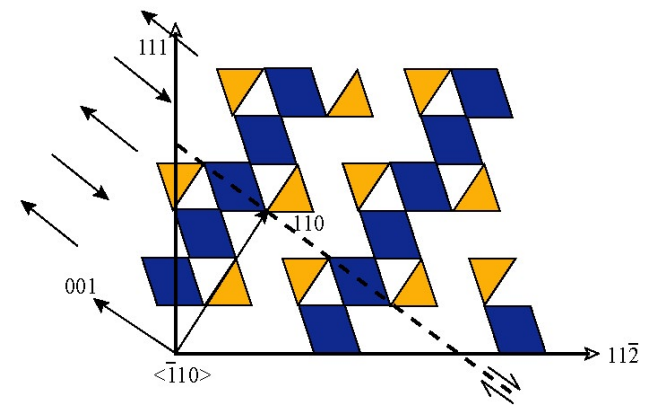
a

Wadsleyite
Imma
O-lattice c.c.p.
in $\langle 01\bar{1} \rangle$ direction



b

Ringwoodite
Fd3m
O-lattice c.c.p.
in $\langle 111 \rangle$ direction



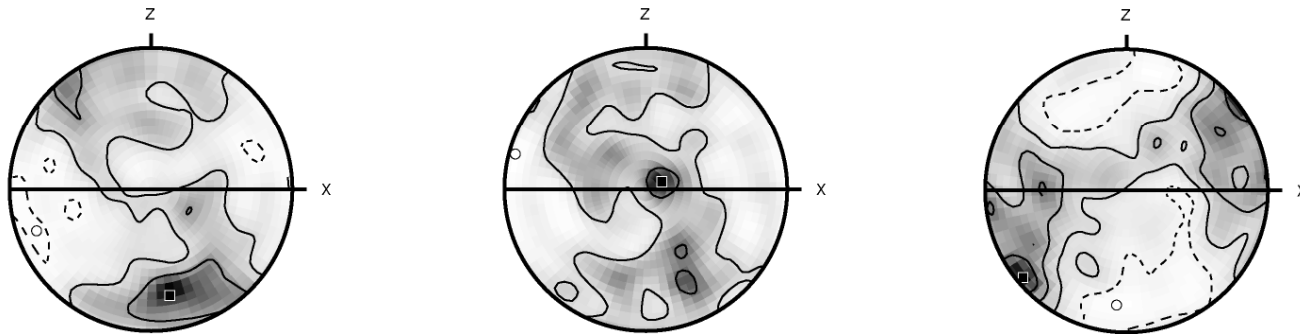
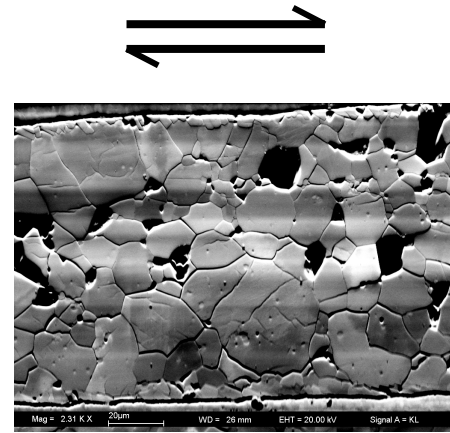
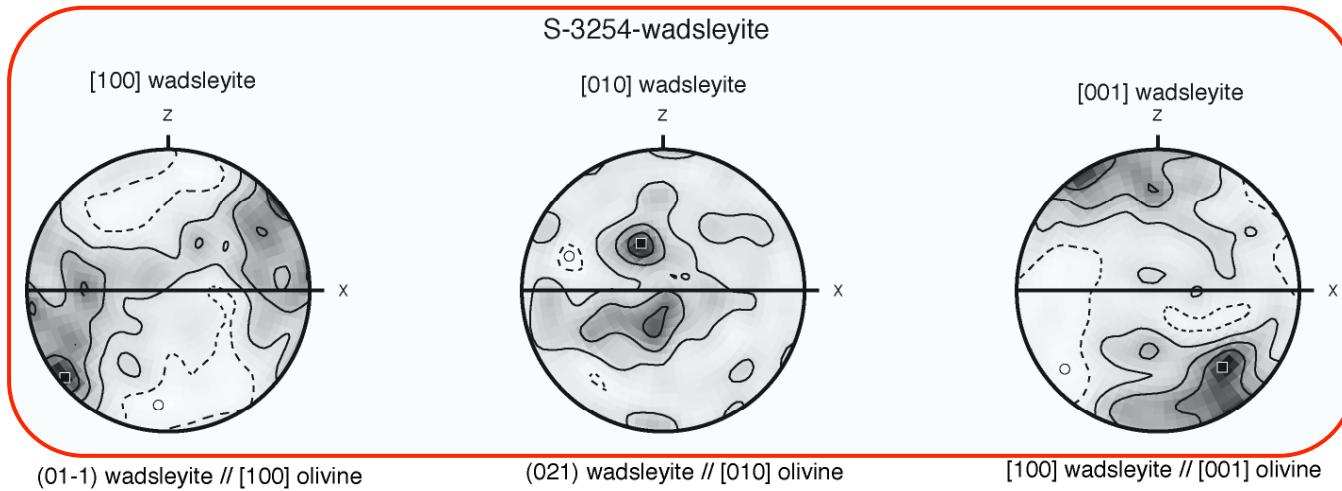
g

$$(100)_{\alpha} \parallel (01\bar{1})_{\beta} \parallel (111)_{\gamma}$$

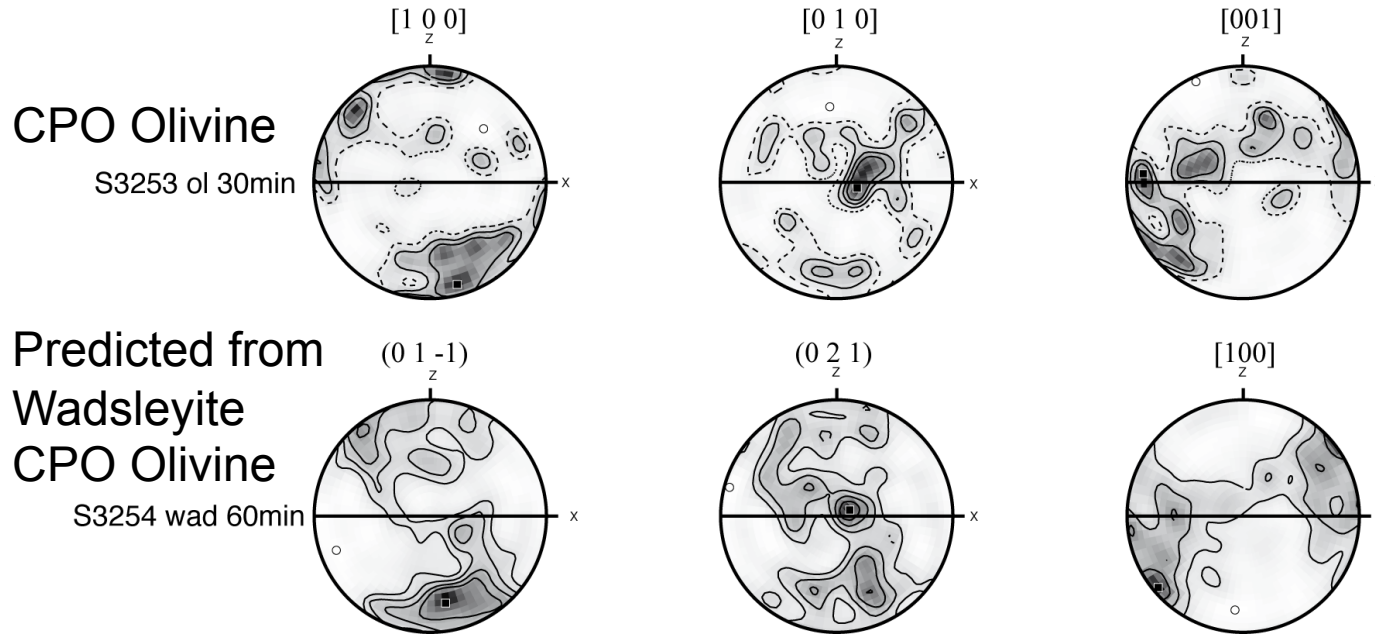
$$(010)_{\alpha} \parallel (012)_{\beta} \parallel (\bar{1}\bar{1}2)_{\gamma}$$

$$[001]_{\alpha} \parallel [100]_{\beta} \parallel [\bar{1}\bar{1}0]_{\gamma}$$

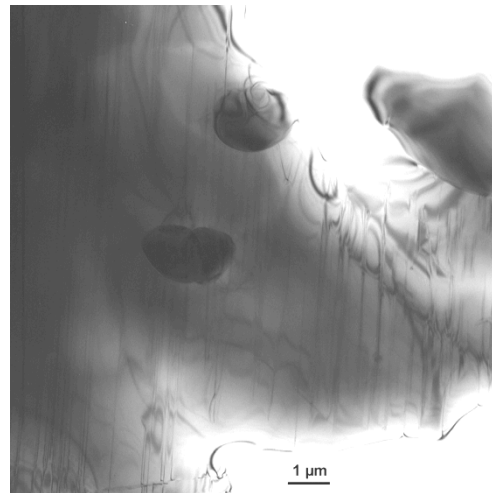
S 3254 - Wadsleyite 60 min



Wadsleyite CPO inherited from Olivine

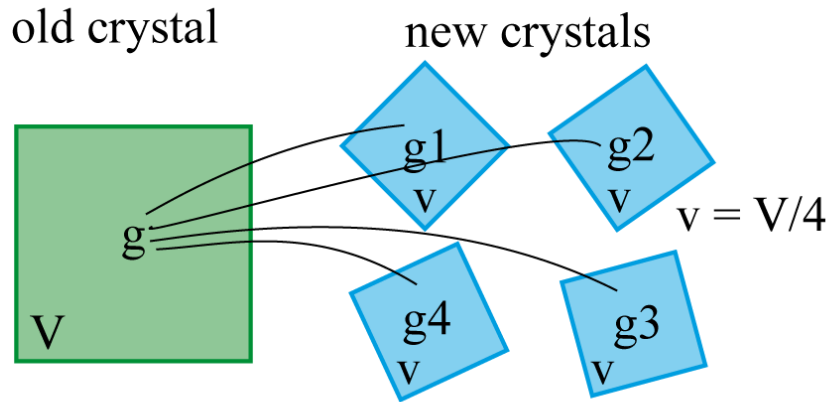


TEM Photo of S3253 (olivine)
Wadsleyite inclusions in Olivine

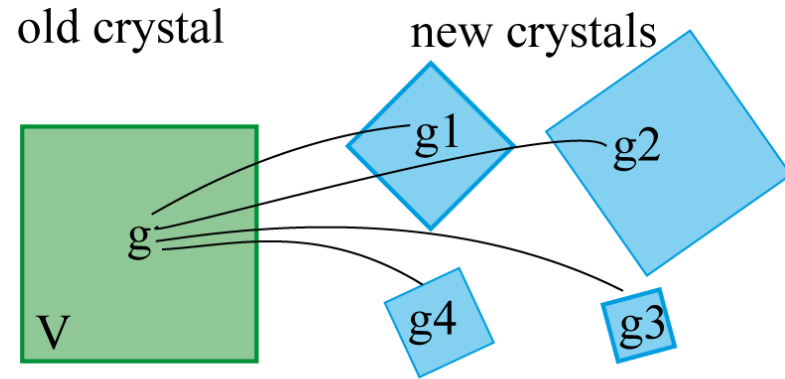


Phase transformation and Variant selection

Case 1 : No variant selection



Case 2 : Variant selection - stronger CPO.



Case for olivine (orthorhombic) to wadselyite (orthorhombic)

g = orientation

Δg = misorientation olivine to wadselyite

S = point group rotations (4 for olivine, so 4 new crystals)

wt = volume fraction weighting

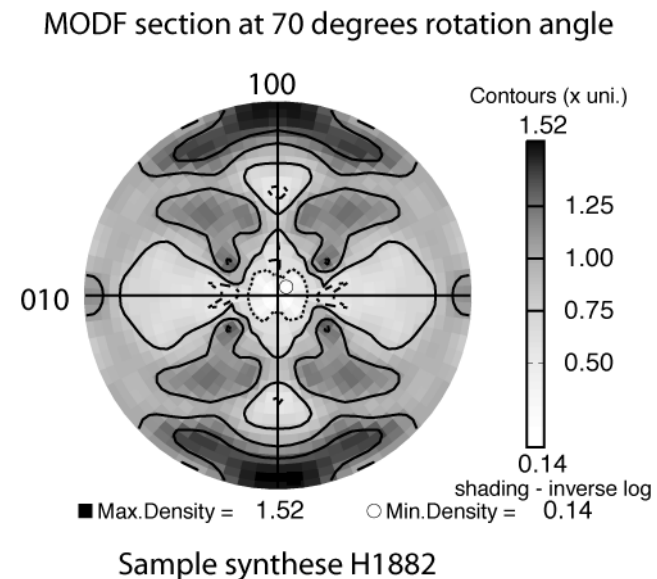
$$g(i...4)^{new} = \Delta g \cdot S(i...4)^{old} \cdot g^{old}$$

$$g(i...4)^{new} = \Delta g \cdot S(i...4)^{old} \cdot g^{old} \cdot wt(i...4)$$

Predicted Misorientation for phase transformation

Predicted misorientation in Wadselyite : 72 degrees rotation about [100] axis.

Found in MisOrientation Distribution Function (MODF)

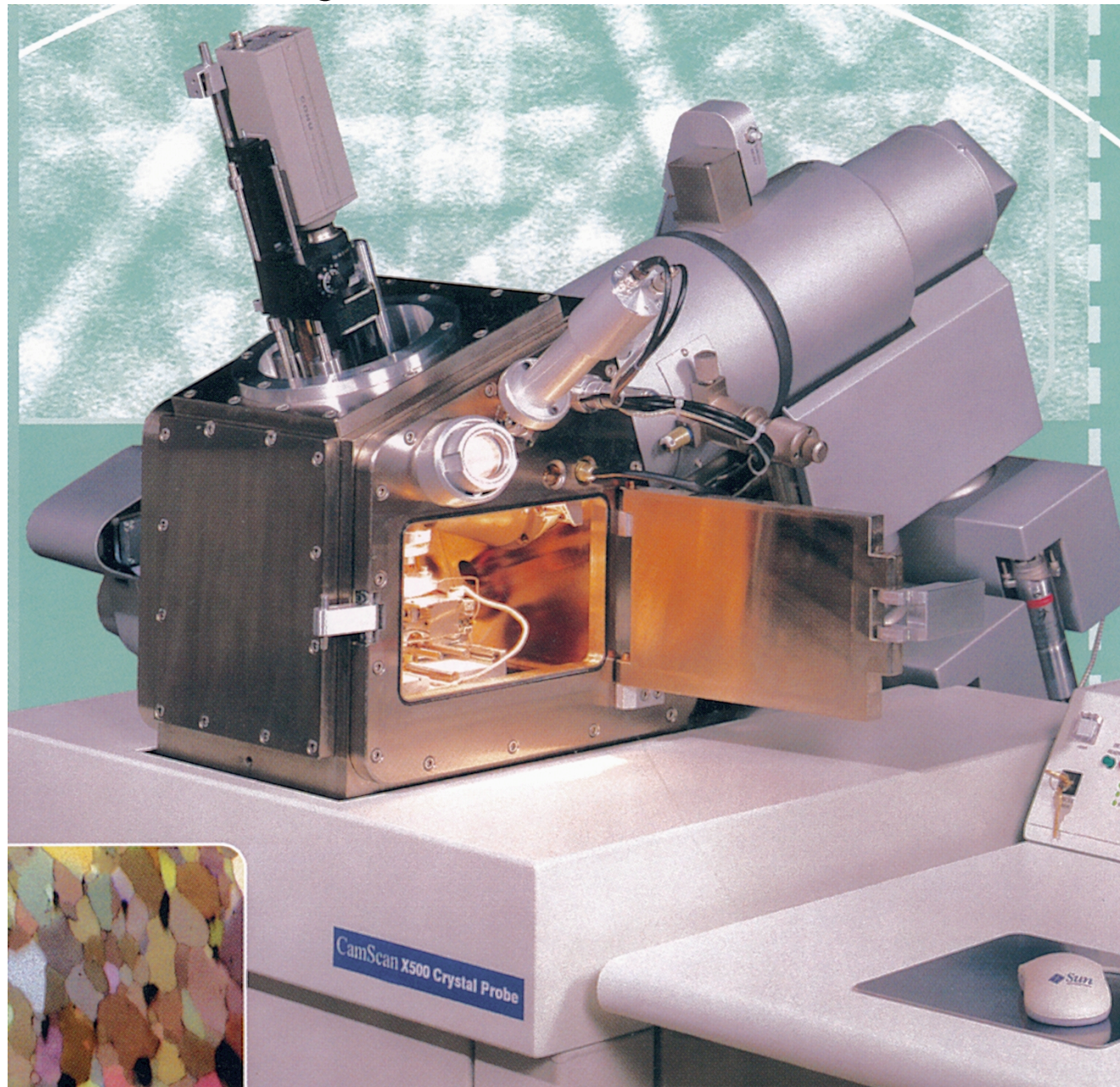


1. What is EBSD ?
2. Symmetry and EBSD
3. Applications
- 4. Future developments**

Future developments

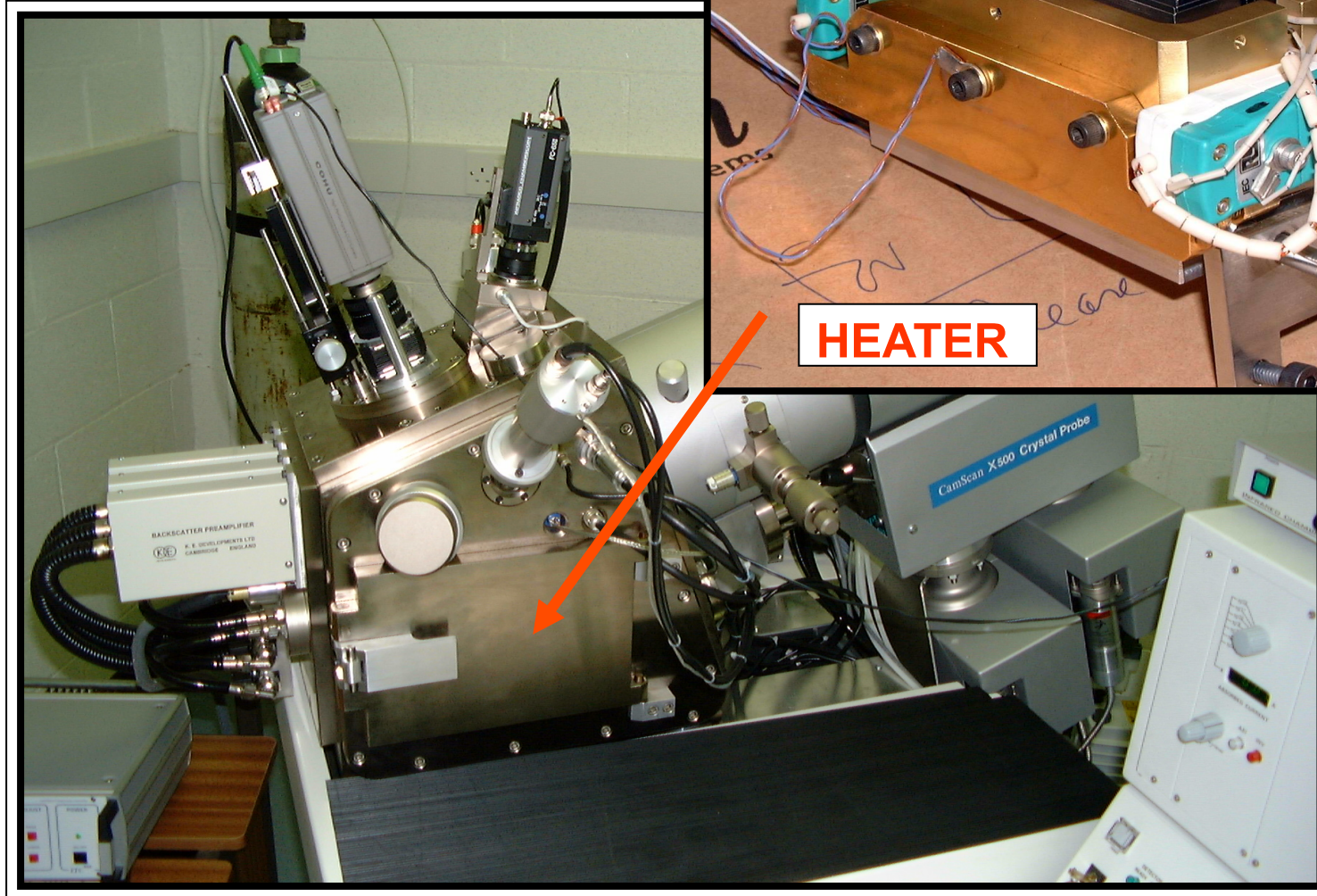
In-situ high temperature EBSD

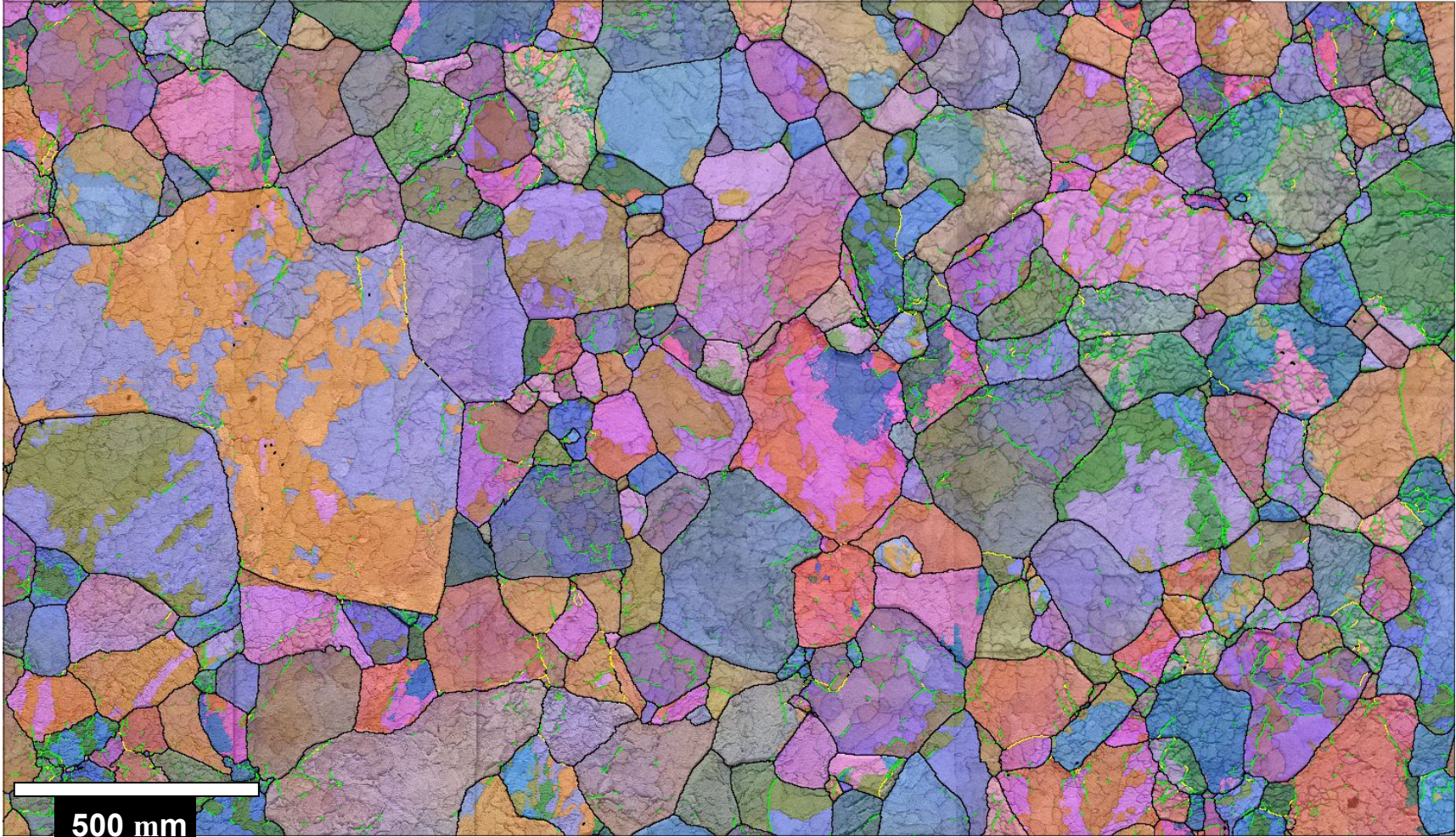
Crystal Probe

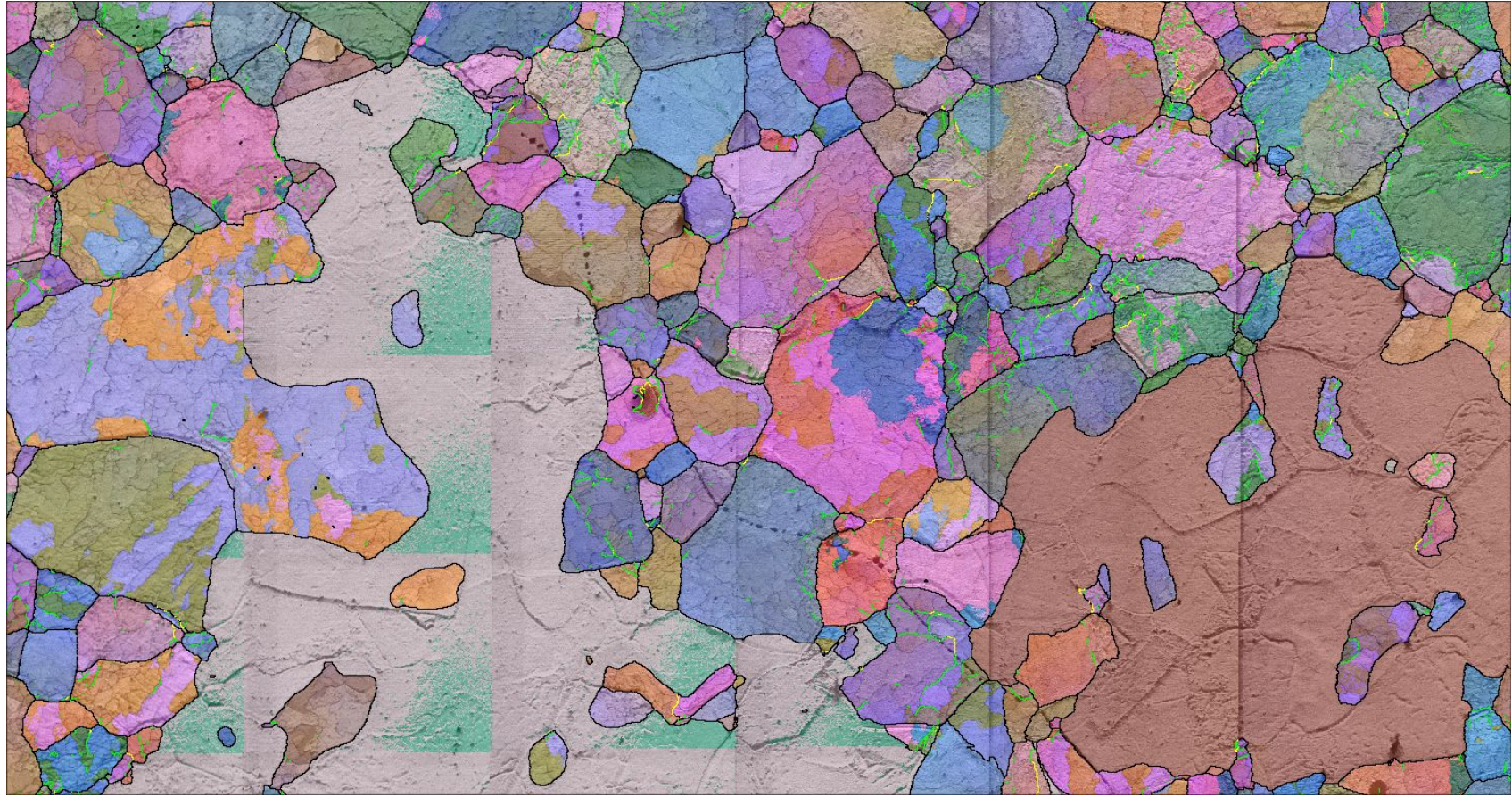


In-situ experiments in SEM

Seward et al., 2000 *Scanning*, 24, 232-240.



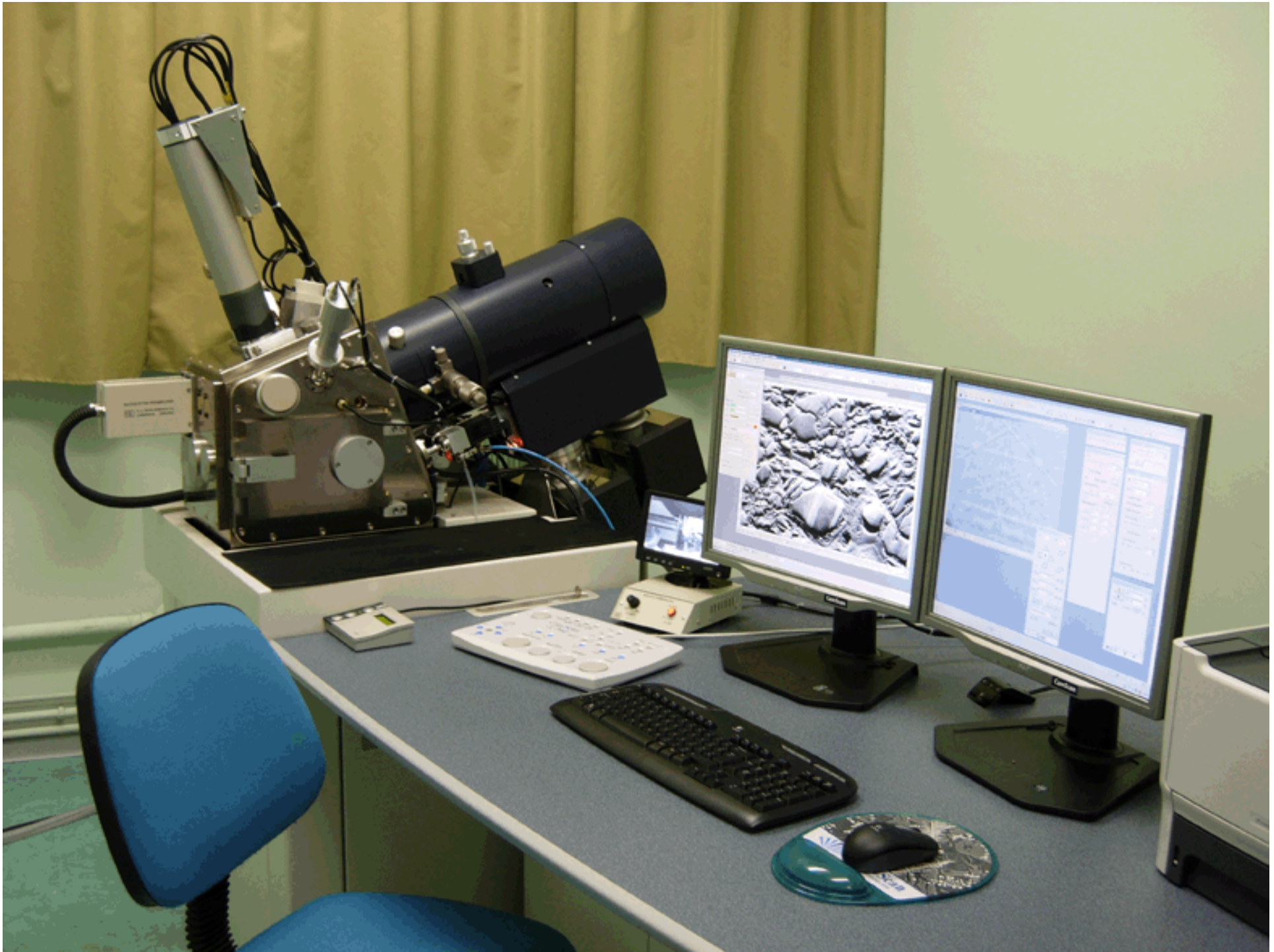


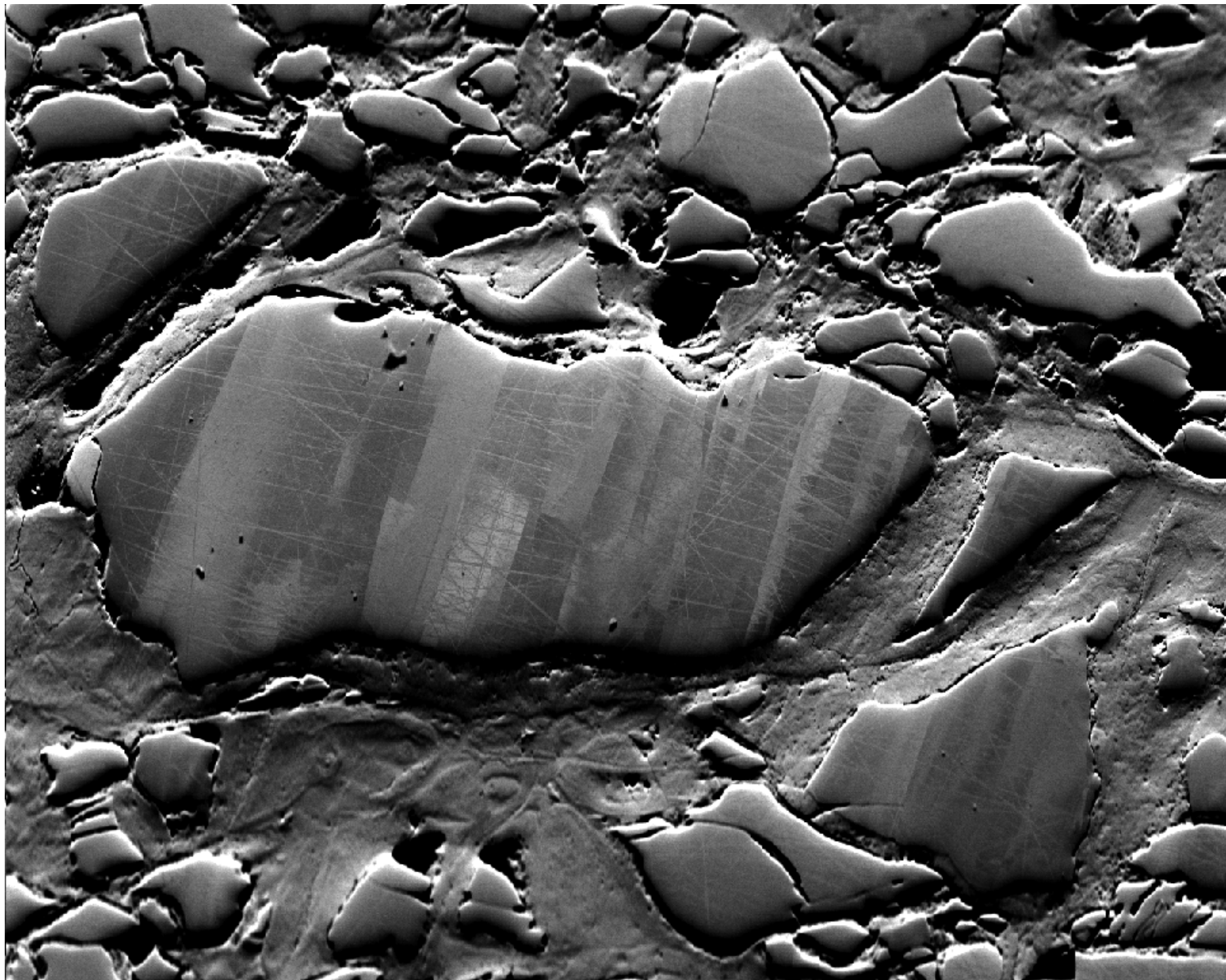


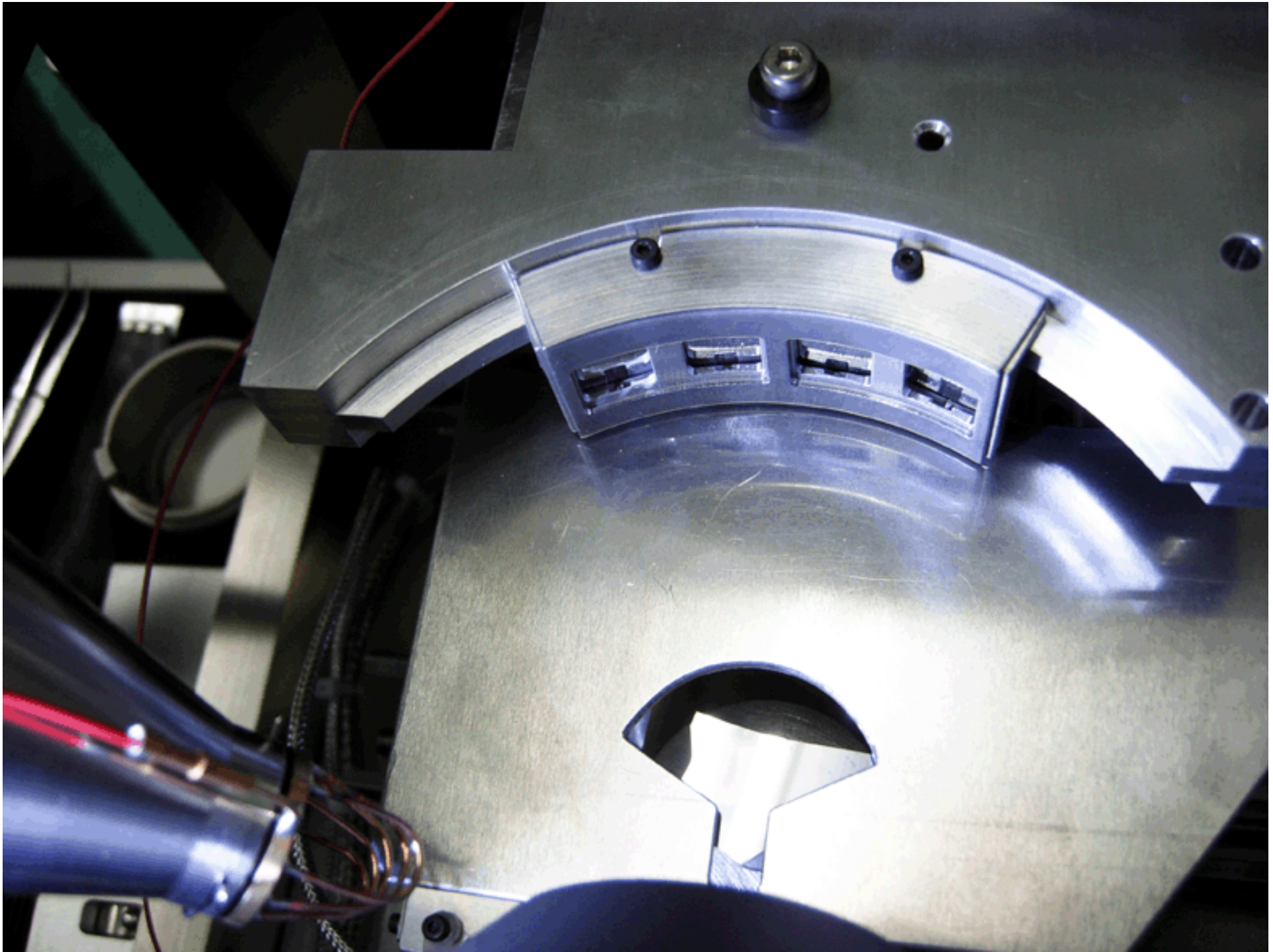
500 mm

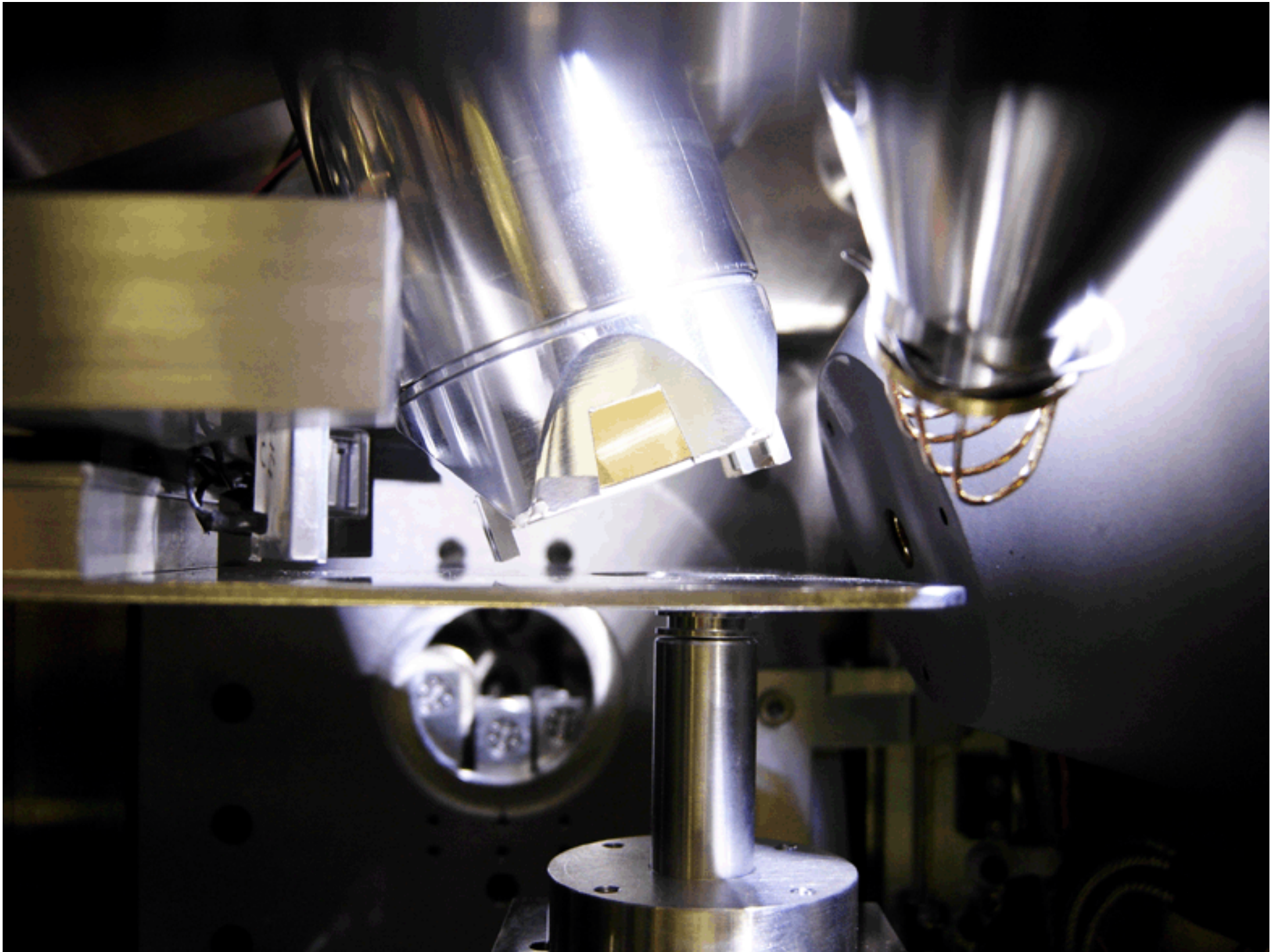


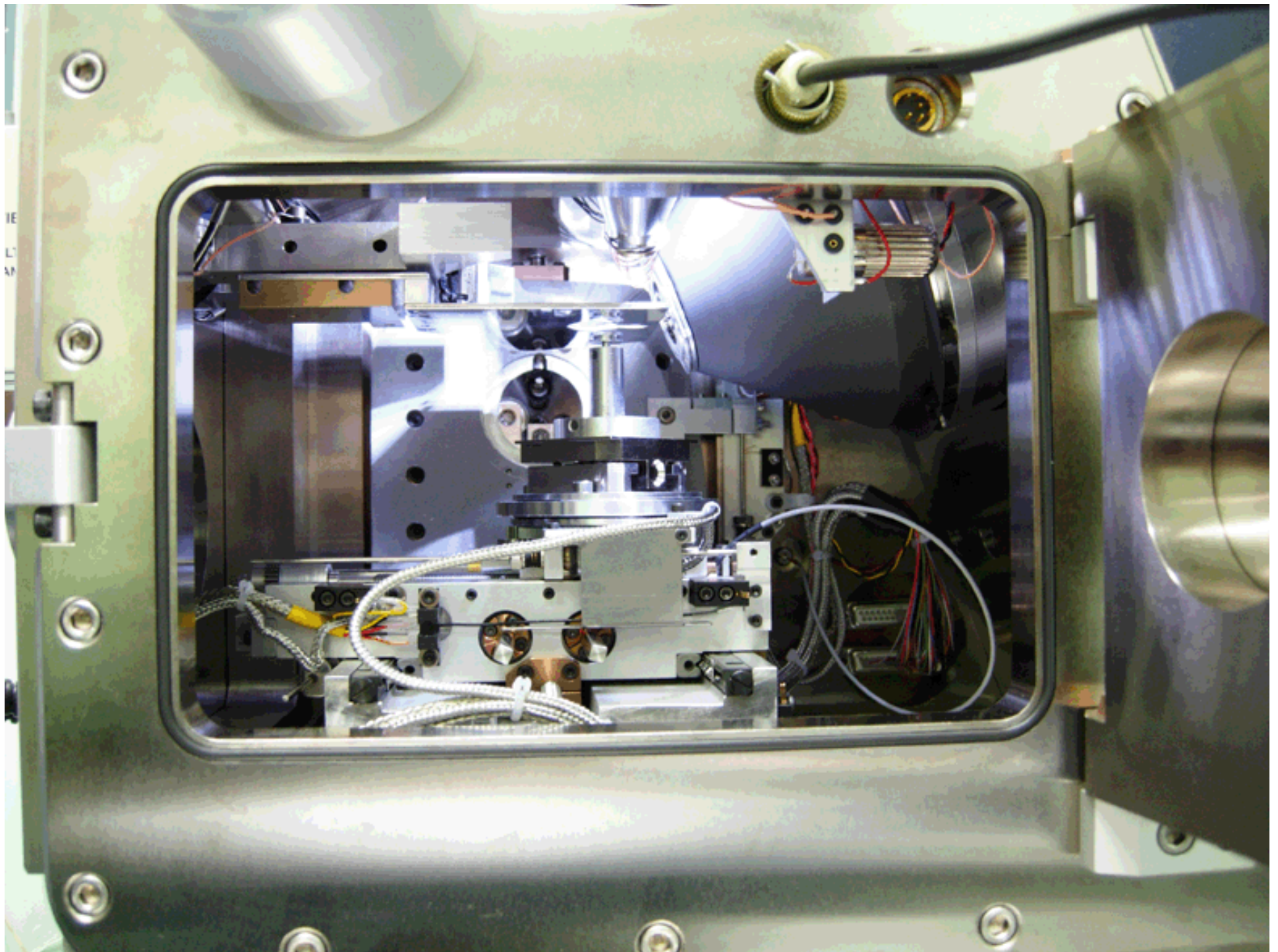
500 mm

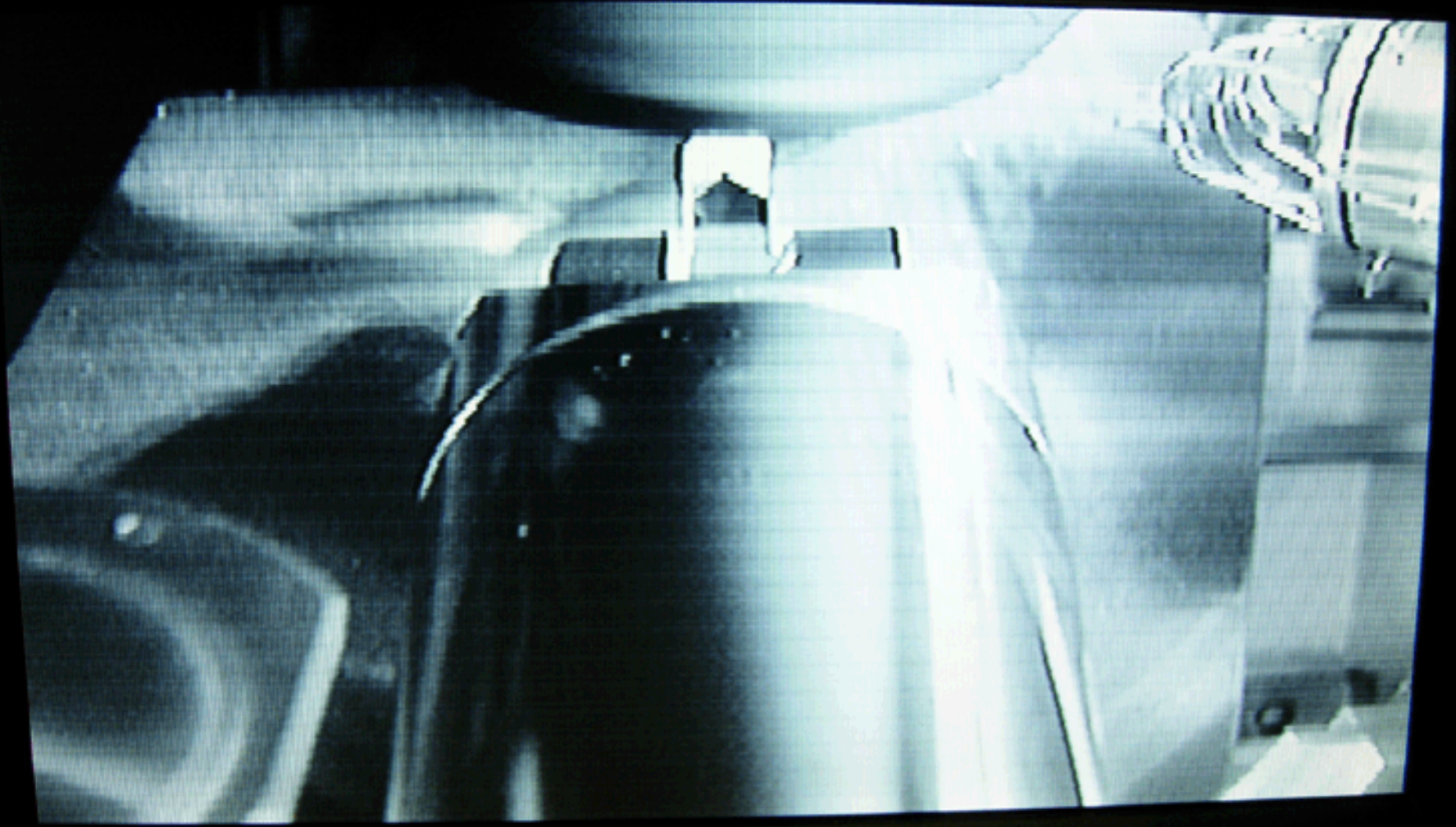












▼ DN

UP ▲

DISP

SEL



PWR